Project Altus Final Report

Preliminary Design and Project Proposal for a Sustainable Upper Atmospheric Vehicle

AE3200: Design Synthesis Exercise

Project Group 25

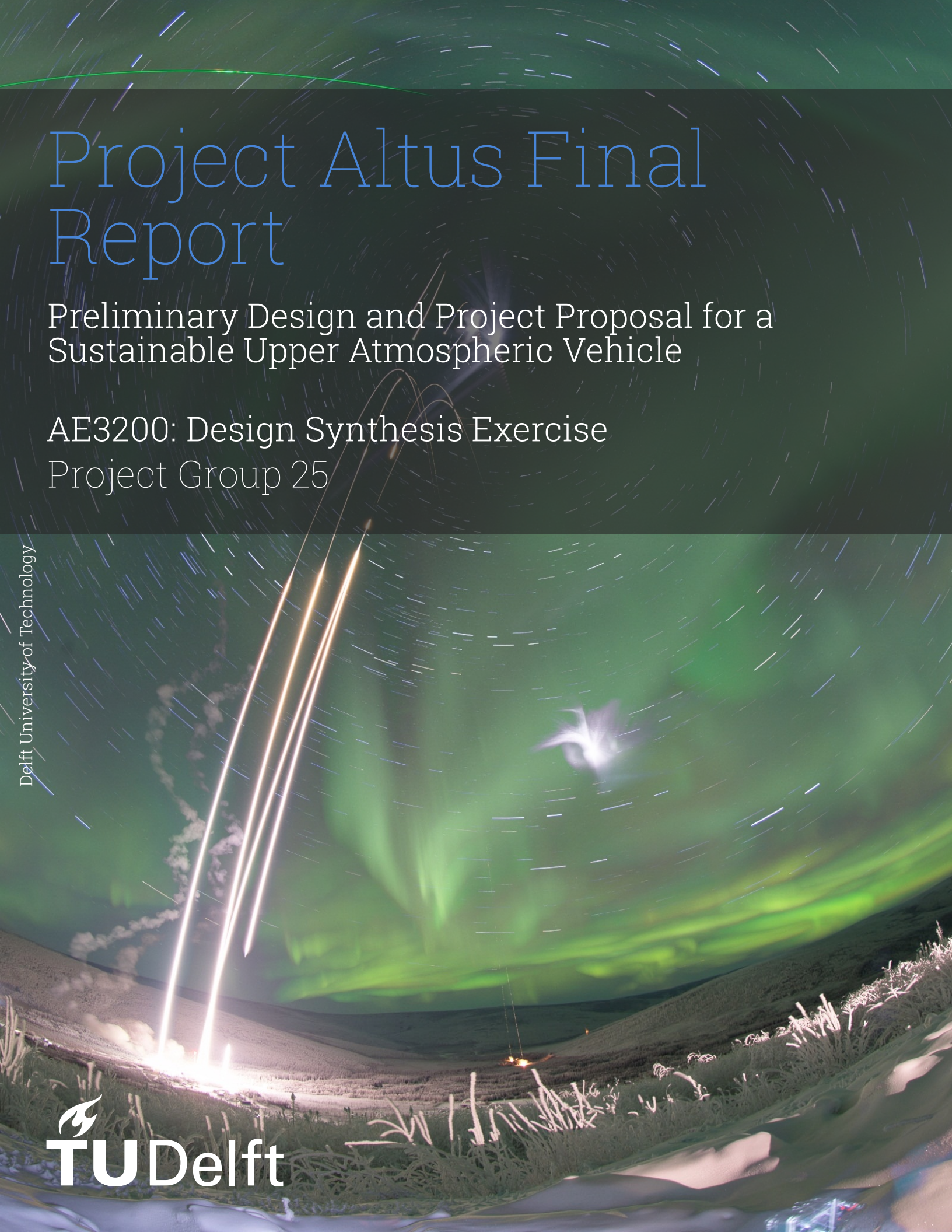

Delft University of Technology

TU Delft

Project Altus Final Report

Preliminary Design and Project Proposal for a Sustainable Upper Atmospheric Vehicle

by

Project Group 25

Student Name	Student Number
Luca Alonso	5239575
Sarissa Aurori	5075939
Mauro Beenders	5084164
Elvin Chen	5296358
Charles Kendall	4815971
Daniël Norbart	5069521
Thijmen Odijk	4771486
Martijn Rusch	4782631
Laura Tabaksblat	5003555
Stefaan Yorucu	5227666

Instructor:	I. Akay
Coaches:	A. Başkaya & P. Piron
Project Duration:	April 2023 - June 2023
Faculty:	Faculty of Aerospace Engineering, Delft

Cover:	Sounding Rockets Launch Into an Aurora by NASA/Jamie Adkins
Style:	TU Delft Report Style, with modifications by Daan Zwaneveld

TU Delft

Executive Overview

Altus Mission

Author: D. Norbart
Editor: C. Kendall

The goal of project Altus is to do an in-situ investigation of Polar Mesospheric Clouds (PMCs). These clouds form around an altitude of 84 km, and only for 60 to 80 days per year, during the summer. Normally, these clouds only form in the polar regions, from around 50° latitude north and south. Recently, however, PMCs have been observed as low as 40° north. There are theories linking this change in location, and other unexpected behaviours of PMCs, to climate change. However, further research is still required to confirm these theories. As these changes are happening at a slow rate, a database of PMC measurements would be extremely beneficial to track indicator values over time. Project Altus sets out to bridge this knowledge gap by taking regular measurements of PMCs over an extended period of time.

To acquire the data necessary for useful scientific study to take place, in situ measurements of PMCs are needed. This stands in contrast to the remote sensing with satellites and ground-based infrastructure that currently dominates PMC research. For definitive answers to other major unanswered questions about PMCs, such as the cause of their radar reflectivity, a thorough analysis of the cloud particles is necessary. This necessitates a sample return mission to retrieve physical particles from the clouds. As aircraft fly too low and satellites too high to retrieve cloud particles, a sounding rocket is the only way of obtaining these samples. A secondary customer requirement is that the sounding rocket vehicle must be sustainable since climate research should not contribute to climate change.

The sustainability aspect of the Altus mission is a very important one since the launcher industry as a whole is quite unsustainable due to the wide use of hazardous chemicals and expending launch vehicles after a single mission. Orbital launch vehicles that use solid propellants (including Europe's next-generation Ariane 6 and Vega-C vehicles) nearly universally use Ammmonium Perchlorate Composite Propellant (APCP). These compositions produce a significant quantity of hydrogen chloride in their exhaust, which harms the environment by damaging the ozone layer and causing acid rain. The Altus mission, therefore, demonstrates an Ammonium DiNitramide (ADN)- and Ammonium Nitrate (AN)-based propellant, which eliminates hydrogen chloride from the exhaust entirely. The lower Technology Readiness Level (TRL) of this propellant and the prohibitive cost of ADN compared to AP currently precludes the use of this type of propellant in orbital vehicles. By demonstrating ADN at a smaller scale, and by encouraging the establishment of bulk-production facilities for this chemical, the Altus mission will therefore pave the way for the wider use of ADN. This will significantly ameliorate the environmental impact of the launch vehicle industry, beyond anything that the Altus mission could achieve when considered in isolation. The chosen mission need statement is therefore to:

Catalyse a shift towards sustainable rocketry by means of a polar mesospheric cloud research mission, demonstrating technologies that can be applied to reduce the environmental impact of rockets.

The properties of the PMCs that will be measured to achieve this goal are: pressure, temperature, and water vapour density, in addition to the collected sample. These will be stored indefinitely, such that future researchers will be able to access an archive of PMC samples. This strategy has proven to be effective in similar situations; for example with the Cape Grim Air Archive. The database will cover 26 years, equal to the maximum recorded duration of two solar cycles. As the solar cycle has a significant influence on the formation of PMCs, it is important to provide data over a sufficient time period to decrease the impact of this confounding variable. The effect of the sidereal rotation of the sun must also be accounted for in the rate of measurements, which leads to a requirement for one

measurement (launch) to be taken per week for the eight weeks in which PMCs form every year.

Two major milestones are implemented. The first milestone, after 10 successful launches, represents the demonstration of the sustainable rocketry technologies. The second, after the completion of measurements for the first solar cycle, represents the halfway point for the nominal mission profile. On both occasions, the progress of the project and the performance of the vehicle will be evaluated, and additions or changes to the program or vehicle can be made.

Market Assessment

Author: D. Norbart
Editors: E. Chen, C. Kendall

When considering the government agencies that have funded PMC research in the past, there is a steady cash flow to a range of research projects. Across the world, a few million dollars are made available for research related to PMCs per year. The AIM satellite is an example of such a project. This is a dedicated mission to measure Polar Mesospheric Clouds, with a total budget of $140MM over several years. Based on this data, it is estimated that the total cost for the proposed Altus mission, at €35MM, can be provided by governments from around the world.

In addition to providing a platform for upper-atmospheric research, sounding rockets are adaptable for use in a variety of areas. This includes flying research missions for auroral science, astrophysics, geoscience, and solar physics, the testing of space hardware as single modules or as complete CubeSats, and microgravity research. It is estimated that the Altus vehicle can provide a microgravity environment for around two minutes at a time, and this is expected to make up the bulk of the commercial market for the vehicle. Aircraft can, however, provide 20 seconds of microgravity repeatedly for a significantly lower price than Altus can offer, while satellites offer effectively infinite time in microgravity. The testing of space hardware is feasible, but it is not possible to compete with state-of-the-art ground testing equipment to capture this market segment and, therefore, at this point in time Altus is not expected to fly a great number of such payloads. However it is possible that new markets will emerge during the operational life of the vehicle, that can be captured with minimal adjustment.

Systems Engineering Approach

Author: M. Rusch

Project Altus has attempted to make use of an integrated systems engineering approach. This consists of connecting the requirements with the risk assessment and then combining these aspects into the trade-off selection criteria. This process starts with the performance requirements. Since there always exists an associated performance risk that the requirement is not met. Usually, multiple individual risks contribute to this performance risk, and all of these are mitigated individually. These mitigation strategies subsequently drive new system requirements, and the verification and validation plan. This allows for a good base on which to conduct the preliminary design. Afterwards, the previously outlined verification and validation is used to test compliance of the design to the requirements, to reassess the risks, and to generate extra requirements. This is the starting point of the next design cycle. The application of this process has not been flawless, but important lessons have been learnt and recommendations made for the future.

The conclusion is that the preliminary design of the Altus vehicle complies with the majority of requirements, however the design is not mature enough to assess compliance with all. The recommendation is to outline a detailed Verification and Validation plan at the start of the next project phase, this will address these deficiencies and their associated risks.

Preliminary design

Author: D. Norbart
Editor: C. Kendall

After the trade-off was completed, the preliminary design of the vehicle was performed with an in-house developed

iterative simulation and sizing tool written in Python. The estimated vehicle characteristics from the conceptual design were used as the starting point of the iterative design loop. To evaluate the output values of the program, a parametric simulation of the rocket vehicle was made. Based on the results of that simulation, the parameters could be adjusted for the next iteration. This process continued until the parameters converged to a stable value.

The environmental sensor package that will measure the PMC ambient properties consist of a sonic thermometer (for temperature), a Dual Absolute Pressure Measuring Transducer (for pressure) and a Lyman-α hygrometer (for humidity). The sample collection mechanism is positioned at the nose of the vehicle, capturing particles by a velocity differential. The particles will be captured and stored in a cooled aerogel, which also keeps the particles dry.

The propulsion system has been designed to bring the vehicle to 110 km. The open-source tool *OpenMotor* was used to design the motors of the Altus vehicle. The design of the lower-stage motor was driven by the launch tower length and exit velocity, as these give requirements on the thrust, while the second-stage motor thrust was selected based on the likely achievable burn rate of the propellant. By integrating the thrust over the burn time, the total impulse was defined. The selected propellant, a Ammonium DiNitramide composite propellant bound with Hydroxyl-Terminated PolyButadiene, was already selected. The exact composition, with burn inhibitors (including a significant quantity of Ammonium Nitrate) and other additives was selected at this point. This gave the density and mass of the propellant, such that the total motor size and mass could be calculated. A finocyl geometry was used for the lower stage motor and an aft finocyl configuration for the upper stage motor. These were designed to give approximately neutral thrust profiles.

A proposal for a backup propellant formulation was also made. This backup propellant formulation is less experimental than the ADN formulation, and emits significantly less hydrogen chloride than ordinary Ammmonium Perchlorate Composite Propellant propellants, but fails to entirely eliminate hydrogen chloride from the exhaust products and therefore is less desirable.

The casing of the motor is made of aluminium 6082, as this is a lightweight and effective solution that can also resist saltwater corrosion. A paper phenolic liner protects the casing from the heat of combustion. The nozzle of both stages is a three-part aluminium-phenolic-graphite construction, in line with the current industry state of the art. Ignition of the propellant is from the nozzle side for the first stage, triggered by the ground equipment. The second stage uses a head-end ignition system to air-start the motor at an altitude of around 10 km.

For the rocket to remain stable in flight, the centre of mass of the rocket must remain in front of the centre of pressure. Fins are used to shift the centre of pressure aft. Furthermore, the fins induce a spin in the rocket, giving it gyroscopic stability. The fins have been sized to prevent aeroelastic flutter. This phenomenon will break up the rocket if the fins are not made strong enough. After the fins have spun up the rocket, it will have to be de-spun, to allow the payload to take high-quality measurements. This is achieved with a yo-yo de-spin device. When a true microgravity environment is needed, any residual rotation will be cancelled by a reaction control wheel in an additional microgravity control module.

For the nosecone, a Haack series is chosen. This minimises the drag from the nosecone in the transonic and supersonic regimes. More analysis is needed to make sure that the nose cone can handle the thermal loads. The body tube carries the loads of the rocket. A stress and buckling analysis have been performed, both of which gave a very small minimum thickness of the skin. To make the tube manufacturable, a thickness of 1 mm has been chosen. The shoulder of the first stage has been sized to also include the first stage recovery section, and the vehicle is passively staged at first stage burnout by the differential drag between the first and second stages. Radial-Axial joints are used to permanently connect parts of both stages, while both motors are attached with screw threads. To ensure that the rocket can handle the conditions in which it has to operate, multiple analyses have been performed. The ground impact, vibrational environment and fatigue can all be handled by the structure. Only one resonance frequency has to be taken into account; further analysis is required to make sure the rocket can handle this.

The recovery of the rocket will be done for both stages individually. The first stage will only have a main parachute, while the second stage also includes a drogue before its main. Based on the desired landing velocity of $8\,\mathrm{m\,s^{-1}}$, the area of the parachute was sized. The first stage has a cross shape parachute, while the second stage has an annular

main and a ribbon hemisflo drogue. The deployment altitudes were selected based on the simulations made in OpenRocket. With this acceleration and the shock load factor, the loads on deployment were calculated and sized. The deployment will be done with the use of a Cold Gas Deployment Device for both stages.

Two systems are used to store the flight data: a flight recorder, and telemetry. This makes the data recovery redundant. Both stages have two fully-redundant avionics stacks, for improved reliability. Cameras are added on both stages to give video data to confirm that all the necessary functions in flight are carried out correctly. The telemetry ground systems of Esrange are used, which sets standards for all the data transmission on board the vehicle. Power is provided to the vehicle by Lithium-Polymer batteries.

For all the subsystems designed in this chapter, cost and mass budgets were made. The budgets will be tracked and updated over the further design process. The margins on the budgets will continue to decrease as the design converges to its final production configuration.

Quality Assessment

Author: D. Norbart
Editors: C. Kendall, M. Rusch

An important aspect of Quality Assessment is checking if the preliminary design complies with requirements. However, due to the maturity of the design in combination with the detail of some requirements, it is not possible to check compliance with all of them. For this reason, the Compliance Matrix, shown in Table 9.1, features 'Indend to Comply' for these detailed requirements. A verification plan for compliance with these will have to be developed in the next phase of the project.

To trust the output of the design software, it needs to be verified and validated. A large number of unit tests were performed, all of which were passed by the code. The individual sub-system modules underwent system tests. Finally, the whole system was tested for sensitivity to the input values. The code also passed these tests by converging to similar results on a range of inputs. All verification tests are therefore passed.

Validation more complex as rocket data is not widely available. The program was therefore compared to OpenRocket, which is independently validated already. It was found that the in-house simulation calculates too much drag compared to OpenRocket. The same conclusion was drawn after comparing the T-Minus DART data to the simulation; the simulated drag was approximately double that of the actual vehicle. Further validation and tuning should be done in the drag calculations of the simulation tool in the upcoming design stages.

Vehicle Overview

Author: D. Norbart
Editors: E. Chen, C. Kendall

Figure 1 shows a render of the preliminary Altus vehicle that has been designed. It is capable of flying a 12 kg payload to an altitude of 110 km. Furthermore Table 1 and Table 2 give an overview of the size, mass, and velocities of the vehicle. More details can be found in Chapter 11.

Figure 1: A render of the preliminary vehicle

Table 1: Vehicle Size Characteristics

Parameter	Value
Total length	6.23 m
Booster length	2.59 m
Sustainer length	3.64 m
Booster outer diameter	0.2 m
Sustainer outer diameter	0.15 m

Parameter	Value
Total mass	157.96 kg
Total dry mass	62.46 kg
Booster mass	90.95 kg
Booster dry mass	26.95 kg
Sustainer mass	67.01 kg
Sustainer dry mass	35.51 kg

Subsystem	Value
Payload	12 kg
Propulsion	125 kg
Stability	7.07 kg
Structure	7.22 kg
Recovery	1.83 kg
Avionics	4.83 kg

Table 2: Main vehicle flight parameters influencing the aerodynamics

	Combined stage	Stage 2
Max velocity [m/s]	578.00	1525.90
Max acceleration [g]	4.94	19.27
Max dynamic pressure [pa]	125299.43	126926.31
Max Mach number [-]	1.80	5.17

Operational Assessment

Author: D. Norbart

Editors: E. Chen, C. Kendall

The payload will be manufactured, tested, and calibrated by an external contractor. Manufacturing and casting will take place in the Netherlands, while the raw materials will be sourced from the European Union (EU) as much as possible. As the flights will happen in Sweden, transportation of the rockets and the propellant is needed. Especially when transporting propellants, careful consideration of the legal requirements and logistics is required.

Using satellites and ground-based observations, the Polar Mesospheric Clouds will be monitored. Around once every week, when the PMCs are present, the rocket will be launched. During flight, telemetry data will be transmitted and the rocket will be tracked from the ground. This aids with vehicle recovery. When the rocket is brought back to base, the data is extracted and stored for scientific research. Additionally, particles from the sample collection system are extracted and stored. All rockets are brought back to the Netherlands at the end of the summer for refurbishment. To ensure that the cost is kept within the budget, it is split into different factors, which have been given estimates. Labour and launch site costs will be significant expenses. As the rockets will be used multiple times, the physical cost of the vehicles is not very significant. In total, it is concluded that the budget is within the allocated margins.

Sustainable Rocketry Industry Proposal

To be able to make a fair assessment of the sustainability improvement that the Altus vehicle will bring, a baseline is needed. For this, the environmental effect of current launchers needs to be assessed. A large number of orbital launchers use solid rocket motors, which nearly always consume APCP. The hydrogen chloride produced by these motors is linked to acid rain in the regions surrounding rocket launches, as well as fish killings and damage to vegetation around launch sites. The ozone layer is also negatively impacted by solid rocket motors. In the production of these motors, there is also a human safety hazard present, as there is an increasing body of evidence linking Ammonium Perchlorate to a decreased performance of the endocrine system.

The EU has started a program called GReen Advanced Space Propulsion (GRASP), which involves 11 research parties that together establish performance and hazard characteristics of a range of propellants. GRASP however, focuses on liquid propellants. Therefore, a new consortium is proposed with the focus solely on solid rockets, with the aim to move away from APCP.

Contents

Acronyms and abbreviations

6DOF Six Degrees Of Freedom.

ADCS Attitude Determination and Control System.

ADN Ammonium DiNitramide.

ADR Accord relatif au transport international des marchandises Dangereuses par Route.

AHP Analytic Hierarchy Process.

AN Ammonium Nitrate.

AP Ammonium Perchlorate.

APCP Ammmonium Perchlorate Composite Propellant.

BMS Battery Management System.

CAN Controller Area Network.

CGAA Cape Grim Air Archive.

CGDD Cold Gas Deployment Device.

College van B&W College van Burgemeester en Wethouders.

CRM Continuous Risk Management.

DAPMT Dual Absolute Pressure Measuring Transducer.

DBP DiButyl Pthalate.

DOA DiOctyl Adipate.

DOD depth of discharge.

DSE Design Synthesis Exercise.

ERC European Research Council.

ESA European Space Agency.

EU European Union.

EUC End-User Certificate.

FBS Functional Breakdown Structure.

FFD Functional Flow Diagram.

FTS Flight Termination System.

GNSS Global Navigation Satellite System.

GRASP GReen Advanced Space Propulsion.

HGDD Hot Gas Deployment Device.

HTPB Hydroxyl-Terminated PolyButadiene.

IenW Infrastructuur en Waterstaat.

ILT Inspectie Leefomgeving en Transport.

IMU Inertial Measurement Unit.

ISA International Standard Atmosphere.

LiPo Lithium-Polymer.

MAI Manufacturing, Assembly, and Integration.

MDI Methylene Diphenyl diIsocyanate.

MEOP Maximum Expected Operating Pressure.

NASA (United States) National Aeronautics and Space Administration.

NSF National Science Foundation.

NWO Nederlandse organisatie voor Wetenschappelijk Onderzoek.

P-POD Poly Picosatellite Orbital Deployer.

PD&DL Project Design & Development Logic.

PDD Project Design and Development Logic.

PMC Polar Mesospheric Cloud.

Radax Radial-Axial.

RBF Remove Before Flight.

REACH Registration, Evaluation, Authorisation and restriction of CHemicals.

REXUS Rocket EXperiments for University Students.

RF Radio-Frequency.

RTV Room Temperature Vulcanising.

SNR Signal-to-Noise Ratio.

SRB Solid Rocket Booster.

SRM Solid Rocket Motor.

TRL Technology Readiness Level.

TVC Thrust Vector Control.

UN United Nations.

UV Ultra Violet.

WHO World Health Organization.

ZARM Zentrum für Angewandte Raumfahrttechnologie und Mikrogravitation.

Symbols

A	Area	[m^2]
a_{pres}	Pressure coefficient	[-]
a	Speed of sound	[$m\,s^{-1}$]
A_x	Area of x	[m^2]
AR	Fin aspect ratio	[-]
B	Bandwidth	[MHz]
b_x	Fin semi-span of x	[m]
$\bar{c}$	Mean aerodynamic chord	[m]
c^*	Characteristic Velocity	[$m\,s^{-1}$]
C_{D_x}	Drag coefficient of x	[-]
C_r	Fin root chord	[m]
C_t	Fin tip chord	[m]
C_{fr}	Frictional drag coefficient	[-]
C_{fr_c}	Drag coefficient with compressibility correction	[-]
C_{L_α}	Lift coefficient slope	[rad^{-1}]
C_{N_α}	Normal force coefficient slope	[rad^{-1}]
$C_{X_{max}}$	Parachute shock load factor	[-]
cc	Specific impulse correction factor	[-]
D_x	Diameter of x	[m]
d_x	Diameter of x	[m]
d_{rocket}	Transmission distance	[m]
dod	Depth of discharge	[%]
E	Youngs modulus	[MPa]
F_x	Force of x	[N]
f_B	Body fineness ratio	[-]
f_{nc}	Nosecone fineness ratio	[-]
f	Frequency	[Hz]
f_c	Carrier frequency	[GHz]
g	Gravitational acceleration	[$m\,s^{-2}$]
G	Shear modulus	[MPa]
G/T	Ground station antenna noise ratio	[$dB\,K^{-1}$]
G_{Rx}	Receiver antenna gain	[dB]
G_{Tx}	Transmission gain	[dB]
h	Altitude	[m]
I	Mass moment of inertia	[$kg\,m^2$]
I_t	Total impulse	[N s]
I_{sp}	Specific impulse	[s]
L	Length	[m]
L_x	Length of x	[m]
L_{FS}	Free space path loss	[dB]
l_{tower}	Launch tower length	[m]
M	Mach number	[-]
m	Mass	[kg]
M_E	Mass of the Earth	[kg]
$M_{propellant}$	Propellant mass	[kg]
m_{rocket}	Mass of the rocket	[kg]
$\dot{m}$	Mass flow rate	[$kg\,s^{-1}$]
n_{mol}	Number of moles	[mol]
n	Integer	[-]
n_{pres}	Pressure exponent	[-]
P	Pressure	[MPa]
P_C	Combustion pressure	[MPa]
P_{Rx}	Received power	[W]
P_{sensor}	Sensor power	[W]
$P_{telemetry}$	Telemetry power	[W]
P_{Tx}	Transmission power	[MHz]
P_{yield}	Yield pressure	[MPa]
q	Dynamic pressure	[Pa]
r	Radius	[m]
R_{data}	Data rate	[$Mbit\,s^{-1}$]
R_{air}	Specific gas constant of air	[$J\,kg^{-1}\,K^{-1}$]
R	Universal gas constant	[$J\,K^{-1}\,mol^{-1}$]
R_E	Radius of the Earth	[m]
Re_{crit}	Critical Reynolds number	[-]
R_s	Surface roughness	[µm]
S_0	Nominal parachute surface area	[m^2]
S_x	Surface area of x	[m^2]
SF	Safety factor	[-]
t	Thickness	[m]
t_{bat}	Battery duration	[hrs]
T	Temperature	[K]
v	Velocity	[$m\,s^{-1}$]
v_e	Equilibrium velocity	[$m\,s^{-1}$]
v_R	Rocket velocity	[$m\,s^{-1}$]
v_{tower}	Launch tower exit velocity	[$m\,s^{-1}$]
Δv	Ideal change in velocity	[$m\,s^{-1}$]
V_x	Volume of x	[m^3]
V_l	Volumetric loading	[-]
V_{avg}	Average Voltage	[V]
x_{CG}	Centre of gravity location	[m]
x_{CP}	Centre of pressure location	[m]
x_{crit}	Laminar transition location	[m]
β	Subsonic mach correction factor	[-]
η	Antenna efficiency	[-]
γ	Heat capacity ratio	[-]
Γ_{LE}	Leading edge slant angle	[°]
Λ	Mid-chord sweep angle	[°]
ρ	Density	[$kg\,m^{-3}$]
σ	Stress	[MPa]
σ_y	Yield strength	[MPa]
σ_{ts}	Ultimate tensile stress	[MPa]
ε	Unit test margin	[-]
ϵ	Strain	[-]
ϕ	Nosecone angular profile	[°]
λ	Taper ratio	[-]

1 Introduction

Authors: C. Kendall, M. Rusch

Rocket vehicles, although flying far less regularly than commercial or civilian aviation, have a disproportionately large impact on the environment. In the past, this has been regarded as inevitable, as performance requirements have been considered far more important than those of protecting the environment. This has led to extensive use of hydrazine, nitric acid, and Ammonium Perchlorate (AP), as well as expendable launch vehicles. With the development of more sustainable alternatives to hydrazine and nitric acid, such as GReen Advanced Space Propulsion (GRASP), and a focus on vehicle reusability as the wider industry responds to SpaceX, many of these harmful materials and practices are either resolved or in the process of being phased out. However, the state-of-the-art in solid rocket propulsion, in terms of propellant formulation, has remained effectively the same since 1969, when Hydroxyl-Terminated PolyButadiene (HTPB) was first introduced as a binder [1]. The Altus project aims to catalyse an industry shift by demonstrating and validating the use of an Ammonium DiNitramide (ADN) and Ammonium Nitrate (AN)-based propellant, and a full-vehicle recovery system.

The initial demonstration mission, and the case for which the vehicle is sized, is an aeronomy mission to study Polar Mesospheric Clouds (PMCs). These clouds form in the upper regions of the atmosphere, above 80 km, and are largely formed of water ice. In recent years, the number of these clouds has been increasing, and they have been observed at increasingly lower latitudes. This is thought to be linked to the effects of global warming, and therefore studying PMCs is a priority for climate research.

Further to this primary mission, it is intended for the Altus vehicle to act as a general-purpose sounding rocket for aeronomy, microgravity and space research payloads. Since a two-stage design has been chosen, it is relatively trivial to substitute a larger booster as the first stage. This potentially allows the apogee of the flight to be raised to 200 km or higher, allowing microgravity research with the addition of a micro-gravity control module (reaction wheel(s)/control moment gyroscope for attitude control).

In Chapter 2 the project goals, timeline, and scientific relevance are outlined, afterwards in Chapter 3, the technological relevance and market analysis are discussed. Chapter 4 explores the post-Design Synthesis Exercise (DSE) phases of the project, together with the functionality of the system and its sustainability. Subsequently, Chapter 5 outlines the stakeholder and system requirements and Chapter 6 discusses the risk assessment and proposes a risk management strategy for future project phases. Chapter 7 gives an overview of the trade-off between concepts and Chapter 8 expands this concept into a preliminary vehicle design. In Chapter 9, compliance of this design to the requirements is assessed and verification and validation is performed on the design and simulation tools used in the process. Chapter 10 explores the functions and interfaces of the various sub-systems in more detail. Next Chapter 11 outlines the performance of the vehicle, also in the realm of sustainability. In Chapter 12, the Manufacturing, Assembly, and Integration (MAI) plan and the operational and logistical concept are presented together with the cost budget for the entire mission. Finally, Chapter 13 aims to provide a solution to the large environmental impact of the rocketry industry at large. This report will be closed with a conclusion and recommendations in Chapter 14 and Chapter 15, respectively.

2
Altus Mission

The mission defines the goal of the project and when it is deemed successful. It is therefore essential to define the mission clearly and to set concise, achievable goals for the project. Furthermore, it is important to determine the relevance of the mission in case the desired research has already been performed. The goal of this chapter is to describe the mission and its goals, milestones, and life cycle.

In this chapter the project objective, which includes the scientific objective, the technological objective, and the mission need statement, is described in Section 2.1. In Section 2.2, the scientific relevance of the mission is described and examples of a similar project are provided. The most important mission milestones of the project are described in Section 2.3. This is followed by the payload description and the reasoning for the chosen payload in Section 2.4. Finally, the project life cycle including the various phases and milestones of the project are described in Section 2.5.

2.1. Project Objectives

Author: L. Tabaksblat
Editor: C. Kendall

The project objective is divided into three parts. The first part is defining the scientific mission in terms of the quantities measured, and the aim of the research. The second part defines the technological objectives, and how they are relevant to the mission. Finally, the third part combines both the scientific mission and the technological objectives into a comprehensive mission need statement.

2.1.1. Scientific Objective

PMCs are a rare form of cloud that form only in the upper mesosphere. These clouds appear for 60 to 80 days of the year, in the summer, as the mesospheric temperature is sufficiently low for the clouds to form only during this period [2]. Researchers are interested in investigating PMCs, as it is currently believed that they may be an indication of climate change [3]. There have been changes observed recently in cloud brightness [4], frequency of appearance [5], and in location [6]. In the past, PMCs only formed in the range from 50° to 65° north and south. However, the clouds have recently been observed as low as 41.7° north [7]. There is, therefore, a desire to research these phenomena.

PMCs need three conditions to form. The first condition is a water vapour density of at least 4 partspermillionvolume to 5 ppmv for visible clouds [8], as the clouds cannot form if there is too little water. The second condition is a temperature below around $-120\,^{\circ}\mathrm{C}$; as the pressure in the mesosphere is extremely low, the freezing point of water also becomes extremely low. As the Polar Mesospheric Clouds are ice clouds, this is an essential factor. The final requirement is a nucleation point around which the ice particles can form. These are usually dust particles, which are currently thought to come from the vaporisation of meteorites in the upper atmosphere [9].

There are two leading theories with regard to linking climate change to the change in cloud behaviour. The first is driven by an increase in methane in the mesosphere. This methane then oxidises, turning into water. As the water vapour density increases, the probability of Polar Mesospheric Clouds forming also increases. This would also explain the increase in brightness of PMCs [10]. The second theory is that an increase in the concentration of CO_2, which is known to cool the middle atmosphere, is leading to a larger area of the mesosphere being cold enough for Polar Mesospheric Clouds to form. This would also explain the appearance of PMCs at lower latitudes

[3]. Furthermore, both of these theories could be influencing PMCs behaviour at the same time.

Although there have already been a large number of Polar Mesospheric Cloud observations performed by satellites such as AIM [11], there are still problems establishing the statistical significance of the current data. As stated by Plane et al. (2023) [12]: "Trends in the cloud brightness and cloud ice water content have been deduced from satellite observations (e.g., [4]), but the statistical significance of these trends remains limited". There is a lack of long-term data that spans multiple solar cycles, as the monitoring of Polar Mesospheric Clouds using satellites is a relatively recent development. Furthermore, there are a lot of factors limiting the usefulness of visual reports created in the past [13].

The solar radiation cycle has a large influence on the frequency of appearance of Polar Mesospheric Clouds. This is because an increase in Ultra Violet (UV)-radiation hitting the mesosphere leads to more water being broken down and therefore a decrease in the water vapour density. This then affects the frequency of appearance of Polar Mesospheric Clouds [14]. However, a new study of the data recorded by AIM found no dependency on the solar radiation cycle [15]. The UV-radiation also changes with solar sidereal rotation (the rotation of the sun about its own axis). This cycle lasts 27 days, during which the number of sunspots visible will vary. Therefore the amount of UV-radiation the mesosphere is exposed to will also change. This connection is further supported by the fact that a 27-day signature has been detected in Polar Mesospheric Cloud frequency [16, 17].

Project Altus has therefore decided to launch for 26 years, 8 times a year during the summer in Esrange. The reason 26 years was chosen is to eliminate the influence of the aforementioned solar radiation cycle on the data, due to its influence on temperature and water vapour density in the mesosphere. To be able to remove this effect from the equation, measurements will be made over two solar cycles. Although a solar cycle on average lasts 11 years, they are known to vary in length significantly. For this reason, the longest two consecutive solar cycles over the last 200 years were calculated and this was decided upon to be the duration of the mission [18].[1] The reasoning for the 8 days is similar to the 26 days, removing the influence of the 27-day cycle on the data by measuring over 2 cycles. This leads to 4 days per cycle, which is done for the sake of redundancy and averaging. This leads to a total of 208 launches over the duration of the mission. Since each vehicle is supposed to be used a minimum of ten times at least 20.8 vehicles are needed. This is rounded up to 22 vehicles in order to have a spare vehicle that can be lost.

2.1.2. Technological Objectives

Because of the requirements of the customer to use a sustainable vehicle, a new vehicle is required, as there are currently no vehicles commercially available that meet all of the requirements. During the initial phase of project Altus, the slow pace of progress within the general launch vehicle industry towards more sustainable alternatives was noted. This is partially due to the reliability and ease of use of technologies currently standardised within the industry, and partially due to the high risk of orbital rockets being designed with technologies that have not been tested on a commercial scale (i.e. it is an unacceptable commercial risk to design orbital launch vehicles around technologies with low Technology Readiness Levels (TRLs)).

For this reason, a secondary objective has been created: to create a technology demonstrator for sustainable technologies, capable of being scaled up for use orbital launch vehicles. To achieve this, it is necessary not only to develop the technologies themselves but also the surrounding logistics and operations. The goal is to push the industry, as a whole, towards a more sustainable approach to rocketry as the cadence of orbital launches continues to increase in the future [19].

[1] `https://www.sws.bom.gov.au/Educational/2/3/7`[11-05-2023]

2.1.3. Mission Need Statement

As there is both a scientific mission and a technological objective, the mission need statement must reflect both goals. The scientific mission will be used to demonstrate the reliability of the sustainable technologies used and to measure the anthropogenic impact on the mesosphere. The mission need statement is:

Catalyse a shift towards sustainable rocketry by means of a polar mesospheric cloud research mission, demonstrating technologies that can be applied to reduce the environmental impact of rockets.

2.1.4. Project Objective Statement

The scientific mission and technological objective also need to be reflected in the objective of the mission. The project objective statement needs to reflect on both these goals and the mission timeline. The scientific objective is to gather data on the clouds and this will be done with a sustainable vehicle. Thus, the project objective statement is:

Demonstrate by means of an in situ investigation of Polar Mesospheric Clouds, a cost-competitive rocket utilising sustainable technologies by 10 students in 10 weeks.

2.2. Scientific Relevance of the Mission

Authors: L. Tabaksblat, D. Norbart
Editor: C. Kendall

As stated in Section 2.1.1, there is a lack of long-term data to support current theories on the cause of change in cloud behaviour [12]. Specifically, proving the theory that Polar Mesospheric Clouds behaviour has been changing due to climate change and not due to natural processes in the mesosphere has, thus far, been impossible. The only way to draw more definitive conclusions is by removing confounding variables by measuring the same characteristics under different conditions, and over a period of several years. For this reason, a long-term database of PMC data must be set up. This long-term database will measure several important atmospheric properties, connected to the conditions necessary for PMCs to form, as discussed in Section 2.1.1.

However, with only these measurements it is still impossible to answer several important research questions surrounding PMCs. For example, the exact origin and composition of the nucleus of PMC ice particles is still not definitively established [20, 9]. Furthermore, the radar reflectivity of these clouds, predicted to come from a sodium-iron coating, is also an area of interest [21]. To give a definitive answer to these questions, a thorough analysis of the cloud particles is necessary. This is not possible to achieve on a sounding rocket in situ. Large machines such as electron microscopes and mass spectrometers are necessary for a full analysis, as well as the analysis requiring more time than is possible to achieve with a sounding rocket vehicle. Therefore, it is necessary that a sample of Polar Mesospheric Cloud particles is returned by every flight.

Long-term atmospheric databases are very useful for the scientific community. A good example of this is the Cape Grim Air Archive (CGAA). The CGAA collects 4 to 6 high-pressure air cylinders per year and has been doing so since 1978 [22]. There have already been over a hundred articles written based on the data collected from sample analysis. This type of database helps with detecting small and long-term changes [23]. The samples also allow for reanalysis in case of doubt or conflict theories [24]. It is, for these reasons, extremely useful to build a database of measurements and samples.

Another reason to do long-term research is connected to the secondary goal of producing a technology demonstrator for sustainability. This is the suspected correlation between rocket launches and an increase in frequency of appearance of Polar Mesospheric Clouds and their appearance at lower latitudes.[2] As rocketry is a growing industry, it is important to monitor the environmental impact it has. This is where the scientific data collected by the mission can be used to monitor the increase in water vapour density in the mesosphere potentially caused by rocketry.

[2] https://www.nasa.gov/feature/goddard/2022/sun/rocket-launches-can-create-night-shining-clouds-away-from-poles-nasa-aim-mission [15/06/2023]

2.3. Mission Milestones

Author: L. Tabaksblat
Editor: C. Kendall

The goal of project Altus is to complete both a scientific mission and to act as a small-scale technology demonstrator for a more sustainable propellant and full vehicle reusability, as mentioned in Section 2.1.3. As the timeline for the technology demonstrator is a lot shorter than the timeline for the scientific mission, it is useful to place milestones to evaluate the current state of the mission. Furthermore, as the scientific mission takes 26 years, a lot can change with regard to both current technology and the needs of the scientific community. Two main milestones are therefore proposed.

The first major milestone is set after the rocket has been launched at least ten times without failure. At that point, around 2 years will have passed since the start of the mission. The goal of the milestone is to evaluate whether the reliability of the technology demonstrator has been proven; Technology Readiness Level (TRL) 6 will need to be reached such that orbital-scale rockets can start using the technology. The main things to be evaluated are the logistics and operations of the propellant, the reliability of the propellant, and the ease of scalability. In case the TRL is not deemed sufficient for larger-scale rocketry further development will need to be performed. At this point, sufficient confidence in the rocket is reached such that commercial customers can start flying on the Altus vehicle.

The second milestone is after the completion of a full set of measurements from the first solar cycle of the mission. At this point, a large set of data measurements will have been collected and presented to the scientific community. The goal of the milestone is to evaluate the needs of the scientific community and the state of the rocket compared to the current state of the art. If the scientific community has no further need for data and the rocket is competitive with other contemporary vehicles, then the project will be fully converted to a commercial launcher. Otherwise, upgrades will be made to continue to be competitive in the market. However, if there is a need for more data, then the project will continue to finish its full mission of two complete solar cycles.

2.4. Payload Description

Author: L. Tabaksblat
Editor: C. Kendall

The chance of PMCs appearing is determined by three conditions. These conditions are the water vapour density, temperature, and a nucleation point. For this reason, the water vapour density and temperature will be measured. Additionally, pressure is useful to measure as this affects the sublimation point and relates the water vapour density to the absolute water content and humidity. To measure the final requirement for PMC formation, a sampling mechanism will be implemented, which captures nucleus samples of the cloud to analyse later.

As the goal of the instrumentation is to measure the characteristics of the mesosphere, the sensors need to be able to measure a relevant range. The temperature sensor should be able to measure a range of 90 K to 300 K [2]. Similarly, the hygrometer should be able to measure a range of 0.1 ppmv to 20 ppmv [25]. Finally, the pressure sensor should be able to measure a range of 0.0001 Torr to 0.1 Torr [26]. The sensors selected to achieve these goals are detailed in Section 8.3.

2.5. Project Life Cycle

Author: L. Alonso
Editor: C. Kendall

The project life cycle consists of various different phases, as shown in Figure 2.1. The DSE consists of the following phases: project definition, concept generation and selection, as well as the preliminary design phase. These will be further discussed in this report. Additionally, all post-DSE phases are discussed in Section 4.1.

For each phase in the project life cycle, it is necessary to incorporate reviews and reports to track and assess the team's progress. Most of the reviews act as gates that only open up the next phase when the review is successful. This allows for effective and efficient use of time and resources while advancing through various quality assessments. The abbreviations of the review names are taken from literature [27, p. 18]. The customised list of reviews and

reports for this project are summarised below:

- Mission Concept Review: A mission proposal document is formulated which affirms the need of the mission.
- Project Plan: A report including the team's approach to the technical and management aspects of the DSE, with the use of Work-Flow diagrams and a Gantt Chart.
- Baseline Report A report including top-level requirement analysis, a Functional Flow Diagram (FFD) and Functional Breakdown Structure (FBS), and design option trees.
- Baseline Review: A formal briefing on the planning phase and the technical requirements.
- Mid-term Report: A report including the results of the analysis and design activities leading to a selected concept that meets requirements.
- Mid-term Review: A formal briefing on the progress of the Mid-term Report.
- Final Report: This report, also known as the preliminary design report.
- Preliminary Design Review or Final Report - A complete and formal briefing including a summary on the development process and results up until the Mid-term Review, followed by the details and design justifications of the final concept that complies with the requirements.
- Production Readiness Review: It is a review of the product to ensure that the production phase can begin.
- Flight Readiness Review: This is a review to determine the system readiness for launch.
- Decommissioning Review: This review confirms the decision to stop the mission. It makes sure that the project is ended in the correct manner.

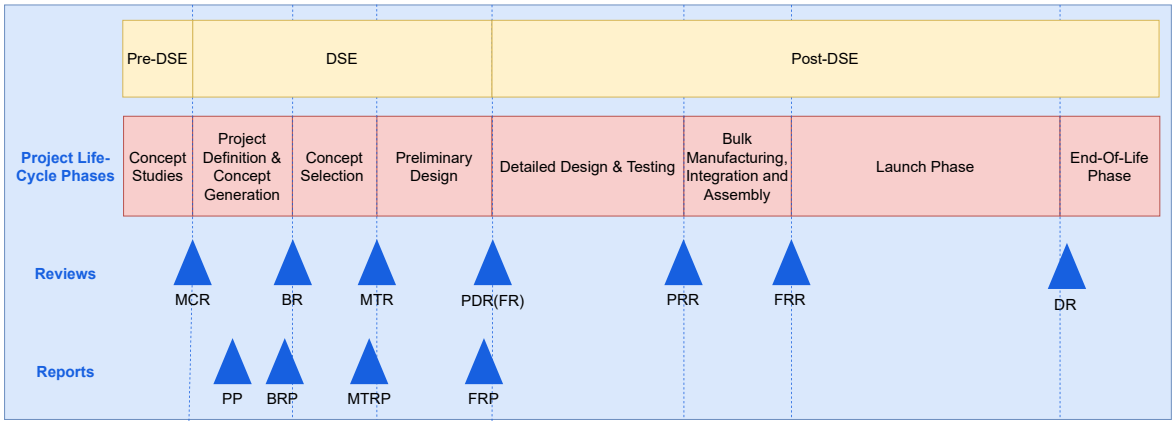

Figure 2.1: Project life cycle showing time of reviews and report deadlines

3
Technology Assessment

3.1. Technological Relevance of the Mission

Author: D. Norbart
Editor: C. Kendall

Further to collecting data on the Polar Mesospheric Clouds, the vehicle is also a technology demonstrator. With this development program, a new type of propellant for civilian rocket vehicles is being investigated. ADN-based propellants are still in their infancy (having been developed in the Soviet Union in 1971, and independently discovered in the west in 1989).[3] This low technology readiness level is a major reason why launch vehicle corporations are not using ADN over Ammmonium Perchlorate Composite Propellant (APCP) [28]. ADN is, however, better for the environment than APCP, as it does not produce hydrogen chloride. Hydrogen chloride in rocket propellant exhausts has been linked to fish killings [29], and to damage to the ozone layer [19]. For orbital rockets to switch from APCP to ADN as the primary solid oxidiser, the TRL must be sufficient and the performance penalty must be marginal. The technology will get closer to these thresholds when developed for the Altus sounding rocket.

ADN is currently not produced in large quantities, which greatly increases costs. Further to the low TRL, it is economically unfeasible to buy ADN for orbital vehicles at current prices, further preventing the implementation of this propellant in civil rocketry. In comparison, the overall costs of the Altus mission are dominated by launch site costs and so, as a fraction of overall operating costs, the increased expense of using a more costly propellant is marginal. By choosing this propellant, the Altus sounding rocket serves as a technology demonstrator. If larger companies, like Arianespace, switch to ADN, a far greater positive environmental impact can be made than the Altus mission ever could in isolation. With the Altus mission, 4.2×10^6 kg of propellant will be used in 26 years. A single Ariane 5 has 475 600 kg of a APCP propellant,[4] and has launched 115 times in the last 26 years.[5] Many other orbital vehicles also use ammonium perchlorate propellants, including the Space Launch System, Atlas V, and Delta IV.[6] To this day, orbital rockets are being developed that use APCP, including Europe's new Ariane 6 and Vega rockets.[7]

3.2. Market Analysis

In order to investigate the market for the scientific research and technologies involved with the mission, a market analysis is performed. Section 3.2.1 describes the specific organisations performing PMC research. Section 3.2.2 outlines the various use cases for sounding rockets that are possible and the market opportunities that exist for Altus.

3.2.1. Stakeholders for the PMC Data

Author: D. Norbart
Editor: C. Kendall

In the United States, the National Science Foundation (NSF) is responsible for the distribution of funding. The European Union (EU) has an equivalent, the European Research Council (ERC). The NSF has allocated $3.67MM

[3] https://web.archive.org/web/20120526005446/http://www.sri.com/psd/research/adn.html [09/06/2023]
[4] https://www.arianespace.com/vehicle/ariane-5/ [09/06/2023]
[5] https://en.wikipedia.org/wiki/Ariane_5 [09/06/2023]
[6] https://en.wikipedia.org/wiki/Solid-propellant_rocket [09/06/2023]
[7] https://en.wikipedia.org/wiki/P120_(rocket_stage) [09/06/2023]

to pure PMC research since 2008. Furthermore, $2.21MM was allocated to research where PMCs were one of the research topics. The total budget allocated to the NSF in this period was $111.2B.[8] The NSF states that they support 24% of all federally funded research at academic institutions [30]. With the assumption that this NSF money is one fourth of the available grants for PMC research in the United States, that would mean that around $1.57MM is available per year. This would result in a total of $40.8MM allocated over the mission duration of 26 years, which would be sufficient to provide €35MM for the entire Altus mission. It is, however, inconceivable that (nearly) all funds available for this research area would be funnelled to a single project.

The ERC has supported one project in which PMCs were one of the topics, which was granted €2.48MM. The EU is organised less federally than the United States. The individual countries in the EU also have substantial national research funding organisations. In the Netherlands, for example, the Nederlandse organisatie voor Wetenschappelijk Onderzoek (NWO) has an annual budget of around €1B [31]. With all of these institutions combined, enough funds are dedicated to Polar Mesospheric Cloud research to fund the mission already. Furthermore, there examples of funds being directed to big projects that try to answer great questions, like telescopes and particle accelerators. The (United States) National Aeronautics and Space Administration (NASA) AIM satellite, which studies PMCs, cost a total of $140MM, but remains an unusual one-time investment [11]. It remains a question however if there exists enough interest in this specific type of PMC data to justify the spending of €35MM on the Altus mission. This is mainly a political question, but based on this analysis, the answer is expected to be positive.

3.2.2. Market Opportunities for Sounding Rockets

Author: M. Rusch

Editor: C. Kendall

Historically, sounding rockets have had various use cases. According to NASA, sounding rockets have been used in the following fields of science: Atmospheric Science, Auroral Science, Astrophysics, Geo-science, Solar Physics, and Micro-Gravity research.[9] Sounding rockets can also serve as a proving ground for new space technologies. Prototypes for instrumentation and other technologies can for example be flight tested prior to their deployment in orbit. NASA conducts around 20 sounding rocket flights per year for these purposes – these carry payloads provided by NASA itself, research institutes, universities, and students. It should be noted, when considering this segment of the market, that the payload masses often exceed 100 kg and typical apogees are in the range of 200 km to 1400 km. This is especially the case for auroral science, astrophysics, geo-science, and solar physics payloads.[10] These types of missions are, therefore, not possible with the Altus vehicle. However, use cases for atmospheric research and micro-gravity research can be further explored.

When investigating the micro-gravity market on the European side of the Atlantic, a more probable option is found. Micro-gravity research is an active field in Europe. The European Space Agency (ESA) performs yearly micro-gravity flight testing campaigns using aircraft;[11] 12 experiments can fly onboard this aircraft and experience approximately 30 min of micro-gravity divided over 93 parabolic manoeuvres of 22 s each. Next to this the Zentrum für Angewandte Raumfahrttechnologie und Mikrogravitation (ZARM) based in Bremen, Germany can conduct up to three experiments per day, with each experiment allowing for 9.3 s of micro-gravity.[12] When taking this into consideration, it is plausible that some use cases exist that need period of microgravity that is longer than these few seconds. An example of this is given by [32]. This group from the Technische Universität Berlin launched a CubeSat on the Rocket EXperiments for University Students (REXUS) rocket. They tested a novel Attitude Determination and Control System (ADCS) system during the approximately 120 s of micro-gravity. The Altus vehicle would be perfectly suited for missions like this, since the apogee and time in micro-gravity are comparable to REXUS. Another example is that of FloripaSat, a CubeSat developed by UFSC in Brazil [33]. This team uncovered several

[8] https://www.nsf.gov/about/congress/119/highlights/cu22.jsp [15/06/23]

[9] https://sites.wff.nasa.gov/code810/files/Sounding%20Rockets_NASA_fact_sheet.pdf [15/06/2023]

[10] https://www.atmosp.physics.utoronto.ca/~workshop/presentations_2010/Sounding%20-%20R%20Pfaff.pdf [15/06/2023]

[11] https://www.esa.int/Education/Fly_Your_Thesis/Fly_Your_Thesis2 [15/06/2023]

[12] https://www.zarm.uni-bremen.de/fileadmin/user_upload/Flyer_Fallturm_EN_digitale_Nutzung.pdf [15/06/2023]

issues with their CubeSat after a flight test on a VSB-30 Sounding Rocket, which ensured the success of their CubeSat in orbit.

It is clear from the previous information that a market for these types of tests and student experiments exists, since the REXUS programme flies 10 similar tests per annum. However, a large hurdle is the cost associated with these launches, and specifically the cost of the launch site as can be seen in the project cost budget presented in Section 12.3. In most cases these high launch costs do not create enough value to warrant investing in a launch. To drive the cost per rocket down, multiple vehicles need to be launched during the same window, since the launch site cost increases with time, not the amount of vehicles launched. This volume is only deemed feasible when the Altus rocket would be employed by the REXUS programme as a sustainable successor to the Improved Orion rocket, since organisations like ESA and the EU place a much higher value on sustainability than commercial clients.

3.2.3. Stakeholders for Technology Demonstration

Author: M. Rusch
Editor: C. Kendall

The main technology that will be demonstrated by the Altus rocket is the use of the sustainable propellants and full-vehicle recovery.

In terms of sustainable propellants, it is clear that with respect to 2050 Climate Goals of the EU and the harmful exhaust products emitted by the industry standard APCP, there is need for a sustainable alternative. It is probable that companies like Arianegroup and their subsidiary Avio, or an organisation like ESA or the EU are interested in demonstrating the operational use of these new propellants and pose it as a viable alternative for the industry standard APCP, which releases harmful hydrogen chloride into the atmosphere.

The full vehicle recovery will be an important technology to demonstrate. This will drive down the costs associated with launching rockets by a strong margin. Entities like T-Minus Engineering or Moraba that launch a lot of sounding rockets each year might be interested in demonstrating this technology.

3.2.4. Market Requirements

Author: M. Rusch
Editor: C. Kendall

Based on the market analysis performed above, two requirements arise from the market: that the rocket shall be able to accommodate a standardised payload format such that it becomes suitable for applications like REXUS, and that the sustainable propellant has to be highly performing so as to pose a viable alternative to APCP in orbital-capable launch vehicles.

4

Project Functionality Assessment

In this chapter the functionality necessary for the project to succeed is analysed. Firstly, this is achieved by investigating the post DSE phases of project Altus in Section 4.1. Afterwards, in Section 4.2.1 and Section 4.2.2, the functions that the vehicle needs to carry out, and the functions that will be performed on the vehicle are outlined. Finally in Section 4.3, the sustainability strategy for these different project phases is explained.

4.1. Project Design and Development Logic

Authors: L. Alonso, D. Norbart
Editors: M. Rusch, C. Kendall, S. Yorucu

As mentioned in Section 2.5, the DSE only covers the initial phases of the project. To fully execute the mission and achieve the goal of building a PMC database, certain steps have to be taken. First, the concept system must be designed and developed. The Project Design and Development Logic (PDD) presents the order of activities to be executed in the post-DSE phases of the project up until the operations phase, as shown in Figure 4.1.

The DSE ends with the preliminary design phase, this phase is concluded with a Final Report, or Preliminary Design Review. This means that the first post-DSE phase is detailed design. After a first iteration of the detailed design phase is performed, a prototype of each subsystem and the payload will be manufactured and tested. A few types of testing will be conducted:

- Vibration testing to ensure the payload can withstand the flight loads on the rocket.
- Vacuum testing to test the functionality of the payload in the mesosphere.
- Spin balancing of the payload to ensure minimal disturbances during flight.
- Wind tunnel testing of the parachutes and the vehicle to determine the descent speeds and to validate the aerodynamic simulations.
- Hydrostatic testing of the motor casings to ensure they can hold the necessary pressure before the hotfire (engine) test.
- Propellant characterisation, this validates the performance characteristics of the propellant that have been used to design the motor.
- Hotfire testing, in which the solid motor is attached to a static test bench, and test fired to validate the motor performance ahead of flight.
- Recovery drop testing to demonstrate that the recovery system functions properly during flight conditions.
- Communications testing to ensure that the telemetry is received by the ground station.
- Hardware/Software in the loop testing, these are tests of the avionics to ensure they function as intended.

The test data will be analysed and the results will serve as the basis of the Production Readiness Review, part of which is compliance with all the requirements. When the Production Readiness Review has a negative outcome, the design is iterated and testing conducted once more. In case of a positive Production Readiness Review, testing will move to dress rehearsals, meaning that the vehicle is completely integrated and the entire launch is practised without actually launching. After the dress rehearsals, the Flight Readiness takes place. In case of a negative outcome, the design is once more iterated on the necessary points. If positive, the project moves to a test flight. If the test flight is

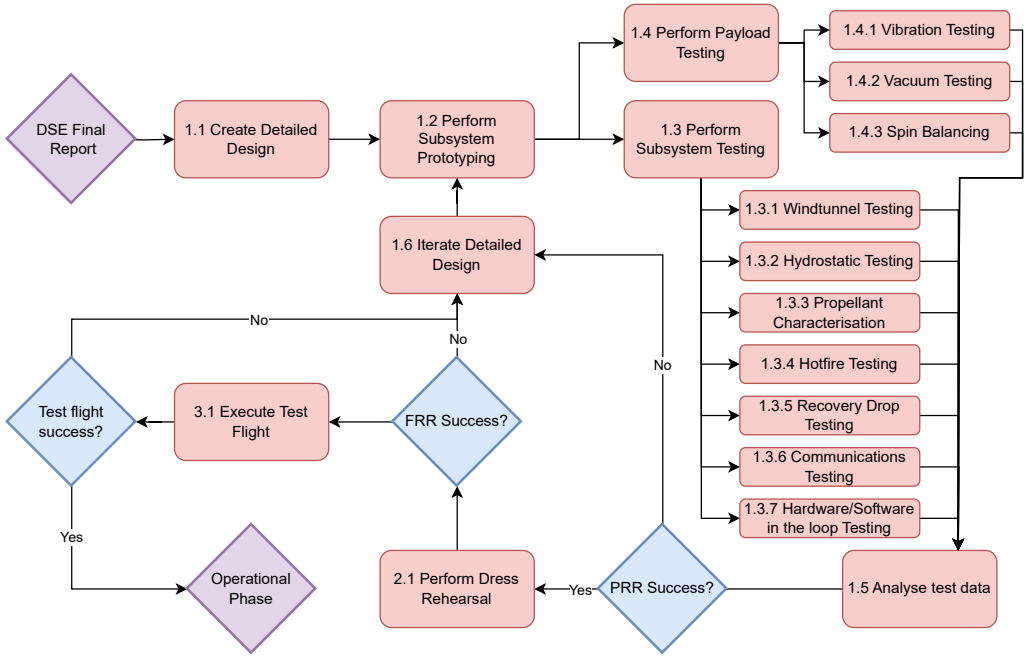

Figure 4.1: Design and development logic of project Altus

not a success, then the detailed design is iterated again. If the full flight test is a success, then the project can move on to the operational phase, further detailed in Chapter 12.

These phases have been compiled in a Gantt chart shown in Figure 4.2. The stakeholder requirement STK-MR-08 places a constraint on the start of the operational phase of the mission. This first operational flight will be in 2026, thus the first launch is scheduled, ten days before the summer solstice on 11/06/2026. Since the PMCs only appear during the summer, and by taking into account the launch cadence and relative appearance, the set launch date makes sense. With this launch date laid down, the intermittent steps can be allocated time windows. Before the operational phase, the vehicles need to be manufactured; for this process, a period of 10 months before the first operational flight is reserved. Manufacturing will begin after the success of the test flight. The month before manufacturing is taken for this test launch. Preceding the test launch, dress rehearsals will be performed to test out the procedures and the subsystem interfaces. Time is also needed to produce the hardware necessary for this phase, and in total two months are allocated for this.

Note that, when designing, it is difficult to determine how long an iteration cycle will last. Also, it is unlikely that everything will work after the first test. Moreover, it is difficult to predict how many design, manufacturing, and test cycles are needed until the system fully works. For now, one year is allocated to this phase. A time of two and a half months, before the iteration phase, is allocated to the testing and test analysis. Six weeks prior to that is for the prototyping and preparation of the tests, and the six months following DSE is for the detailed design.

4.2. Functionality Assessment

Author: T. Odijk

Editors: M. Rusch, C. Kendall, S. Yorucu

The functionality assessment of the product is one of the design steps. The functions required dictate what the vehicle will be capable of. The functions themselves can be derived from the combination of the stakeholder requirements and the project objective statement. In turn, these functions are the input for the functional requirements, which then are linked to the performance requirements. It is therefore important to have a good overview of all the functions

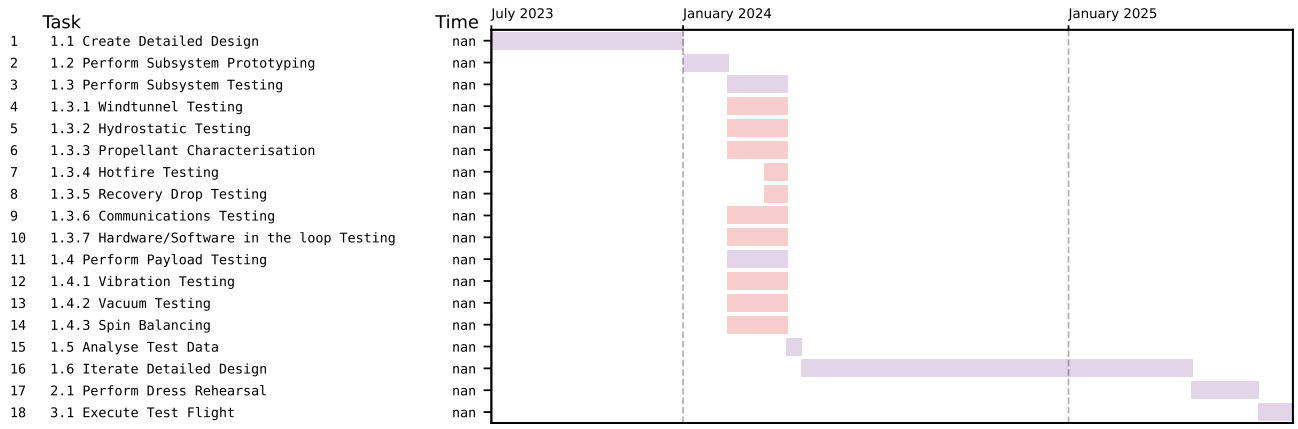

Figure 4.2: Design and Development Logic Gantt Chart

that have to be performed during the mission. The different functions during the mission phases can be found in Section 4.2.1, and a complete overview is given in Section 4.2.2.

4.2.1. Functional Flow Diagrams

Author: E. Chen
Editors: M. Rusch, C. Kendall, S. Yorucu

The vehicle shall perform a number of functions throughout its operation. These functions are required both before, during, and after the mission, and have a defined time-wise order. To illustrate the logical flow of the system functionality, a FFD is used. The high level functional flow diagram is shown in Figure 4.3.

As shown in the FFD, the life cycle of a vehicle is divided into a number of phases:

- Manufacturing, Assembly, and Integration (MAI)
- Launch operations
- Ascent
- Experiments execution
- Descent
- Recovery
- Refurbishment
- Data analysis
- End of Life

In each of these phases, the functional flow is further expanded into specific functionalities. In the MAI phase, the functionality is related to the design, testing, manufacturing, assembly, and integration. During the launch operations phase, the functions of the vehicle are related to the logistics, pre-launch checks, and launch preparations. Then, the ascent phase involves the rocket leaving the tower by propelling and coasting towards the desired altitude.

In the ”Perform experiment” phase, the vehicle and and the payload needs to support the scientific data acquisition process and sample collection.

During the descent phase, the vehicle has to be capable of recovering itself and communicating its landing location for retrieval.

After the landing, the refurbishment phase begins. During this phase, the vehicle has to support the inspection, testing, and refurbishment of individual subsystems.

The data analysis phase includes vehicle functions related to the data extraction and processing. This relates to both

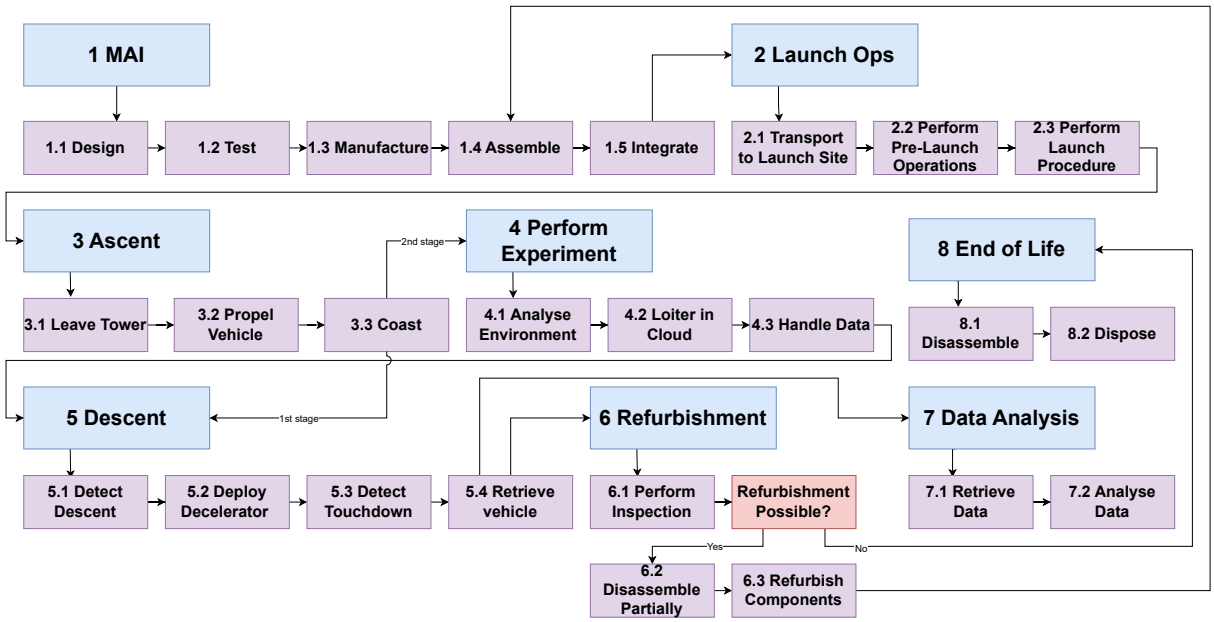

Figure 4.3: High-Level Functional Flow Diagram

the scientific mission and the performance evaluation of the vehicle.

Finally, during the end of life of the vehicle, design for recycling shall aid in the recycling process by allowing the separation of the vehicle into subsystems and recyclable parts.

These high level functions have been expanded into a complete FFD is shown at the end of this chapter. One important note must be made about phase 3.2. Here the vehicle is in the so called Flight Termination System (FTS) loop. Checking constantly if the flight needs to be terminated. This happens both for the first stage burn, second stage burn, and the coast to apogee. Since the functions are identical, they have all been numbered the same, this is why there are functions with code 3.2.x in phase 3.3.

4.2.2. Functional Breakdown Structure

Author: E. Chen

Editors: M. Rusch, C. Kendall, S. Yorucu

The FBS expands upon the elements identified in the FFD. Instead of showing this in a sequential flow diagram, the Functional Breakdown Structure uses a hierarchical tree, where each level of the tree goes into further detail. To allow for cross-referencing between functions, matching functional identifiers are used between the FBS and FFD, with the FBS containing an additional level of detail when compared to the FFD. The detailed FBS is shown at the end of this chapter. The main purpose of the diagram in the context of the project is to allow for a full overview of all the required functions and sub-functions independent of the physical product itself. This allows a common set of functions to be applied for different potential vehicle designs or options [34].

4.3. Sustainable Development Strategy

Author: S. Aurori

Editors: C. Kendall, S. Yorucu

Over the past few years, a large push towards sustainable space flight and engineering has been established [19]. With an increasing interest in the exploration of space, more missions are ongoing both to expand our knowledge of Earth and space. Many initiatives have been started on the research of sustainable space system propellants and propulsion systems, with the purpose of decreasing the damaging effect of these on the environment. This not only ensures the good relation between the systems and the nature around them, but also with the operators and responsible crews tasked with the logistics, testing, maintenance, and functioning of these systems.

This section outlines the considered sustainability aspects within each mission phase. With the main focus is on the handling of the vehicle, components, and systems during manufacturing, testing, operations, and end of life. Various procedures, such as nondestructive testing, apply for multiple phases. However, each procedure will be outlined only once. Further detail on the vehicle specific performance sustainability is outlined later within the report, in Chapter 9. An overview of the socio-economic aspects taken into account within the sustainability assessment of the project is developed in the early mission stages. Ensuring an inclusive environment, prioritising operational safety, and respecting the environment, is of top priority within the Altus mission.

4.3.1. Mission Phases

Engineering sustainability is a principle that needs to be included not only during the design phase, but throughout all phases of the Altus project. It entails the establishment and adherence to a framework that connects engineering projects to socio-economic aspects [35].

4.3.2. Project Planning and Initial Design

The project planning and initial design phase is when the first steps towards project and system sustainability are taken. Various factors of social, economic, and technical character influence the way in which the project needs to be approached. It is of utmost importance to assess the impact of rocketry, not only on an operational model, but to implement sustainability within all its phases and to document properly the link between such a framework and the technical design.

Starting with the initial project phases, as outlined in Chapter 2, there are various preliminary steps that need to be taken within the design phase: the project definition, concept selection and the preliminary design. These influence the next project milestones. To prevent a waste of resources, margins are allocated to the various budget distributions within the planning phase. This is necessary to ensure that enough time is allocated for iterations, testing and the qualification of both hardware and concepts.

Within the design phase, a high importance is given to the use of software tools and pre-existing technical literature. The Altus project is focused on the use of already existing knowledge and shifting towards a sustainable engineering mindset. With this, the use of open source tools is implemented (e.g. OpenRocket, used for the preliminary trajectory simulations, and OpenMotor, similarly used for the design of the propulsion system). More detail on these tools is given in Chapter 8 and Section 4.1. This allows for external members of both the scientific and the engineering community to replicate and understand the systems developed within the Altus project.

An important aspect of social sustainability included within the project is ensuring that the knowledge gathered both through the qualification of the Altus vehicle, as well as the data gathered on the PMC, is widely made available to external parties. Proper documentation of all the milestones, outlined in Section 2.3 and Section 2.5, is needed to ensure that feedback can be received from outside the project crew, as well as to ensure that the public understands the need and importance of such missions and research. Transparency allows for both further concept improvement, from effective peer reviews, as well as connecting the project to a broader audience.

Furthermore, project Altus will ensure the inclusion of a diverse crew, both from a nationality, gender, and professional point of view. To set an example within the Science, Technology, Engineering, and Mathematics (STEM) community, the project will include, to its best capability, experienced professionals from all backgrounds,

allowing them to set an example for their peers. Chapter 2 outlines the milestones and timeline of the project: a minimum of two years for technical qualification, and 11 years of scientific data gathering. Thus, due to this wide time-span, the Altus mission should properly set an environment for young professionals to learn and to develop new skills and knowledge. This can be applied throughout the mission phases, as the concepts developed during the design phase are verified and validated through testing and iterations within the three year development period of the mission.

Finally, one of the key aspects of sustainable design is the impact that sustainability actually has on the design decisions. In that regard, it is useful to firstly look into fail-safe and safe-life designs. A fail-safe design allows for some members within a structure to fail, due to the presence of contingent structural components to accommodate for it, without having critical failure of the entire system [36]. On the other hand, a safe-life entails a system that is guaranteed to fulfil its purpose for a defined period of time [36]. This allows for a clear replacement strategy of various subsystems, which can aid with a efficient resource distribution. As an example, this is reflected by the use of a replaceable graphite nozzle insert. Designing a very durable nozzle, for the entire duration of the vehicle, translates quickly into high mass and financial costs [36].

Furthermore, a safe failure methodology is taken into account as well, as for example in the solid motor design, outlined in more detail in Chapter 8. The casing is designed for significantly higher loads (in the case of the Altus motors, 1.452 times higher) than the Maximum Estimated Operating Pressure (MEOP) of the combustion chamber. Furthermore, a safe and predetermined nozzle shear-out design failure mode is implemented. This helps to ensure that the payload does not get damaged in case of an over-pressurisation event, with the energy dissipated away from the vehicle.

4.3.3. Manufacturing

The sustainability of the manufacturing process can be assessed from two different perspectives: the material outsourcing, and the production process. Firstly, ensuring that the materials that are needed for the system are acquired from reliable, ethical sources. Secondly, it is important to look into the operational safety of the manufacturing process, as well as the way the resources are being used and the amounts of materials that are being processed, yet scrapped through manufacturing [37].

Table 4.1: Waste analysis for FOI and EURENCO syntheses of ammonium dinitramide [38]

	Waste (kg/ton ADN)	
Process	**FOI**	**EURENCO**
Water	194100	21000
Non-solvent	30000	30000
Alcohol	8420	3150
Nitrates	18170	310
Sulfates	13540	5110
Neutralizing agent	50	0
Dinitramide	250	420
Granulated activated carbon	700	0
Guanylurea	0	1165
Others	990	1115
Total	266220	62270

Starting with the materials used within the system, it has been decided in the early stages of the concept selection that the predominant materials used for the structures, motor casing, and supporting parts of the vehicle shall be metal based. A deeper assessment of the specific alloys is presented in later chapters of this report, namely Section 11.4. The machining process is a topic of main sustainability focus, as the vehicle is mostly made of metal, and thus has to be machined a significant amount. Moreover, machining metal introduces high operational risks and large amounts of resources spent on the production of metal components. An evaluation of the sustainability of metal-machining suggests that 80% of skin diseases developed through these operations are due to metal working fluids, specifically, cooling fluids [37]. The storage and usage of such fluids can also cost twice as much as the creation of the part itself [37]. Safer options for the operators are proposed, such as cryogenic, or air based cooling, or solid lubricants which would reduce both the cost and the operational hazards that arise within this process. The usage of vegetable oil as a safer fluid is also an option, within a Minimum Quantity Lubrication (MQL) framework, in which only the necessary amount of fluid is dispersed during the machining process [37].

As approximately 90% of the dry mass of the launcher is made of various aluminium alloys, a closer look is taken at the recyclability of this metal. A detailed overview of the mass distribution through the vehicle is given in Table 11.1. According to a study on the reusability of aluminium, 75% of the entire amount of extracted raw aluminium is still in use today Currently, a third of the used aluminium is made of scraps, but it is expected that this fraction can rise to 50% by 2050. Machining processes are well-known for their high fraction of scrap production, meaning that the recyclability of the material pays a very important role in the sustainability of the process.

The propellant manufacturing and outsourcing is a topic of main focus within the Altus project. With the task of establishing a new sustainable framework, as well as demonstrating cleaner propulsion technologies, it is necessary to ensure operational and environmental safety within the propellant manufacturing process. An overview of the different waste products obtained by the Swedish Defense Research Agency (FOI) and the French provider EURENCO can be seen in Table 4.1. Based on the analysis performed in 2023 by Fu-yao Chen et al. in [38, Section 2.4], FOI results in 4.27 times more kilograms of waste per ton of produced ADN, making EURENCO the desired source of oxidiser for the Altus mission. Furthermore, ensuring that HTPB is also environmentally sustainable, an alternative synthesis route for 1,3-butadiene C_4H_6 is looked into. Previous production methods based on bio-derived ethanol exist, in the United States during World War II, as well as in the Soviet Union within the synthetic rubber industry [39]. Presently, butadiene is derived from fossil fuels, which entails the need for an alternative ethanol based process, proven in the last century.

4.3.4. Assembly, Integration, and Testing

The reusability of the vehicle, is not only paramount for sustainability, but also is a key stakeholder requirement. This not only entails the reuse of the vehicle itself, as its operations and logistics also need to be well documented and transmittable. From qualifications motor testing, to vibration loading of the payload and electronics, the Altus vehicle will be subjected to a series of tests and integration phases. Further detail on the tests is given in Section 4.1. Traceability in decision and results is key when trying to replicate or assess a system. Thereby, for the effective transfer of knowledge gathered throughout the Altus mission, proper documentation needs to be written.

Non-destructive testing methods have been developed since the early 1960's [40]. These methods are a very sustainable means of flaw detection within various structures. Within the Altus project, various non destructive processes are considered, such as: liquid penetrating tests, microwave detection, ultrasonic testing, and industrial computed tomography imagery detection [41, 40, 42]. The qualification of the metal stock for the structures of the vehicle can be assessed by means of these methods. Furthermore, microwave, ultrasonic and computer tomography detection are used within the industry for checking the quality of solid propellant grains [40]. The propulsion system of the Altus vehicle uses an ADN-AN-HTPB composite propellant, and so thorough inspection of the grain after casting is necessary for to ensure low risk of an over-pressure occurring. The non-destructive assessment of the materials attained for the assembly and integration of the main vehicle subsystems, such as the joints, motor casing, staging articulations, nosecone structure and deployment mechanism is planned as a precaution. Ensuring that the metal stock is up to specification is necessary such that failure, due to operational related factors, is prevented.

4.3.5. Operations

To further strengthen the technological and scientific aspect of the mission, it is of great importance to develop a strong set of procedures to be used throughout the vehicle operations. This not only helps with, reducing time costs, and effectively using resources, but also ensures a safe and proper way of passing through various high risk activities. These include explosives handling in the case of the ADN-based solid propellant, the payload integration, and launch.

As with most launcher systems, the Altus vehicle contains a wide variety of hazardous items: high power lithium polymer batteries, two solid ADN-based motors, solid motor igniters, and parachute deployment devices. Chapter 8 outlines the characteristics of these subsystems. The handling of these systems entails the addition of proper safety precautions to ensure that the test crews, operators, maintenance crew, and the system itself are safe. This will ensure the durability and sustainability of the mission throughout its entire duration.

Considering the safe handling and storage of the motors, the following factors need to be taken into account: accidental ignition of the motor during handling, toxic exhausts and chemicals, impact sensitivity, and shelf life [43]. More details on the operational steps and procedures are outlined in Section 12.2. The shelf life of the motors can be increased by reducing the thermal and physical loads of the motors are going through. By means of a proper storage facility, with the necessary temperature and humidity controls, the shelf life of the propellant can be extended [43]. Ensuring that the compounds in the motor composition are compatible with each other is needed. It is expected that the propellants shall be classified as 1.1 or 1.3 explosives under the Accord relatif au transport international des marchandises Dangereuses par Route (ADR), meaning that special transportation of the motors, and full handling procedures are needed.[13]

Furthermore, the vehicle electronics and power systems require special storage facilities. Well ventilated and dry rooms are required, with average temperatures of 5 °C, acid immune coated walls, and floors covered in anti-static varnishes. Proper ventilation is advised to reduce the amount of hydrogen gas accumulation in the room [44]. This factor also influences the positioning of the illumination items, which shall not be placed above the battery containers to avoid the buildup of hydrogen gas [44].

Finally, the deployment system, as outlined later, contains pressurised gas vessels. These also have to be stored properly. Pressurised containers need to be treated with great care ensuring that they are not damaged by impact, nor exposed to high temperatures. The expiration date needs to be assessed and ensure that operation only occurs within the allowed time period.

4.3.6. Refurbishment

As previously outlined in Section 4.3.4, non-destructive testing is highly useful in the quality assurance process of the systems within the Altus launcher. This can be further applied within the refurbishment phase. Having the requirement of reusing the launcher hardware for at least 10 missions, not including consumables such as sealing elements and the propellant, entails that the hardware needs to be checked and its quality ensured before reuse. Again, by means of non-destructive testing, the aluminium structures can be scanned and assessed [41]. In this case, it is the already-processed hardware that is investigated, not the metal stock as in the ATI phase. Special attention needs to be paid towards the hardware parts that are exposed to severe thermal stresses, such as: the motor casings, the nose cone, and nozzle inserts. The graphite nozzle insert, is assumed to last for two missions. Its low mass allows it to be replaced, while respecting STK-RE-1, detailed in Section 5.2.

4.3.7. End of Life

Within the End of Life phase of the mission, both the vehicle as well as the knowledge gathered within the mission need to be properly assessed. Moreover, taking into account the high proportion of recyclable metals within the vehicle, all of those compounds can be recycled and reused for other future systems. Furthermore, the documentation written within the mission can be used as inspiration for future missions. Taking into account the progress in sustainability, both from a technical and socio-economic way of the Altus mission, this will enhance the pool of knowledge in the field of sustainable sounding rocketry.

[13] https://business.gov.nl/regulation/transport-dangerous-goods-road/[20/06/2023]

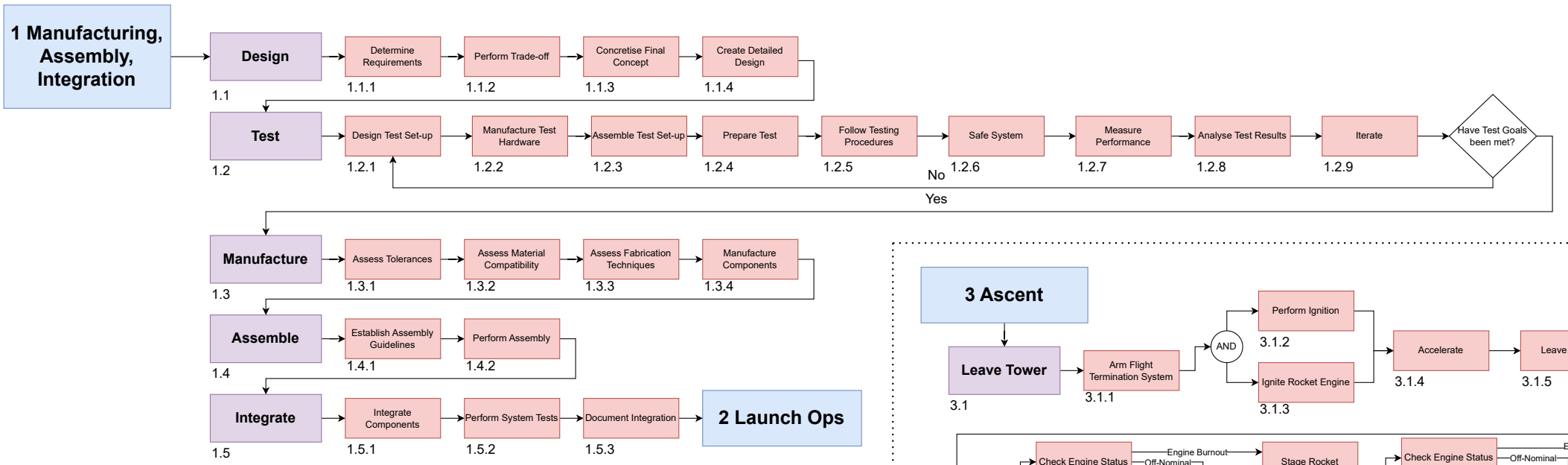
1 Manufacturing, Assembly, Integration
Design
1.1
Determine Requirements
1.1.1
Perform Trade-off
1.1.2
Concretise Final Concept
1.1.3
Create Detailed Design
1.1.4
Test
1.2
Design Test Set-up
1.2.1
Manufacture Test Hardware
1.2.2
Assemble Test Set-up
1.2.3
Prepare Test
1.2.4
Follow Testing Procedures
1.2.5
Safe System
1.2.6
Measure Performance
1.2.7
Analyse Test Results
1.2.8
Iterate
1.2.9
Have Test Goals been met?
No
Yes
Manufacture
1.3
Assess Tolerances
1.3.1
Assess Material Compatibility
1.3.2
Assess Fabrication Techniques
1.3.3
Manufacture Components
1.3.4
Assemble
1.4
Establish Assembly Guidelines
1.4.1
Perform Assembly
1.4.2
Integrate
1.5
Integrate Components
1.5.1
Perform System Tests
1.5.2
Document Integration
1.5.3
2 Launch Ops

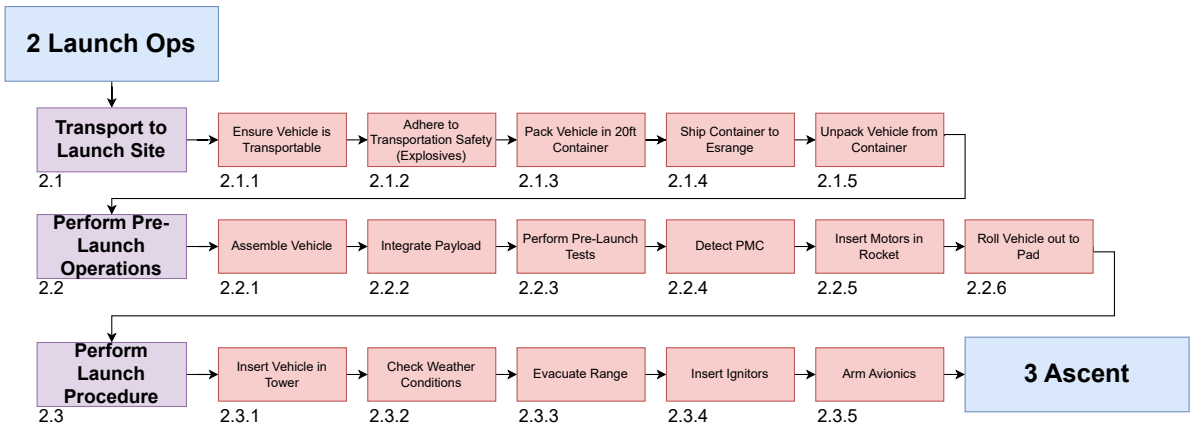
2 Launch Ops
Transport to Launch Site
2.1
Ensure Vehicle is Transportable
2.1.1
Adhere to Transportation Safety (Explosives)
2.1.2
Pack Vehicle in 20ft Container
2.1.3
Ship Container to Esrange
2.1.4
Unpack Vehicle from Container
2.1.5
Perform Pre-Launch Operations
2.2
Assemble Vehicle
2.2.1
Integrate Payload
2.2.2
Perform Pre-Launch Tests
2.2.3
Detect PMC
2.2.4
Insert Motors in Rocket
2.2.5
Roll Vehicle out to Pad
2.2.6
Perform Launch Procedure
2.3
Insert Vehicle in Tower
2.3.1
Check Weather Conditions
2.3.2
Evacuate Range
2.3.3
Insert Ignitors
2.3.4
Arm Avionics
2.3.5
3 Ascent

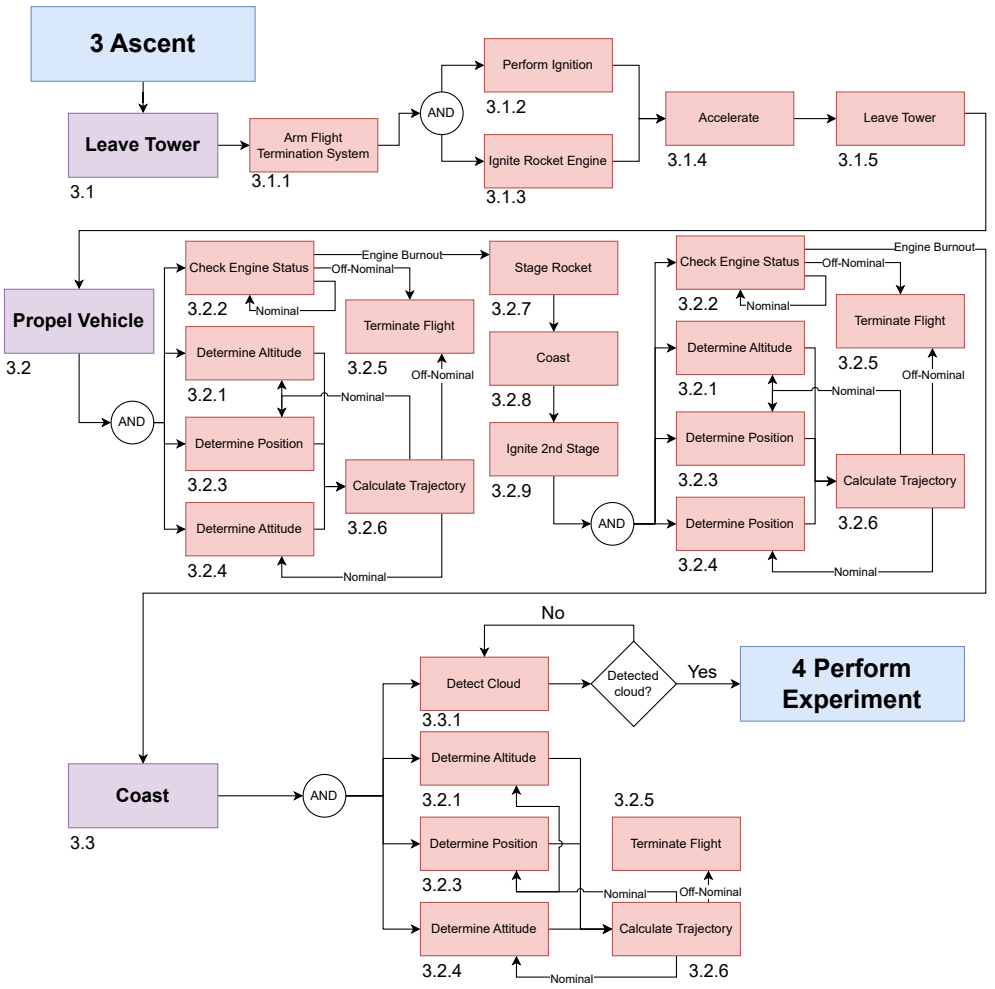
3 Ascent
Leave Tower
3.1
Arm Flight Termination System
3.1.1
AND
Perform Ignition
3.1.2
Ignite Rocket Engine
3.1.3
Accelerate
3.1.4
Leave Tower
3.1.5
Propel Vehicle
3.2
AND
Check Engine Status
3.2.2
Engine Burnout
Off-Nominal
Nominal
Determine Altitude
3.2.1
Determine Position
3.2.3
Determine Attitude
3.2.4
Terminate Flight
3.2.5
Calculate Trajectory
3.2.6
Stage Rocket
3.2.7
Coast
3.2.8
Ignite 2nd Stage
3.2.9
AND
Check Engine Status
3.2.2
Engine Burnout
Off-Nominal
Nominal
Determine Altitude
3.2.1
Determine Position
3.2.3
Determine Position
3.2.4
Terminate Flight
3.2.5
Calculate Trajectory
3.2.6
Coast
3.3
AND
No
Detect Cloud
3.3.1
Detected cloud?
Yes
4 Perform Experiment
Determine Altitude
3.2.1
Determine Position
3.2.3
Determine Attitude
3.2.4
Terminate Flight
3.2.5
Calculate Trajectory
3.2.6
Nominal
Off-Nominal
Nominal

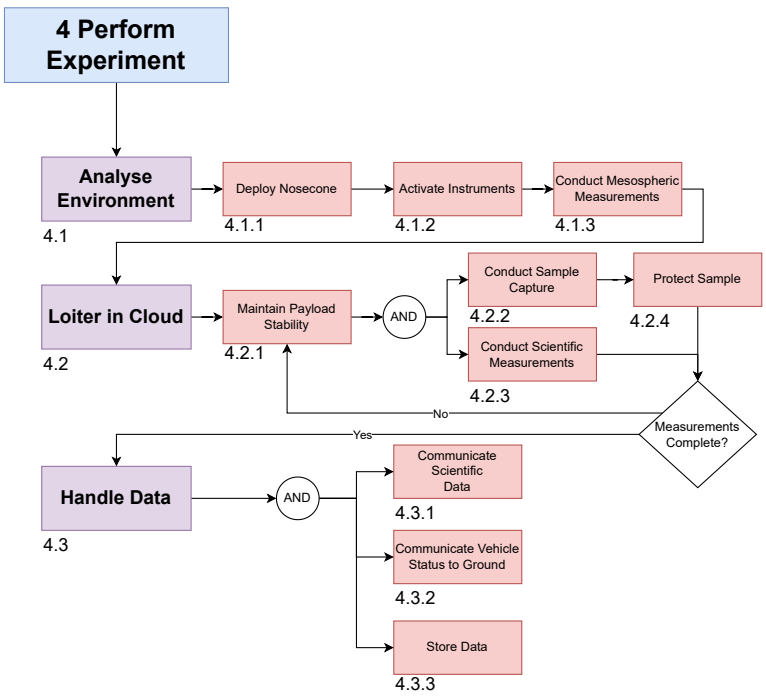
4 Perform Experiment
Analyse Environment
4.1
Deploy Nosecone
4.1.1
Activate Instruments
4.1.2
Conduct Mesospheric Measurements
4.1.3
Loiter in Cloud
4.2
Maintain Payload Stability
4.2.1
AND
Conduct Sample Capture
4.2.2
Conduct Scientific Measurements
4.2.3
Protect Sample
4.2.4
No
Yes
Measurements Complete?
Handle Data
4.3
AND
Communicate Scientific Data
4.3.1
Communicate Vehicle Status to Ground
4.3.2
Store Data
4.3.3

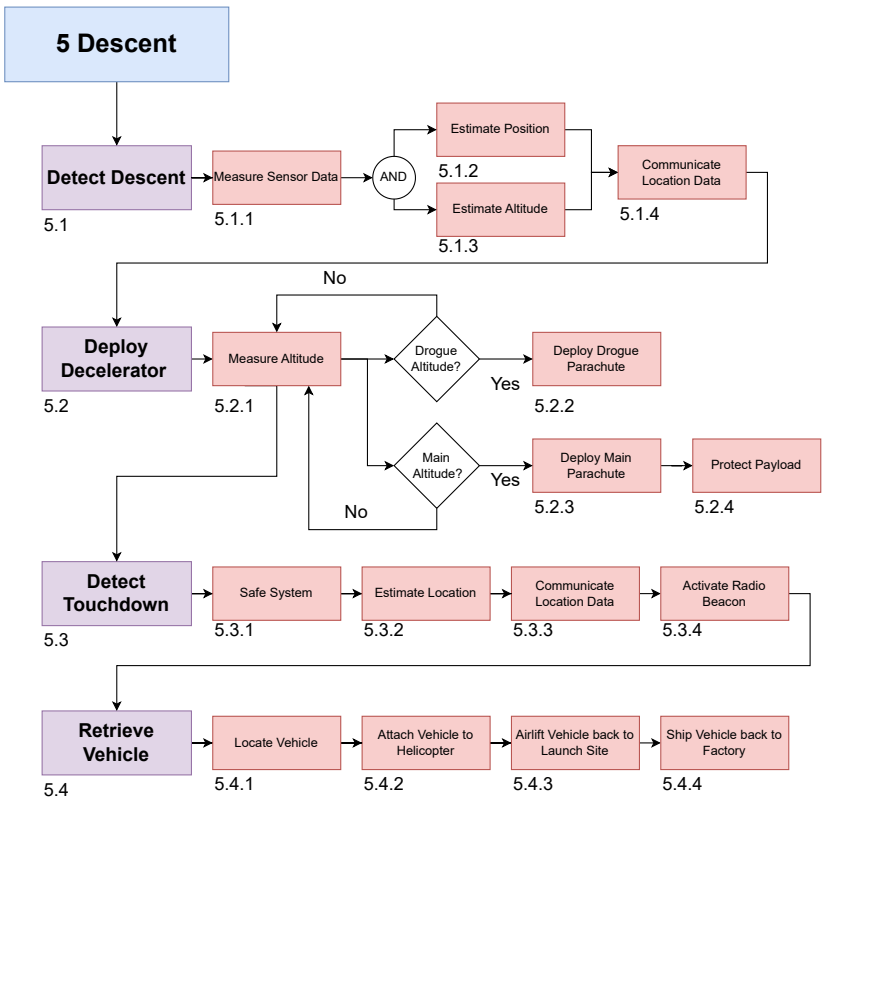
5 Descent
Detect Descent
5.1
Measure Sensor Data
5.1.1
AND
Estimate Position
5.1.2
Estimate Altitude
5.1.3
Communicate Location Data
5.1.4
No
Deploy Decelerator
5.2
Measure Altitude
5.2.1
Drogue Altitude?
Yes
Deploy Drogue Parachute
5.2.2
Main Altitude?
Yes
Deploy Main Parachute
5.2.3
Protect Payload
5.2.4
No
Detect Touchdown
5.3
Safe System
5.3.1
Estimate Location
5.3.2
Communicate Location Data
5.3.3
Activate Radio Beacon
5.3.4
Retrieve Vehicle
5.4
Locate Vehicle
5.4.1
Attach Vehicle to Helicopter
5.4.2
Airlift Vehicle back to Launch Site
5.4.3
Ship Vehicle back to Factory
5.4.4

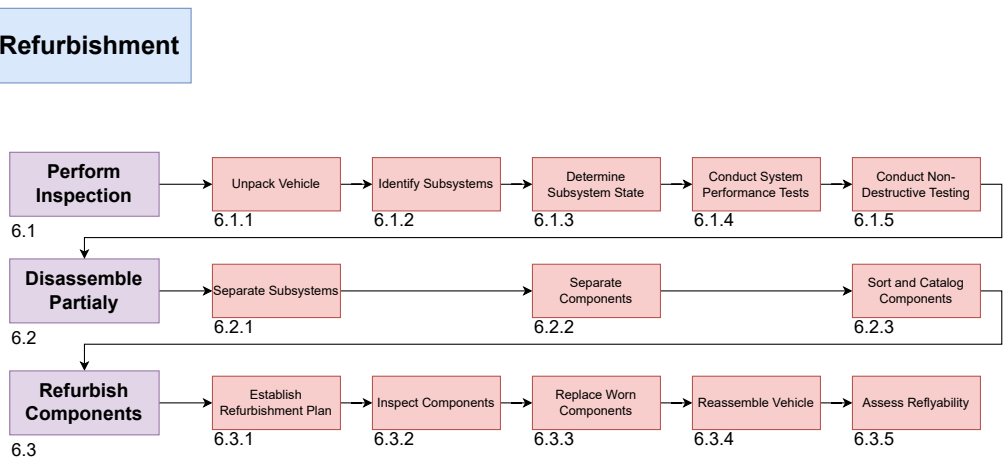
6 Refurbishment
Perform Inspection
6.1
Unpack Vehicle
6.1.1
Identify Subsystems
6.1.2
Determine Subsystem State
6.1.3
Conduct System Performance Tests
6.1.4
Conduct Non-Destructive Testing
6.1.5
Disassemble Partialy
6.2
Separate Subsystems
6.2.1
Separate Components
6.2.2
Sort and Catalog Components
6.2.3
Refurbish Components
6.3
Establish Refurbishment Plan
6.3.1
Inspect Components
6.3.2
Replace Worn Components
6.3.3
Reassemble Vehicle
6.3.4
Assess Reflyability
6.3.5

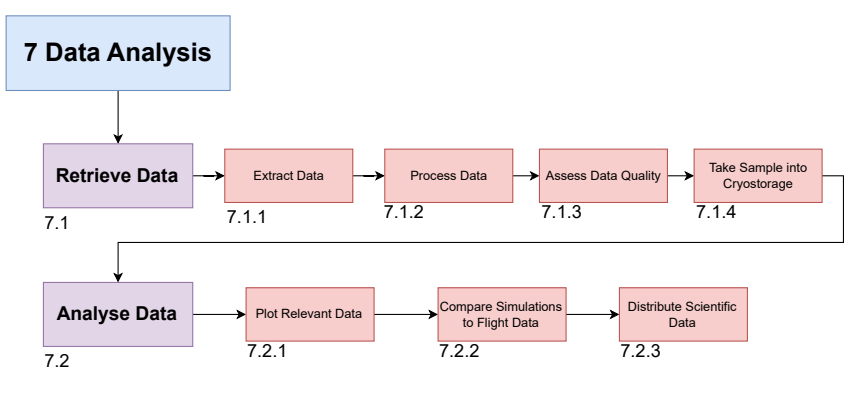
7 Data Analysis
Retrieve Data
7.1
Extract Data
7.1.1
Process Data
7.1.2
Assess Data Quality
7.1.3
Take Sample into Cryostorage
7.1.4
Analyse Data
7.2
Plot Relevant Data
7.2.1
Compare Simulations to Flight Data
7.2.2
Distribute Scientific Data
7.2.3

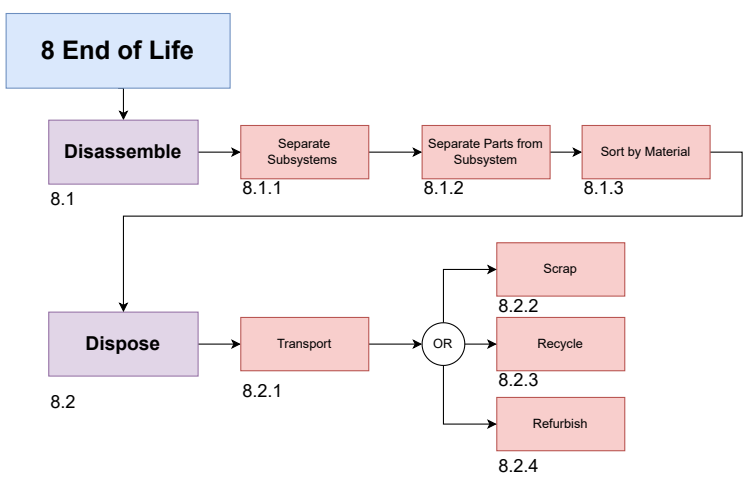
8 End of Life
Disassemble
8.1
Separate Subsystems
8.1.1
Separate Parts from Subsystem
8.1.2
Sort by Material
8.1.3
Dispose
8.2
Transport
8.2.1
OR
Scrap
8.2.2
Recycle
8.2.3
Refurbish
8.2.4

Phase

Functional Group

Function

Subfunction

Mission

1 MAI

1.1 Design
- 1.1.1 Determine Requirements
  - 1.1.1.1 Determine Stakeholder Requirements
  - 1.1.1.2 Determine Scientific Requirements
  - 1.1.1.3 Determine Vehicle Requirements
- 1.1.2 Perform Trade-off
  - 1.1.2.1 Determine Trade-off Criteria
  - 1.1.2.2 Determine Options to be Considered
  - 1.1.2.3 Analyse each Criterium for each Option
  - 1.1.2.4 Visualize with a Matrix
  - 1.1.2.5 Choose Best Option
- 1.1.3 Concretise Final Concept
  - 1.1.3.1 Do Preliminary Calculations
  - 1.1.3.2 Create Preliminary Design
  - 1.1.3.3 Make Rough CAD Design
- 1.1.4 Create Detailed Design
  - 1.1.4.1 Create Computer Models
  - 1.1.4.2 Perform Simulations
  - 1.1.4.3 Create Technical Drawings

1.2 Test
- 1.2.1 Design Test Set-up
  - 1.2.1.1 Asses System to be Tested
  - 1.2.1.2 Asses Test Goals
  - 1.2.1.3 Create Test Set-up Diagrams
- 1.2.2 Manufacture Test Hardware
  - 1.2.2.1 Create Overview of Components
  - 1.2.2.2 Manufacture Individual Components
- 1.2.3 Assemble Test Set-up
  - 1.2.3.1 Assemble Test Set-up Subsystems
  - 1.2.3.2 Assemble Complete Test Set-up
  - 1.2.3.3 Perform Integration Tests
- 1.2.4 Prepare Test
  - 1.2.4.1 Write Test Procedures
  - 1.2.4.2 Assign Test Roles
  - 1.2.4.3 Assign Safety Roles
  - 1.2.4.4 Prepare Testing Facility
  - 1.2.4.5 Asses Testing Operations
- 1.2.5 Follow Testing Procedures
  - 1.2.5.1 Assemble Prototype
  - 1.2.5.2 Perform Actuation Checks
  - 1.2.5.3 Perform Electronics Checks
  - 1.2.5.4 Perform Safety Checks
  - 1.2.5.5 Ensure Appropriate PPE is Used
- 1.2.6 Safe System
  - 1.2.6.1 Have Visual Safety Indicators/Labels
- 1.2.7 Measure Performance
  - 1.2.7.1 Have Target Performance Characteristics
  - 1.2.7.2 Ensure Performance Requirements met
- 1.2.8 Analyse Test Results
  - 1.2.8.1 Perform Data Analysis
  - 1.2.8.2 Summarise Test Conclusions
- 1.2.9 Iterate
  - 1.2.9.1 Implement Design Changes
  - 1.2.9.2 Adapt Tests for new Changes

1.3 Manufacture
- 1.3.1 Assess Tolerances
  - 1.3.1.1 Determine Materials Thermal Behaviours
  - 1.3.1.2 Determine Vehicle Environment Conditions
  - 1.3.1.3 Determine Materials Stress Behaviours
- 1.3.2 Assess Material Compatibility
  - 1.3.2.1 Determine Difference in Thermal Behaviour
  - 1.3.2.2 Check Polarity of Materials
  - 1.3.2.3 Check Reactivity between Materials
  - 1.3.2.4 Check Radiation Interference
- 1.3.3 Assess Fabrication Techniques
  - 1.3.3.1 Check Toxic By-products
  - 1.3.3.2 Establish Part Traceability
- 1.3.4 Manufacture Components
  - 1.3.4.1 Machine Parts
  - 1.3.4.2 Additively Manufacture Parts
  - 1.3.4.3 Mould Parts

1.4 Assemble
- 1.4.1 Establish Assembly Guidelines
  - 1.4.1.1 Have Adequate Tolerances
  - 1.4.1.2 Check Assembly Accessibility
  - 1.4.1.3 Document Order of Operations
  - 1.4.1.4 Check Mounting Clearances
- 1.4.2 Perform Assembly
  - 1.4.2.1 Gather all Components
  - 1.4.2.2 Document Assembly Parts and Process
  - 1.4.2.3 Combine Components
  - 1.4.2.4 Put in Bolts and Rivets

1.5 Perform Integration
- 1.5.1 Integrate Components
  - 1.5.1.1 Connect Wiring
  - 1.5.1.2 Bolt and Rivet Sub-systems Together
- 1.5.2 Perform System Tests
  - 1.5.2.1 Have Hardware Test Interfaces
  - 1.5.2.2 Have Electronic Test interfaces
  - 1.5.2.3 Perform Dress Rehearsal
- 1.5.3 Document Integration
  - 1.5.3.1 Have Photographic Documentation
  - 1.5.3.2 Have Procedural Documentation

2 Launch Ops

2.1 Transport to Launch Site
- 2.1.1 Ensure Vehicle is Transportable
  - 2.1.1.1 Check Vehicle
  - 2.1.1.2 Check Transportation System
  - 2.1.1.3 Check Connection
- 2.1.2 Adhere to Transportation Safety (Explosives)
  - 2.1.2.1 Assess what licenses are required
  - 2.1.2.2 Obtain required licenses
- 2.1.3 Pack Vehicle in 20ft Container
  - 2.1.3.1 Acquire Container
  - 2.1.3.2 Pack Hardware with Adequate Protection
- 2.1.4 Ship Container to Esrange
  - 2.1.4.1 Organize Means of Transportation
  - 2.1.4.2 Perform Transport of System
- 2.1.5 Unpack Vehicle from Container
  - 2.1.5.1 Unpack Container
  - 2.1.5.2 Set up Workspace

2.2 Perform Pre-Launch Operations
- 2.2.1 Assemble Vehicle
  - 2.2.1.1 Assemble Subsystems
  - 2.2.1.2 Assemble Complete System
  - 2.2.1.3 System Health Checks
- 2.2.2 Integrate Payload
  - 2.2.2.1 Unpack Payload
  - 2.2.2.2 Attach Payload to Rocket
  - 2.2.2.3 Payload Health Checks
- 2.2.3 Perform Pre-Launch Tests
  - 2.2.3.1 Arm the Avionics as a Test
  - 2.2.3.2 Ensure Flight Termination System is Unarmed
  - 2.2.3.3 Ensure Deployment System is Unarmed
  - 2.2.3.4 Run Range Simulations Based on Updated Weather Conditions
  - 2.2.3.5 Perform Communication Checks
- 2.2.4 Detect PMC
  - 2.2.4.1 Observe the Sky
  - 2.2.4.2 Detect Polar Mesospheric Clouds
  - 2.2.4.3 Determine Polar Mesospheric Cloud Location
  - 2.2.4.4 Assess Reachability
  - 2.2.4.5 Decide on Target
- 2.2.5 Insert Motors in Rocket
  - 2.2.5.1 Evacuate Unnecessary People
  - 2.2.5.2 Insert Motor
- 2.2.6 Roll Vehicle out to Pad
  - 2.2.6.1 Load Vehicle in Transport Cart
  - 2.2.6.2 Attach Transport Cart to Tractor
  - 2.2.6.3 Drive to the Launchpad

2.3 Perform Launch Procedure
- 2.3.1 Insert Vehicle in Tower
  - 2.3.1.1 Arrive at the Launchpad
  - 2.3.1.2 Attach Vehicle to Launchrail
  - 2.3.1.3 Raise the Launchtower
  - 2.3.1.4 Check Tower Angles
  - 2.3.1.5 Attach Ground Infrastructure to Vehicle
- 2.3.2 Check Weather Conditions
  - 2.3.2.1 Gather Low Level Wind Data
  - 2.3.2.2 Gather High Level Wind Data
  - 2.3.2.3 Gather Lightning Probabilities
  - 2.3.2.4 Determine Precipitation Intensity
- 2.3.3 Evacuate Range
  - 2.3.3.1 Sound Evacuation Alarms
  - 2.3.3.2 Check Airspace with Radar
- 2.3.4 Insert Ignitors
  - 2.3.4.1 Insert Ignitors in Rocket
  - 2.3.4.2 Attach Ignitors to Firing Line
- 2.3.5 Arm Avionics
  - 2.3.5.1 Boot Avionics
  - 2.3.5.2 Arm Avionics
  - 2.3.5.3 Unshunt Ignitors

3 Ascent

3.1 Leave Tower
- 3.1.1 Arm Flight Termination System
  - 3.1.1.1 Insert Detonators
  - 3.1.1.2 Arm Detonators
  - 3.1.1.3 Evacuate Launchpad
  - 3.1.1.4 Turn on FTS
  - 3.1.1.5 Activate FTS Receiver
- 3.1.2 Perform Ignition
  - 3.1.2.1 Power Pyro Circuit
  - 3.1.2.2 Measure Actuation
- 3.1.3 Ignite Rocket Engine
  - 3.1.3.1 Start Burning Propellant
- 3.1.4 Accelerate
  - 3.1.4.1 Have Adequate Thrust
  - 3.1.4.2 Have launch Guidance
- 3.1.5 Leave Tower
  - 3.1.5.1 Decouple Ground Interfaces
  - 3.1.5.2 Measure Combustion Pressure Peak
  - 3.1.5.3 Detect Acceleration
  - 3.1.5.4 Detect Threshold Velocity

3.2 Propel Vehicle
- 3.2.1 Determine Altitude
  - 3.2.1.1 Determine Pressure
  - 3.2.1.2 Integrate Inertial Measurements
- 3.2.2 Check Engine Status
  - 3.2.2.1 Measure Chamber Pressure
  - 3.2.2.2 Measure Burn Time
- 3.2.3 Determine Position
  - 3.2.3.1 Receive GNSS Signal
  - 3.2.3.2 Determine GNSS Position
- 3.2.4 Determine Attitude
  - 3.2.4.1 Read out Inertial Measurements
  - 3.2.4.2 Read Magnetometer
  - 3.2.4.3 Determine Orientation
- 3.2.5 Terminate Flight
  - 3.2.5.1 Send Termination Command
  - 3.2.5.2 Receive Termination Command
  - 3.2.5.3 Fire FTS Detonators
  - 3.2.5.4 Disintegrate Vehicle
  - 3.2.5.5 Track Debris with Radar
- 3.2.6 Calculate Trajectory
  - 3.2.6.1 Determine Instantaneous Impact Point (IIP)
  - 3.2.5.2 Check IIP is in range
  - 3.2.5.3 Check Trajectory is in range
  - 3.2.5.4 Send Termination Command if Off-nominal
  - 3.2.5.5 Transmit Information to Ground
- 3.2.7 Stage Rocket
  - 3.2.7.1 Engine Burns out
  - 3.2.7.2 Drag Separates the Stages
- 3.2.8 Coast
  - 3.2.8.1 Maintain Stability
  - 3.2.8.2 Count Down until Next Stage
- 3.2.9 Ignite 2nd Stage
  - 3.2.9.1 Power Pyro Circuit
  - 3.2.9.2 Detect Actuation

3.3 Coast
- 3.3.1 Detect Cloud
  - 3.3.1.1 Measure Altitude
  - 3.3.1.2 Check Altitude Against Prediction

4 Perform Experiment

4.1 Analyse Environment
- 4.1.1 Deploy Nosecone
  - 4.1.1.1 Actuate CGDD
  - 4.1.1.2 Deploy Nosecone
- 4.1.2 Activate Instruments
  - 4.1.2.1 Activate Payload Power
  - 4.1.2.2 Mechanically Deploy Payload
- 4.1.3 Conduct Mesospheric Measurements
  - 4.1.3.1 Measure Pressure
  - 4.1.3.2 Measure Temperature
  - 4.1.3.3 Measure Altitude
  - 4.1.3.4 Measure Water Vapour Density
  - 4.1.3.5 Measure Atmospheric Composition
  - 4.1.3.6 Measure Solar Flux and Terrestrial Flux

4.2 Loiter in Cloud
- 4.2.1 Maintain Payload Stability
  - 4.2.1.1 Measure Payload Altitude
  - 4.2.1.2 Control Parachute
- 4.2.2 Conduct Sample Capture
  - 4.2.2.1 Expose Payload to Cloud
  - 4.2.2.2 Containing Sample
  - 4.2.2.3 Keep Sample Sterile
- 4.2.3 Conduct Scientific Measurements
  - 4.2.3.1 Measure Pressure
  - 4.2.3.2 Measure Temperature
  - 4.2.3.3 Measure Altitude
  - 4.2.3.4 Measure Water Vapour Density
  - 4.2.3.5 Measure Atmospheric Composition
  - 4.2.3.6 Measure Solar Flux and Terrestrial Flux
- 4.2.4 Protect Sample
  - 4.2.4.1 Seal Sample
  - 4.2.4.2 Protect Sample Mechanically

4.3 Handle data
- 4.3.1 Communicate Scientific Data
  - 4.3.1.1 Encode Data
  - 4.3.1.2 Transmit Data
- 4.3.2 Communicate Vehicle Status to Ground
  - 4.3.2.1 Encode Data
  - 4.3.2.2 Transmit Data
- 4.3.3 Store Data
  - 4.3.3.1 Encode Data
  - 4.3.3.2 Save Data Persistently
  - 4.3.3.3 Protect Data

5 Descent

5.1 Detect Descent
- 5.1.1 Measure Sensor Data
  - 5.1.1.1 Read Data
  - 5.1.1.2 Detect Errors
  - 5.1.1.3 Feed Data to System
- 5.1.2 Estimate Position
  - 5.1.2.1 Check Gyroscopes
  - 5.1.2.2 Compare to Launch Position
- 5.1.3 Estimate Altitude
  - 5.1.3.1 Read all Detected Accelerations
  - 5.1.3.2 Detect Errors
  - 5.1.3.3 Integrate Acceleration Twice
  - 5.1.3.4 Read Barometric Static Pressure
  - 5.1.3.5 Compare to Standard Atmosphere
  - 5.1.3.6 Read GNSS Location
  - 5.1.3.7 Combine Data with Kalman Filter
- 5.1.4 Communicate Location Data
  - 5.1.4.1 Encode Location Data
  - 5.1.4.2 Transmit Location Data

5.2 Deploy Decelerator
- 5.2.1 Measure Altitude
  - 5.2.1.1 Transmit Altitude to Ground Station
- 5.2.2 Deploy Drogue Parachute
  - 5.2.2.1 Ensure Clear Access to Surrounding Air
  - 5.2.2.2 Eject Drogue Parachute
  - 5.2.2.3 Inflate Drogue Parachute
- 5.2.3 Deploy Main Parachute
  - 5.2.3.1 Eject Main
  - 5.2.3.2 Inflate Main
- 5.2.4 Protect Payload
  - 5.2.4.1 De-expose Fragile Parts of the Payload

5.3 Detect Touchdown
- 5.3.1 Safe System
  - 5.3.1.1 Disarm Flight Termination System
- 5.3.2 Estimate Location
  - 5.3.2.1 Read GNSS Location
- 5.3.3 Communicate Location Data
  - 5.3.3.1 Encode Location Data
  - 5.3.3.2 Transmit Location Data
- 5.3.4 Activate Radio Beacon
  - 5.3.4.1 Power Radio Beacon
  - 5.3.4.2 Start Transmission

5.4 Retrieve Vehicle
- 5.4.1 Locate Vehicle
  - 5.4.1.1 Follow GNSS Data
- 5.4.2 Attach Vehicle to Helicopter
  - 5.4.2.1 Turn Off Avionics
  - 5.4.2.2 Attach Vehicle to Helicopter
- 5.4.3 Airlift Vehicle back to Launch Site
  - 5.4.3.1 Fly to Launch Site
  - 5.4.3.2 Detach Vehicle from Helicopter
- 5.4.4 Ship Vehicle back to Factory
  - 5.4.4.1 Pack Vehicle into 20ft Container
  - 5.4.4.2 Arrange Transportation
  - 5.4.4.3 Transport Container to Factory

6 Refurbishment

6.1 Perform Inspection
- 6.1.1 Unpack Vehicle
  - 6.1.1.1 Set Up Workspace
- 6.1.2 Identify Subsystems
  - 6.1.2.1 Identify System Interfaces
  - 6.1.2.2 Identify Key Components
- 6.1.3 Determine Subsystem State
  - 6.1.3.1 Determine Wear Level
  - 6.1.3.2 Determine Flight History
- 6.1.4 System Performance Tests
  - 6.1.4.1 Compare with Pre-flight Data
  - 6.1.4.2 Ensure Performance Requirements met
- 6.1.5 Conduct Non-destructive Testing
  - 6.1.5.1 Internal NDT
  - 6.1.5.2 Surface NDT

6.2 Disassemble Partially
- 6.2.1 Separate Subsystems
  - 6.2.1.1 Have Standardised Fasteners
- 6.2.2 Separate Components
  - 6.2.2.1 Identify Component Interfaces
  - 6.2.2.2 Separate Components
- 6.2.3 Sort and Catalog Components
  - 6.2.3.1 Document Wear Level
  - 6.2.3.2 Document Flight History

6.3 Refurbish Components
- 6.3.1 Establish Refurbishment Plan
  - 6.3.1.1 Inventorise Wear of Parts
- 6.3.2 Inspect Components
  - 6.3.2.1 Have Components Specifications
- 6.3.3 Replace Worn Components
  - 6.3.3.1 Assess Reusability of each Part
  - 6.3.3.2 Dispose of Unusable Parts
  - 6.3.3.3 Repair Components
- 6.3.4 Reassemble Vehicle
  - 6.3.4.1 Combine Components
  - 6.3.4.2 Combine Sub-systems
- 6.3.5 Assess Reflyability
  - 6.3.5.1 Perform System Tests

7 Data Analysis

7.1 Retrieve Data
- 7.1.1 Extract Data
  - 7.1.1.1 Connect to Avionics
  - 7.1.1.2 Extract Data
- 7.1.2 Process Data
  - 7.1.2.1 Apply Noise Filtering
  - 7.1.2.2 Apply Calibration
  - 7.1.2.3 Assess Data Quality
  - 7.1.2.4 Process Data with Scientific Tools
- 7.1.3 Assess Data Quality
  - 7.1.3.1 Assess Noise Levels
  - 7.1.3.2 Estimate Errors
  - 7.1.3.3 Identify Possible Improvements
- 7.1.4 Take Sample to Cryostorage
  - 7.1.4.1 Prevent Ice Crystals from Melting

7.2 Analyse Data
- 7.2.1 Plot Relevant Data
  - 7.2.1.1 Combine Relevant Data
  - 7.2.1.2 Display Plotted Data
- 7.2.2 Compare Simulations Flight Data
  - 7.2.2.1 Assess Flight Path
  - 7.2.2.2 Improve Flight Simulations
- 7.2.3 Distribute Scientific Data
  - 7.2.3.1 Pack Scientific Data
  - 7.2.3.2 Send Scientific Data to Researcher

8 End of Life

8.1 Disassemble
- 8.1.1 Separate Sub-systems
  - 8.1.1.1 Disconnect Powerlines
  - 8.1.1.2 Take Out Bolts
  - 8.1.1.3 Drill Out Rivets
- 8.1.2 Separate Parts from Sub-system
  - 8.1.2.1 Take Out Bolts
  - 8.1.2.2 Drill Out Rivets
  - 8.1.2.3 Desolder Wires and Components
  - 8.1.2.4 Remove Adhesives
- 8.1.3 Sort by material
  - 8.1.3.1 Isolate Recycleable Materials
  - 8.1.3.2 Isolate by Metal Types
  - 8.1.3.4 Collect Scrap Components
  - 8.1.3.5 Collect Refurbishable Components
  - 8.1.3.6 Collect Recyclable Components

8.2 Dispose
- 8.2.1 Transport
  - 8.2.1.1 Load Parts
  - 8.2.1.2 Unload Parts
- 8.2.2 Scrap
  - 8.2.2.1 Scapyard
  - 8.2.2.2 Incineration
- 8.2.3 Recycle
  - 8.2.3.1 Shred
  - 8.2.3.2 Melt Metal
- 8.2.4 Refurbish
  - 8.2.4.1 Check Sub-system Performance

5 Requirements

In this chapter, the stakeholder, launch, and system requirements are presented. In Section 5.1 the the generation of requirements and their categorisation is discussed. Afterwards, in Section 5.2 and Section 5.3, the stakeholder requirements and the launch and system requirements, respectively, are presented.

5.1. Origin and Categorisation of Requirements

Author: T. Odijk
Editor: C. Kendall

The requirements that have been identified can be grouped into categories adapted from Section 4.2.2 of the NASA Systems Engineering Manual (2016) [27]. For the current phase, the most critical distinction is between the functional need requirements, performance requirements, and interface requirements. It should be noted that the three categories mentioned are not exhaustive and, as the project matures, the categorisation will become more extensive.

The functional requirements state the functions that need to be accomplished. The functional requirements are established from the functions that the product must perform, and thus can be identified from the functional breakdown structure. More information on the functional breakdown may be found in Section 4.2.2.

The performance requirements dictate how well these functions need to be performed. These performance requirements are also linked to the risks that need to be analysed. Each performance requirement has an associated performance risk (elaborated upon in Chapter 6).

Lastly, the interface requirements dictate the interaction between the product and external world. For example, these are requirements derived from the launch site, or from how the system operator interacts with the system. These requirements can also follow from the market analysis, as seen in Section 3.2.

5.2. Stakeholder Requirements

Author: M. Rusch
Editor: C. Kendall

Table 5.1 shows the stakeholder requirements that have been negotiated with the customer, as well as one requirement, STK-MK-01, that has followed from the market analysis. The requirements are divided over the following categories with their respective code:

- Mission Requirements (STK-MR-xx)
- Launch Site Requirements (STK-LS-xx)
- Propulsion Requirements (STK-PR-xx)
- Re-usability Requirements (STK-RE-xx)
- Market Requirements (STK-MK-xx)
- Financial Requirements (STK-FI-xx)

Table 5.1: Stakeholder Requirements

ID	Requirement
STK-MR-01	The sounding rocket shall have a minimum apogee of 90 km.
STK-MR-02	The rocket shall have a maximum total payload of 40 kg.
STK-MR-03	The scientific instruments shall be capable of making in-situ measurements of the physical properties of the PMCs.
STK-MR-05	The scientific instruments shall be capable of making in-situ measurements of the chemical properties of the PMCs.
STK-MR-06	The payload shall be able to collect an atmospheric sample from inside the Polar Mesospheric Cloud.
STK-MR-07	The vehicle shall gather engine and flight performance data.
STK-MR-08	The first operational flight shall take place in 2026.
STK-LS-01	The rocket shall meet the safety requirements of the launch site.
STK-LS-02	The rocket shall be capable of being launched at the Esrange Space Center.
STK-PR-01	The rocket propulsion system shall not use propellants that are derived from fossil fuels.
STK-PR-02	The rocket propellants shall not be toxic to the environment.
STK-PR-03	The rocket exhaust products shall abide by the WHO Global Air Quality Guidelines.
STK-RE-01	The rocket shall have less than 9% of its parts by dry mass replaced per mission, averaged over 10 missions.
STK-RE-02	No more than 1 vehicle shall be lost, on average, over a span of 20 missions.
STK-MK-01	The payload section shall be able to accommodate a payload of 6U.
STK-FI-01	The total mission development cost shall be no more than 35 million euros.

5.3. Launch and System Requirements

Author: M. Rusch

Editor: C. Kendall

The requirements from the launch site have been divided into categories. Each category of requirement is displayed in an reference table:

- General launch site and ground system requirements (LCH-GN-xx & LCH-GS-xx) – Table 5.2
- Safety and simulation requirements (LCH-SF-xx & LCH-SM-xx) – Table 5.3

The system requirements have been divided into categories according to subsystems and the payload:

- Avionics requirements (SYS-AV-xx) – Table 5.4
- General system requirements (SYS-GN-xx) – Table 5.5
- Payload requirements (SYS-PL-xx) – Table 5.6
- Propulsion and power (SYS-PR-xx & SYS-PW-xx) – Table 5.7
- Recovery (SYS-RC-xx) – Table 5.8.

Table 5.2: General Launch Site and Ground System Requirements

Code	Type	Requirement	Motivation	V&V	Traceability
LCH-GN-01	Interface	The vehicle shall be able to be interfaced with the Esrange ground equipment.	To ensure less production of launch equipment, the available Esrange equipment should be used.	Demonstration	STK-LS-02
LCH-GN-02	Functional	A simulation tool shall be able to determine the vehicle trajectory ahead of launch.	To ensure that the vehicle will not leave the safety zone, simulations shall be performed to predict the landing site and debris dispersal zones.	Analysis and Demonstration	STK-LS-02
LCH-GN-03	Interface	The flight termination system shall be able to be activated from the ground.	To ensure that there will not be a range safety violation, a manual actuation method for the FTS needs to exist.	Demonstration	STK-LS-01
LCH-GN-04	Functional	The vehicle shall be able to be transported in a 20 ft shipping container.	Ensures that the vehicle can be transported easily, decreasing the transport logistics complexity.	Inspection	STK-LS-02
LCH-GN-05	Performance	The vehicle shall be able to reach the PMC within 7 hours of it being sighted.	The minimum lingering time of a polar mesospheric cloud is 7 hours.	Demonstration	STK-MR-06
LCH-GN-06	Performance	The vehicle shall be able to be left in an unarmed, but otherwise prepared for flight, condition for a period of at least 5 days.	To ensure that the rocket will be ready for the appearance of a PMC, the rocket will be set up as soon as possible so minimum work needs to be done before launch. This means that the rocket needs to be in an assembled state for a max of 5 days.	Demonstration	STK-MR-06
LCH-GS-01	Interface	All Ground System equipment shall be designed in such a way that the system can be remotely switched ON/OFF from outside the danger area.	Enable remote switching ON/OFF of Ground System equipment from a safe location.	Testing	STK-LS-01
LCH-GS-02	Functional	At least two independent tracking systems shall provide real-time positional/instantaneous impact point (IIP) data during launch.	Using multiple independent tracking systems to provide real-time positional/IIP data is required by Esrange for redundancy [45].	Inspection	STK-LS-01
LCH-GS-03	Functional	The tracking systems shall be designed in such a way that no single-order vehicle failure mode or ground system failure mode could cause the loss of both systems.	Prevent loss of both tracking systems due to single-order vehicle or ground system failure.	Inspection	STK-LS-01
LCH-GS-04	Interface	The vehicle shall be capable of communicating with the Esrange ground system.	Necessary for tracking the state of the vehicle and being able to terminate its flight in case of emergency.	Demonstration	STK-LS-02

Table 5.3: Launch Site Safety and Simulation Requirements

Code	Type	Requirement	Motivation	V&V	Traceability
LCH-SF-01	Functional	The vehicle shall carry a flight termination system.	A flight termination system is required by Esrange for unproven vehicles [45].	Inspection	STK-LS-01
LCH-SF-02	Functional	Materials selected for use in hazardous chemical systems shall be compatible with the hazardous chemical used.	Compatible materials for hazardous chemicals, in case hazardous chemicals are used, are required by Esrange [45].	Analysis and Testing	STK-LS-01
LCH-SM-01	Performance	Probability of casualty (Pc) for individuals shall be below 1e-6.	Ensure probability of casualty for individuals is below a specified threshold.	Analysis	STK-LS-01
LCH-SM-02	Performance	The Casualty Expectation (CE) shall be below 30e-6.	Ensure the Casualty Expectation is below a specified threshold.	Analysis	STK-LS-01
LCH-SM-03	Performance	The probability of hitting an aircraft (Pi) shall be below 0.1e-6 for each impact area.	Ensure probability of hitting an aircraft is below a specified threshold for each impact area.	Analysis	STK-LS-01
LCH-SM-04	Performance	The probability of spent stages, experiment bodies, or other vehicle debris impacting on protected property areas shall be below 1e-3.	Ensure probability of debris impacting protected property areas is below a specified threshold.	Analysis	STK-LS-01
LCH-SM-05	Performance	The 1σ Gaussian impact dispersion shall be less than 20 km.	Limit the one σ Gaussian impact dispersion to less than a specified distance.	Analysis	STK-LS-01
LCH-SM-06	Functional	At least one tracking or other data source shall be utilized to determine impacts (either during the mission or through post-mission analysis) of vehicle components.	Utilize tracking or other data sources to determine impacts of vehicle components.	Inspection	STK-LS-01

Table 5.4: Avionics Requirements

Code	Type	Requirement	Motivation	V&V	Traceability
SYS-AV-01	Functional	The avionics shall be able to detect launch.	Important to determine required actions for the flight computer.	Analysis and Testing	STK-MR-07
SYS-AV-02	Functional	The avionics shall be able to detect apogee.	Important to determine required actions for the flight computer.	Analysis and Testing	STK-MR-07
SYS-AV-03	Functional	The avionics shall be able to detect touchdown.	Important to determine required actions for the flight computer.	Analysis and Testing	STK-MR-07
SYS-AV-04	Functional	The avionics shall be able to detect separation.	Important to determine required actions for the flight computer.	Analysis and Testing	STK-MR-07

Table 5.4: Continuation of the Avionics Requirements

Code	Type	Requirement	Motivation	V&V	Traceability
SYS-AV-05	Functional	The avionics shall be able to detect payload deployment.	Important to determine required actions for the flight computer.	Analysis and Testing	STK-MR-07
SYS-AV-06	Functional	The avionics shall have thermal protection against overheating.	In the mesosphere, electronics cannot be air-cooled. Need to ensure proper cooling even in near vacuum or by isolating the electronics.	Demonstration and Testing	STK-MR-01
SYS-AV-07	Interface	All avionics boards shall be capable of communicating with the ground stations.	To be able to monitor the rocket.	Demonstration and Testing	LCH-SM-02
SYS-AV-08	Functional	The avionics shall be able to store data on a flight recorder.	To ensure recovery of the data.	Inspection	STK-MR-07
SYS-AV-09	Functional	The avionics shall be able to monitor combustion chamber pressure.	To ensure triggering of FTS in the worst-case scenario.	Analysis and Testing	STK-MR-07
SYS-AV-10	Functional	The avionics shall be able to monitor engine temperature.	To ensure triggering of FTS in the worst-case scenario.	Analysis and Testing	STK-MR-07
SYS-AV-11	Functional	Each stage of the rocket shall contain an independent avionics board.	To ensure both stages can deploy their parachute.	Inspection	STK-RE-02
SYS-AV-12	Functional	Each stage shall contain 2 identical independent avionics boards for redundancy.	Redundancy to prevent failure.	Inspection	STK-RE-02
SYS-AV-13	Functional	The avionics shall have redundant flight recorders.	Redundancy to prevent failure.	Inspection	STK-RE-02
SYS-AV-14	Functional	All avionics sensors shall be redundant.	Redundancy to prevent failure.	Inspection	STK-RE-02
SYS-AV-15	Performance	The avionics shall be able to operate in a range of at least 90-315 K.	Expected temperature range of the environment.	Testing	STK-MR-01
SYS-AV-16	Performance	The avionics shall be capable of working in an environment of up to 90% humidity.	Expected humidity range of the environment in a worst-case scenario.	Testing	STK-MR-01
SYS-AV-17	Functional	The avionics shall be able to determine current position.	Required for tracking and recovery.	Analysis and Testing	STK-RE-02
SYS-AV-18	Functional	The avionics shall have at least one camera to monitor the stage separation.	Monitor proper deployment of the 2nd stage and allow for easier determination of the cause in case of failure.	Inspection	STK-MR-07
SYS-AV-19	Functional	The avionics shall have at least one camera to monitor payload deployment.	Monitor proper deployment of the payload deployment and allow for easier determination of cause in case of failure.	Inspection	STK-MR-07
SYS-AV-20	Functional	The avionics shall have at least one camera in the 1st stage to monitor recovery deployment.	Monitor proper deployment of the 1st stage recovery and allow for easier determination of cause in case of failure.	Inspection	STK-MR-07

Table 5.4: Continuation of the Avionics Requirements

Code	Type	Requirement	Motivation	V&V	Traceability
SYS-AV-21	Functional	The avionics shall have at least one camera in the 2nd stage to monitor recovery deployment.	Ensure proper deployment of the 2nd stage recovery and allow for easier determination of cause in case of failure.	Inspection	STK-MR-07
SYS-AV-22	Performance	The engine bay pressure sensor shall have a precision of at least 2 bar.	Minimum precision required for detecting engine failure.	Testing	SYS-AV-09
SYS-AV-23	Performance	The engine bay temperature sensor(s) shall have a precision of at least 3 K.	Minimum precision required for detecting engine failure.	Testing	SYS-AV-10
SYS-AV-24	Performance	The positioning system shall have a precision of ±20m.	Minimum precision required for recovering the rocket.	Testing	STK-RE-02
SYS-AV-25	Performance	The signal-to-noise ratio (G/T) shall be a minimum of 12 dBK^{-1}.	Minimum G/T required by the Esrange satellites to pick up the signal.	Inspection	STK-LS-02
SYS-AV-26	Interface	The telemetry shall adhere to IRIG standards.	Standard used by Esrange for downlink and FTS.	Inspection	STK-LS-02
SYS-AV-27	Performance	The telemetry system shall use a frequency between 2300–2400 MHz.	Frequency recommended by Esrange for standardization.	Inspection	STK-LS-02
SYS-AV-28	Performance	The telemetry system shall have a range of at least 150 km	To communicate with the ground, taking into account approximate flight profile.	Analysis and Testing	STK-MR-01

Table 5.5: General System Requirements

Code	Type	Requirement	Motivation	V&V	Traceability
SYS-GN-01	Functional	The vehicle shall have a propulsion system.	To reach the cloud, the vehicle shall be able to move itself.	Inspection	STK-MR-01
SYS-GN-02	Functional	The vehicle shall have a recovery system.	To reuse the vehicle, a recovery system should be fitted to make sure as much of the vehicle as possible survives.	Inspection	STK-RE-02
SYS-GN-03	Functional	The vehicle shall remain stable through the entire ascent phase of the flight.	To make the vehicle recoverable, it needs to be stable throughout the flight.	Inspection and Simulation	STK-RE-02
SYS-GN-04	Functional	The vehicle shall expose the payload to the environment during the measurement phase.	To prevent damage to the instrumentation, the payload will only be exposed to the environment when measurements are needed.	Demonstration	STK-MR-05

Table 5.5: Continuation of the General System Requirements

Code	Type	Requirement	Motivation	V&V	Traceability
SYS-GN-05	Performance	The tower exit velocity of the vehicle shall be at least 40 ms^{-1}.	Establishes the stability of the rocket while attached to the launch tower.	Analysis	SYS-GN-03
SYS-GN-06	Performance	The vehicle touchdown velocity shall be no more than 10 ms^{-1}.	Ensures that the payload and sensitive subsystems within the vehicle reach the ground safely.	Analysis and Testing	SYS-GN-02
SYS-GN-07	Functional	The rocket shall not be damaged during flight.	To minimize the parts needed to be replaced, the vehicle should not sustain damage during flight.	Inspection	STK-RE-01
SYS-GN-08	Functional	The rocket shall not be damaged during touchdown.	To minimize the parts needed to be replaced, the vehicle should not sustain damage during touchdown.	Inspection	STK-RE-01
SYS-GN-09	Functional	The rocket shall be locatable once landed.	To improve the chance of reusing the vehicle, it needs to be located after flight.	Demonstration	STK-RE-02
SYS-GN-10	Functional	The vehicle shall be able to measure its altitude throughout the entire flight.	Altitude is necessary to determine the correct deployment time of the payload.	Analysis and Testing	STK-MR-03
SYS-GN-11	Functional	The vehicle shall be able to measure its position throughout the entire flight.	The position data will be used to determine whether the payload actually deployed in the cloud and to prove the vehicle did not go out of bounds.	Analysis and Testing	STK-MR-03
SYS-GN-12	Functional	The vehicle shall be able to determine its attitude throughout the entire flight.	The attitude data can be used to determine whether sample capture occurred correctly and whether the vehicle was in the right orientation.	Analysis and Testing	STK-MR-03
SYS-GN-13	Functional	The vehicle shall be able to record the accelerations throughout the entire flight.	The acceleration data can be used to ensure that the instruments did not experience acceleration above their ratings and to confirm the vehicle adhered to the desired flight profile.	Analysis and Testing	STK-MR-07
SYS-GN-14	Functional	The vehicle shall provide measurement calibration data throughout the entire flight.	Certain instruments might need calibration parameters such as the temperature of the rocket body during flight.	Analysis and Testing	STK-MR-03
SYS-GN-15	Interface	The vehicle shall be able to support the mass of the payload.	The structural rigidity of the vehicle should be strong enough to not flex under the weight of the payload.	Analysis and Testing	STK-MR-02
SYS-GN-16	Interface	The vehicle shall not interfere with the functioning of the payload.	The vehicle exhaust and other factors should not influence measurements or cause interference.	Analysis and Testing	STK-MR-03

Table 5.5: Continuation of the General System Requirements

Code	Type	Requirement	Motivation	V&V	Traceability
SYS-GN-17	Functional	The vehicle shall shield the payload from the outside environment when non-operational.	To prevent damage to the instrumentation, the payload will only be exposed to the environment when measurements are needed.	Demonstration	STK-MR-06
SYS-GN-18	Performance	A single vehicle shall be able to be reused at least 10 times.	To promote sustainability, the requirement of 10 reuses is set.	Demonstration	STK-RE-01
SYS-GN-19	Performance	The vehicle shall withstand longitudinal accelerations of 25 g.	Ensures that the vehicle maintains structural integrity during flight. Value taken from OpenRocket simulation.	Analysis and Demonstration	STK-RE-02
SYS-GN-20	Interface	The payload shall be mountable to the vehicle.	The vehicle will need a physical interface with the payload to ensure structural rigidity.	Demonstration	STK-MR-02
SYS-GN-21	Performance	The vehicle shall have a stability margin of at least 2 when the speed is Mach 0.3.	Ensuring that the rocket is stable during flight.	Simulation	SYS-GN-03
SYS-GN-22	Performance	The vehicle shall have a stability margin of no more than 6 when the speed is Mach 0.3.	Ensuring that the rocket is stable during flight.	Simulation	SYS-GN-03
SYS-GN-23	Performance	The vehicle shall withstand lateral accelerations of 20 g.	Ensures that the vehicle maintains structural integrity during flight. Value taken from OpenRocket simulation.	Analysis and Demonstration	STK-RE-02
SYS-GN-24	Performance	The maximum dynamic pressure shall be 200 kPa.	Ensures that the vehicle will not go through extreme loads, even at high supersonic mach numbers.	Analysis	STK-RE-02
SYS-GN-25	Performance	Second stage engine shutoff shall be achieved at maximum 50km altitude.	Necessary to ensure that there are no exhaust products released into the mesosphere.	Analysis	STK-MR-06

Table 5.6: Payload Requirements

Code	Type	Requirement	Motivation	V&V	Traceability
SYS-PL-01	Performance	The payload shall be able to operate in a temperature range of 90-315 K.	The lower boundary is the temperature of the mesosphere, the upper boundary the temperature of the air at sea level	Testing	STK-MR-01
SYS-PL-02	Functional	The electronics shall have thermal protection against overheating.	To let the electronics function properly, they should not be overheated.	Testing	STK-MR-01
SYS-PL-03	Performance	The electronics shall be capable of working in an environment of up to 95% humidity.	Expected humidity range of the environment in a worst case scenario.	Testing	STK-MR-01

Table 5.6: Continuation of the Payload Requirements

Code	Type	Requirement	Motivation	V&V	Traceability
SYS-PL-04	Performance	The payload shall be capable of working in an environment of up to 95% humidity.	Expected humidity range of the environment in a worst case scenario.	Testing	STK-MR-01
SYS-PL-05	Performance	The payload shall be able to survive a maximum acceleration of 50 g.	The sounding rocket will launch with a high acceleration, afterwards the payload should still be able to make measurements.	Testing	STK-MK-01
SYS-PL-06	Interface	The payload instruments shall be capable of being mounted onto a baseplate.	Needed To ensure that the payload can be properly and easily integrated in the vehicle.	Inspection	STK-MK-01
SYS-PL-07	Functional	The payload shall have redundant flight recorders.	Ensures that the data gathered by the payload can be retrieved even in case one of the blackboxes fails.	Inspection	STK-MR-07
SYS-PL-08	Performance	The payload flight recorder shall be capable of storing at least 8 Gb of data.	Ensures that all the necessary data gathered can be stored properly.	Inspection	STK-MR-03
SYS-PL-09	Performance	The payload system shall pass vibrational qualification testing.	Necessary to ensure that the payload can withstand more vibrations than the worst case scenario load during launch.	Testing	STK-MK-01
SYS-PL-10	Performance	The payload system shall pass pressure qualification testing.	Necessary to ensure that the payload can withstand lower pressures than the worst case scenario load during launch.	Testing	STK-MK-01
SYS-PL-11	Performance	The payload system shall pass temperature qualification testing.	Necessary to ensure that the payload can withstand more extreme temperatures than the worst case scenario load during launch.	Testing	STK-MK-01
SYS-PL-12	Interface	The payload system shall be integrable in the vehicle.	Ensures that the vehicle can support the payload and its deployment possible, throughout all the mission phases.	Inspection	STK-MK-01
SYS-PL-13	Performance	The vehicle acceleration shall not exceed the maximum allowable accelerations of the instruments.	To complete the mission, the instrumentation cannot be damaged by the accelerations experienced during flight.	Analysis and Demonstration	STK-MK-01
SYS-PL-14	Functional	The experiment data shall be recoverable.	For the experiment to be useful, the data needs to be recovered.	Demonstration	STK-MR-03
SYS-PL-15	Functional	The payload activation altitude shall be adjustable until 90 seconds before launch.	In order for the rocket to deploy at the correct moment, the required altitude needs to be determined with the most recent simulations.	Demonstration	STK-MK-01
SYS-PL-16	Performance	The payload shall measure the water vapor density of the mesosphere with a range of at least 0-20 parts per million by volume.	This is the expected range of values for the mesosphere.	Analysis and Testing	STK-MR-05

Table 5.6: Continuation of the Payload Requirements

Code	Type	Requirement	Motivation	V&V	Traceability
SYS-PL-17	Performance	The payload shall measure the water vapor density of the mesosphere with an accuracy of at least 10%.	Current feasible resolution for measurements below 10 ppmv.	Analysis and Testing	STK-MR-05
SYS-PL-18	Performance	The payload shall be able to measure the temperature of the mesosphere with a range of at least 90-300 K.	Expected range of temperature experienced by the rocket.	Analysis and Testing	STK-MR-03
SYS-PL-19	Performance	The payload shall be able to measure the temperature of the mesosphere with a resolution of dT less than or equal to 0.1 K.	Minimum resolution required to detect a temperature trend.	Analysis and Testing	STK-MR-03
SYS-PL-20	Performance	The payload shall be able to measure the pressure of the mesosphere with a range of at least 0.1-100 mbar.	Expected range of pressure measured in the mesosphere.	Analysis and Testing	STK-MR-03
SYS-PL-21	Performance	The payload shall be able to measure the pressure of the mesosphere with an accuracy of at least 5%.	Minimum resolution for the data to be useful.	Analysis and Testing	STK-MR-03
SYS-PL-22	Functional	The payload shall be able to capture a sample of a polar mesospheric cloud.	To create a library of samples that can be analyzed in the future.	Demonstration	STK-MR-06
SYS-PL-23	Performance	The payload shall be able to sustain the transportation loads.	To complete the mission, the instrumentation cannot be damaged by the loads experienced during transportation.	Analysis and Testing	STK-MR-02
SYS-PL-24	Performance	The payload shall be able to sustain the flight loads.	To complete the mission, the instrumentation cannot be damaged by the loads experienced during flight.	Analysis and Testing	STK-MR-02
SYS-PL-25	Performance	The payload shall be able to sustain the launch loads.	Derived from SYS-PL-27	Analysis and Testing	SYS-PL-24
SYS-PL-26	Performance	The payload shall be able to sustain the coast loads.	Derived from SYS-PL-27	Analysis and Testing	SYS-PL-24
SYS-PL-27	Performance	The payload shall be able to sustain the recovery loads.	Derived from SYS-PL-27	Analysis and Testing	SYS-PL-24

Table 5.7: Propulsion and Power Requirements

Code	Type	Requirement	Motivation	V&V	Traceability
SYS-PR-01	Functional	The propellants used shall not contain any fossil fuel derivatives.	Related to the stakeholder requirement, ensures that the propellant trade-off is sustainable.	Inspection	STK-PR-01
SYS-PR-02	Functional	The ignition systems shall have at least 2 redundant safety mechanisms.	Ensures a safe handling process during rocket integration and launch procedures.	Inspection	STK-LS-01
SYS-PR-03	Functional	The ignition should have at least 2 indications of the triggering of the pyro.	Ensures a safe handling process during rocket integration and launch procedures.	Inspection	STK-LS-01
SYS-PR-04	Functional	The rocket motor shall have a failure mode of nozzle shear-out.	Ensures that in case of engine failure, the payload does not get damaged.	Analysis and Testing	STK-LS-01
SYS-PR-05	Performance	The rocket motors shall pass two qualification hot fire tests.	Requirement derived from Esrange qualification requirements.	Testing and Inspection	STK-LS-02
SYS-PR-06	Performance	The combustion chambers shall pass qualification hydrostatic testing.	Necessary to ensure that the combustion chamber can withstand hotfiring conditions. The testing pressure depends on the vehicle.	Testing and Inspection	STK-LS-01
SYS-PW-01	Performance	The power system shall power the vehicle for at least 60 minutes without external charging.	Necessary to account for possible time delays and nominal pre-launch procedures.	Inspection	LCH-GN-08
SYS-PW-02	Performance	The telemetry transmission power shall not be higher than 10W.	Defined based on Esrange power recommendations.	Inspection	STK-LS-02
SYS-PW-03	Functional	The payload and avionics shall have separate power systems.	Ensures that the power system is redundant and that not all electronics on board the vehicle are affected.	Inspection	SYS-AV-17
SYS-PW-04	Functional	The payload shall have redundant power systems.	Ensures that the payload is powered in case of a power system malfunction.	Inspection	SYS-AV-17
SYS-PW-05	Functional	The avionics shall have redundant power systems.	Ensures that the avionics are powered in case of a power system malfunction.	Inspection	SYS-AV-17
SYS-PW-06	Functional	The power systems shall be able to be externally charged from the tower.	Ensures that the vehicle can be powered after full integration, maximizing the amount of power on board the vehicle at the moment of launch.	Inspection	LCH-GN-08

Table 5.8: Recovery Requirements

Code	Type	Requirement	Motivation	V&V	Traceability
SYS-RC-01	Performance	The recovery system of the first stage shall have a reliability of 97.5%.	The system should have a total recovery rate of 95%; with two stages this means 97.5% for both.	Demonstration	STK-RE-02
SYS-RC-02	Performance	The recovery deployment system of the first stage shall have a reliability of 97.9%.	With an inflation reliability rate of 0.996 for space parachutes [46], the deployment will need a reliability of 97.9% to achieve 97.5% total.	Demonstration	STK-RE-02
SYS-RC-03	Performance	The recovery system of the second stage shall have a reliability of 97.5%.	The system should have a total recovery rate of 95%, with two stages this means 97.5% for both.	Demonstration	STK-RE-02
SYS-RC-04	Performance	The recovery deployment system of the second stage shall have a reliability of 97.9%.	With an inflation reliability rate of 0.996 for space parachutes [46], the deployment will need a reliability of 97.9% to achieve 97.5% total.	Demonstration	STK-RE-02
SYS-RC-05	Performance	The parachutes shall withstand the flight loads.	The flight loads depend on dynamic pressure, vehicle dimensions and mass, and deployment altitude.	Analysis and Testing	SYS-GN-04
SYS-RC-06	Performance	The parachutes shall withstand shock loads.	The shock loads can be quantified once the payload shock requirements are defined. The reaction also depends on the type of parachute used.	Analysis and Testing	SYS-GN-04
SYS-RC-07	Performance	The parachutes shall maintain stability.	Parachute stability can be quantified using angles of oscillation, dependent on the type of parachute, deployment altitude, and speed.	Analysis and Testing	SYS-GN-04
SYS-RC-08	Functional	The parachutes shall be orange.	To ensure clear visibility, orange is the best color.	Inspection	SYS-GN-04
SYS-RC-09	Performance	The deployment actuation system shall have a reaction timing of less than 0.5s.	Ensure that deployment occurs under the expected conditions	Demonstration	SYS-GN-04

6
Risk Assessment

Authors: M. Rusch, T. Odijk
Editor: C. Kendall
In this chapter, the risk assessment for the Altus mission is discussed. In Section 6.1 some background information on the Risk Management process is given. Section 6.2 explains the different types or risks that can be identified. Section 6.3 explains the Continuous Risk Management (CRM) approach and Section 6.4 shows how CRM can be applied to the risks for Project Altus. In Section 6.5 an overview of all identified risks is given.

6.1. Background

One of the most important aspects to understand about the mission are the risks involved. The design and handling risks of the system are important for the engineers and operators to understand , but it is also important to identify the biggest risks for the stakeholders in the project. The stakeholders are mostly interested in the performance risks, as these are directly related to the set requirements. For the engineering side all risks become important as the best way to prevent an accident, also referred to as departure, is to eliminate the root causes.

In risk management there is a split into two phases: the phase before the departure occurs, and the phase after the departure has occurred. This split is illustrated in Figure 6.1. To decrease the likelihood of a departure occurring, it is important to identify the causes of the potential departure. By putting prevention strategies in place, the probability of a departure is lowered. There should be mitigation steps in place to limit the the severity of the consequences of a departure, in case the prevention strategies fail to prevent a departure.

It is important to note that the difference between prevention and mitigation is based on the frame of reference used. When looking at a departure on a high level in the fault tree, mitigation methods for the low level departures may become prevention measures, and vice versa.

During the DSE, the above description of risk assessment was not known to the project group prior to performing the risk analysis. As such, the risks were found by globally analysing the system and identifying the biggest causes of departures. It is highly recommended that the risk analysis is revisited and worked out in more detail, according to the above methods, if the project proposal is accepted (discussed in Section 15.1.3).

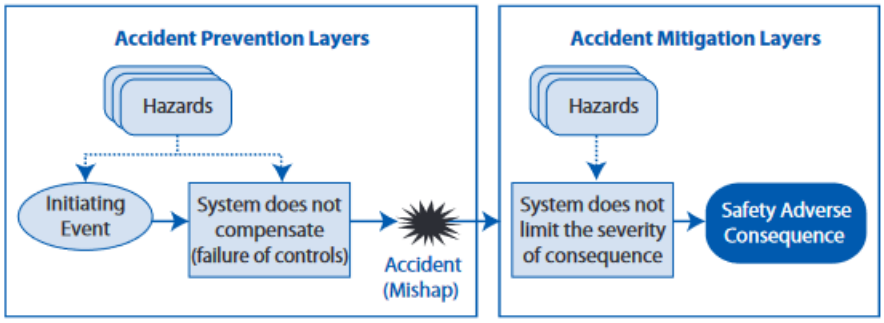

Figure 6.1: The difference between the prevention and mitigation phase. Taken from: [27]

A thorough understanding of the risks involved in the project is needed to ensure that no departures occur. Further to this, the risks also influence the design process. For instance, some of the prevention and mitigation methods can lead to new requirements for the system. The steps that need to be taken to minimise the likelihood and severity of a

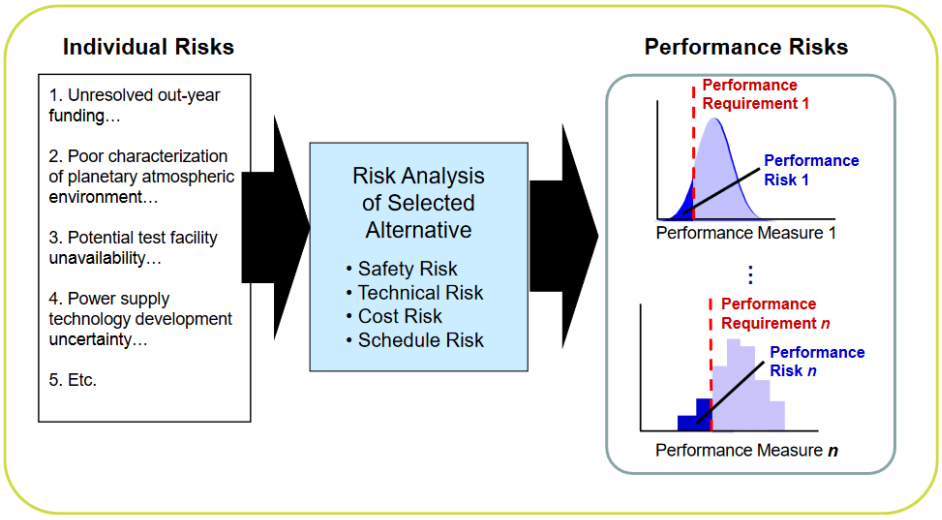

Figure 6.2: How individual risks gather to make performance risks. Taken from: [47]

departure are taken into consideration when designing the logistics and operations of the system. The steps relating to the control of the design should be taken into the verification and validation plan.

6.2. Risk Categorisation

Risks can be split into a number of different categories. The first split is for the level of the risk. There are performance risks which can be directly related to the risk of not meeting the performance requirements, as seen in Section 5.1. Individual risks can combine to form factors that cause a performance risk to occur, as shown in Figure 6.2. Further information on this phenomenon can be found in the NASA systems engineering handbook (2007) [27, ch. 6] and the NASA risk management handbook (2011) [47, ch. 2]. For instance, the vehicle not reaching the desired apogee is a performance risk, for which an individual risk is that the performance requirements were not properly communicated.

Individual risks are a specific issue of concern to one or more stakeholders which are presenting a risk to the achievement of one or more performance requirements.

Next to this the risks can be split over a number of mission execution domains.

- Safety, denoted with RSK-xx-SAF-xx (Making sure injuries are avoided, destruction of property, etc.)
- Technical, denoted with RSK-xx-TCH-xx (Performance of the system)
- Cost, denoted with RSK-xx-CST-xx (Will the project be within budget)
- Schedule, denoted with RSK-xx-SCH-xx (Will the project be on time)

6.3. Risk Management

The risk management process can be broken down into multiple steps and methods. One of these methods is Continuous Risk Management [27, 47]. CRM can be applied to multiple levels of the organisational hierarchy, and can be broken down into five steps: identify, analyse, plan, track and control.

Step 1: Identify

The first step – identify – focus on capturing the stakeholders' concerns about the performance requirements. This would mean that the stakeholder requirements are linked to an associated performance risk. For instance, the first stakeholder requirement – STK-MR-01: "The sounding rocket shall have a minimum total payload of 40 kg" – will be accompanied by a performance risk – "RSK-P-MR-01: The vehicle does not reach 90 km".

Step 2: Analyse

After the risks have been identified, they need to be characterised, such that they can be properly treated. The characteristics, that need to be identified first, are the likelihood of the departure occurring and the consequences of the departure. Once the likelihood and consequences of the risk are known, the time and date at which the risk was identified during the risk management process, and the time at which the departure can occur need to be documented. This, combined with the magnitude of uncertainty, allows for the risk to be properly addressed.

To give a more practical example of how this method works, a previously identified risk has been elaborated upon. One of the individual risks that has previously been found is engine over-pressurisation, as this can cause a failure of the engine. This risk has been investigated in more detail as it is one of the originally identified risks, and as it will have an impact on multiple performance risks. This investigation is described in Section 6.4.

Step 3: Plan

In this step the action points are established to mitigate the risk if needed.

- Accept: If a risk is tolerable, it will be accepted without mitigation
- Mitigate: Mitigation actions can be developed to address the drivers of the performance risks
- Watch: Risk drivers can be noted down for observation and development of contingency plans
- Research: A risk can be studied further to better understand the drivers and reduce the uncertainty
- Elevate: A risk can be elevated to a higher management level
- Close: A risk can be closed if all drivers are no longer considered potentially significant

Step 4: Track

The track step is where observable data and metrics on the risks are collected. Information is collected that could lead to the following.

- The discovery of a previously unidentified associated risk .
- A change in the analysis of risks.
- Changes in previously agreed upon plans.
- A previously agreed upon contingency needs to be implemented.

Step 5: Control

The last step is to analyse all measures that are in place to prevent or mitigate the risks. If these steps are not adequate new control actions need to be implemented to increase their effectiveness. These control actions can consist of revisions to the plan, or the creation of a new plan.

6.4. Risk Discovery

We have taken the risk, **RSK-PR-TCH-02**: “Engine over-pressurisation” as an example to work out in full detail, as seen in Figure 6.3. This risk was taken as the point of reference for the analysis. From this point of reference there is both a prevention and mitigation side. The mitigation side leads up to the stakeholder requirements via the performance risks and mitigation. The prevention side leads down to the root causes of the departure with prevention strategies in between to reduce the likelihood of reaching the chosen departure. During this process new risks were found and these were given an identifier. This is not reflected in the later tables as there is not enough time within the DSEs to fully complete this process. However, we did find that **RSK-P-MR-01** is equivalent to the already identified risk **RSK-LR-TCH-08**. From the mitigation and prevention layers a couple of links to different systems engineering tools can be identified. These links are to the requirements, verification and validation steps, logistics and operations, budgets and market analysis.

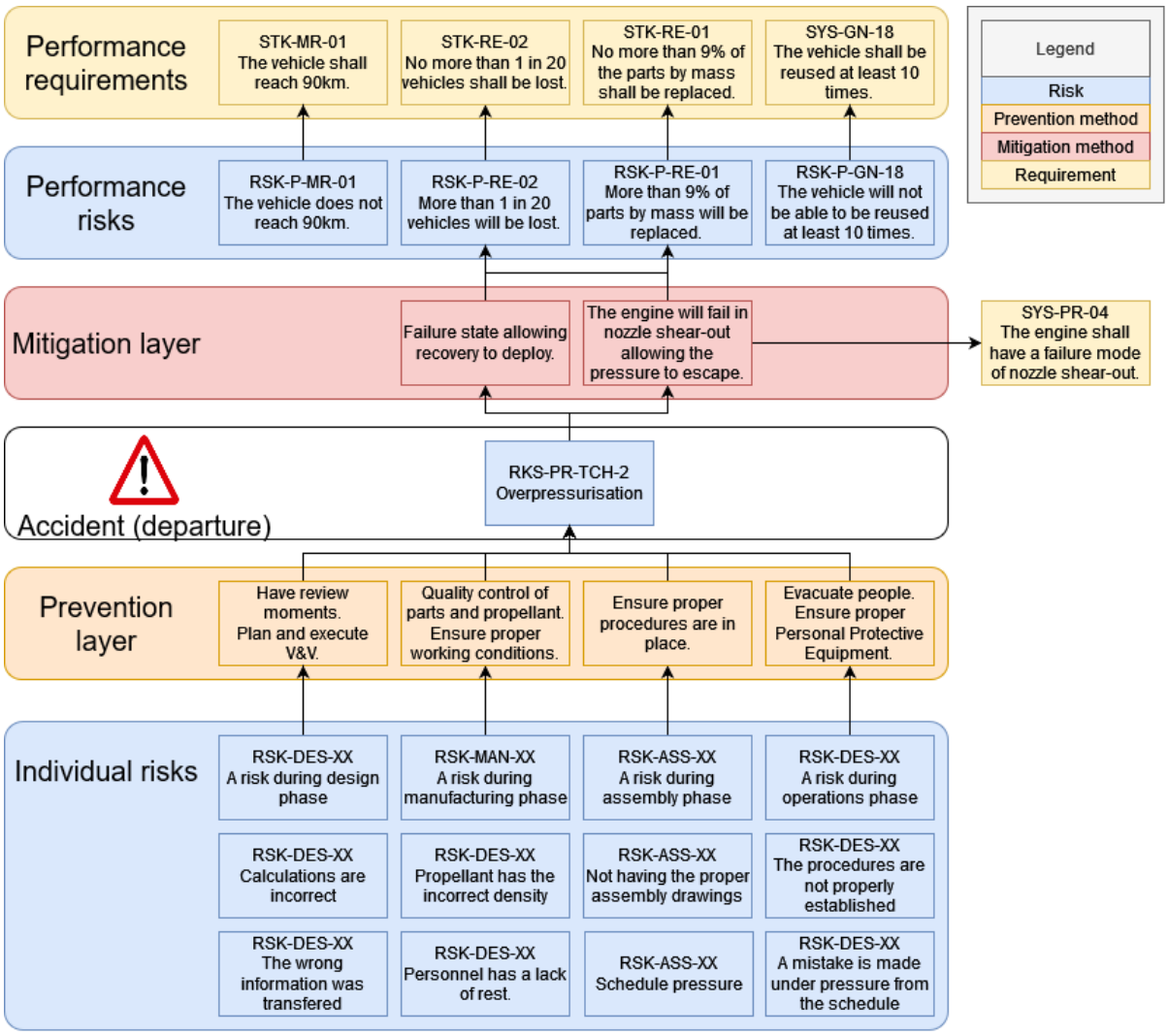

Figure 6.3: An exploration of risks, mitigations and contingencies from a departure point.

6.5. Overview of Risks

The risks that have previously been identified are sorted according to four categories: safety, technical, cost and schedule. Additionally, the prevention strategies are no longer split between probability and severity as all prevention measures will decrease the likelihood of a departure occurring. The mitigations, previously marked as severity mitigations, have been moved to the mitigation plan as these are all measures to reduce the consequences of the departure. This, however, means that not all risks have mitigation strategies as this is not always possible. Pre-mitigation risks are shown in the risk map in Figure 6.4, post-mitigation risks are shown in the risk map in Figure 6.5. The risks have, however, not been linked to other risks and requirements yet. This was deemed to be beyond the scope of the current project phase. The risks have also been grouped in a number of categories:

- Avionics – Table 6.1
- Integration risks – Table 6.2
- Launch and recovery phase – Table 6.3
- Manufacturing – Table 6.4
- Post-flight – Table 6.5
- Payload – Table 6.6
- Propulsion – Table 6.7
- Research and development – Table 6.8
- Recovery – Table 6.9
- Complete system – Table 6.10

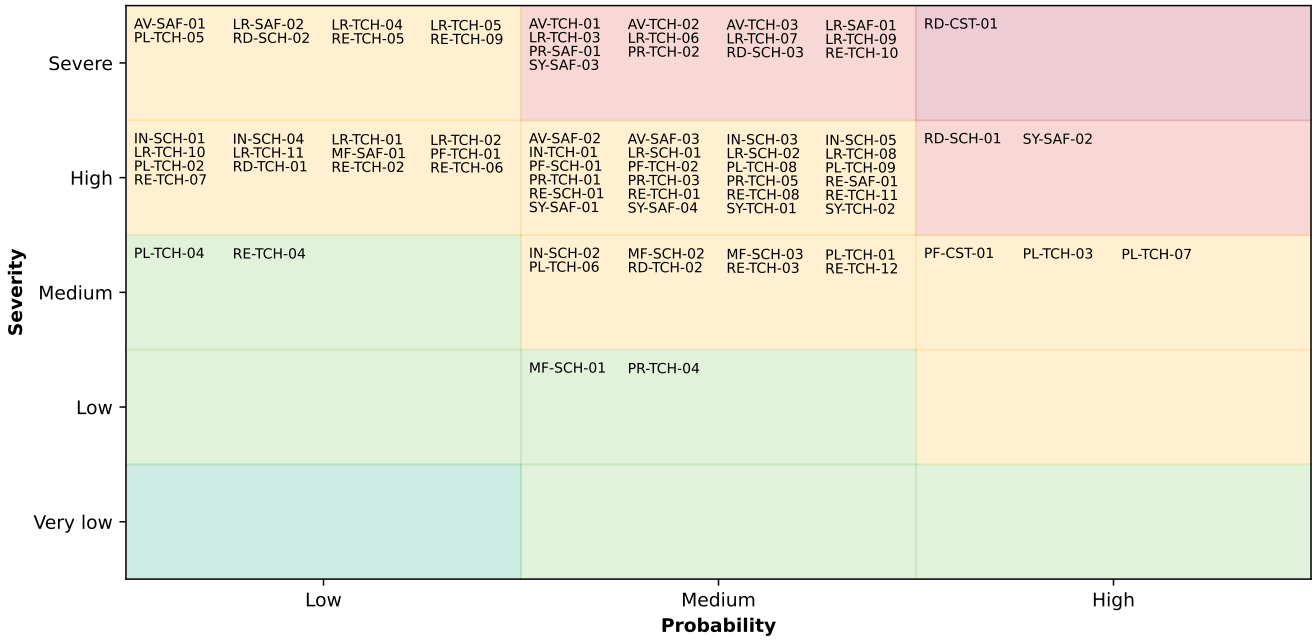

Figure 6.4: Risk map before management strategies

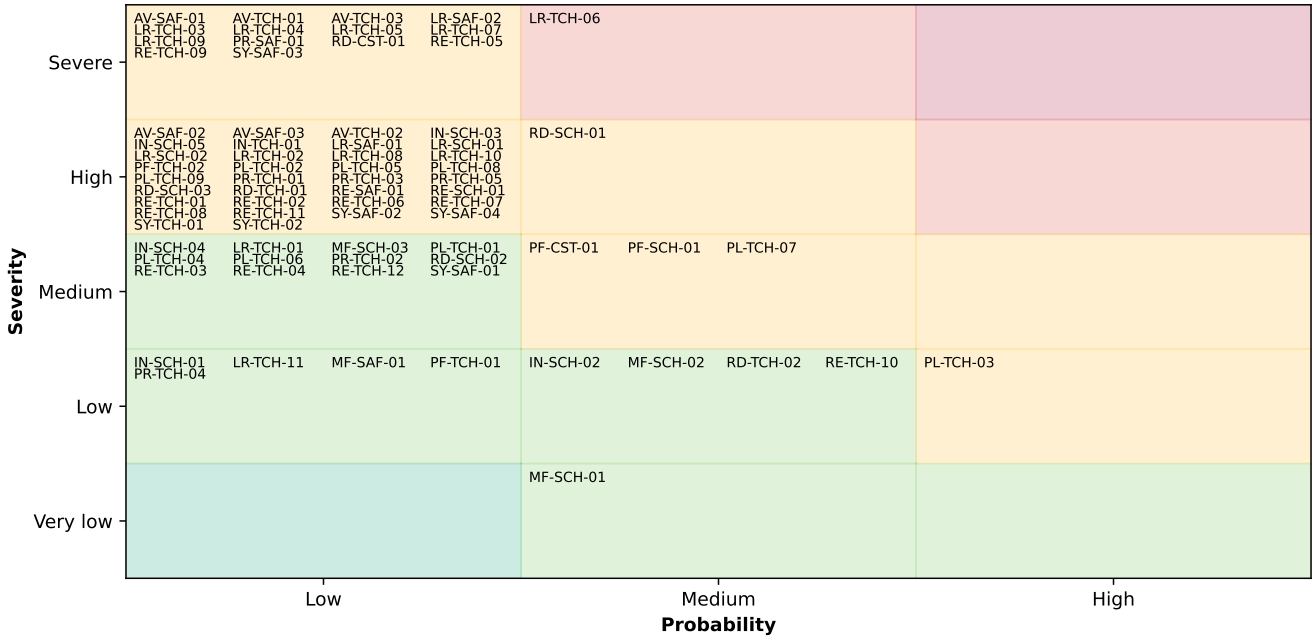

Figure 6.5: Risk map after management strategies

Table 6.1: Risks associated with the avionics

Risk ID	Risk	Probability	Severity	Prevention Strategy	Mitigation Plan	Post Probability	Post Severity
RSK-AV-SAF-01	Incorrect triggering of 2nd stage ignition	Low	Severe	Ensure multiple requirements for triggering ignition	Clear sufficient downrange area	Low	Severe
RSK-AV-SAF-02	Incorrect triggering of 1st stage parachute deployment	Med	High	Ensure multiple requirements for triggering deployment	Allow for margins in deployment time	Low	High
RSK-AV-SAF-03	Incorrect triggering of 2nd stage parachute deployment	Med	High	Ensure multiple requirements for triggering deployment	Allow for margins in deployment time	Low	High
RSK-AV-TCH-01	Loss of connection to groundstation	Med	Severe	Redundant systems and ensuring that nobody else is using that frequency in the area as well	Schedule more time during the window and backup windows	Low	Severe
RSK-AV-TCH-02	Battery fire	Med	Severe	Use battery protection and monitoring systems	Have fire fighting equipment close to battery at all times	Low	High
RSK-AV-TCH-03	Wires get pulled out	Med	High	Use latching and robust connectors	-	Low	High
RSK-AV-TCH-03	Electronics board failure	Med	Severe	Extensive testing of the board along with redundancy and an inspection before final assembly along with testing of the electronics in the expected environment (humidity, temperature, vibrations)	-	Low	Severe

Table 6.2: Risks associated with the integration phase

RSK-IN-SCH-01	Loss of essential personnel	Med	High	Ensure healthy work environment	Document suffiently and distribute expertise over people	Low	Low
RSK-IN-SCH-02	Delays and losses due to shipping	Med	Med	Contact suppliers ahead of time and make orders early	Find placeholder, use adaptive scheduling	Med	Low
RSK-IN-SCH-03	Hardware is damaged during integration and testing	Med	High	Proper integration procedures need to be written out. Allows for enough time to be allocated for each integration phase, and proper handling procedures.	Have spares on hand if possible	Low	High

Table 6.2: Continuation of risks associated with the integration phase

Risk ID	Risk	Probability	Severity	Prevention Strategy	Mitigation Plan	Post Probability	Post Severity
RSK-IN-SCH-04	Testing facility gets damaged	Low	High	Extensive verification before testing, clear Go/No-Go conditions specified	Establish relations that allow for the quick acquisition of a new location	Low	Med
RSK-IN-SCH-05	Delays in mission duration due to testing	Med	High	Prepare extensively for the testing campaign	Allow for margins in the schedule	Low	High
RSK-IN-TCH-01	Incompatible subsystems	Med	High	Set up proper system interfacing standards and guidelines early in the design process. These standards should be known during the design of all subsystems	Redesign the interfaces between the subsystems	Low	High

Table 6.3: Risks associated with the Launch and Recovery Phase

RSK-LR-SAF-01	Violation of allocated airspace	Med	Severe	Extensive Simulations thoughout the design process	Use FTS to terminate the flight	Low	High
RSK-LR-SAF-02	Unplanned/accidental launch	Low	Severe	Shunt igniter with Remove Before Flight (RBF) pin, test electronic safety features	Evacuate downrange before rocket is in tower, terminate flight	Low	Severe
RSK-LR-SCH-01	Improper Launch Conditions	Med	High	Plan launch window using historical weather statistics, plan suffient time on site	-	Low	High
RSK-LR-SCH-02	Unable to attain airspace clearance	Med	High	Plan launch window far in advance and reserve airspace accordingly	Move launchwindow	Low	High
RSK-LR-TCH-01	Loss of vehicle power	Low	High	Redundant power system and battery charging strategy.	-	Low	Med
RSK-LR-TCH-02	Loss of communication/telemetry	Low	High	Redundant communication systems and performing hardware checks during integration. Proper handling integration handling procedures of hardware.	-	Low	High
RSK-LR-TCH-03	In-flight stability problem	Med	Severe	Aerodynamic stability and control simulations need to be performed during the design and testing phases.	-	Low	Severe

Table 6.3: Continuation of risks associated with the Launch and Recovery Phase

Risk ID	Risk	Probability	Severity	Prevention Strategy	Mitigation Plan	Post Probability	Post Severity
RSK-LR-TCH-04	Unplanned structural disintegration	Low	Severe	Perform vibration and load tests during the integration/testing phases. Include strict safety margins on the structural properties of the vehicle in the early design stages.	-	Low	Severe
RSK-LR-TCH-05	Failure of flight termination system	Low	Severe	Design with redundancy in mind	-	Low	Severe
RSK-LR-TCH-06	Instrumentation failure	Med	Severe	Get instruments rated for the environment and conduct both vacuum and vibration testing. Essential instruments should have redundancy	-	Med	Severe
RSK-LR-TCH-07	Failure of recovery system	Med	Severe	Conduct extensive wind tunnel and drop testing of the parachute system to identify and mitigate failure modes. Recovery system can include redundancy	-	Low	Severe
RSK-LR-TCH-08	Target altitude not reached	Med	High	Target with a margin above the minimum required altitude, verify motor performance	-	Low	High
RSK-LR-TCH-09	Payload Deployment Failure	Med	Severe	Have a redundant deployment system	-	Low	Severe
RSK-LR-TCH-10	Data Logging Malfunction	Low	High	Have a redundant data system, on board storage and telemetry.	-	Low	High
RSK-LR-TCH-11	Ground station failure	Low	High	Extensive testing of the communications	Work with the backup ground system or scrub launch	Low	Low

Table 6.4: Risks associated with manufacturing

Risk ID	Risk	Probability	Severity	Prevention Strategy	Mitigation Plan	Post Probability	Post Severity
RSK-MF-SAF-01	Work and health safety incident	Low	High	Train personnel in proper safety practises.	Have people with first aid training and keep first aid supplies available	Low	Low
RSK-MF-SCH-01	Breakdown of fabrication tools	Med	Low	Ensure tooling is well maintained and not abused	Keep additional tooling and budget available to replace broken fabrication tools	Med	Very low
RSK-MF-SCH-02	Supply chain issues	Med	Med	Design the systems with standardised and widely available parts if possible. Keep backup options for critical components.	Redesign with available parts	Med	Low
RSK-MF-SCH-03	Manufacturing issues	Med	Med	Use proper technical drawings to communicate the manufacturing details to the machinists.	Remanufacture the parts	Low	Med

Table 6.5: Risks associated with the post flight phase and payload

RSK-PF-CST-01	Refurbishment cost higher than expected	High	Med	Design for refurbishment	Use margins in the budget and renegociate pricing	Med	Med
RSK-PF-SCH-01	Unable to refurbish vehicle	Med	High	Design the system for refurbishment	Construct new vehicle	Med	Med
RSK-PF-TCH-01	Data loss or corruption	Low	High	Backup data immediately after receiving, in the cloud and on a harddrive.	Attempt data recovery	Low	Low
RSK-PF-TCH-02	Unable to retrieve vehicle	Med	High	Use a satellite locator beacon	Reconstruct vehicle, don't leave harmful substances in vehicle	Low	High
RSK-PL-TCH-01	Sample collection malfunction	Med	Med	Test the system extensively on the ground	-	Low	Med
RSK-PL-TCH-02	Payload outgassing interferes with measurements	Low	High	Test interference on the ground	Deploy nosecone earlier to outgas quicker	Low	High
RSK-PL-TCH-03	Sensor malfunction	High	Med	Use redundant sensors	-	High	Low
RSK-PL-TCH-04	Radiation environment interfers with measurements	Low	Med	Use radiation hardend sensors and electronics	Use redundant sensors to increase accuracy	Low	Med

Table 6.6: Continuation of payload risks

Risk ID	Risk	Probability	Severity	Prevention Strategy	Mitigation Plan	Post Probability	Post Severity
RSK-PL-TCH-05	Loss of communication between payload and rocket	Low	Severe	Redundant logging and communication systems on the payload side to prevent loss of data	-	Low	High
RSK-PL-TCH-06	Errors in calibration of sensors	Med	Med	Do sensibility check on data, recalibrate sensors often	Try to retreive useful data after recalibrating the sensors	Low	Med
RSK-PL-TCH-07	Contamination of sample	High	Med	Create strict handling procedures and only open and close the sample container manually in a clean room	-	Med	Med
RSK-PL-TCH-08	Mechanical failure of payload	Med	High	Ensure mechanical robustness during testing of the payload	-	Low	High
RSK-PL-TCH-09	Payload integration error	Med	High	Have detailed integration procedures	-	Low	High

Table 6.7: Risks associated with propulsion

RSK-PR-SAF-01	2nd engine ignites after 1st stage failure	medium	Severe	Implement a number of electronic failsafes	Prevent ignition or terminate the flight using the FTS	Low	Severe
RSK-PR-TCH-01	Engine casing burn through	Med	High	Check for erosive burning and use ticker battleship chambers to characterise the engine. Use a thermal liner	-	Low	High
RSK-PR-TCH-02	Engine overpressurisation	Med	Severe	Implement the correct safety factor and characterise the engine properly	Design for the safest failure mode to occur first	Low	Med
RSK-PR-TCH-03	Combustion instability	Med	High	Check quality of the grains	Characterise motor behaviour better	Low	High
RSK-PR-TCH-04	Failed ignition 1st stage	Med	Low	Use redundant ingintion system	After safe light given, start preparing the same rocket again with a new igniter	Low	Low
RSK-PR-TCH-05	Failed ignition 2nd stage	Med	High	Use redundant ignition system	Attempt recovery without stage 2 ignition	Low	High

Table 6.8: Risks associated with the research and development phase

Risk ID	Risk	Probability	Severity	Prevention Strategy	Mitigation Plan	Post Probability	Post Severity
RSK-RD-CST-01	Budget overrun	High	Severe	Allow for sufficient margin in budget allocation	Find more funding or renegotiate with customer	Low	Severe
RSK-RD-SCH-01	Timeline overrun	High	High	Make planning flexible, such that you can make up for extended phases duration by shortening other phases, add margins	Extent the project timeline to launch later, make deadlines flexible.	Med	High
RSK-RD-SCH-02	Unable to attain permits	Low	Severe	Apply for permits early in the process	Get external help to fulfil permit obligations	Low	Med
RSK-RD-SCH-03	Unable to find system testing facility	Med	Severe	Locate multiple possible testing locations early in the design and have backup options.	Build relations that allow quick acquisition of alternative sites	Low	High
RSK-RD-TCH-01	Loss of design data	Low	High	Keep both local and remote backups, Constantly monitor data quality and status.	Start over from the last kept backup	Low	High
RSK-RD-TCH-02	Unsuitable Concept	Med	Med	Evaluate the concepts critically and in detail early on in the process in order to catch unfeasible projects before going into the design phase.	Plan an extra design iteration, start over with the conceptual design.	Med	Low

Table 6.9: Risks associated with the recovery system

RSK-RE-SAF-01	Collision during descend	Med	High	Check with the simulations the expected landing site and the probability of collosion	-	Low	High
RSK-RE-SCH-01	Extreme weather	Med	High	Lay out detailed Go/No-Go conditions. Plan time for delays	Wait until later date	Low	High
RSK-RE-TCH-01	Parachute gets tangled	Med	High	Create strict procedures for folding and packing the parachute and perform an inspection before final assembly	-	Low	High
RSK-RE-TCH-02	Parachute melts itself together	Low	High	Choose a parachute material that can handle the expected temperatures of the environment and provide protection for the parachute against the pyrotechnic exhaust	-	Low	High

Table 6.9: Continuation of recovery system risks

Risk ID	Risk	Probability	Severity	Prevention Strategy	Mitigation Plan	Post Probability	Post Severity
RSK-RE-TCH-03	Parachute drogue doesn't deploy	Med	Med	Extensive testing in a wind tunnel	Open the main parachute slowly to decrease it's chance of failing	Low	Med
RSK-RE-TCH-04	Parachute main not properly connected to drogue	Low	Med	Inspection before final assembly to check for proper connection to drogue	-	Low	Med
RSK-RE-TCH-05	Parachute not properly connected to rocket	Low	Severe	Inspection before final assembly to check for proper connection to rocket	-	Low	Severe
RSK-RE-TCH-06	Shock loads too high for parachute	Low	High	Perform simulations to check expected shockloads and to confirm the parachute can handle them and implement correct safety factors	-	Low	High
RSK-RE-TCH-07	Parachute doesn't inflate	Low	High	Use certified riggers for packing the parachute in the correct way	-	Low	High
RSK-RE-TCH-08	Mortar destroys parachute	Med	High	Test the mortar extensively on the ground	-	Low	High
RSK-RE-TCH-09	Pyrotechnics don't produce enough pressure	Low	Severe	Test the mortar extensively on the ground and use redundant pyrotechnics	-	Low	Severe
RSK-RE-TCH-10	Primary pyrotechnics don't fire	Med	Severe	Include redundant pyro	Use redundant pyrotechnics	Med	Low
RSK-RE-TCH-11	Structural misfabrication	Med	High	Inspect each parachute and fly them in a windtunnel	-	Low	High
RSK-RE-TCH-12	Incorrect deployment	Med	Med	Test the system extensively and use multiple conditions to determine when to fire the parachute (timer, dynamic pressure and Global Navigation Satellite System (GNSS))	Check complience with safety zone, terminate if exceeded	Low	Med

Table 6.10: Risks associated with the complete system

Risk ID	Risk	Probability	Severity	Prevention Strategy	Mitigation Plan	Post Probability	Post Severity
RSK-SY-SAF-01	Unstable rocket	Med	High	Perform simulations and testing of the dynamic and static vehicle stability for the relevant mach regimes	Terminate flight using FTS	Low	Med
RSK-SY-SAF-02	Rapid Unscheduled Disassembly	High	High	Implement correct safety factors and ensure all parts are checked extensively before during and after assembly	Evacuate the area and document the failure and debris. Perform a failure investigation to avoid similar failures in the future	Low	High
RSK-SY-SAF-03	Range Violation	Med	Severe	Create accurate similations to predict the change of the rocket leaving the range	Terminate flight when trajectory is off nominal	Low	Severe
RSK-SY-SAF-04	Launch attachment failure	Med	High	Design with a high safety factor, taking into account shocks and handling	Safe the system if still on the pad, otherwise, evacuate area	Low	High
RSK-SY-TCH-01	Staging malfunctions	Med	High	Test the separation in simulated environments to ensure correct and reliable staging	Terminate flight using FTS	Low	High
RSK-SY-TCH-02	Thermal loads too high	Med	High	Ensure that relevant safety factors are applied to the thermals	-	Low	High

7
Trade-off

To converge on a final vehicle architecture, the following approach was applied. First, design option trees were created for the various subsystems of the vehicle. These were made as exhaustive as possible. The next step was to prune these design option trees, since various options could be identified as unsuitable, and therefore, could be excluded from the list of feasible options. The remaining options could then be traded off so that the most suitable option could be identified. An important part of this process was that all the necessary trade-offs were identified. Afterwards, it was possible to evaluate if the result of a particular trade-off would be driving, independent, or dependent. A driving trade-off is one that will affect the design to a disproportionate amount. An independent trade-off does not depend on choices made for the other systems, while a dependent trade-off will depend on the others and thus needs to be analysed in greater depth. The classification of each trade-off can be found in Section 7.1.

All trade-offs were combined into configurations. These were then worked out such that some basic characteristics were known, such as a mass distribution over the sub-systems, as seen in Section 7.2. An estimation of the vehicle emissions and environmental costs was performed. The differences in handling procedures for each concept were identified. Finally, a cost estimate was attached to the configuration. Based on these data, the final vehicle configuration was chosen from the developed concepts. The further development of the chosen vehicle concept is detailed in Chapter 8. To increase confidence in the results, the robustness of the trade-offs has been investigated. This further allowed sensitive trade-offs to be identified and investigated such that their robustness can be increased. Sensitivity analysis is covered in Section 7.3.

7.1. Overview of the Trade-off

Author: T. Odijk

Editors: C. Kendall, L. Alonso

To make fair and consistent trade-offs, the method for all sub-system trade-offs was the same. The chosen method is the Analytic Hierarchy Process (AHP). This method includes a check to ensure that the assignment of the criteria weights happens in a consistent way. For this the criteria of the trade-off need to be established. After the method selection, this was the first step taken. These criteria followed from the stakeholder requirements that have been set for the project (detailed in Section 5.2). These requirements also drive the performance risks which have to be considered in the complexity criteria (detailed in Chapter 6).

The following list of systems was considered for this first round of trade-offs:

- Propulsion architecture
- Propellant(s)
- Structural materials
- Stage separation
- Recovery system
- Recovery deployment
- Nose cone deployment
- Stability and control
- Number of stages

Configuration-independent trade-offs

From this list, the propulsion type trade-off (between liquid, hybrid, and solid propellants), was deemed to be a trade-off that would drive the overall vehicle design. For this reason, it was treated as the first trade-off to be performed. It was found that solid propulsion would be the best option, in line with the current industry state-of-the-art.

There were also a number of trade-offs that were independent of all other trade-offs. The first of these was the propellant selection, in which the combination of ADN and HTPB was chosen. Secondly, the structural material that was selected is independent of the other systems. It was chosen to construct the vehicle fuselage from 7075 T6 aluminium. For the staging of the vehicle, the choice was made to use aerodynamic staging. This was deemed to be independent of the other systems. Finally, the recovery system trade-off additionally did not depend on the choices made in the other trade-offs. For the first stage, a single stage method was chosen, using only a main parachute. For the second stage, a dual stage recovery method was chosen. Dual stage recovery deploys a drogue to slow down the vehicle at high altitude and provide stability, followed by a main parachute deployment close to the ground for the final deceleration.

Configuration-dependent Trade-offs

After completing the driving configuration-independent trade-offs, the remaining configuration-dependent trade-offs are:

- Nose cone deployment method
- Stability and control
- Number of stages

All of these were deemed to be either too closely interlinked with other systems or too sensitive to be analysed in isolation. To alleviate this, five different configurations were made such these configuration-dependent systems can be examined in context.

7.2. Selection of Configurations

Author: T. Odijk
Editor: C. Kendall

The final trade-off for the vehicle configuration was performed using a number of established configurations. These configurations share the following common systems:

- Solid propulsion
- ADN + HTPB for the propellant
- Aluminium 7075-T6 for the structure of the rocket
- Aerodynamic staging (if applicable)
- The recovery method used is a drogue and main chute

The differences between the configurations are in the recovery and nose cone deployment, the stability and control, and the number of stages. An overview of the concepts is given in Table 7.1. To analyse the concepts, first-order simulations were performed to assess the total mass of the vehicle. This was mainly to differentiate between the single and dual-stage options. Further to this, the sustainability, handling and costs were analysed to find the most suitable option.

Table 7.1: Vehicle concepts including sensitive trade-off results

Concept	1	2	3	4	5
Stages	1	2	2	1	2
Deployment	Hot gas	Cold gas	Hot gas	Cold gas	Cold gas
Stability	No spin	No spin	Yo-yo de-spin	Yo-yo de-spin	Yo-yo de-spin

At the end of the analysis, the results were put together in a AHP style trade-off. The selected concept was number 5: the two stage, cold gas deployment with the yo-yo de-spin concept. This concept is further developed in Chapter 8.

7.3. Sensitivity Analysis

Author: M. Rusch

Editors: C. Kendall, L. Alonso

The robustness of the trade-offs was tested by means of a sensitivity analysis. The procedure for this is relatively straightforward. One by one, the weights of the trade criteria are varied, first upwards until the outcome of the trade-off changes, and subsequently downwards until the outcome changes. This yields a range of weights for which the result of the trade-off stays the same. The larger this stability interval is, the more robust the trade-off is to changes in weight for that particular criterion. Using this method, three trade-offs were identified that are sensitive.

The first of these is the propellant choice. When the importance of sustainability decreases, AP based propellants will win as opposed to the selected ADN based propellants. However, due to the nature of the stakeholders, this is very unlikely, so this trade-off is also considered robust.

The second trade-off that is considered sensitive is that of stability and control. Currently, the winner is the low spin rate with yo-yo de-spin. However, if the importance of feasibility decreases, and that of reliability, sustainability, and mass increases, the rolleron will come out as the winner of the trade-off. Further analysis has been performed on both options and when factoring in cost and TRL to the analysis, the confidence in the yo-yo de-spin being the most suitable option has increased.

The final trade-off that was found to be sensitive is that for the recovery deployment method. The Hot Gas Deployment Device (HGDD) is the original winner, but if the importance of sustainability increases, and that of reliability decreases, a Cold Gas Deployment Device (CGDD) is preferred. To increase the robustness of the choice, this trade-off has been categorised as a dependant trade-off and the design options were evaluated as part of the full vehicle concept instead of as a single subsystem. This resulted in the CGDD coming out as the definitive winner.

8
Preliminary Design

Determining the preliminary design of the vehicle is done using a sizing tool written in Python. This tool consists of a global program, which is discussed in Section 8.1. In Section 8.2 the simulation tool is explained, which is used to find the performance of the rocket at every iteration. Next, the payload is discussed Section 8.3 which drives the rocket diameter and the rocket mass. Lastly, the sizing of the propulsion, stability & control, structure, recovery, and avionics subsystems are explained in Section 8.4, Section 8.5, Section 8.6, Section 8.7, and Section 8.8, respectively.

8.1. Design Methodology

Author: M. Beenders
Editor: L. Tabaksblat

The preliminary design of the rocket relies on interdependencies between variables, such as the mass and the length of the rocket. Therefore, a sizing program has been devised to iterate the rocket until it meets all its requirements. This method allows for all subsystem sizing tools to be created in parallel, without the need to wait on values from other subsystems. When individual subsystem sizing tools are created, they can be combined into the main program, which can then run through tens of iterations in the span of a few minutes.

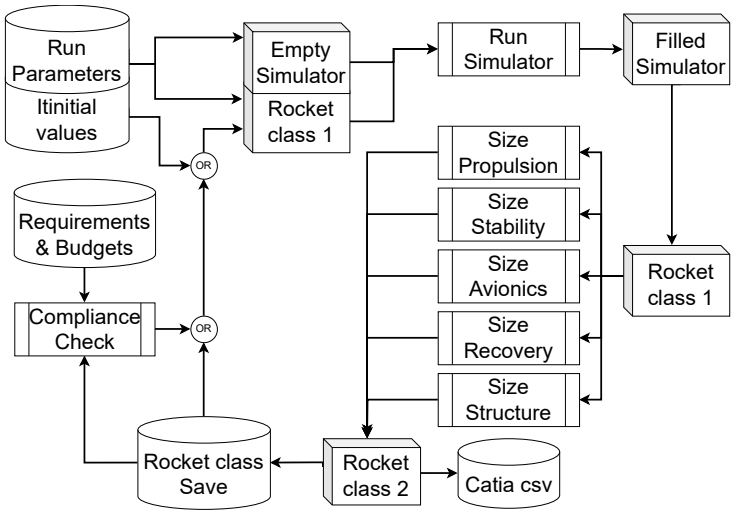

Figure 8.1: Code overview

To ensure that all the subsystem sizing programs are running on the same data, the sizing program has been designed around a global rocket data class, which houses all the variables about the rocket and its subsystems. When the program starts, this rocket class is loaded with initial values, which are a combination of constants, like propellant density, and educated guesses about, for example, the rocket mass. The educated guesses can also be randomised, which will be further discussed in Section 9.2. With the values initialised, the program sums its subsystem values, like mass and length, for the stages and then for the total rocket. This way the separate sizing tools and the simulation code can also use the total mass and length of the rocket. The rocket class is now fully initialised and ready for use.

The next step for the sizing tool is to simulate the rocket class, the workings of which will be further explained in Section 8.2. Running the simulation will output the apogee, maximum velocity and other trajectory-related values, which can be used as inputs for the sizing tools. Next, the program makes a copy of the rocket class, which it then distributes over the separate sizing programs. It makes these copies so that the sizing programs do not change each other's values during a concurrent iteration. During sizing, the program sizes the propulsion, stability and control, structure, recovery and avionics subsystems. These are elaborated upon, from Section 8.4 to Section 8.8. After the sizing tools have returned their values, the program checks if there are any double changes for the same variable to make sure nothing gets overwritten. The code then

combines all the changed values into a new rocket data class, which can then be used to start a new iteration.

To check if a rocket iteration complies with the requirements, the program checks all the variables, which are specified by a separate requirements file and checks their compliance. This analysis then outputs a small report of all values that do not comply with the requirements. Moreover, to ensure confidence in the code, such that it works as intended, it is verified and validated in Section 9.2.

8.2. Simulation

Author: M. Beenders
Editor: L. Alonso

One of the most important requirements is reaching a minimum altitude of 90 km (STK-MR-01). For the simulation, an apogee of 110 km was chosen to include a margin, additionally allowing more time for experimental measurements. This apogee target is also the main sizing parameter for the engine subsystem. Hence, the sizing program is equipped with a simulation algorithm that can quickly (≈26 ms) estimate the trajectory of the rocket and return the apogee and other variables, such as maximum velocity and the speed of sound.

The simulator works iteratively by first calculating all the forces, which are then converted to acceleration, and then integrated into velocity and location. Using the new location and velocity, the forces are recalculated and the cycle continues, until the vertical velocity reaches zero, indicating that the rocket has reached apogee. The simulator does not calculate the downward trajectory, as it cannot predictably mimic the effects of the recovery system and does not take into account wind effects, making it unusable for both recovery deployment simulations and downrange predictions.

The forces that are considered are gravity, thrust and aerodynamic drag, the forces created by the launch tower are neglected in this stage. However, the tower angle is taken into account and is taken to be 83°, as this is an often-used angle. This angle is simulated by keeping the rocket inclination locked until it reaches the tower exit velocity, which is chosen as an initial condition. The gravity force (F_G) is calculated using equation (8.1).

$$F_G = G\frac{M_E m_{rocket}}{(R_E + h)^2} \tag{8.1}$$

Where the gravitational constant $G = 6.6743 \times 10^{-11}\,\mathrm{m^3 kg^{-1} s^{-2}}$, the mass of the earth $M_E = 5.972 \times 10^{24}\,\mathrm{kg}$, the radius of the earth $R_E = 6.371 \times 10^{6}\,\mathrm{m}$, along with, h and m_{rocket} being the rocket altitude and mass, respectively. The thrust is simulated as a rectangular thrust curve, with a constant thrust for the duration of the burn time. The aerodynamic drag is calculated using analytical estimations discusses in Section 8.2.1.

8.2.1. Drag

Author: S. Yorucu
Editor: C. Kendall

Correctly assessing a vehicle's performance through simulation is significantly impacted by the accurate representation of the vehicle's environmental effects. One of the environmental effects being imposed on the entire vehicle is drag. For example, the drag allows for the conservative assessment of certain performance metrics, such as the thrust-to-weight ratio of the rocket. Also, the perfectly parabolic flight profile of a rocket is deviated due to drag, giving more realistic flight profiles.

Air flowing around a solid body induces some form of drag, which resists any movement of an object. In this case, the rocket will have to overcome drag, in the forms of skin friction drag and body pressure drag, also known as wave drag during the supersonic speed regime. Friction drag is due to the surface roughness of the rocket body and fins, while the body pressure drag is caused by the energy that is lost in pushing the air around the rocket, as well as by shock wave effects [48].

The drag sources are analysed using the Barrowman method, where the drag components are computed for both partially-laminar and fully turbulent boundary layers. However, it is assumed that the rocket will only be assessed using fully turbulent boundary layers, as it will be in the supersonic speed regime for the majority of its flight.

The different sources of drag, imposed on the different segments of the rocket, are elaborated upon in Section 8.2.1 and Section 8.2.1. The segments of the rocket that are considered are: the rocket body, nose cone, shoulder, fins, and base.

Skin Friction Drag

Author: S. Yorucu

The rocket experiences viscous flow around its body, generating frictional forces on its skin that disrupts flow. Several equations were used to assess the skin friction drag, using the vehicle dimensions to calculate the wet areas of the rocket segments. Additionally, corrections were made for compressibility effects during transonic and supersonic flight.

Firstly, the skin friction drag calculations are initiated by considering the surface roughness height (R_s) of the vehicle, which is assumed to be uniform and constant at a value of 50 µm. Another initial parameter is the critical Reynolds number (Re_{crit}), where transition of the flow from laminar to turbulent occurs. This is assumed to be a constant value of $5 \cdot 10^5$. Even though fully turbulent flow is assumed, it is important to assess the relation of transition with rocket speed. The position of transition, given by x_{crit}, Re_{crit} and the rocket speed (v_R), illustrated in equation (8.2).

$$x_{crit} = 1.5 \cdot 10^{-5} \left(\frac{Re_{crit}}{v_R} \right) \tag{8.2}$$

Below, in equation (8.3), x_{crit} is combined with R_s to obtain an initial estimate for the frictional drag coefficient, given by C_{fr}.

$$C_{fr} = 0.032 \cdot \left(\frac{R_s}{x_{crit}} \right)^{0.2} \tag{8.3}$$

Moreover, C_{fr} needs a compressibility correction for the high subsonic and supersonic speed regime, respectively, as provided in equation (8.4). Note that, a compressibility correction is necessary for taking into account changing atmospheric properties due to higher Mach numbers.

$$C_{fr_c} = \begin{cases} C_{fr}(1 - 0.1M^2) & \text{if } M \leq 1 \\ C_{fr}(1 + 0.15M^2)^{-0.58} & \text{if } M > 1 \end{cases} \tag{8.4}$$

where the corrected frictional drag coefficient is given by C_{fr_c}. Note that, in equation (8.5), a limiting case for the frictional drag coefficient is assessed. If the value of C_{fr_c} is greater in equation (8.5) than in equation (8.4), then the frictional drag coefficient is taken as the value provided by equation (8.5). This limiting case is due to surface roughness effects [48, p. 45].

$$C_{fr_c} = C_{fr}(1 + 0.18M^2)^{-1} \tag{8.5}$$

C_{fr_c} is now combined with geometrical parameters, to determine the total skin friction drag coefficient ($C_{D_{fr}}$) of the entire rocket, including the body and the fins. Equation (8.6) provides the relation;

$$C_{D_{fr}} = C_{fr_c} \frac{\left(1 + \frac{1}{2f_B}\right) S_{body_w} + \left(1 + \frac{2t_f}{\bar{c}}\right) S_{fins_w}}{S_{ref}} \tag{8.6}$$

where the fineness ratio (length-over-diameter) of the body is given by f_B and S_{ref} is the cross-sectional area of the vehicle, t_f is the thickness, and $\bar{c}$ is the mean aerodynamic chord of the fins. S_{body_w} is the wet area of the rocket body. S_{body_w} is calculated in equation (8.7):

$$S_{body_w} = S_{nc_w} + S_{sh_w} + S_{stage_w} \tag{8.7}$$

Hereafter, the subscripts: *nc*, *sh*, *u*, and *l*; are used to refer to the: nose cone, shoulder, upper stage, and lower stage, respectively. The wet areas of these segments are provided in equation (8.8)-equation (8.10).

$$S_{nc_w} = \pi D_u \frac{R}{\sqrt{\pi}} \sqrt{\phi_{nc} - 0.5\sin(2\phi_{nc})}, \quad \phi_{nc} = \arccos\left[1 - 2\left(\frac{X_{nc}}{L_{nc}}\right)\right] \tag{8.8}$$

The angular profile of the nose cone is ϕ_{nc}, and the length of the nose cone is L_{nc}. X_{nc} is the axial distance from the tip ($X_{nc} = 0$) to L_{nc} [49, p. 6].

In equation (8.9), the shoulder (otherwise referred to as the transition stage) wet area is conveyed;

$$S_{sh_w} = \frac{\pi D_l L_t}{\cos\left[\arctan\left(\frac{D_l - D_u}{2L_t}\right)\right]} \tag{8.9}$$

where the vertical transition length is given by L_t. The transition stage is located between the upper and lower stage. Their respective wet areas are given in equation (8.10) below.

$$S_{stage_u} = \pi D_u L_u \quad S_{stage_l} = \pi D_l L_l \tag{8.10}$$

Also, the upper and lower stages each have their own set of fins to ensure stability, elaborated upon in Section 8.5.1. This is illustrated in equation (8.11);

$$S_{fins_u} = 2n\frac{b_u}{2}\left(C_{r_u} + C_{t_u}\right) \quad S_{fins_l} = 2n\frac{b_l}{2}\left(C_{r_l} + C_{t_l}\right) \tag{8.11}$$

where the number of fins on each stage is given by n(=4). Regarding the geometrical properties, the root and tip chord is given by, C_r and C_t, respectively, as well as the semi-span by b. Note that a factor of 2 is applied to equation (8.11), as the wet area is seen on both sides of the fins. Finally, S_{ref} is conveyed in equation (8.12), where it is the outermost cross-sectional area of the rocket.

$$S_{ref} = \frac{\pi}{4} D_l^2 \tag{8.12}$$

Body Pressure Drag

Author: S. Yorucu

Pressure drag, or wave drag, is generated by the forcing of air around an object, in this case, the rocket. Wave drag is used while discussing the drag caused by shock waves. In this section, the pressure drag, experienced by the nose cone, shoulder, fins, and rocket base, will be covered and elaborated up on using formulae from literature [48, 50, 51, 52, 53].

Nose Cone Pressure Drag

From Section 8.6.1, the nose cone chosen for the vehicle was the LD Haack nose cone, which is mathematically derived to have the lowest drag theoretically possible [49]. The nose cone pressure drag coefficient ($C_{D_{nc}}$) is derived from empirical data [48, App. B]; is conveyed in equation (8.13);

$$C_{D_{nc}} = C_{nc_B}\left(\frac{C_{nc_0}}{C_{nc_B}}\right)^{\frac{\ln(f_{nc}+1)}{\ln 4}}, \quad C_{nc_B} = 0.85\left(\frac{q_{stag}}{q}\right) \tag{8.13}$$

where C_{nc_B} is the drag coefficient assuming a blunt cylinder as the nose cone, and is calculated using the stagnation factor (q_{stag}/q). Moreover, a reference nose cone drag coefficient, given by C_{nc_0}, is derived from literature [50, p. 16]. It has a value of 0 at subsonic speeds, and a value of 0.1 at supersonic speeds. The stagnation factor also depends on the speed regime, as conveyed in equation (8.14), below.

$$\frac{q_{stag}}{q} = \begin{cases} 1 + \frac{M^2}{4} + \frac{M^4}{40}, & \text{if } M \leq 1 \\ 1.84 - \frac{0.76}{M^2} + \frac{0.166}{M^4} + \frac{0.035}{M^6}, & \text{if } M > 1 \end{cases} \tag{8.14}$$

As a result, the nose cone pressure drag, is solely dependent on the Mach number and its fineness ratio (f_{nc}).

Shoulder Pressure Drag

The shoulder pressure drag is due to the air being forced around the conical separation stage of the rocket. It is assumed that the shoulder has the same drag coefficient as the nose cone ($C_{D_{sh}} = C_{D_{nc}}$) throughout its speed regime [48, p. 48].

The surface area that the airflow sees to generate the pressure drag above, is given in equation (8.15), below.

$$S_{sh} = \frac{\pi}{4}\left(D_l^2 - D_u^2\right) \tag{8.15}$$

Fin Pressure Drag

The following calculations for fin pressure drag ($C_{D_{fin}}$) are simplified, and only applicable, for fins with tapering trailing edges. The fin pressure drag formula changes in the speed regime, as can be seen in, equation (8.16), below.

$$C_{D_{fin}} = \begin{cases} -1 + (1 - M^2)^{-0.417}, & \text{if } M \leq 0.9 \\ 1 - 1.785(M - 0.9), & \text{if } 0.9 < M \leq 1 \\ 1.214 - \frac{0.502}{M^2} + \frac{0.1095}{M^4}, & \text{if } M > 1 \end{cases} \tag{8.16}$$

The leading edge slant angle (Γ_{LE}) is used to correct for cross-flow, as shown in equation (8.17).

$$C^*_{D_{fin}} = C_{D_{fin}} \cos(\Gamma_{LE})^2 \tag{8.17}$$

Note that, it is assumed that there is no additional drag from the trailing edge as it has a forward sweep, thus is tapered [48, p. 50]. Finally, the surface area of the entire fin is determined in equation (8.18), to be used in equation (8.22).

$$S_{fin} = \frac{b \cdot t_f}{\cos(\Gamma_{LE})} \tag{8.18}$$

Base Drag

The aftmost point of the rocket experiences drag due to there being a decreasing pressure gradient. Empirical formulae were created to determine the amount of base drag a rocket generates [48, p. 50]. The empirical formula was created, based on subsonic and supersonic speed regimes, and is provided in equation (8.19).

$$C_{D_{base}} = \begin{cases} 0.12 + 0.13M^2, & \text{if } M < 1 \\ 0.25/M, & \text{if } M > 1 \end{cases} \tag{8.19}$$

The surface area of the base (S_{base}) of the rocket is given in equation (8.20), to be used in equation (8.22).

$$S_{base} = \frac{\pi}{4} D_l^2 \tag{8.20}$$

Drag Summary

Combining the formulae provided in Section 8.2.1 and Section 8.2.1, the total drag coefficient of the rocket (C_D) can be calculated at any point in flight, given the rocket speed and atmospheric properties. The drag coefficient formula is given below in equation (8.21), along with the dynamic pressure (q_∞), relating the rocket speed (v_r) to the atmospheric properties, such as density (ρ_∞). The density in this model is calculated using the International Standard Atmosphere (ISA), which relates the altitude of the rocket to the current atmospheric properties.

$$\begin{aligned} C_D &= C_{D_{fr}} + C_{D_{nc}} + C_{D_{sh}} + C^*_{D_{fin}} + C_{D_{base}} \\ q_\infty &= 0.5\rho_\infty v_r^2 \end{aligned} \tag{8.21}$$

Thereby, the total drag force (F_D) of the rocket is given in equation (8.22):

$$F_D = q_\infty \left(C_{D_{fr}} S_{ref} + C_{D_{nc}} S_{nc} + C_{D_{sh}} S_{sh} + 4C^*_{D_{fin}} S_{fin} + C_{D_{base}} S_{base} \right) \tag{8.22}$$

where the surface areas (S) of each relevant structural component, are combined with their respective drag coefficients. Note that, $C_{D_{fin}}$ has a factor of 4 in front of it as there are 4 fins.

For easier implementation of the drag phenomena into the program, several assumptions had to be made. These assumptions are listed below in Table 8.1.

Assumption	Effect
Non-smooth surface	Introduces more energetic flow allowing for turbulence
Fully turbulent boundary layer	No laminar separation
High Reynolds number flight	$Re > Re_{crit}$
Interference drag small	Interference drag component zero
Fin tip vortices small	Ignore fin tip wave drag component

Table 8.1: Assumptions and their implications on calculations.

8.3. Payload

Authors: C. Kendall, D. Norbart

The payload is the driving element for many aspects of the vehicle design, including the diameter of the sustainer (which indirectly drives the diameter of the lower stage, since a sufficient diameter difference must be present to ensure aerodynamic stage separation) and the overall vehicle sizing.

The payload section has an outer diameter of 150 mm. This enables a standard cubesat (of diagonal length $100\sqrt{2} \approx 141.42$ mm) to just fit inside the payload bay if a 3 mm skin is used. The instruments used in Altus' primary scientific mission all have diameters of less than 150 mm and so are not driving in this case. Additionally, the payload will also use the empty space in the nose cone to decrease the length of the rocket.

The primary scientific mission is to investigate PMCs, a suite of instruments is needed. The environment in which the three parameters will be measured is very harsh. The pressure at 80 km is around 0.89 Pa and the temperature $-77\,^{\circ}$C [2], which makes it very challenging to have measurement instruments that have a good accuracy. Normal thermometers, for example, will not work at these ranges (as the thermal inertia of the thermometer itself tends to dominate the measurement rather than the actual air temperature).

Sample Collection

The sample collection mechanism will be located in the nose of the rocket. It will be protected by the nose cone during the first part of the flight. When the rocket approaches the altitude of the PMCs, at around 60 km the nosecone is ejected and the sample collection device is exposed. As the nosecone will not reattach, the collection device itself also has a turning disc containing a few holes. This disc can be turned such that its holes line up with the outside holes of the device, or that all of them are offset. This last state prevents contamination with particles from outside the Polar Mesospheric Clouds. The holes on the collection device will be in the axial direction, on the front of the rocket [54].

PMCs are a thin layer of cloud, normally not thicker than 1 km [55]. The sounding rocket will travel unguided in a parabolic arc through the mesosphere. Furthermore, due to dynamics in the atmosphere like wind and the unpredictability of the exact performance of the engine, it is impossible to tell exactly what the apogee of the rocket will be. Especially as the clouds do not always appear at the exact same height [13], it was deemed impossible to target the apogee of the rocket exactly in the clouds. The solution chosen is to fly through the clouds on vehicle ascent, and again during descent.

The sample collection device is passive, which means that there is a difference in speed necessary between the PMC particles and the rocket. As the movement of the clouds is assumed to be slow, this means that the rocket will need to have a high enough speed in the sample collection phase. Additionally, care must be taken with where the sample collection device is located in the rocket. Based on the initial analysis, it will be in the nose with the opening axially

forward. In the normal travelling direction, particles can flow into the collection system from the top. On descent however, the rocket will most likely not be in the correct orientation for sample recovery. Therefore, only the ascent phase though the clouds will be used to collect samples. The descent will be used to make extra measurements of temperature, pressure and humidity.

The particles consist of ice, which is very fragile and can also melt. To minimise damage to the particles before analysis, the particles must be stored in the correct way. When the particles are collected, they impact on the aerogel sample plate and get trapped in the material. This slows the particles over a longer distance than, for example, metals would do [56]. The particles will sustain minimal damage in this way; this technique has been demonstrated with cosmic dust [57]. An added benefit is that the aerogel conducts heat very poorly, make it easy to keep the particles at their low temperature. The compartment will be climate controlled, such that the humidity can be kept to a minimum. This prevents the particles from growing further from humidity trapped within the rocket during the descent phase of the flight.

Environmental Sensing

Additionally to the sample collection, it is necessary that the environmental properties of the PMCs are measured. The chosen properties to measure were the external temperature, humidity and pressure. These measurements can only be taken by specialised measurement equipment optimised for measurements in near-vacuum conditions. Such equipment is not available off the shelf, and so custom equipment must be used.

Temperature Measurement

To measure temperature at low pressures and temperatures, with a low thermal inertia, a sonic thermometer is used. This system does not use thermal conductivity, as the thermal inertia of the device would be hindering the measurements. Instead, it derives the temperature from the speed of sound, as they are directly linked by the equation $a = \sqrt{\gamma R_{air} T}$. The thermometer sends out a sound wave and listens on the other side of the instrument, which has air in between. The phase shift, with a known distance between sender and receiver, can be linked to the speed of sound. A sonic thermometer has been shown to be capable of measurements from 78 K to 293 K, with an accuracy of 0.1 K [58].

Pressure Measurement

For measuring pressure, a Dual Absolute Pressure Measuring Transducer (DAPMT) sensor will be used. This system works by ionising the air and measuring the conductivity. From the conductivity measurement, the pressure of the air can be calculated. This sensor is specifically made for flight on a sounding rocket [59]. The demonstrated measurement range is from 0.13 Pa to 1333 Pa. Within this range, the DAPMT has an accuracy of 7%, as the conductivity of the air is not perfectly predictable. However, this has been judged to be sufficient for the measurements necessary for the mission.

Humidity Measurement

Normal humidity sensors rely on measuring the dew point of the water vapour. At mesospheric conditions, this is not possible. Therefore, a Lyman-α hygrometer [60] will be used. This device depends on the absorption of light by the water molecules in the air. UV-radiation is sent out at the frequency which is absorbed; the amount of light received on the other side of the device corresponds to the water vapour in between (similar to how a smoke detector may detect smoke by the blocking of radiation within the device). Some development is still necessary to get this method to work on a sounding rocket, but this is expected to be feasible [61].

Structure

The payload mass cannot be properly calculated yet, as the exact payload shapes and connectors are still hard to determine. Therefore, these will only be calculated during the final design. To account for this unknown, a factor of 1.3 on the mass is used to approximate the payload mass and add a margin to the mass in general. As the structure mass will be relatively low, a factor of only 1.1 is added to the payload costs.

Budgets

In Table 8.2 the mass and cost of the payload are presented. This information was sourced from the references of the individual instruments from the previous sections. The budgets regarding the power and data are further discussed in Section 8.8.

Table 8.2: Summary of the Payload

Name	Mass [kg]	Cost [€]
Pressure Gauge	<2.5	10,500
Thermometer	0.7	14,251
Hygrometer	2	18,444
Sample Collector	4	25,000
Factor	x 1.3	x 1.1
Total	<12	75,015

8.4. Propulsion Sub-System

The main function of the propulsion system is to provide the necessary thrust force to ensure that the payload, onboard the Altus vehicle, will reach the desired apogee of 110 km. The system is comprised of two solid motors, for each of the two stages of the launcher.

To design the propulsion system for the two stages of the rocket, three software tools have been used: proPEP, a custom Python sizing tool and OpenMotor. Their input and output parameters are outlined in Figure 8.2, as well as their functionalities. These parameters are outlined within this section, alongside an overview of the main propulsion system parts: propellant, grain, casing, liner, nozzle and igniter. each of these propulsion system parts are detailed in their respective subsections.

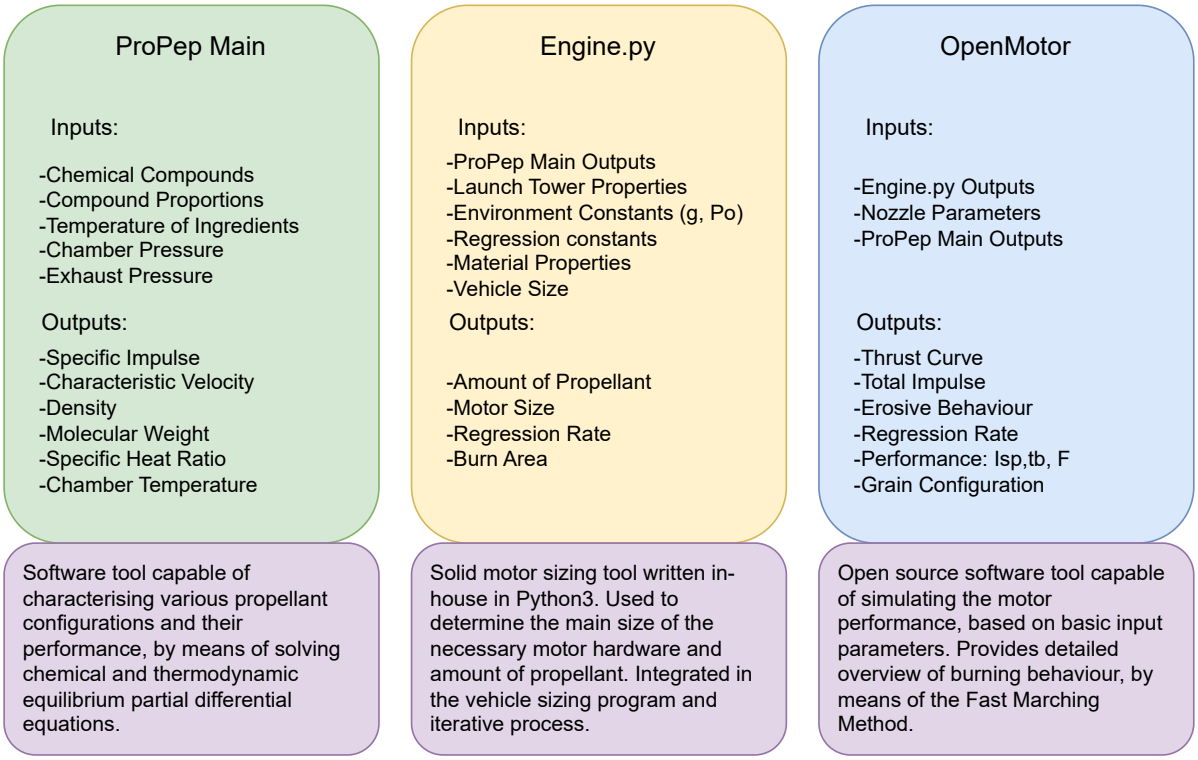

Figure 8.2: High-Level Functions of Propulsion System Software Tools

8.4.1. Design Parameters

Author: S. Aurori
Editor: C. Kendall

The desired output of the propulsion system sizing process is the size in terms of mass, length-to-diameter ratio, and the performance regarding produced thrust to propel the vehicle to 110 km. Beside this, it is required to ensure that the solid motors are feasible to produce and operate, hence, an assessment of the regression rate, erosive behaviour and obtained thrust curves is performed, by means of OpenMotor simulations. The outputs of these parameters are analysed based on values recommended by literature. The ballistic operators, such as total impulse, burn time, combustion pressure and propellant composition are varied in steps during the iterative process, within the developed Python sizing program.

In order to design the propulsion system, it is necessary to distinguish the independent design variables from the dependent ones. The first category can be further split into control and design variables [62]. The control variables are the ones that influence the dependent parameters. Finally, there are factors that influence the design and performance of the system, which fit into the uncontrolled variable category, such as environmental factors. For the specific design of the Altus vehicle propulsion system, the variables and their designated category can be found in Table 8.3. The control variables are related to the tower parameters, which flow from the launchsite requirements and system requirements. The fixed and later, iterated upon variables within the engine.py tool, OpenRocket, ProPEP and OpenMotor, are outlined under design variables. The dependent variables are results of simulations within the tools used, based on the input variables. An explanation of the origin and usage of the parameters through the three used software tools is provided in Figure 8.2.

Table 8.3: Overview of Propulsion System Variable Types [62]

Independent Variables			
Control	Design	Dependent Variables	Uncontrolled Variables
Effective Tower Length	Propellant Composition	Specific Impulse	Ambient Pressure Sea Level
Tower Exit Velocity	Grain Configuration	Propellant Density	Ambient Pressure End Burn Time
	Nozzle Throat	Characteristic Velocity	
	Nozzle Exit Area	Specific Heats Ratio	
	Pressure Coefficient	Regression Rate	
	Pressure Exponent	Port-to-throat Ratio	
	Total Impulse	Casing Thickness	
	Thrust	Casing Length	
	Chamber Pressure	Propellant Mass	
	Casing Outer Diameter	Casing Mass	

The design of the system starts with identifying the interactions between the solid motors with the rocket, and the propulsion subsystems. The vehicle is required, according to the system requirement SYS-GN-05 to exit the launch tower with a velocity of at least $40\,\mathrm{m\,s^{-1}}$, from Table 5.5. This further influences the initial amount of thrust required and the acceleration of the booster stage of the rocket. According to preliminary simulations conducted in an earlier design stage in OpenRocket, the burn times of both the booster and the sustainer are approximated to 15 seconds and 10 seconds, respectively, which allow for the initial value of the Total Impulse to be determined, as 125 547.6 N s and 75 622.45 N s. These are calculated based on the product between the thrust force and motor burn time. These values are further used as input variables, which are iterated upon in the Python tool, in order to ensure that the vehicle reaches the desired altitude of 110 km.

Furthermore, it is needed to assess the propellant composition and performance. The main chosen propellants are ADN and HTPB, in a proportion of 36% and 12%. These compounds, together with ammonium nitrate, aluminium, diocyl adipate, and oxamide in proportions of 28%, 14.5%, 6%, and 2%, needed as binding compounds and as

stabilisers of the propellant combustion, are plugged into the ProPEP software (described in Brown (1995) [63]). An overview of these values can be found in Table 8.5. The tool contains base files with information on these chemicals. The chemical equilibrium at the selected combustion pressure is calculated, based on the chemical principle of the minimisation of Gibbs free energy.[14] The program then outputs: specific impulse, characteristic velocity, combustion temperature, specific heat ratio, and density. The values for these parameters can be found in Table 8.4.

Having the propellants characterised and the initial thrust (F), total impulse (I_t) and specific impulse (I_{sp}) determined, the amount of propellant needed and its consumption can be found. The propellant mass, $M_{propellant} = I_t/(I_{sp} \cdot g)$ is found to be approximately 64 kg for the booster and 32 kg for the sustainer. Furthermore, the mass flow rate, $\dot{m} = F/(I_{sp} \cdot g)$ is determined to be approximately $4.27\,\mathrm{kg\,s^{-1}}$ for the first stage and $3.15\,\mathrm{kg\,s^{-1}}$ for the upper stage. These values are varied throughout the iteration phase, until convergence between the values characterising all the subsystems and the desired apogee is achieved.

Table 8.4 outlines the inputs for all the propulsion system subsystems: the propellant characteristics, environment constants, nozzle dimensions, rocket body dimensions, launch tower parameters,and casing material properties. These are the values used at the beginning of the iterative process. Values such as the total impulse for both the first and second stage, combustion pressures, launch tower length, and exit velocity have been altered during the iterations.

Table 8.4: Propulsion System Input Variables

Parameter Name	Symbol	Assigned Value	SI Units
Launch Tower Length	l_{tower}	17	m
Launch Tower Exit Velocity	v_{tower}	40	$\mathrm{m\,s^{-1}}$
Gravitational Acceleration	g	9.80665	$\mathrm{m\,s^{-2}}$
Ambient Pressure	P_0	101325	Pa
Total Impulse First Stage	$I_{t,1}$	125547.6	N s
Total Impulse Second Stage	$I_{t,2}$	75622.45	N s
Combustion Pressure First Stage	$P_{C,1}$	4	MPa
Combustion Pressure First Stage	$P_{C,2}$	2.5	MPa
Volumetric Loading	V_l	0.8	–
Specific Impulse First Stage	$I_{sp,1}$	200	s
Specific Impulse Second Stage	$I_{sp,2}$	245	s
Specific Impulse Correction Factor	cc	0.95	–
First Stage Diameter	D_1	0.2	m
Second Stage Diameter	D_2	0.15	m
Characteristic Velocity	c^*	1490	$\mathrm{m\,s^{-1}}$
Propellant Density	$\rho_{propellant}$	1570	$\mathrm{kg\,m^{-3}}$
Ratio of Specific Heats	γ	1.26	–
Yield Strength Al6082	σ_y	260	MPa
Al6082 Density	ρ_{casing}	2700	$\mathrm{kg\,m^{-3}}$
Safety Factor	SF	1.425	–
Pressure Coefficient	a_{pres}	0.000001	–
Pressure Exponent	n_{pres}	0.56	–

Alongside the propellant mass, determining the propellant's volume and distribution in the vehicle is necessary. In order to find the propellant volume, some factors need to be taken into account: the propellant mass that was determined earlier, the proportion of propellant to port space, the diameter of the rocket, and the propellant density. The mass, density, and diameter are easily determined, however, the proportion of empty space in the grain depends

[14] `http://www.nakka-rocketry.net/th_prope.html` [10/06/2023]

on the grain port configuration, which is not included in the iterative process automatically, since it is determined by human design decisions, validated in OpenMotor simulations. To account for this, the volumetric loading figure, V_l, is assumed to have a value of 0.8, which allows for both bi-dimensional and three-dimensional port configurations [64, Figure 1]. The volumetric loading is defined as $V_l = V_{propellant}/V_{available}$, the ratio between the propellant volume and the available volume within the combustion chamber [64].

To determine the volume of a grain and its length, which includes the empty port volume as well, equation (8.23) is used [64]. The port volume entails the empty volume found in the centre of the propellant grain.

$$V_{ch} = \frac{m_p}{\rho_{prop} \cdot V_l}, \quad l_{ch} = \frac{4 \cdot V_{ch}}{\pi \cdot d_{grain}^2}, \quad d_{grain} = d_{stage} - 2 \cdot t_{casing} \tag{8.23}$$

8.4.2. Propellant

Authors: C. Kendall, S. Aurori

Editor: L. Tabaksblat

An ADN-based propellant, with HTPB binder was selected in the propellant trade-off. This propellant combination removes hydrochloric acid from the rocket exhaust products, which is the main environmental pollutant when considering conventional APCP motors. It is also performant and highly industry relevant compared to propellants based only on ammonium nitrate, which do not have sufficient performance for orbital applications.

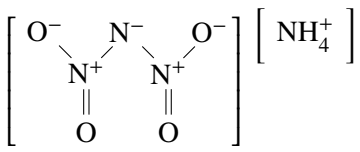

(a) Chemical structure of Ammonium DiNitramide

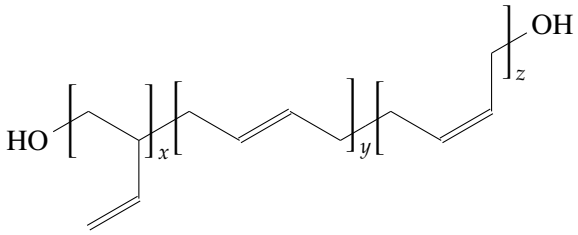

(b) Chemical structure of HTPB

Literature indicates a higher burn rate for ADN propellants than is desirable for Altus. Of note is, that it is currently extremely difficult to give quantitative predictions of solid rocket propellant regression characteristics, although machine learning approaches are showing some promise in this area [65].

Propellant burn rate is usually characterised according to equation (8.24) [66, p. 12].

$$v = a_{pres} P_{chamber}^{n_{pres}} \qquad (n < 1) \tag{8.24}$$

The burn rate is dependent on the combustion pressure, $P_{chamber}$, the pressure coefficient a_{pres} and the pressure exponent n_{pres}. A value of $n_{pres} < 1$ is necessary for stability of operation, as a motor with $n_{pres} > 1$ will undergo pressure runaway. This means that small changes in the burn area caused by grain casting imperfections or particle size difference can translate into a significant pressure increase. Any change in pressure will result in a diverging overall pressure, which is not desirable. Typical values of n_{pres} for composite rocket propellants are between 0.2 and 0.6 [67, Section 11.1].

Table 8.5: Propellant Components

Component	%w/w
Ammonium Dinitramide	36
Ammonium Nitrate	28
Aluminium	14.5
Oxamide	2
HTPB R45	12
Dioctyl Adipate	6
MDI	1.5

ADN-based propellant typically have high burn rates, which results in higher thrusts than are desirable in this application. The burn rate is moderated by the addition of ammonium nitrate (a slower burning oxidiser) and oxamide (a burn rate inhibitor) to the propellant [28, Figure 3.6]. These additions result in a performance penalty, but do result in a final propellant with a density and I_{sp} comparable to the current industry state-of-the-art. A comparison between these standards and an ADN-based propellant can be checked in [28, Figure 3.2]. The addition of these stabilisers is necessary to ensure

that combustion instabilities are not likely to occur, due to the high ranging pressure exponent between 1 and 1.5 for ADN dominated propellant configurations [28, Figure 3.6]. A significant portion of the development time of the Altus vehicle is expected to be devoted to manufacturing a propellant that gives the regression rate parameters desired for optimum operation of the vehicle. For the purposes of initial vehicle design and I_{sp} calculations, a formulation expected to burn at approximately the correct rate is estimated from literature. The regression rates for ADN based propellant, in combination with HTPB start at values of at least $10\,\mathrm{mm\,s^{-1}}$, which result in pressure coefficients between 0.83 and 0.98, which as previously stated, increase the probability of extreme overpressure if any propellant imperfections are present [68]. [68, Figure 10] showcases the influence of the ADN - AN ratio on the regression rate, when using HTPB as binder. The results are computed at a 7 MPa combustion pressure, and the regression rates show desired values below 10 mm/s for ratios below 90% to 10% of ADN to AN. The chosen ratio for the preliminary design of the propulsion system is of 56.25% ADN to 43.75% AN, which translates to a regression rate of approximately $4\,\mathrm{mm\,s^{-1}}$, with a chosen pressure exponent of approximately 0.6, based on literature. The final value, based on OpenMotor iterations, was found to be 0.56.

For initial propellant composition calculations, Methylene Diphenyl diIsocyanate (MDI) is used as the hardener in proPEP. This is a well-known chemical, for which the values of heat of formation and density are readily available. However, it is known and acknowledged that an incompatibility between ADN and isocyanate curatives exists [69]. Therefore, an alternative curing agent will be required for the final propellant formulation. However, it is judged that the departure from the estimated propellant resulting from this substitution will be small, and as such MDI may be used for initial calculations.

Pthalate-based plasticisers such as DiButyl Pthalate (DBP) have been explicitly avoided in the propellant owing to their inclusion as a substance of very high concern under the EU Registration, Evaluation, Authorisation and restriction of CHemicals (REACH) regulations.[15] The selected plasticiser is therefore DiOctyl Adipate (DOA), which is commonly used, cheap, and gives good performance. This substance also has no notable toxicities and is relatively safe to work with.[16]

Backup Propellant Formulation

Author: C. Kendall

Editor: L. Tabaksblat

It is possible that, in the development of the propellant, it is found that a propellant with suitable performance is not possible to be formulated using ammonium dinitramide. Given that this is a mission-critical element for the vehicle development process, a backup propellant is proposed that is better-developed than the ADN-based formulation.

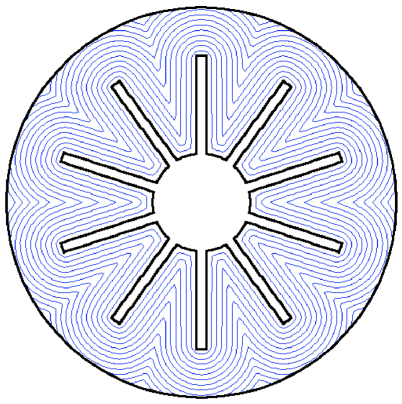

Figure 8.4: Regression profiles for a finocyl grain geometry [70]

The fallback propellant is based on a 1979 NASA study of alternative propellant formulations for the Space Shuttle Solid Rocket Booster (SRB) [71]. The basis of this propellant type is a blend of ammonium nitrate and ammonium perchlorate as the oxidiser. This type of propellant was evaluated in the initial propellant tradeoff, and rejected as less sustainable than the ADN-based propellant formulation, since the exhaust products still contain hydrogen chloride. However, the quantity is vastly reduced compared to traditional APCP propellants, and as such validating the use of this propellant formulation in a flight vehicle would still represent a significant step towards sustainable rocket propellants for the European rocket industry, even if does not achieve the goal of completely eliminating hydrogen chloride from the exhaust products.

[15] https://echa.europa.eu/substance-information/-/substanceinfo/100.001.416 [12/06/2023]

[16] https://echa.europa.eu/substance-information/-/substanceinfo/100.004.231 [12/06/2023]

8.4.3. Grain Geometry

Authors: S. Aurori, C. Kendall

Editor: L. Tabaksblat

As previously outlined, the grain geometry is determined by means of OpenMotor simulations. The port configuration is chosen based on the outputted thrust curve, which is on its own chosen based on maximum accelerations and loads allowed by the payload. Different port configurations allow for different thrust levels during flight, which contribute to various acceleration levels, based on the vehicle decreasing wet mass [67, Section 11.3]. The desired thrust profile lies between a neutral or a regressive configuration, since avoiding high thrust values for a lower mass of the vehicle induces high accelerations. Reducing the acceleration intensity is beneficial for the payload and the rocket subsystems.

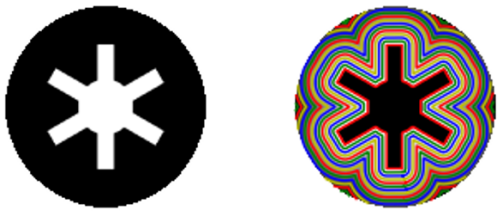

Figure 8.5: Booster Grain Configuration Cross-sectional area and burn pattern resulted from OpenMotor simulations

The thrust and pressure curve of a solid rocket motor is directly linked to the burning surface area as the grain regresses. To achieve the targeted thrust curve and volumetric loading fraction, two main port geometries were considered. These were finocyl, and aft finocyl. A finocyl grain (a portmanteau of "finned cylinder", and illustrated with its regression profile in Figure 8.4) is a grain geometry that can be carefully tuned. An overview of the exact chosen configuration for the booster motor can be seen in Figure 8.5. These plots have been outlined by means of OpenMotor simulations, based on an iterative process. The resulting thrust curve is assessed, and the finocyl is altered based on the thrust. The desired thrust setting entails having a high thrust concentration in the first seconds of flight to achieve a successful tower exit.

Additionally, the configuration chosen for the sustainer motor consists of an aft finocyl grain, as can be seen in Figure 8.6. Two thirds of the grain use a BATES (circular grain port) configuration, alongside the aft third consisting of a finocyl section. This allows for more performance, as well as a more constant thrust setting. The red line in Figure 8.6 showcases the spot on the grain where the cross-section view of the grain is shown below. The circular port diameter of both finocyl and the tubular grain sections measures the same value.

Figure 8.6: Booster Grain Configuration Cross-sectional area and burn pattern resulted from OpenMotor simulations

8.4.4. Motor Casing

Author: S. Aurori

Editor: C. Kendall

To design the casings for the booster and sustainer solid motors, a material needs to be chosen. The most important parameters looked into when choosing a material are strength, reusability and resistance to salt-water corrosion. As

the motor casings are decided upon to be the load bearing structure of the launcher sections that they entail. This means that the outer diameter of the motor casings is set to that of the respective stage, 0.15 m for the upper stage and 0.2 m.

A preliminary comparison between five metal alloys, suitable for both salt water operations, as well as withstanding the combustion loads has been performed. Only metals have been selected due to sustainability reasons, as outlined in Section 4.3. A more in depth comparison between composites and metal structures is showcased in Section 11.4. The inverse of the product between the density and the required thickness for withstanding a pressure load of 7 MPa, $1/\rho_{alloy} \cdot t$, has been computed. Based on this assessment, the alloy with the lowest value, Aluminium 6082 with T6 temper has been chosen as the winner, partially due to its good resistance to salt-water corrosion. This material has a suggested maximum service temperature of 160 °C [72]. Given that the expected combustion temperature is in the order of 2200 °C, a thermal liner is required to protect the casing from the heat of combustion. This liner is discussed in Section 8.4.5.

Having chosen a material, the wall thickness of the casing, as well as its weight and length can be calculated. The wall thickness is found by use of equation (8.26), where the P_{yield} is based on the product between a safety factor SF and the Maximum Expected Operating Pressure (MEOP), which is based on the chamber pressure P_C multiplied by a safety factor. The safety factor SF is determined based on the calculation equation (8.25) [43, Section 8]. The values are based on the calculations for the assumed yield pressure, where the MEOP is equal to $1.1 \cdot P_C$, followed by the proof pressure $P_{proof} = 1.2 \cdot MEOP$.

$$SF = (1.1) \cdot (1.1) \cdot (1.2) \qquad SF = 1.452 \tag{8.25}$$

$$P_{yield} = \frac{2 \cdot \sigma_{yield} \cdot t_{casing}}{D_{inner}} \qquad P_{yield} = SF \cdot P_c \tag{8.26}$$

The total mass of the casing can be determined based on the length of the grain, the inner and outer diameter of the casing, and the density of the Aluminium 6082 alloy. The casing mass may be calculated by firstly finding the cross-sectional area of the tubular motor casing $\pi \cdot (R_{outer}^2 - r_{inner}^2)$, where R_{outer} is derived from the rocket stage outer diameter, and r_{inner} being the thickness subtracted from the outer radius. The cross-section area multiplied by the length of the grain results in the volume of the casing shell which, when multiplied by the density of the material, results in the mass of the casing. These calculations do not include the mass of the nozzle, as this will be outlined in Section 8.4.6. The final values for the measurements of the motor casings are outlined in Table 8.6. Moreover, due to the early stage of the design process, a preliminary calculation for the size and weight of the bulkhead has been computed, assuming that it weighs up to 10% of the casing mass, and that it has a thickness of 1 cm.

Table 8.6: Motor Casings Dimensions and Mass

Parameter Name	Final Value	Units
First Stage Casing Length	1.81	m
Second Stage Casing Length	1.41	m
First Stage Casing Thickness	5.2	mm
Second Stage Casing Thickness	4.1	mm
First Stage Casing Mass	15.46	kg
Second Stage Casing Mass	7.03	kg
First Stage Casing Outer Diameter	20	cm
Second Stage Casing Outer Diameter	15	cm

8.4.5. Liner

Author: C. Kendall
Editor: L. Tabaksblat

There are two main forms of thermal liner typically used to protect solid rocket motor casings from the heat of

combustion. These are rigid and elastomeric liners. A rigid liner consists of a solid tube of material (such as cloth- or paper-reinforced phenolic, or other temperature resistant composites), to which the grain is directly bonded. An elastomeric binder uses a polymer material such as HTPB, with additional additives. This mixture is either spun-cast or sprayed onto the pre-prepared casing where it bonds to the casing.

Because of the difficulty of replacing an elastomeric liner (the liner must be scraped from the inside of the casing then reapplied, which requires a significant amount of time and equipment investment), a solid liner made of paper phenolic has been selected. This has the added advantage that the propellant may be cast into the liner and stored independently, rather than cast into the casing directly. Therefore, the propellant quality (identification of potential cracks and voids) can be assessed with the use of a low-power X-ray machine, rather than requiring a machine capable of penetrating aluminium. The propellant-liner 'cartridge' can be very quickly and easily assembled into the rocket motor by one or two crew members, during the motor assembly process. Within the propulsion sizing tool implementation, a liner thickness of 0.003 m is assumed. This can further be iterated upon in future design phases.

8.4.6. Nozzle

Authors: C. Kendall, S. Aurori
Editor: L. Tabaksblat

Because of the extremely high heat flux in the rocket nozzle, solid rocket motors of this scale typically use a graphite insert for the nozzle throat. These inserts are produced from fine-grained isomolded graphite to ensure sufficient structural properties to withstand the forces without shattering. Their profiles are visible in Figure 8.7a and Figure 8.7b. This graphite insert is usually bonded to a cloth phenolic main nozzle body, which is supported by an aluminium structure that transfers the loads into the phenolic section. This aluminium structure can also act as an extension to the nozzle expansion section, where the temperature of the exhaust gases has dropped sufficiently. The relations to derive heat transfer into the nozzle are established [73], but fall beyond the scope of the preliminary design phase.

The nozzle throat insert is designed with a taper such that the insert is pressed into its mounting by the internal pressure of the engine, giving a good seal. The insert is also bonded to the phenolic nozzle body using high temperature Room Temperature Vulcanising (RTV) silicone, such as Permatex 81160.[17]

In order to determine whether erosive burning occurs in the solid motor, which would negatively impact its performance, the nozzle throat area needs to be determined. This allows for the performance of the motor to be validated by means of OpenMotor simulations. Erosive burning is possible when the ratio between the area of the grain port and the nozzle throat area is less or equal to 4 [67, Section 12.1]. The area of the grain port is determined in OpenMotor, hence, it is decided to keep the throat area constant. This can be determined based on the combustion pressure, the massflow and the characteristic velocity, according to equation (8.27).

$$A_{throat} = \frac{\dot{m} \cdot c^*}{P_C} \tag{8.27}$$

Next, the exit area of the nozzle can be determined which can be used to quantify the size and performance of the nozzle. The exit area can be found based on the throat area and the passing Mach numbers of the flow through both surfaces. The Mach numbers are influenced by the pressures at the respective points of interest, and can be calculated by use of the isentropic flow relations seen in equation (8.28) and equation (8.29) [67, Section 3.2].

$$P_C = P_{ambient} \cdot \left[1 + \frac{1}{2} \cdot (\gamma - 1) \cdot M_{exit}^2\right]^{\frac{\gamma}{\gamma - 1}} \tag{8.28}$$

[17] https://www.permatex.com/products/gasketing/red-gasket-makers/permatex-ultra-red-rtv-silicone-gasket-maker-3-35-oz/ [19/06/2023]

$$\frac{A_{exit}}{A_{throat}} = \frac{M_{exit}}{M_{throat}} \cdot \sqrt{\left(\frac{1 + \frac{\gamma-1}{2} \cdot M_{exit}^2}{1 + \frac{\gamma-1}{2} \cdot M_{throat}^2} \right)^{\frac{\gamma+1}{\gamma-1}}} \tag{8.29}$$

The Mach number can be calculated from equation (8.28), based on the combustion pressure, the ambient pressure at the highest altitude the motor is required to burn at and the ratio of specific heats. This is applied for both nozzles, for both the sustainer and the booster, by applying the respective ambient pressures that apply, as well as the different combustion pressures. Having determined the Mach number at the exit of the nozzle, the area there can be computed as well. The Mach number at the throat is 1, and the throat area has been previously calculated as well. By solving equation (8.29), the nozzle exit area can then be found. An indication of the flow direction is also shown, with the red arrow symbol.

Now that the areas are determined, the final measurement of the nozzle, its length, can be calculated. Based on the nozzle type, with a conical shape and a 15° divergent half angle, the length is found due to its dependency towards the nozzle exit area, throat area and diameter [67]. The convergent half angle of the first stage motor measures 50°, while for the second stage it measures 60°. Based on [67, figure 3.12], the nozzle length can be approximated. The profile of the booster and sustainer nozzles can be seen in Figure 8.7a and Figure 8.7b.

(a) Booster Motor Nozzle Profile

(b) Sustainer Motor Nozzle Profile

8.4.7. Igniters

Author: C. Kendall

The first stage igniter for the rocket may take many forms, which each have roughly equivalent performance. Given the small impact on performance, a copper(II) oxide - aluminium thermite igniter was selected, based on previous experience with this igniter type. These igniters are very well characterised, and work by producing a shower of molten copper droplets that impinge onto the propellant face [74]. The chemical process for the thermite reaction is given in equation (8.30).

$$3\,CuO + 2\,Al \longrightarrow Al_2O_3 + 3\,Cu + Heat \tag{8.30}$$

The igniter for the first stage can be inserted through the nozzle and directly controlled from the ground system. This has the benefit of decreasing the vehicle complexity compared to an igniter controlled by an on-board computer. However, an Radio-Frequency (RF) filter must be used in the igniter lines to prevent inadvertent activation of the igniter resulting from induced currents from high-power radar and other RF systems at the launch site. Similar devices have been in use in rocket ignition circuits since the 1950's [75, Section 11-4].

The first stage igniter is relatively insensitive to sizing, as the igniter itself generates no gases. Reese, Wright and Son indicate an igniter mass relationship based on chamber volume, and note a variation between their calculated igniter mass and other calculations from literature [74].

For the second stage igniter, on-board control is unavoidable as the second stage must be ignited in flight. Therefore, the igniter for the second stage is integrated directly into the sustainer bulkhead. Furthermore, the ignition composition must operate nominally at the reduced pressures resulting from the high-altitude ignition. A commonly used formulation to solve this issue is Boron - Potassium Nitrate ($BKNO_3$ – n.b. that this is a shorthand term, and not a molecular formula), which has been in use since the 1960s [76]. This compound is often prepared according to the industry standard US MIL-P-46994 [77], though other formulations are also used.

It is necessary to size the upper stage igniter to fully pressurise the upper stage motor to operating pressure, such that impulse is not wasted bringing the motor to operating pressure (as the propellant burn rate is affected by the chamber

pressure – see equation (8.24)). The igniter may be initially sized by use of the ideal gas law, equation (8.31), owing to the high temperature of the produced gas.

$$PV = n_{mol}RT \tag{8.31}$$

Taking the formulation used by Kerr-McGee, given by Piper [76] (Table 8.7), as the reference formulation, proPEP gives $T = 3065\,\mathrm{K}$ and a specific gas production of $0.018\,05\,\mathrm{mol\,g^{-1}}$.

The mass of the igniter is estimated based on the ideal gas law and the empty volume of the motor. An estimation of the amount of pressurised gas formed post ignition needs to be computed, however this is recommended to be determined in later stages of the design, since it is closely linked to the final propellant formulation resulting from strand burning tests. The mass of the igniter may be revised based on these test firings.

Table 8.7: Kerr-McGee $BKNO_3$ formulation

Chemical	Percentage
Potassium Nitrate	73
Boron	19
Nitrocellulose Lacquer	8

8.4.8. Propulsion Budgets

Author: S. Aurori
Editor: C. Kendall

Within this subsection the propulsion system budgets are outlined. Firstly, the system is split into three categories: the motor casing, propellant and igniter. These sections are further outlined from a mass and financial point of view. These two budgets are closely related, due to the fact that the great majority, namely the casing, propellant and igniter, disregarding the nozzle insert and electric match, are priced based on raw material costs and component mass. The two budgets are outlined separately, starting with the mass budget, followed by the financial one.

Propulsion Mass Budget

Author: S. Aurori

An overview of the mass budget for the propulsion system for both the booster motor and the sustainer can be found in Table 8.9 and Table 8.8. As the system contains both reusable, refurbishable and consumable items, an indication of the first time budgets, as well as the budget over the span of 10 missions is given. The first time budgets entail the mass for the first use of the system, where all components are brand new.

The mass of the items is estimated based on the preliminary sizing results, and margins are included. The values originally found in sources are rounded up to the closest integer. The propulsion system is split into three categories, namely: motor casing, propellant and igniter. All the main components within each category are outlined in the *Item* column.

The reusability and reliability of these components is taken into account in the mass distribution. The following components from the outlined items in Table 8.9 are assumed to last for 10 missions: combustion chambers, bulkheads, nozzle retainer rings. The nozzle graphite insert and phenolic composites are assumed to last for 2 flights, meaning that they have to be replaced 5 times over the span of 10 missions.

Table 8.8: First time mass estimate for the propulsion system

Distribution	First Time Value	
Budget	Mass (kg)	
Item	Booster	Sustainer
	Motor Casing Items	
Combustion Chamber	15.5	7.0
Bulkhead	1.5	0.7
Oring Seals	0.04	0.04
Nozzle Graphite Insert	0.4	0.3
Phenolic Composites	0.4	0.3
Nozzle Retainer Ring	0.2	3.1
	Propellant Compounds	
Ammonium Dinitramide	23	11.3
HTPB	7.7	3.8
Aluminium Powder	9.3	4.6
Ammonium Nitrate	17.9	8.8
Oxamide	1.3	0.6
Dioctyl Adipate	3.8	1.9
MDI	1	0.5
	Igniter Items	
Potassium Nitrate	0.015	0.007
Boron	0.004	0.002
Nitrocellulose	0.000	0.001
Electric Match	-	-
Total per motor:	82.1	43.0
Total Propulsion System	126	

Table 8.9: Ten missions mass estimate for the propulsion system

Distribution	10 Missions Value	
Budget	Mass (kg)	
Item	Booster	Sustainer
	Motor Casing Items	
Combustion Chamber	15.5	7.0
Bulkhead	1.5	0.7
Oring Seals	0.4	0.4
Nozzle Graphite Insert	2.0	1.4
Phenolic Composites	0.4	0.3
Nozzle Retainer Ring	0.2	3.1
	Propellant Compounds	
Ammonium Dinitramide	230	113
HTPB	77	38
Aluminium Powder	93	46
Ammonium Nitrate	179	88
Oxamide	13	6
Dioctyl Adipate	38	19
MDI	10	5
	Igniter Items	
Potassium Nitrate	0.15	0.07
Boron	0.04	0.02
Nitrocellulose	0.002	0.01
Electric Match	-	-
Total per motor:	660	328
Total Propulsion System	998	

Propulsion Sub-System costs

Author: S. Aurori

An overview of all the materials and chemicals needed is kept, where a unit cost is attributed based on prices found on the market, which can be seen in Table 8.10. These unit costs are multiplied by the weight of each part, sourced from Table 8.8. The margins attributed in the previous section are carried further into the cost estimations.

It is assumed that only the costs of the materials and the compounds themselves are included, disregarding the manufacturing costs. For the main items such the motor casing, the propellant casting and igniter preparation, the respective costs are included within the operations and logistics chapter. An exception is made, in the case of the nozzle graphite insert item, where an invoice is sourced to give a cost estimation. This invoice includes the material, manufacturing and transport costs.

Table 8.10: Overview of cost per unit for the propulsion system items

	Compound	Price/unit [€]
Motor Casing Items		
Combustion Chamber [kg]	Al 6082	24 [18]
Bulkhead [kg]	Al 6082	24 [19]
Oring Seals [part]	Rubber	3
Nozzle Graphite Insert [part]	Graphite	300 [78]
Phenolic Composites [kg]	Phenolic Resin	2 [20]
Nozzle Retainer Ring [kg]	Al 6082	24 [21]
Propellant Compounds [kg]		
Oxidiser	ADN	150
	AN	1
Fuel	HTPB	35 [79]
	Al	15
Binder	Oxamide	200 [22]
	Dioctyl Adipate	1 [23]
Curative	MDI	3 [24]
Igniter Items		
Potassium Nitrate [kg]	KNO_3	5 [25]
Boron [kg]	B	3564 [26]
Nitrocellulose [kg]	Nitrocellulose	116 [27]
Electric Match [part]	E-Match	1 [28]

The cost breakdown shows the strong influence of the propellant on the cost of the system, as it is accounting for 97% of the total cost over 10 missions, and for 87.3% of the one time cost of the entire system. However, the costs shown in Table 8.12 and Table 8.11 are estimated based on a "per kilogram" assessment of the costs of each raw material of chemical needed for the development of the motor. It is expected that during the manufacturing process, larger batches of each product will be acquired, drawing the price down significantly. Since ADN is a new propellant, still in its infancy, it is expected that in the next years its production will increase. Project Altus is expected to be the main civilian customer for ADN producers, meaning that the mission will drive the majority of civilian ADN demand, which will incentivise a switch to a continuous production method.

[18] https://www.exportersindia.com/product-detail/epoxy-phenol-novolac-resin-5622299379.htm [01/06/2023]

[19] https://www.exportersindia.com/product-detail/epoxy-phenol-novolac-resin-5622299379.htm [01/06/2023]

[20] https://www.exportersindia.com/product-detail/epoxy-phenol-novolac-resin-5622299379.htm [01/06/2023]

[21] https://www.exportersindia.com/product-detail/epoxy-phenol-novolac-resin-5622299379.htm [01/06/2023]

[22] https://www.fishersci.nl/shop/products/oxamide-98-thermo-scientific/10269393#?keyword=oxamide [01/06/2023]

[23] https://www.indiamart.com/proddetail/dioctyl-adipate-liquid-23857631048.html [01/06/2023]

[24] https://www.chemanalyst.com/Pricing-data/methylene-diphenyl-diisocyanate-mdi-1111#:~:text=CFR%20JNPT%20(India)%20pricing%20of,2464%2FMT%20in%20Q3%202021. [01/06/2023]

[25] https://www.lmine.com/nitratesbases-c-1_7_221/potassium-nitrate-prills-technical-grade-kno3-55-lb-bag-p-4560.html#:~:text=Potassium%20Nitrate%20PRILLS%20Technical%20Grade,%5D%20%

Table 8.11: First time cost estimate for the propulsion system

Distribution	First Time Value	
Budget	Financial (€)	
Item	Booster	Sustainer
	Motor Casing Items	
Combustion Chamber	369	168
Bulkhead	37	17
Oring Seals	0.1	0.1
Nozzle Graphite Insert	120	84
Phenolic Composites	1	1
Nozzle Retainer Ring	5	74
	Propellant Compounds	
Ammonium Dinitramide	3457	1700
HTPB	269	132
Aluminium Powder	139	68
Ammonium Nitrate	18	9
Oxamide	255	125
Dioctyl Adipate	4	2
MDI	3	2
	Igniter Items	
Potassium Nitrate	0.07	0.03
Boron	13.54	6.77
Nitrocellulose	0.02	0.09
Electric Match	0.80	0.80
Total per motor:	4691	2389
Total Propulsion System	7080	

Table 8.12: Ten missions cost estimate for propulsion system

Distribution	First Time Value	
Budget	Financial (€)	
Item	Booster	Sustainer
	Motor Casing Items	
Combustion Chamber	369	168
Bulkhead	37	17
Oring Seals	1	1
Nozzle Graphite Insert	600	420
Phenolic Composites	1	1
Nozzle Retainer Ring	5	74
	Propellant Compounds	
Ammonium Dinitramide	34566	16996
HTPB	2688	1322
Aluminium Powder	1392	685
Ammonium Nitrate	176	86
Oxamide	2548	1253
Dioctyl Adipate	43	21
MDI	33	16
	Igniter Items	
Potassium Nitrate	0.7	0.3
Boron	135.4	67.7
Nitrocellulose	0.2	0.9
Electric Match	8.0	8.0
Total per motor:	42603	21137
Total Propulsion System	63740	

8.5. Stability & Control Sub-System

Author: S. Yorucu
Editor: C. Kendall

To ensure that the rocket keeps true to its trajectory, and carries out its mission as intended, a fully functioning stability and control subsystem is essential. For example, if a too-low spin rate is achieved, then the rocket would start to wobble and deviate from its trajectory. Sufficient spin stabilisation can be obtained through the sizing of fins, elaborated upon in Section 8.5.2. To prevent the rocket from deviating from its path due to cross-flow, a sufficient stability margin must be taken, as further explained in Section 8.5.1. Additionally, the rocket must provide adequate experimental conditions for the effective measuring of the scientific payload. For example, to properly experiment in microgravity, the rocket must be completely de-spun to avoid errors due to centrifugal acceleration. This is expanded on in Section 8.5.3.

8.5.1. Stability Margin

Author: S. Yorucu
Editor: C. Kendall

2D%20%24103.89%20%3A%20Legend%20Inc. [01/06/2023]

[26] https://www.ottokemi.com/boron/boron-powder-50um-99-b-0063.aspx [01/06/2023]

[27] https://kolba.pl/en/product/50744,vihtavuori-n550-nitrocellulose-powder-1-kg [01/06/2023]

[28] https://wirelessfireworks.co.uk/product/electric-match-igniters/ [01/06/2023]

A stability margin, for rocketry, is defined as a dimensionless parameter calculated as the distance from the rockets centre of pressure to its centre of gravity, divided by the outermost diameter of the rocket.[29] This value is often given in calibres (cal.), i.e. multiples of the diameter of the vehicle. Determining the centre of pressure of the rocket is paramount in assessing its stability during flight, as it counteracts aerodynamic moments. It is important that this point lies a certain distance *behind* the centre of gravity to ensure a sufficient restoration moment to act against disturbances to the angle of attack. As a result, the stability margin (SM) of the rocket at Mach 0.3 (the reference value used by OpenRocket [48]) must be between 2-6 cal, as the centre of pressure has a tendency to move forward as the vehicle mach increases, decreasing the stability margin. Therefore, a stability margin of 4 was chosen for sizing the stability of the rocket.

Method & Assumptions

The method used to find the centre of pressure of the vehicle, and thus its stability, is taken from literature [48, p. 11-13]. It mainly varies with the angle of attack (α) of a rocket, again primarily cause by cross-flow, or side-wind. Moreover, several assumptions were made, depicted below.

- Small angle approximation (Normal force = Lift force).
- Steady, non-rotational flow around the body.
- The rocket is a rigid body.
- The nose tip is a point.
- The fins are flat plates.
- The rocket body is axially symmetric.
- The centre of pressure location is primarily affected by the fins.
- The segments' centre of pressure location is at their respective centroid.

Initially, the centre of pressure location is calculated by breaking the rocket up into segments. These segments are comprised of: the nose cone, payload section, upper and lower stage, body, and fins. The centres of pressure, and flow areas (A_{fl}), of these individual segments are found using equation (8.32) [48, p. 22, eq. 3.19].

$$A_{fl} = C_{N_\alpha} \cdot S_{ref} = C_{L_\alpha} \cdot S_{ref} = 2 \cdot [A(l) - A(0)] \tag{8.32}$$

Note that, the flow area is the product of, the reference area of a segment (S_{ref}), with its lift-angle derivative (C_{L_α}). $A(l)$ and $A(0)$, are the cross sectional areas of the two ends of a segment. As these areas are identical for cylindrical shapes, namely the body and payload section; that respective segment has no contribution to lift and/or stability.

The flow area of the fins is calculated using, equation (8.33) for the subsonic speed regime and equation (8.34) for the supersonic speed regime; where, Λ_c is the fin mid-chord sweep angle, and b is the semi-span of the fin.

$$A_{fl_f} = \frac{2\pi \cdot b^2}{1 + \sqrt{1 + \left(\frac{\beta \cdot b^2}{S_{fins} \cdot \cos \Lambda_c}\right)^2}}, \quad \beta = \sqrt{1 - M_\infty^2} \tag{8.33}$$

$$A_{fl_f} = S_{fins}\left(\frac{2}{\beta} + K_2\alpha + K_3\alpha^2\right), \quad K_2 = \frac{(\gamma+1)M^4 - 4\beta^2}{4\beta^4}, \quad K_3 = \frac{(\gamma+1)M^8 + (2\gamma^2 - 7\gamma - 5)M^6 + 10(\gamma+1)M^4 + 8}{6\beta^7} \tag{8.34}$$

Moreover, the locations of the fins' centre of pressure (x_{CP_f}) are at the aftmost positions of the rocket, and are approximated by equation (8.35). This is done by assuming that x_{CP_f} lies on the centroid of the fin, and that the centroid lies on the semi root chord. Note that, at higher Mach numbers ($M > 2$), empirical formulas are used, given in equation (8.36) [53, p. 33], where AR is the aspect ratio of the fin.

$$x_{CP_{f_u}} = L_{nc} + L_u + \frac{1}{2}C_{r_u}, \quad x_{CP_{f_l}} = L_{nc} + L_u + L_t + L_l + \frac{1}{2}C_{r_l} \tag{8.35}$$

[29] `https://www.apogeerockets.com/Tech/Rocket_Stability` [19-06-2023]

$$
\begin{aligned}
x_{CP_{f_u}} &= L_{nc} + L_u + \frac{AR_u \cdot \beta - 0.67}{2AR_u \cdot \beta - 1}, \quad AR_u = \frac{b_u^2}{S_{fins_u}} \\
x_{CP_{f_l}} &= L_{nc} + L_u + L_t + L_l + \frac{AR_l \cdot \beta - 0.67}{2AR_l \cdot \beta - 1}, \quad AR_l = \frac{b_l^2}{S_{fins_l}}
\end{aligned}
\tag{8.36}
$$

In terms of the body, the nosecone and shoulder have varying cross-sectional areas, thus have an appreciable effect on the centre of pressure location. The centre of pressure locations for the nosecone and shoulder, are given below in equation (8.37);

$$
x_{CP_{nc}} = \frac{5}{2} \cdot D_{nc}, \quad x_{CP_{sh}} = \frac{2}{3} \cdot L_t \frac{2 \cdot D_u + D_l}{D_u + D_l} + 5 \cdot D_u + L_u \tag{8.37}
$$

and the flow areas are given by equation (8.38);

$$
A_{fl_{nc}} = 2\pi \left(\frac{D_{nc}}{2} \right)^2, \quad A_{fl_{sh}} = 2\pi \left[\left(\frac{D_l}{2} \right)^2 - \left(\frac{D_u}{2} \right)^2 \right] \tag{8.38}
$$

Furthermore, the entire rocket's centre of pressure location (x_{CP}), is given by a weighted sum of the individual centre of pressure locations and their respective flow areas, in equation (8.39), below.

$$
x_{CP} = \frac{\left(x_{CP_{f_u}} + x_{CP_{f_l}} \right) \cdot A_{fl_f} + x_{CP_{nc}} \cdot A_{fl_{nc}} + x_{CP_{sh}} \cdot A_{fl_{sh}}}{A_{fl_f} + A_{fl_{nc}} + A_{fl_{sh}}} \tag{8.39}
$$

To summarise, the x_{CP}, needs to be at least twice, and at most six times, the outer-rocket diameter (D_l) aft of the location of the centre of gravity (x_{CG}), illustrated in equation (8.40), below.

$$
\frac{x_{CP} - x_{CG}}{2 \cdot D_l} \leq SM \leq \frac{x_{CP} - x_{CG}}{6 \cdot D_l} \tag{8.40}
$$

8.5.2. Fins

Author: S. Yorucu

Editor: C. Kendall

Fins are crucial to retain stability during flight for sounding rockets. Fins stabilise a rocket by moving the vehicle centre of pressure aftward. They can also be canted (or, equally, given an asymmetric profile) to induce a spinning motion in the rocket. This spin ensures that the rocket does not deviate from its trajectory through gyroscopic stability, and by ensuring that thrust misalignments do not compound (i.e. a spinning rocket with a thrust misalignment will tend to move in a helical motion, while a non-spinning rocket will tend to fly in an arc as the thrust misalignment compounds [80]). The degree of stability and control that fins can provide depends on several parameters, which are mainly: the number, location, size, and shape of the fins. For the first iteration of the vehicle, certain parameters were fixed. These fixed parameters were given a value based on engineering judgement and literature [81, 82, 83, 84]. This is summarised in Table 8.13.

Table 8.13: Initial design parameters for the rocket fins.

Parameter	Decision	Reasoning
Number	4	High stability with good performance [81]
Location	Max aft positions	Provides max stability margin
Shape	Trapezoidal fins	Most efficient shape for both subsonic and supersonic missiles. Reduces shock wave formation and drag at supersonic speeds. [82]
C_{r_l}	0.4 m	Arbitrary value chosen to meet *SYS-GN-21*
C_{t_l}	0.4 m	*Idem dito*
b_l	0.4 m	*Idem dito*
t_{f_l}	5 mm	*Idem dito*
C_{r_u}	0.4 m	*Idem dito*
C_{t_u}	0.4 m	*Idem dito*
b_u	0.4 m	*Idem dito*
t_{f_u}	5 mm	*Idem dito*

Iterations were done after simulations to optimise the fin parameter configuration. An important aeroelastic phenomenon was considered during iterations; fin flutter, which must be avoided to ensure the structural integrity and functionality of the fins during flight [83].

Fin flutter is a form of dynamic instability, caused by the interaction of inertial, aerodynamic and elastic forces, which generate vibrations in the fins. Air is used as an effective damper to reduce the amplitude of the oscillatory motion generated by the interaction of forces [83]. The fin flutter motion has a critical vehicle speed at which the effect will become noticeable. To avoid flutter, the fin flutter velocity must be greater in magnitude than the maximum rocket velocity. Equation (8.41) gives the fin flutter velocity.

$$v_f = SF \cdot a \cdot \sqrt{\frac{2G(AR+2)\left(\frac{t_f}{C_r}\right)^3}{1.337 p_\infty (1+\lambda) AR^3}} \tag{8.41}$$

The above equation conveys the relation between the fin flutter velocity and the atmospheric, material, and geometrical properties of the environment and fins. From the atmospheric properties, one can determine the speed of sound (a) and free-stream pressure (p_∞). The taper ratio is given by $\lambda = {}^{C_t}/_{C_r}$, where C_t and C_r are the tip and root chord, respectively. Additionally, the aspect ratio (AR), which depends on the semi-span (b) and wet area (S_{fins}), along with the thickness (t_f), are the geometrical parameters used to size the fins. The shear modulus (G), is the only material property that is taken into account for fin flutter. Lastly, a safety factor (SF) of ${}^2/_3$ was taken to have confidence in the fin geometry and its dimensions.

It should be noted that the apogee and stability of the rocket vary most with fin span and thickness [82] (rather than with root chord, for instance). Fins with smaller spans are more effective in resisting flutter, as they become more stiff, and they also have less drag. However, there still exists a minimum effective area of the fins where the rocket can be controlled [84].

The final values attained for the trapezoidal fin geometry, are provided in Table 8.14. Note that, the total mass of the fins and their raw material costs, are illustrated in Section 8.6.8.

Table 8.14: Final values for the fins.

Parameter	Upper Fins Final Values	Lower Fins Final Values	SI Units
C_r	0.35	0.50	m
C_t	0.10	0.230	m
b	0.139831	0.209	m
Λ_{LE}	30.0	30.0	°
t_f	6.021	4.590	mm
Mass	0.5323	0.9839	kg/fin
Number of fins	4	4	[-]
Cost	156.2745	288.9361	€

8.5.3. De-Spin

Author: C. Kendall
Editor: S. Yorucu

Given that the chosen stabilisation method of the Altus vehicle is spin stabilisation, it is necessary to to de-spin the vehicle to provide a stable measurement platform for the scientific instruments or other payloads that the vehicle carries. To carry out the de-spin manoeuvre, the simplest and most straightforward method is the use of a yo-yo de-spin mechanism. This method uses a pair of weights which extend radially on long lines or wires to cancel the spin rate of the vehicle, analogous to the way a figure skater decreases their rotation rate by extending their arms. The angular momentum is removed from the rocket system by expelling the weights from the vehicle once all of the angular momentum has been transferred. A key advantage of this system is that the lengths of the lines and the mass of the weights depend only on the ratio of final to initial spin rate ω_f/ω_i along with the rotational inertia and the radius of the vehicle [85]. The yo-yo de-spin is therefore completely insensitive to the initial rate of rotation of the vehicle as long as the targeted final rotation rate is 0 Hz, allowing the rotational rate, induced by the fins, to be varied later in the design process without affecting this subsystem.

In equation (8.42) below, the yo-yo de-spin mechanism geometry is related to the vehicle geometry, to determine the length l of the lines and the mass of the released weights $m_{weights}$;

$$\frac{I}{M(l+a)^2} = \frac{1+r}{1-r} \tag{8.42}$$

where:

$$l = \text{length of wire} \quad a = \text{vehicle radius} \quad I = \text{vehicle moment of inertia} \quad M = m_{weights} + \frac{1}{3}m_{lines}.$$

For the purposes of microgravity experiments, this form of de-spin is not sufficient, as the vehicle attitude must be precisely maintained. Therefore, a microgravity control module will be installed to the vehicle in the later phases of design for this kind of flight, which uses reaction control wheels to counter any remaining spin, while maintaining attitude. Although the yo-yo de-spin mechanism removes the majority of the vehicle spin, the reaction control wheels are necessary in further minimising spin to a negligible amount. Again, the sizing of this module is beyond the scope of the preliminary design phase, as it is not relevant for the primary mission of PMC measurements.

The de-spin mechanism is currently estimated to have a total mass of around 0.5 kg to 1.0 kg. However, the exact design of the despin mechanism, because of the dependency on the vehicle moment of inertia, varies with payload configuration and the exact design of the vehicle. Because of this, and the small mass of the de-spin mechanism relative to the entire vehicle, the despin mechanism is neglected from the initial sizing calculations and mass budget.

The cost of the de-spin mechanism will be dominated by the pyrotechnic wire cutter uses to actuate the weight deployment. These have a nearly 100% reliability,[30] and have a cost of around €165.[31] Therefore the estimated

[30] https://www.cypres.aero/sparepart/pulley-part/ [21/06/2023]
[31] https://www.chutingstar.com/cypres-aad-replacement-cutter [21/06/2023]

total cost of the yo-yo de-spin mechanism is less than €250.

8.5.4. Stability & Control Budgets

The stability and control subsystem is broken down into its respective components and their mass and cost are conveyed in Table 8.15. The upper range of the mass of the de-spin mechanism is chosen to account for the maximum mass.

Table 8.15: Mass and cost values for the components of the stability & control subsystem

Parameter	Mass (kg)	Cost (€)
Lower stage fins	2.13	288.94
Upper stage fins	3.94	156.27
De-spin mechanism	1.00	250.00
Total	**7.07**	**695.21**

8.6. Structure Sub-System

This section covers the design of the structure of the rocket. Section 8.6.1 will explain the design of the nosecone, Section 8.6.2 covers the main body of the vehicle. In Section 8.6.3 the shoulder and staging mechanism are discussed, next Section 8.6.4 covers the possible types of joints that can be used in the vehicle. Section 13.1 analyses impact survivability, afterwards Section 8.6.6 elaborates on the natural frequencies in the rocket and Section 8.6.7 explores the fatigue in the vehicle, which is relevant because of reuse. Finally, Section 8.6.8 outlines the mass and cost budgets for the structures of the vehicle.

8.6.1. Nose Cone

Author: S. Yorucu

Editor: C. Kendall

The nose cone is vital in minimising the friction drag experienced by the entire rocket during flight. The shape and size of the nose cone are the main parameters that manipulate the airflow and determine the drag performance of the entire rocket. The optimal shape of a nose cone depends on the speed-region of flight [86]. The initial nose cone parameters are conveyed in Table 8.16.

Table 8.16: Initial and final design parameters of the nose cone.

Parameter	Decision	Reasoning
Shape	LD Haack	Mathematically derived shape for theoretically lowest wave drag [49]
Fineness ratio	5	Minimal drag point [50, p. 16]
Diameter	150 mm	Preliminary outer diameter of sustainer stage

As the nose cone tip is the first point on the rocket to decelerate the air, it heats up, especially at high supersonic and hypersonic speeds. As a result, the maximum temperature of the tip of the nose cone must be calculated to ensure that it does not melt or undergo degradation during flight. This also ensures the longevity of the nose cone, where its temperature (T_{nc}) is calculated using equation (8.43).[32]

$$T_{nc} = T_{\infty} \cdot \left[1 + \frac{2\gamma}{1+\gamma}(M_{\infty}^2 - 1)\right] \cdot \left[\frac{2 + (\gamma - 1)M_{\infty}^2}{(1+\gamma)M_{\infty}^2}\right] \tag{8.43}$$

The above equation is solely dependent on the atmospheric conditions, including the specific heat ratio (γ), free

[32] https://www.grc.nasa.gov/www/k-12/airplane/normal.html [08-06-2023]

stream temperature (T_∞), speed of sound, and the rocket velocity (M_∞). Lastly, the final values for the nosecone, is given in Table 8.17, below, where the mass and raw material cost is given in Section 8.6.8.

Table 8.17: Final values for the nosecone.

Parameter	Final values	SI Units
Diameter	0.15	m
Length	0.75	m
t_{nc}	5.0	mm

8.6.2. Body tube

Author: D. Norbart
Editor: E. Chen

The loads during launch will be carried by the main structure of the rocket. The flight loads will be carried by the engine casing or a load carrying skin. For the initial calculations the main body of the rocket will consist out of a two constant cross section tubes to represent the stages. There will also be a shoulder connecting the two tubes. The outer diameter of the lower stage is set to 0.2 m, while the outer diameter of the upper stage will be 0.15 m. The maximum force that the lower stage engine exerts is 8370 N, this is 7562 N for the second stage. The yield strength of the material used is 260 MPa. A conservative safety factor of two is used. The mass of the tube pressing on the lower parts of the tube can be neglected. Using $\sigma = \frac{F}{A}$ the minimum area can be calculated to give a stress lower than 130 MPa. This area is 6.44×10^{-5} m^2 for the lower stage and 5.82×10^{-5} m^2 for the upper one. The formula $A = 0.25\pi(d_o^2 - d_i^2)$ can be used to calculate the inner diameter, thus thickness. The inner diameter will be 0.1998 m and 0.1498 m, for the first and second stage respectively. The skin thickness is therefore 0.0002 m. This is however very thin. A buckling analysis is thus needed, as that will most likely be the failure mode for such a thin structure.

According to NASA [87], the critical buckling stress in a thin-walled cylinder is given by equation (8.44). With the equation for stress, this can be rewritten to equation (8.45). Here only the inner diameter (d_i) is unknown, so the equation can be solved. With E = 72 GPa, this gives an inner diameter of 0.1998 m for the lower stage and the upper stage needs 0.1498 m. Since these results are the same, the buckling does not put a more stringent condition on the thickness of the body.

$$\sigma = 0.605E\frac{t}{r} \tag{8.44}$$

$$F = 0.605E \cdot \frac{d_o - d_i}{d_o} \cdot 0.5\pi \cdot (d_o^2 - d_i^2) \tag{8.45}$$

Even though this initial analysis shows that the structure will withstand the axial forces with a thickness of only 0.2 mm, this is not very probable. Due to vibrations there will be side forces too. Dents easily form in such a thin skin, which decrease the performance. Due to these reasons, a skin thickness of 1 mm was chosen. Further analysis is required in this field, but considered too extensive for this stage of the design.

The mass of the structure can now be calculated. Excluding the length of the nose cone, the upper structure has a length of 2.887 m and the lower structure 2.589 m. With the density of 2810 kg m^{-3} this brings the mass of the lower stage structure to 2.28 kg and to 1.90 kg for the upper one. The total mass of the skin will therefore be 4.18 kg. As aluminium 7075 costs €18.35 kg^{-1}.[33] this brings the raw material cost of the entire body tube to €76.70.

8.6.3. Shoulder and Staging Mechanism

Authors: L. Alonso, E. Chen

The shoulder is the structural connection between the first and second stage of the sounding rocket. The use of the shoulder is to additionally contain the recovery system of the first stage. To size the shoulder of the rocket,

[33] https://onlinealuminium.nl/en-aw-7075-t651/ [21/06/2023]

equation (8.9) is used to calculate the surface area of the shoulder, S_{sh_w}. Therefore, the mass of the shoulder, m_{sh}, is determined using equation (8.46).

$$m_{sh} = S_{sh_w} t_{skin} \rho_{skin} = \frac{\pi D_l L_t}{\cos\left[\arctan\left(\frac{D_l - D_u}{2L_t}\right)\right]} t_{skin} \rho_{skin} = 1.78\,\text{kg} \tag{8.46}$$

Where D_l and D_u is the diameter of the lower stage and upper stage equal to 0.2 m and 0.15 m, respectively. These values are derived from the payload in Section 2.4. L_t is the height of the shoulder chosen to be 0.2 m. While, t_{skin} is the thickness of the outer body skin equal to 5 mm and ρ_{skin} is the outer body skin density of the chosen aluminium (Al7075-T6) equal to $2810\,\text{kg}\,\text{m}^{-3}$. These values and the chosen material was determined in the trade-off in Section 7.1. This results in a total structural mass of the first stage recovery bay equal to 1.78 kg.

The staging mechanism is located in this shoulder. To establish a connection between the two stages, a slip fit is used. This connection consists of a cylindrical section aft of the fins on the second stage slipping into a tubular section located inside the shoulder. The sections need to have a correct tolerance for a smooth separation at engine burnout. This separation approach is used by some sounding rockets such as the Loki-Dart [88].

8.6.4. Vehicle Joints

Author: C. Kendall

Editors: S. Yorucu, E. Chen

Given that, the structural loads experienced by hypersonic vehicles are very high, sufficient reinforcement of the structure is compulsory to ensure the proper functioning said structure. Adequate reinforcement can be achieved through joining structures by high-load bearing joints, such as lap joints, radial-axial joints, and screws. Moreover, these joining structural components are not only effective in supporting the main structure of the vehicle, but also effective for easy disassembly, necessary for maintenance and transport. Henceforth, it is paramount to consider these joints that are used to connect sections of the rocket together.

The characteristics of *stiffness*, *linear rotation rate* and *low hysteresis*, are desirable for rocket vehicle joints [89]. The first of these, stiffness, reduces the overall elasticity of the vehicle and its flexing, which helps to minimise aeroelastic effects that can introduce additional stresses. Secondly, the linear rotation rate helps to provide predictable behaviour of the vehicle and joint, and finally, having low hysteresis means that the rocket will return to its original state when load is removed rather than remaining bent.

Three types of joint have been selected for use for connecting the sections of the rocket vehicle.

Lap Joint

The lap joint is the simplest joint that is commonly used. This joint tends to give relatively poor stiffness, as any screws used can only provide radial preload. This joint also exhibit an extremely high degree of hysteresis. While it is possible to reduce these effects by increasing the length of the lap section, this unacceptably increases mass compared to other joint options. Therefore, this joint is only used for the separation between the first and second stages of the vehicle.

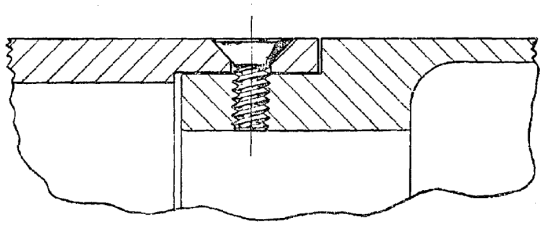

(a) Lap Joint

Radial-Axial

Radax joints are commonly used in modern sounding rocket vehicles. They are high-stiffness, low-hysteresis joints that allow both radial and axial preload of the joint. Radax joints on REXUS use helicoil thread inserts

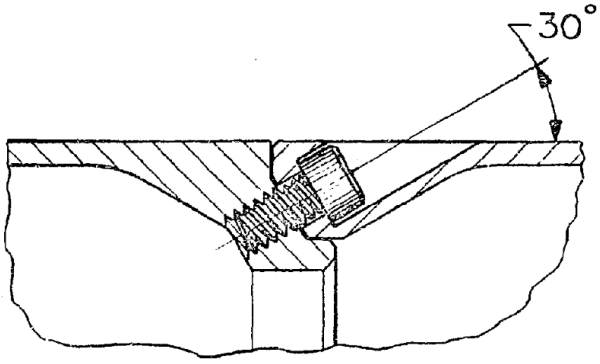

(b) Radial-Axial (Radax) Joint

in the aluminium modules such that the joints can be
repeatedly assembled and disassembled without damaging the threads [90].

Screw

Screw joints were used to attach the Nike and Cajun motors to the main vehicle section on the rockets using these motors [75]. These joints provide good preload and do not require particularly tight tolerances. The joint is also much quicker to assemble than other types, and may be preferred when ease of assembly is preferred.

8.6.5. Survivability on Impact

Author: D. Norbart

When landing the rocket on the ground, all kinetic energy will have to be dissipated. If the landing speed is too high, the rocket might crumple or fail in any other way. To make sure this doesn't happen, a first estimate analysis will be done. The assumption will be made for the simplest case, the rocket is modelled as a continuous tube with constant mass. This tube lands straight on the ground, with the small circular area. If the rocket lands diagonally, it falls over, which makes the deceleration distance a lot longer. Therefore, the impact force here is a lot lower. To make this possible, the fins do not protrude below the body. For this analysis, the ground is assumed to be completely rigid, such that the elastic compression of the tube is the only thing absorbing the force of impact.

With the yield strength (σ_y) and Youngs modulus (E) of a material, one can calculate the strain (ϵ) of a material before plastic deformation starts occurring [91]. As the rocket has to be launched multiple time, no plastic deformation should be allowed. The crumple zone of the rocket is thus this elastic deformation regime, it can be calculated from the maximum strain times the length of the rocket (l). The force on the rocket (F_e) can be calculated through the difference in kinetic energy, divided by this deformation distance. As the kinetic energy at the end is zero, this is the beginning kinetic energy divided by the distance. The kinetic energy is the square of the landing speed (V^2) times half the mass of the vehicle (m). Combining all of these, the force can be calculated that is exerted on the rocket if the entire elastic regime is used as crumple zone.

$$F_e = \frac{0.5 \cdot m \cdot v^2 \cdot E}{l \cdot \sigma_y} \tag{8.47}$$

The maximum force that the rocket can experience before deforming (F_a) permanently is calculated. For that, the yield strength is multiplied with the area of impact. This area is assumed to be the cylinder cross section. With the previously made assumptions, this is the mass of the rocket divided by the length and density (ρ).

$$F_a = \frac{\sigma_y \cdot m}{l \cdot \rho} \tag{8.48}$$

When the force experienced in the elastic regime, equation (8.47), is greater than the acceptable force, calculated with equation (8.48), the structure will have plastic deformation. As this should be avoided, the system has to be designed such that $F_a > F_e$. The two equations can be combined to get equation (8.49), the fraction has to be lower than 1. The parameters that can be varied to achieve this objective are the material of the rocket and the decent velocity, which is linked to the area of the parachute, given in equation (8.56).

$$\frac{F_e}{F_a} = \frac{v^2 \cdot E \cdot \rho}{2 \cdot {\sigma_y}^2} < 1 \tag{8.49}$$

Table 8.18: Landing shock initial parameters first (left) and second stage (right)

Parameter	Value	Unit
Yield strength	260	MPa
Density	2700	$\mathrm{kg\,m^{-3}}$
Youngs modulus	72000	MPa
Length of the stage	2.59	m
Dry mass of the stage	24.38	kg
Landing velocity	8	$\mathrm{m\,s^{-1}}$

Parameter	Value	Unit
Yield strength	260	MPa
Density	2700	$\mathrm{kg\,m^{-3}}$
Youngs modulus	72000	MPa
Length of the stage	3.64	m
Dry mass of the stage	27.3	kg
Landing velocity	8	$\mathrm{m\,s^{-1}}$

As the rocket is made up of two stages, who will land independently, two analyses need to be performed too. The values for the first and second stage are provided in Table 8.18.

Taking all of these values into account, the first stage can handle a force of 907 kN. While only 83.4 kN acts on it during the landing. This means that the first stage, in its current configuration, can easily handle the landing loads. For the second stage, only the mass and the length are different. Which means that the fraction $\frac{F_e}{F_a}$ is the same, at 0.092. So the second stage will easily handle the landing loads too.

8.6.6. Natural Frequency

Author: D. Norbart

Editor: E. Chen

Every solid rocket engine will vibrate when producing thrust. This is the effect of unstable flow in the combustion chamber [92]. To make a basic estimation, the frequency at which it will vibrate can be estimated by equation (8.50). Here a is the speed of sound, which itself is calculated with equation (8.51). The temperature (T), inside the chamber is really high, at 3000 K. With $\gamma = 1.26$ and R = 287, this leads to a speed of sound of a = 1042 $\mathrm{m\,s^{-1}}$. With a length of the propulsion chamber of L = 1.805 m for the first stage and L = 1.408 m for the second stage, multiple frequencies can be calculated. Here, n denotes the longitudinal acoustic mode number [93].

Based on the data, this gives a ground forcing frequency of 288.5 Hz for the first stage and 369.9 Hz for the second stage. Taherinezhad and Zarepour (2020) [94] recommend looking at the first four natural frequencies, so n = 1,2,3,4. These frequencies are given in Table 8.19.

$$f = \frac{n \cdot a}{2 \cdot L} \tag{8.50}$$

$$a = \sqrt{\gamma \cdot R_{air} \cdot T} \tag{8.51}$$

Table 8.19: Forcing frequencies by the engine

Forcing frequency [Hz]	1st stage	2nd stage
First harmonic	288.5	369.9
Second harmonic	577.0	739.7
Third harmonic	865.6	1110
Fourth harmonic	1154	1480

Table 8.20: Natural frequencies of the Altus vehicle

	1st stage		2nd stage	
Frequency [Hz]	Dry	Wet	Dry	Wet
Longitudinal frequency	14.6	7.66	5.48	3.73
Lateral frequency	317	167	226	154

To make sure that the structure can handle these vibrations, its natural frequencies should be sufficiently different from these excitation frequencies. If this is not the case, resonance will start appearing, which may damage the vehicle. The natural frequency will be calculated in the longitudinal and lateral axes for the assumption that the rocket is a constant cross section hollow tube.

The natural frequency is given by equation (8.52). Here, m represents the mass and k the spring stiffness. For lateral

loads k is given by equation (8.53), for longitudinal loads equation (8.54) is used [95].

$$f = \frac{1}{2\pi}\sqrt{\frac{k}{m}} \tag{8.52}$$

$$k_{lateral} = \frac{3\pi \cdot E \cdot (d_o^4 - d_i^4)}{64L^3} \tag{8.53}$$

$$k_{longitudal} = \frac{EA}{L} \tag{8.54}$$

The data from Table 8.18 is again used. The mass here is dry mass, next to doing the calculations with the dry mass, it will also be done with the wet mass. This will give two extremes, all natural frequencies that the rocket will experience along the flight, will be between these two values. For determining the stiffness, only the dry mass is used, as the fuel is not a structural member. The fuel mass (64.0 kg for the lower stage and 31.5 kg for the upper stage) is only taken into account in equation (8.52).

The calculations are made for the first and second stage alone, as the connection is assumed to dampen the vibrations enough to not pose any issues. The area of the stage is calculated by $A = \frac{m}{L\rho}$. With the outer diameter set (15 cm for the upper stage and 20 cm for the lower stage), the inner one can be calculated.

In Table 8.20, the results of the calculations are shown. These numbers need to be compared to those in Table 8.19. It can immediately be seen that there won't be any resonance in the longitudinal direction. The eigenfrequencies are one to two orders of magnitude lower than the forcing frequencies in that direction. For the second stage of the rocket, no issues seem to be present either, as the first harmonic falls outside the range of the natural frequencies. The first stage however, the first harmonic falls between the two bounds on the natural frequency. This means that, according to this analysis, somewhere during the burn a point will be hit where resonance will occur. Further analysis is needed to see if the rocket can handle this and if the assumptions produced adequate results. Accurate computational models and testing are necessary to do these analyses in greater detail. These are however beyond the scope of the preliminary design.

8.6.7. Fatigue

Author: D. Norbart

As the rocket will be used multiple times, in which it will endure high vibrational and thermal loads, a fatigue analysis is desired. Furthermore, the rocket will go through a full pressure cycle every launch. From around 0.1 MPa to near vacuum and back.

As fatigue is something that comes with a lot of cycles, the vibrations are the most important part to look at. These vibrations stress the structure in different directions with a high frequency. The first harmonic of the forcing frequency, being the dominant source of vibrations, will be used for the calculations.

The first stage engine will burn for 15 s, at a frequency of 288.5 Hz, as calculated in Section 8.6.6. Multiplying the burn time by the vibration frequency gives a total of 4328 cycles experienced by the rocket. After separation, the second stage will burn for 10 s with a frequency of 369.9 Hz. This gives another 3699 cycles. But these will only be experienced by the second stage. Taking into account the fact that each vehicle has to launch twenty times, these cycles will be multiplied by that number. This gives 86550 total cycles for the lower stage and 160530 total cycles for the upper stage.

To estimate if the cyclic behaviour of these loads will lead to fatigue failure, the stress level should be known too. The maximum thrust force exerted by the lower stage engine is 8600 N, this is 4400 N for the upper stage engine. With the assumption that the rocket is a hollow, constant cross section tube for both stages, this gives a maximum mean stress (σ_m) of 1.87 MPa for the lower stage and 1.90 MPa for the upper stage. With the tensile strength (σ_{ts}) of Al7075 at 572 MPa, using Goodman's rule equation (8.55), an equivalent stress level ($\Delta\sigma_{\sigma_m}$) to failure at zero mean stress ($\Delta\sigma_{\sigma_o}$) can be calculated [91].

$$\Delta\sigma_{\sigma_m} = \Delta\sigma_{\sigma_o}\left(1 - \frac{\sigma_m}{\sigma_{ts}}\right) \tag{8.55}$$

As the upper and lower stage stress are nearly equal, they are taken together to simplify the calculation. The worst case scenario of 1.90 MPa is taken for both stages. The number of cycles is taken at 160530. This brings Goodman's rule to $\Delta\sigma_{\sigma_m} = \Delta\sigma_{\sigma_o} \cdot (0.997)$. The 7075 aluminium, when cycled for $1.6 \cdot 10^5$ cycles, can handle approximately 310 MPa of stress amplitude [96]. This is the value for a zero mean stress, with the 1.9 MPa mean stress, this brings the maximum stress amplitude to $\Delta\sigma_{\sigma_m} = 309.1$ MPa. According to Guéry et al. (2008)[92], the thrust oscillations are in the range of several percent. Taking a very conservative estimate of 10%, this makes the stress oscillations around 190 kPa strong. This only accounts to 0.06% of the maximum oscillation stress that aluminium 7075 can handle.

Even though testing is preferred and some stress concentration areas need to be investigated in more detail later in the design, this analysis does not indicate that fatigue will be in issue. When the atmospheric conditions and high heat loads make the material a lot weaker, it will still have enough margin to survive.

8.6.8. Structure Budgets

Author: S. Yorucu

Editor: L. Alonso

The structure subsystems are broken down into their respective components and conveyed in Table 8.21, below, where the components total mass and raw material cost is given.[34]

Table 8.21: Mass and cost values for the components of the structural subsystem

Parameter	Mass (kg)	Cost (€)
Nosecone	1.26	23.15
Shoulder	1.78	32.66
Lower stage body	2.28	41.84
Upper stage body	1.90	34.87
Total	**7.22**	**132.52**

[34] https://onlinealuminium.nl/en-aw-7075-t651/ [21/06/2023]

8.7. Recovery Sub-System

Author: L. Alonso

This section outlines the design of the recovery sub-system. First, Section 8.7.1 covers the design of the parachutes themselves. Afterwards, Section 8.7.2 will size the suspension lines, subsequently, Section 8.7.3 the mass and cost budgets for recovery are presented. Section 8.7.4 explains the deployment device and finally, Section 8.7.5 presents the configuration of the recovery system.

8.7.1. Parachutes

Author: L. Alonso

Editor: C. Kendall

Recovery is a crucial aspect for the mission's success, and therefore a sizing is necessary for the recovery system chosen. From the trade-off (Section 7.2), it was concluded that the recovery system of both stages will consist of a drogue followed by a larger main parachute. This combination of two parachute sizes limits the touchdown area and recovery loads on the vehicle. However, with the use of the most current simulations, and assuming an extreme wind speed of $10\,\mathrm{m\,s^{-1}}$, the lateral distance the first stage rocket covers with the use of only a main parachute without a drogue was equal to 9.5 km. This value is well inside the allowed dispersion area at Esrange (120 km by 75 km rectangle). This is mainly due to the relatively low apogee of 9 km reached by the first stage. This does not apply to the second stage because its apogee is substantially larger at around 100 km. Therefore, the first stage recovery will only consist of a main parachute, while the second stage recovery will consist of a drogue chute and a main parachute.

This section aims to determine the parachutes and drogue fabric area, and hence, its mass and cost. The parachute configuration and time of deployment are additionally discussed. Moreover, the suspension lines of the parachutes will be sized, allowing for the calculation of the total mass and cost of the main and drogue parachutes.

Note that the following sections will present the initial sizing for the recovery subsystem. The iterations were performed in Python to account for the whole rocket.

Overview of Parachute Openings

With the use of the OpenRocket simulation, it was chosen that the first stage main parachute will be deployed at its apogee at 9 km. Meanwhile, for the second stage, the drogue will open at 60 km altitude after apogee, continued by the second stage main parachute at 2 km altitude. This is shown in Figure 8.9.

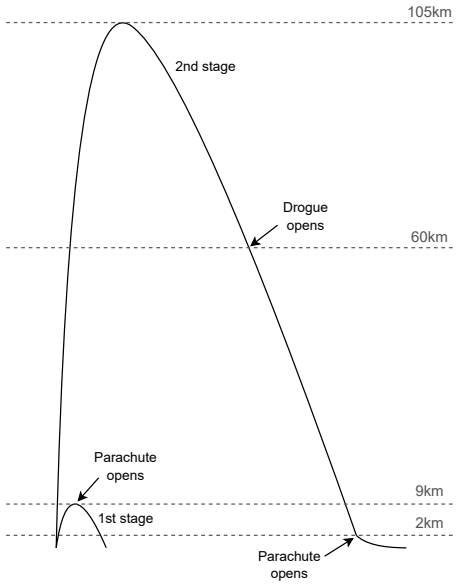

Figure 8.9: Figure displaying the parachute openings

Fabric Area of Parachutes

To calculate the nominal surface (fabric) area, S_o, of the parachutes, the equation of motion at equilibrium must be derived – that is, the equilibrium of the rocket's total weight and the drag caused by the parachute – equation (8.56). This equation is utilised separately to determine the surface area of the parachute canopy for the first stage main parachute and the second stage main parachute and drogue.

$$mg_0 = C_D \frac{1}{2} \rho v_e^2 S_o \tag{8.56}$$

where m represents the the dry mass of the corresponding stage and is approximately 24.4 kg for the first stage and 27.3 kg for the second stage. g_0 is the gravitational acceleration equal to $9.806\,65\,\mathrm{m\,s^{-2}}$.

The equilibrium velocity, or rate of descent, v_e, is chosen for the first and second stage main parachute to be equal to $8\,\mathrm{m\,s^{-1}}$. This value represent the velocity of the rocket with the parachute right before it touches the ground, and is chosen based a similar flight proven vehicle [90, p. 43]. Since this occurs at touchdown, the density of air, ρ, is assumed for the first and second stage main parachute to be equal to the density of air at sea level, $1.225\,\mathrm{kg\,m^{-3}}$.

However, since the drogue chute of the second stage is deployed before the main parachute, the previous assumptions are not valid for the drogue chute. The drogue is designed to open at 60 km altitude after apogee, continued by the second stage main parachute at 2km altitude. Therefore, the drogue is sized to achieve an equilibrium velocity of $25\,\mathrm{m\,s^{-1}}$ at 2 km altitude which results in the density of air, ρ, to be equal to $1.0065\,\mathrm{kg\,m^{-3}}$ with the use of the ISA model.

Lastly, the drag coefficient, C_D, is directly related to the shape of the canopy of the parachute and the drogue chute. Various different shapes of canopies and their respective drag coefficient were found [97]. A table of the various parachute options concisely presents the different fabric areas, S_o, of the parachutes and drogue chutes with varying canopy shapes, and hence, varying drag coefficients. Table 8.22 shows the plausible main parachutes, while Table 8.23 displays the plausible drogue chutes.

For the main parachutes in Table 8.22, the red rows represent unfeasible options because the parachute is either obsolete, or too complex to work with the requirements for the parachute rotation. The light blue rows represent plausible options, and the chosen options are highlighted in a darker blue. For the first stage, a cross shape parachute canopy was chosen because of its ease of manufacture. This leads to a surface area of $9.38\,\mathrm{m^2}$, as shown in the table in turquoise. For the second stage, an annular parachute canopy was chosen because it offers the lowest surface area out of all the plausible options, leading to a surface area of $8.04\,\mathrm{m^2}$, as shown in the table.

For the second stage drogue chute in Table 8.23, the only supersonic drogue, the ribbon hemisflo, was chosen, resulting in a surface area of $2.84\,\mathrm{m^2}$, as shown in the table in turquoise. According to the OpenRocket simulation, the second stage keeps accelerating after apogee, causing the velocity when the drogue chute opens at 60 km to be supersonic at mach numbers higher than 2. Since the ribbon hemisflo drogue chute is the only supersonic drogue that is designed for mach numbers higher than 2, as shown in the table, it is the chosen option.

Table 8.22: Table of the main parachutes surface area with varying parachute canopy shapes

Type:	Name of parachute:	C_D	$C_{X_{max}}$	General Application/ Design Mach (M)	Area (Stage 1)	Area (Stage 2)
Solid textile	Flat circular	0.75	1.7	Obsolete	8.13	9.11
Solid textile	Conical	0.75	1.8	$M \leq 0.5$	8.13	9.11
Solid textile	Biconical	0.75	1.8	$M \leq 0.5$	8.13	9.11
Solid textile	Triconical/Polyconical	0.8	1.8	$M \leq 0.5$	7.62	8.54
Solid textile	Extended Skirt, 10% flat	0.78	1.4	$M \leq 0.5$	7.82	8.76
Solid textile	Ext skirt 14.3 flat	0.75	1.4	$M \leq 0.5$	8.13	9.11
Solid textile	Hemispherical	0.62	1.6	Obsolete	9.84	11.02
Solid textile	Annular	0.85	1.4	$M \leq 0.5$	7.18	**8.04**
Solid textile	Cross	0.65	1.2	Deceleration	**9.38**	10.51
Slotted	Ringslot	0.56	1.05	$0.1 \leq M \leq 0.9$	10.89	12.20
Slotted	Ringsail	0.75	1.1	$M \leq 0.5$	8.13	9.11
Slotted	Disk-gap-band	0.52	1.3	$M \leq 0.5$	11.73	13.13
Rotating	Vortex Ring	1.5	1.2	Small parachutes	4.07	4.55

Table 8.23: Table of the drogue chutes surface area with varying canopy shapes

Type:	Name of drogue:	C_D	$C_{X_{max}}$	General Application/ Design Mach (M)	Area (Stage 2)
Solid textile	Guide surface (ribbed)	0.28	1.2	$0.1 \leq M \leq 1.5$	3.04
Solid textile	Guide surface (ribless)	0.3	1.4	$0.1 \leq M \leq 1.5$	2.84
Slotted	Flat (fist)	0.45	1.05	Obsolete	1.89
Slotted	Conical ribbon	0.5	1.05	$0.1 \leq M \leq 2$	1.70
Slotted	Conical ribbon (varied porosity)	0.55	1.3	$0.1 \leq M \leq 2$	1.55
Slotted	Ribbon (hemisflo)	0.3	1.3	Supersonic ($1 \leq M \leq 3$)	**2.84**
Rotating	Rotofoil	0.85	1.05	-	1.00
Rotating	Sandia RFD	1.25	1.1	-	0.68

The tables additionally present the shock load factor, C_X, for each parachute, which is used to aid the sizing of the altitude of the parachute openings. Since the main parachute of the first stage is deployed at apogee, the shock load is small, as no vertical drag acceleration is present. However, according to the OpenRocket simulation, for the second stage the acceleration of the vehicle at 60 km before the drogue opens is equal to $35\,\mathrm{m\,s^{-2}}$. By applying the shock load factor of the chosen drogue chute equal to 1.3, it results in an acceleration of $45.5\,\mathrm{m\,s^{-2}}$ equal to 4.64 g. Moreover, for the second stage main parachute, the acceleration of the vehicle at 2 km when the parachute opens is equal to $90\,\mathrm{m\,s^{-2}}$. By applying the shock load factor of the chosen parachute equal to 1.4, it results in an acceleration of $126\,\mathrm{m\,s^{-2}}$ equal to 12.84 g. Both these accelerations with the shock loads applied satisfy and are significantly under the payload requirement (SYS-PL-05) of a maximum load of 50 g.

Parachutes Fabric Mass and Cost

The fabric chosen for the parachute canopy is ripstop nylon because of its high reliability and its widely known use for parachutes [97]. The mass of the parachutes canopy fabric can be estimated by multiplying the surface areas found in the previous section by the density of ripstop nylon of $35\,\mathrm{g\,m^{-2}}$ which is determined from commercially available sources.[35] The cost is similarly calculated by multiplying the surface areas by €$9.41\mathrm{m^{-2}}$.[35] The results are shown in Table 8.24.

[35] `http://www.paragear.com/skydiving/10000042/W9110W/` [12/06/2023]

Table 8.24: Table of the parachutes mass

Parachute:	Mass (kg):	Cost (euros):
first stage main parachute	0.33	88.31
second stage main parachute	0.10	26.70
second stage drogue chute	0.28	75.62

8.7.2. Suspension Lines

Author: L. Alonso

The suspension lines are the lines that connect the parachute canopy to the vehicle. To calculate the total mass of all suspension lines in one parachute, the line length to canopy diameter (L/D) ratio, as well as the number of lines and their density are needed. The length of the suspension lines is determined by multiplying the L/D ratio by the nominal diameter of the parachute canopy, which is calculated with Equation (8.57) [97].

$$D_o = \sqrt{\frac{4S_o}{\pi}} \tag{8.57}$$

The total mass of all the suspension lines in one parachute is calculated by multiplying the number of lines by the length of the line and by the mass per metre ($4.976\,\mathrm{g\,m^{-1}}$), determined from a commercially available source.[36] The total cost of the lines is similarly calculated by multiplying the total length of the lines by the cost per metre equal to €$1.1264\mathrm{m}^{-1}$.[36] The results are shown in Table 8.25.

Table 8.25: Table of the suspension lines sizing

Parachute:	D_o (m)	L/D ratio	Line Length (m)	No. of lines	Total mass (kg)	Total cost (euros)
first stage main	3.46	1.40	4.84	8	0.19	43.61
second stage drogue	1.90	2.00	3.80	24	0.45	102.76
second stage main	3.20	1.25	4.00	24	0.48	108.08

8.7.3. Total Mass and Cost

The total mass and cost of the parachutes per vehicle are calculated by adding up the mass and cost values of the fabric and suspension lines, resulting in Table 8.26.

Table 8.26: Table of the total mass and cost of the parachutes

Parachute:	Total mass (kg)	Total cost (€)
first stage main	0.52	131.92
second stage drogue	0.55	129.47
second stage main	0.76	183.70
Total:	**1.83**	**445.09**

8.7.4. Parachute Deployment Device

Author: L. Alonso

Editor: C. Kendall

This section aims to explain the configuration of the parachute deployment devices, as well as determine the total mass and cost of the deployment devices used. The deployment device used for the parachutes and drogue chute was chosen to be CGDDs. This consists of a tank of compressed gas (usually nitrogen or carbon dioxide – in this case, nitrogen is chosen for sustainability reasons) from which the flow is controlled by a valve. When the valve is opened, the compressed gas ejects the parachute out of the vehicle.

[36] `https://sky-shop.eu/lines-spectra1000-yard` [12/06/23]

Mass and Cost of Deployment Devices

The mass of a single CGDD is taken from a commercial manufacturer of CGDDs for amateur high power rockets.[37] The mass is equal to 0.5 kg, and since the rocket uses 3 CGDDs (one for each of the first and second stage parachute systems, and one for the deployment of the vehicle nosecone), the total mass is equal to 1.5 kg. The cost for an equivalent commercial device is €530. This results in a total cost of the deployment devices of €1590 per vehicle. Note that a comparable system may be developed, but the commercial device is taken as representative in terms of mass and cost.

8.7.5. Configuration of Recovery Sub-system

Author: L. Alonso
Editor: C. Kendall

The configuration of the parachute recovery systems needs to be selected for both the first and second stage. While the main purpose of the parachute is for recovery, the parachute can also also aid in retrieval by being clearly visible against the surrounding environment. Vibrant contrasting fabric colours are thus used, with orange being a colour contrasting against most environments.

First Stage Recovery Bay

The configuration of the first stage recovery sub-system inside the recovery bay is shown in Figure 8.10a. The image presents a CAD render of the upper part of the first stage of the rocket. The section where the diameter of the outer skin reduces is the shoulder. It takes advantage of the slip fit mechanism, previously mentioned in Section 8.6.3, to connect with the second stage of the rocket. In this render only the first stage is shown, leaving the opening at the top. The model is cut in half revealing the first stage main parachute highlighted in red, as well as the deployment device. The cold gas tank is represented by the blue tank which when utilised the pressurised air exerts force on the displayed brown disk, known as a sabot. This leads to the sabot which propels the parachute out of the opening, resulting in the configuration shown in Figure 8.10b.

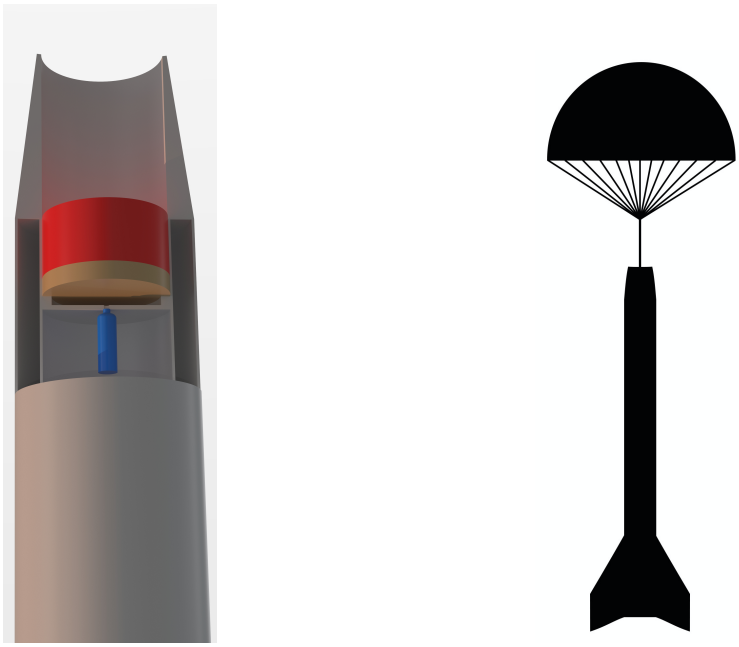

(a) Recovery bay configuration **(b)** Main parachute configuration

Figure 8.10: First stage recovery configuration

[37] `https://shop.fruitychutes.com/products/hawk-co2-system-kit-16-to-45-gram` [13/06/2023]

Second Stage Recovery Bay

For the recovery system of the second stage of the sounding rocket, the recovery bay is sized by taking into account the volume the parachutes occupy. This volume, V_{rb}, is calculated by dividing the mass of the parachute fabric, m_{par}, by a constant packing density, $\rho_{pack} = 217.27\,\mathrm{kg\,m^{-3}}$ based on data from DARE. From this volume, the height of the recovery bay, h_{rb}, can be calculated with the use of equation (8.58).

$$h_{rb} = \frac{V_{rb}}{\pi(\frac{D_u}{2})^2} = \frac{\frac{m_{chutes_u}}{\rho_{pack}}}{\pi(\frac{D_u}{2})^2} = 0.10\,\mathrm{m} \tag{8.58}$$

where the m_{chutes_u} is the added mass of the second stage drogue chute and main parachute fabric, determined in Section 8.7.1 and equal to 0.38 kg. As previously mentioned, D_u is the diameter of the upper stage equal to 0.15 m.

This results in the height of the recovery bay to be 0.10 m, which is used as a parameter in the the sizing of the body tube in Section 8.6.2. The configuration of the second stage recovery subsystem inside the recovery bay is shown in Figure 8.11a. The image presents a CAD render of the top part of the second stage of the rocket after separation, where the bottom part is the beginning of the nosecone. The model is cut in half revealing the second stage drogue chute highlighted in red, the main parachute highlighted in orange, as well as the deployment device. Note that the cold gas tank and the sabot are represented in the exact manner as the first stage recovery bay configuration. When the pressurised gas propels the drogue chute out at 60 km; the configuration is shown in Figure 8.11b. A pyrotechnic line cutter can then be used to deploy the main parachute, which is stored in a bag and bypassed by a line which ensures that the bag and main parachute are unloaded. When the bypass line is severed, the drogue chute becomes the pilot for the main parachute, pulling it out of the bag. The main parachute is deployed at an altitude of 2 km, where its configuration is shown in Figure 8.11c.

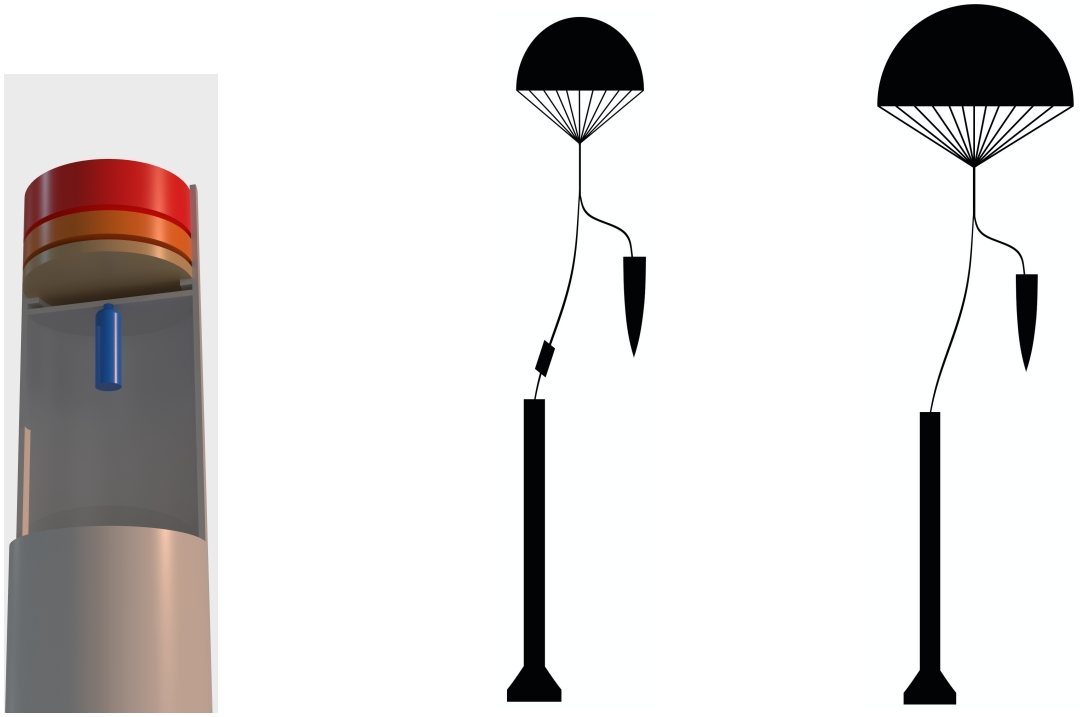

(a) Recovery bay configuration **(b)** Drogue chute configuration **(c)** Main parachute configuration

Figure 8.11: Second stage recovery configuration

8.8. Avionics Sub-System

Author: L. Tabaksblat
Editors: C. Kendall, E. Chen

The avionics are essential for ensuring the successful completion of the mission. Not only are they responsible for the deployment of the recovery system, they are also responsible for ensuring that the payload data is stored. In this section, the sizing and preliminary design of the avionics will be discussed.

As the recovery of the data determines the mission success, it was decided to use two systems for storing the data. The first system is a flight recorder on board of the rocket capable of surviving a possible crash. The second system is a telemetry system sending the payload data to the ground station where it will be stored. This allows for the data to always be recovered, even if the flight recorder fails.

Due to the importance of the avionics, stage will carry fully redundant avionics systems. This means that each stage carries two identical electronics stacks, each with their own flight recorder, battery and power system. The only non-redundant subsystem is telemetry, since this relies on fixed frequency ranges and external antenna mounting. During the detailed design phase, redundancy will also be used for all essential deployment systems such as the parachute deployment and ignition system.This ensures that even if one system fails the a successful mission will still occur.

As failure is still always a possibility, one of the most important forms of data is camera data, as this allows for visual indication regarding the failure of the vehicle. For this reason each stage will have 2 cameras. On the first stage one camera will look up – checking for successful staging and parachute deployment – and a second camera will be looking down to check for correct engine ignition and functioning. The second stage similarly will have one camera looking down to check for engine ignition and staging, and one camera looking up to check for correct payload and parachute deployment.

In addition to adding redundancy to prevent failure, the rocket will also be charged in the launch tower to prevent the electronics from running out of battery power due to potential launch delays. The cable by which the rocket will be powered is called the umbilical. The umbilical will also be responsible for communication in the tower, as cable based communication is more reliable and less prone to errors. The umbilical will also transmit the arming signal to the rocket from the ground software.

As the electronics design will very quickly go into a detailed design, the only systems that will be sized currently are the batteries, telemetry, and storage system. This is because the telemetry is essential for the power and link budget and therefore needs to be sized. Due to the power requirements of the payload and telemetry, the battery mass will be a significant contribution to the mass budget. Furthermore, the storage sizing will be used to make a preliminary data storage budget.

8.8.1. Telemetry

Author: L. Tabaksblat
Editor: C. Kendall

As the ground systems have already been designed by Esrange [98], the link budget can be calculated quite easily. Furthermore, Esrange also gives recommendations for the carrier frequency, maximum transmission power, and maximum bandwidth. The recommended downlink frequency from Esrange is in the range of 2.3 GHz to 2.4 GHz. For this reason, a frequency of 2.4 GHz and 2.3 GHz for the first and second stage were chosen. Different frequencies were chosen to ensure that the signals from both stages would not interfere with each other and were not in each others bandwidth. Furthermore, after multiple iterations, a transmission power of 5 W was chosen as this is sufficient for the required Signal-to-Noise Ratio (SNR) and is less than the recommended maximum power of 10 W.

The first assumption made to calculate the link budget was that the transmitter antenna has a gain of 0 dB. This assumption was made as a fairly omnidirectional antenna is desired to ensure contact with the ground stations occurs. Furthermore, the actual antenna will be chosen in the future and therefore has been set to 0 dB to prevent overestimation of the actual link budget. As it is difficult to estimate losses due to atmospheric losses, polarisation

mismatch, losses due the rocket body, and component losses, it was decided to assume a loss of 10 dB meaning a 10 times reduction in the SNR. This is to prevent an overestimation of the SNR of the system and acts as a safety factor. In the future a much more in depth link budget analysis will be performed. QPSK modulation is chosen based on recommendations in the IRIG-106 telemetry standard for its spectral efficiency at high data rates [99].

Using the parameters shown in Table 8.27, the formulae from "Digital and Analog Communication Systems" by Couch[100] were used to estimate the final SNR and bandwidth. To calculate the SNR, the distance was set to 200 km to calculate the free-space loss (estimated, based on simulations, as the furthest telemetry distance). Furthermore, Esrange has multiple ground stations; for this initial phase, the ground station with the best performance was used. The calculations gave the estimations mentioned in Table 10.7. For the bandwidth the theoretical modulation spectral efficiency was used to estimate the required bandwidth. Quadrature phase shift keying was chosen as it has a theoretical spectral efficiency of 2 meaning that the bandwidth can be equal to half of the data rate. Furthermore, this is a commonly used modulation technique, meaning that it will be easy to find electronics for the telemetry system and that this system is compatible with the Esrange ground systems.

Table 8.27: Telemetry system initial variables

Parameter	Symbol	Initial Value Stage 1	Initial Value Stage 2	SI Units
Carrier frequency	f_c	2.4	2.3	GHz
Data rate	R_{data}	8.95	9.01	$\mathrm{Mbits\,s^{-1}}$
Modulation	-	QPSK	QPSK	-
Transmission gain	G_{Tx}	0	0	dB
Transmission distance	d_{rocket}	60	200	km
Velocity	v	1.8	1.8	$\mathrm{km\,s^{-1}}$
Ground station antenna diameter	$d_{antenna}$	5	5	$\mathrm{m^2}$
Ground Station antenna noise ratio	G/T	12	12	$\mathrm{dB\,K^{-1}}$
Antenna efficiency	η	0.5	0.5	-
Margin	-	25	25	%

In the future, to be compatible with the ground systems of launch sites, a telemetry standard should be chosen. As Esrange will be the primary launch site, the telemetry package standard chosen will be the IRIG-106 standard [99], as mentioned in the Esrange user handbook [98]. This means that the data rate will increase due to the requirements set by the IRIG standard such as, for example, the need for a header and error correction data such as a checksum.

8.8.2. Power Distribution

Author: L. Tabaksblat
Editors: C. Kendall, E. Chen

The two most reasonable options for the vehicle batteries are lithium-ion and Lithium-Polymer (LiPo), due to their high power density, low cost, and high discharge rate. There are also other options commonly used for larger rockets such as NASA's Space Launch System. However, as the size of the Altus rocket is much smaller, and therefore the available volume and mass budget much lower, a high energy density becomes essential. Therefore, Lithium-Polymer was chosen, as it has the highest energy density of the possible battery types. Furthermore, this battery type is commonly used in electronics requiring higher discharge rates. The biggest downside of these batteries is their more complex requirements for charging and discharging, their sensitivity to temperature, and their risk of combustion in case of improper handling.

Based on the power estimations made for all of the avionics, it is estimated that the avionics need 23 W of power excluding the telemetry power. The payload will have a separate battery to reduce to chance of power loss of the payload and will need 36.2 W of power. As these are very basic estimations, a margin will need to be applied to this. Furthermore, the depth of discharge (DOD) needs to be decided as the higher the depth of discharge the more charge cycles the battery can handle. A depth of discharge of around 70% should be sufficient as this would provide around 475 cycles given an acceptable loss of 10% [101]. The total battery energy in Wh can then be determined by

multiplying the power required with the desired battery lifetime and multiplying it with the margin increase divided by the DOD. The continuous battery time for sizing is set to 2 hours. With a flight time of around 20 minutes, the rocket will continue to transmit its location for 1 hour and 40 minutes after touchdown. This should be enough time to get an accurate grasp of the location of the vehicle and to approach the touchdown location.

As batteries are sized in Ah, this is also calculated. For this the average voltage has to be chosen: as six cell LiPos are common commercial batteries their average voltage was chosen, giving an average voltage of 24 V. This is also a commonly used voltage level for valves and actuators. By dividing the total energy by the average voltage, the battery size in Ah can be found. The mass estimation can be made then by dividing the required battery energy with the energy density of a LiPo. In this case the lowest energy density of $140\,\mathrm{W\,h\,kg^{-1}}$ was assumed [102]. This gives a battery mass of 0.36 kg for the avionics per electronics board, and 0.923 kg for the payload.

Table 8.28: Battery system initial variables

Parameter name	Symbol	Initial Value Stage 1	Initial Value Stage 2	Initial Value Payload	SI Units
Battery Duration	t_{bat}	2	2	2	hrs
Telemetry Power	$P_{telemetry}$	5	5	0	W
Sensor Power	P_{sensor}	23	23	36.2	W
Depth of Discharge	dod	70	70	70	%
Average Voltage	V_{avg}	24	24	24	V
Margin	-	25	25	25	%

8.8.3. Data Storage

Author: L. Tabaksblat
Editor: C. Kendall

In Table 10.2, the data rate estimations can be found. As the exact sensors have not been chosen yet due to this design being a preliminary design, a margin of 25% was chosen to prevent an underestimation of the required data rate and therefore the minimum storage size. Furthermore, the required logging time will also be overestimated to reduce the risk of the storage space being too small leading to data being lost. For now, the required logging time was chosen to be equal to the required battery time of two hours to ensure that in the worst case scenario of continuous logging no data would be lost. This leads to a required data storage of 5.03 Gbytes per flight recorder for the avionics. Considering that storage is usually sold in powers of two, the storage size will therefore be 8 Gbytes for all flight recorders. The payload only needs a flightrecorder of 0.1 Gbytes and will therefore use a memory of 1 Gbit or 0.125 Gbytes.

8.8.4. Avionics Mass & Costs

Author: L. Tabaksblat
Editor: C. Kendall

The avionics cost breakdown can be found in Table 8.29. As avionics is heavily dependent on the detailed design the only costs that are relatively precisely known are the estimated battery costs and the cost for the data storage. All other sensors including the cameras are based on similar components but have not been chosen definitively. The antennas were assumed to be relatively inexpensive as they will have to be designed in-house, which results in increased labour costs but significantly reduced material costs. For this reason, antennas were estimated to cost €20 each. The general electronics are extremely dependent on the final design and difficult to estimate at the current design phase due the specifications. For this reason, a large budget was estimated for the general electronics. The cost in Table 8.29 are for all electronics in total meaning two electronics boards per stage for two stages. It also contains the flight recorder, Battery Management System (BMS), and batteries for the payload.

Similarly to the cost budget the only mass estimation that is reliable is the expected battery mass. Due to the mass being dependent on the detailed electronics design any other estimations are difficult. However, this is not a significant problem as the majority of the weight will come from the batteries. Table 8.29 also contains the mass of

the flight recorder, BMS, and batteries for the payload.

Table 8.29: Cost budget for the avionics

Instrument	Amount	Total mass (kg)	Total Cost (€)
IMU [103] [38]	4	0.22	14600
GPS [104] [39]	4	0.08	80
Pressure sensor (engine) [105] [40]	4	0.234	560
Thermocouple [41]	4	0.0004	200
Camera [106] [42]	4	0.504	1600
Telemetry [107] [43]	2	0.04	1548.6
Antenna	4	0.4	80
Battery [44]	5	2.35	700
BMS [108] [45]	5	0.0025	60
Data Storage [109] [46]	5	0.005	100
General	4	1	4000
Total	-	4.83	23528.60

[38] https://www.xsens.com/hubfs/Downloads/Leaflets/MTi-300.pdf [16/06/2023]

[39] https://nl.farnell.com/stmicroelectronics/teseo-vic3da/gnss-dead-reckoning-module-1-57542ghz/dp/3806254[16/06/2023]

[40] https://www.ifm.com/nl/nl/product/PT5502?gad=1gclid=CjwKCAjwp6CkBhB_EiwAlQVyxX9nXOEo7qzJrVLeifDEQMXUZpP3IN1p9Veu1VnQotwOtv92iHXvrhoC9vIQAvD_BwE[16/06/2023]

[41] https://nl.rs-online.com/web/p/thermocouples/8722613[16/06/2023]

[42] https://gopro.com/en/us/shop/cameras/hero8-black/CHDHX-801-master.html[16/06/2023]

[43] https://www.digikey.nl/en/products/detail/texas-instruments/AFE7769IABJ/10445292[16/06/2023]

[44] https://www.rcracingtwente.nl/product/spektrum-22-2v-5000mah-6s-30c-smart-lipo-battery-ic5-spmx50006s30/[16/06/2023]

[45] https://nl.mouser.com/ProductDetail/Texas-Instruments/BQ76PL536ATPAPTQ1?qs=sGAEpiMZZMug9GoBKXZ75%252BV7oilvYIdtgq6XqT5yLsQ%3D[16/06/2023]

[46] https://nl.rs-online.com/web/p/flash-memory/2420193?cm_mmc=NL-PLA-DS3A-_-google-_-CSS_NL_EN_Semiconductors_Whoop-_-(NL:Whoop!)+Flash+Memory-_-2420193&matchtype=&aud-772940708119:pla-340537612551&gclid=CjwKCAjwyqWkBhBMEiwAp2yUFsECUVaBK2K_LtM5q8nC-LfNdwnZ0gklaZ6DwcoC3Z3mzv6ikX8DQhoCmngQAvD_BwE&gclsrc=aw.ds[16/06/2023]

9
Quality Assessment

Editor: L. Tabaksblat

With the preliminary design completed, quality assessment needs to be conducted for both the design and the design tools. In Section 9.1, the design is compared against all the requirements in order to check for compliance. Afterwards, the verification and validation methods of the software are discussed in Section 9.2. This includes results from unit tests of the sizing code, sensitivity testing of the iterative optimisation approach, and the results from the validation of the simulation tool.

9.1. Requirements Compliance and Sensitivity

Author: E. Chen

Editor: C. Kendall

In Chapter 5, the requirements for the vehicle were identified based on the stakeholder requirements and the mission. The design of the vehicle shall be in compliance with all of these requirements, which were taken into account during the preliminary design presented in Chapter 8. This has resulted in a preliminary vehicle design, which is checked for compliance with the requirements. At this point, not every requirement can be checked for compliance, since some cover more detail than is presently available. As such, the compliance will be classified as either "compliant", "non-compliant", or "intend to comply". A requirement intended to be compliant, indicates that the preliminary design does not, for now, violate the requirement, but that it shall be treated during the detailed design. Remarks are made about the sensitivity of the system to requirements compliance. Sensitivity is a metric that is associated with performance requirements,and hence the majority of the requirements are set to 'N.A.' for sensitivity in the compliance matrix. For requirements that are categorised as 'intend to comply' the sensitivity has been set to 'T.B.D.', meaning to-be-determined. For the performance requirements that are compliant, they are either marked as sensitive: 'Yes', or insensitive: 'No', based on the amount of margin. The compliance matrix is shown in Table 9.1.

A special note must be made about *SYS-GN-05*: "The tower exit velocity of the vehicle shall be at least 40 ms^{-1}", which is compliant but sensitive. Currently, due to the nature of the design software, the rocket engine is sized for exactly the requirement. If it's not monitored going forward, this requirement could become non-compliant later in the design. However, this can be solved by adopting an appropriate thrust curve in the detailed design phase.

As indicated in the compliance matrix, the compliance checks show that the current vehicle configuration conforms to the evaluated performance requirements, since these were used during the iterative sizing of the vehicle subsystems. Furthermore, the compliance of additional requirements can be confirmed based on the preliminary design in Chapter 8. The methods for the verification of the remaining requirements are presented in Chapter 5 and are elaborated upon in Table 9.1.

Table 9.1: Requirements Compliance Matrix

Code	Compliance	Sensitive?	Comment
STK-MR-01	Compliant	No	Simulated to 110 km, more than requirement
STK-MR-02	Compliant	No	Payload mass at 12 kg, less than requirement
STK-MR-03	Compliant	No	Adequate sensors are included for PMC study
STK-MR-05	Compliant	No	Adequate sensors are included for PMC study

Table 9.1: Requirements Compliance Matrix

Code	Compliance	Sensitive?	Comment
STK-MR-06	Compliant	No	Vehicle contains a sample collection system
STK-MR-07	Compliant	No	Sensors are included in the design for performance characterisation
STK-MR-08	Intend to comply	T.B.D	A 2026 launch date is the goal, but compliance is uncertain
STK-LS-01	Intend to comply	T.B.D	Preliminary design meets safety requirements, but currently inadequate detail for full compliance
STK-LS-02	Intend to comply	T.B.D	The rocket is designed for the Esrange requirements and recommendations
STK-PR-01	Intend to comply	T.B.D	Viable syntheses are available for the propellant but viability needs to be proven
STK-PR-02	Compliant	No	AND/HTPB is not toxic to the environment
STK-PR-03	Intend to comply	T.B.D	Requires propellant exhaust measurements. Expected to meet the guidelines after dispersal
STK-RE-01	Intend to comply	T.B.D	Requires demonstration during test flights
STK-RE-02	Intend to comply	T.B.D	Requires demonstration during test flights
STK-MK-01	Compliant	No	The payload section allows for a 6U payload
STK-FI-01	Intend to comply	T.B.D	Requires updated cost estimation after detailed design
LCH-GN-01	Compliant	N.A.	Telemetry system is compliant
LCH-GN-02	Intend to comply	N.A.	Requires Six Degrees Of Freedom (6DOF) trajectory simulation
LCH-GN-03	Compliant	N.A.	Vehicle includes FTS
LCH-GN-04	Compliant	N.A.	Each stage is below 5 m and fits within a container
LCH-GN-05	Intend to comply	T.B.D	Requires conducting an integration test for setup time estimates
LCH-GN-06	Intend to comply	T.B.D	Rocket and engine can be prepared in advance
LCH-GS-01	Compliant	N.A.	Remote control possible through umbilical
LCH-GS-02	Compliant	N.A.	Both GNSS tracking and radar are available
LCH-GS-03	Compliant	N.A.	Both tracking systems are independent
LCH-GS-04	Compliant	N.A.	Frequencies are compliant with ESA ground stations
LCH-SF-01	Compliant	N.A.	Vehicle includes FTS
LCH-SF-02	Compliant	N.A.	Compatible materials are used with hazardous chemicals
LCH-SM-01	Intend to comply	T.B.D	Requires 6DOF debris disperson simulation
LCH-SM-02	Intend to comply	T.B.D	Requires 6DOF debris disperson simulation
LCH-SM-03	Intend to comply	T.B.D	Requires 6DOF debris disperson simulation
LCH-SM-04	Intend to comply	T.B.D	Requires 6DOF debris disperson simulation
LCH-SM-05	Intend to comply	T.B.D	Requires 6DOF debris disperson simulation
LCH-SM-06	Intend to comply	N.A.	Not yet explored, requires test flight to prove
SYS-AV-01	Compliant	N.A.	Vehicle includes adequate sensors for launch detection: Inertial Measurement Unit (IMU) for detectin launch acceleration
SYS-AV-02	Compliant	N.A.	Vehicle includes GNSS tracking for apogee detection
SYS-AV-03	Compliant	N.A.	Vehicle includes adequate sensors: IMU for detecting no deceleration and GNSS for detecting touchdown altitude
SYS-AV-04	Compliant	N.A.	Vehicle includes adequate sensors: IMU for detecting sudden change in acceleration
SYS-AV-05	Compliant	N.A.	Avionics communicate with payload
SYS-AV-06	Intend to comply	N.A.	Requires thermal testing of avionics
SYS-AV-07	Compliant	N.A.	Telemetry system uses frequencies compliant with esrange adviced frequencies
SYS-AV-08	Compliant	N.A.	Vehicle includes a flight data recorder

Table 9.1: Requirements Compliance Matrix

Code	Compliance	Sensitive?	Comment
SYS-AV-09	Compliant	N.A.	Vehicle includes engine pressure sensors
SYS-AV-10	Compliant	N.A.	Vehicle includes an engine temperature sensor
SYS-AV-11	Compliant	N.A.	Both stages have avionics systems
SYS-AV-12	Compliant	N.A.	Redundant avionics are present in the design
SYS-AV-13	Compliant	N.A.	Redundant flight data recorders are present in the design
SYS-AV-14	Compliant	N.A.	The avionics use redundant sensors
SYS-AV-15	Intend to comply	T.B.D	Requires thermal testing of avionics
SYS-AV-16	Intend to comply	T.B.D	Requires humidity testing of avionics
SYS-AV-17	Compliant	N.A.	Vehicle includes GNSS tracking
SYS-AV-18	Compliant	N.A.	Separation monitoring camera is present in design
SYS-AV-19	Compliant	N.A.	Payload monitoring camera is present
SYS-AV-20	Compliant	N.A.	Recovery camera is present in first stage
SYS-AV-21	Compliant	N.A.	Recovery camera is present in second stage
SYS-AV-22	Intend to comply	T.B.D	Requires calibration and characterisation of sensor
SYS-AV-23	Intend to comply	T.B.D	Requires calibration and characterisation of sensor
SYS-AV-24	Compliant	No	Within accuracy of GNSS tracking, sufficient margin to prevent sensitivity
SYS-AV-25	Compliant	No	Signal-to-noise ratio is estimated to be 28.1 dB at 120 km which is higher than 12 dB, sufficient margin to prevent sensitivity
SYS-AV-26	Intend to comply	N.A.	Telemetry protocols are not yet designed, but will adhere to IRIG-106
SYS-AV-27	Compliant	No	2300-2400 MHz is used for telemetry, this is not expected to change
SYS-AV-28	Compliant	No	Sizing indicates a telemetry range greater than 120 km, suffcient margin to prevent sensitivity
SYS-GN-01	Compliant	N.A.	The vehicle has a propulsion system
SYS-GN-02	Compliant	N.A.	The vehicle has recovery systems
SYS-GN-03	Compliant	N.A.	Simulations indicate static stability throughout the flight
SYS-GN-04	Compliant	N.A.	The nosecone is ejected to expose the payload
SYS-GN-05	Compliant	Yes	The tower escape velocity is exactly 40 $\mathrm{m\,s^{-1}}$, this needs to be adressed in detail design
SYS-GN-06	Compliant	No	The parachutes are sized for a touchdown velocity of 8 $\mathrm{m\,s^{-1}}$, sufficient margin to prevent sensitivity
SYS-GN-07	Intend to comply	N.A.	Requires flight testing with damage analysis
SYS-GN-08	Intend to comply	N.A.	Requires flight testing with damage analysis
SYS-GN-09	Compliant	N.A.	GNSS tracking is available
SYS-GN-10	Compliant	N.A.	GNSS tracking is available
SYS-GN-11	Compliant	N.A.	GNSS tracking is available
SYS-GN-12	Compliant	N.A.	Avionics include attitude sensors
SYS-GN-13	Compliant	N.A.	Avionics include inertial sensors
SYS-GN-14	Compliant	N.A.	Calibration sensor data required such as rocket temperature is measured throughout the entire flight
SYS-GN-15	Intend to comply	N.A.	Structural analysis and physical testing required
SYS-GN-16	Intend to comply	N.A.	Requires a payload integration test
SYS-GN-17	Compliant	N.A.	The payload is protected by the vehicle nose cone
SYS-GN-18	Intend to comply	T.B.D	Requires demonstration of reuse during test flight
SYS-GN-19	Intend to comply	T.B.D	Requires structural analysis and stress testing

Table 9.1: Requirements Compliance Matrix

Code	Compliance	Sensitive?	Comment
SYS-GN-20	Intend to comply	N.A.	Requires detailed design and integration demonstration
SYS-GN-21	Compliant	No	Simulated stability margin is at 4, sufficient margin to prevent sensitivity
SYS-GN-22	Compliant	No	Stability margin is at 4, margin sufficient to prevent sensitivity
SYS-GN-23	Intend to comply	T.B.D	Requires structural analysis and stress testing
SYS-GN-24	Compliant	No	The maximum dynamic pressure is estimated to be 160 kPa (below 200 kPa limit), margin is sufficient
SYS-GN-25	Compliant	No	Simulated burnout altitude is 25 km (below 50 km limit), sufficient margin to prevent sensitivity
SYS-PL-01	Intend to comply	T.B.D	Requires thermal testing of payload
SYS-PL-02	Intend to comply	N.A.	Requires detailed design and thermal testing
SYS-PL-03	Intend to comply	T.B.D	Requires humidity testing of electronics
SYS-PL-04	Intend to comply	T.B.D	Requires humidity testing of payload
SYS-PL-05	Intend to comply	T.B.D	Requires structural analysis and payload testing
SYS-PL-06	Compliant	N.A.	A standard cubesat payload mounting is used
SYS-PL-07	Intend to comply	N.A.	The payload flight data recorders may differ from mission to mission
SYS-PL-08	Intend to comply	T.B.D	Storage requirements may differ from mission to mission
SYS-PL-09	Intend to comply	T.B.D	Requires vibration testing of payload
SYS-PL-10	Intend to comply	T.B.D	Requires pressure testing of payload
SYS-PL-11	Intend to comply	T.B.D	Requires thermal testing of payload
SYS-PL-12	Compliant	N.A.	The vehicle uses a common cubesat payload form factor
SYS-PL-13	Intend to comply	T.B.D	Max vehicle acceleration is 15 g, 35 g below the payload acceleration limit of 50 g
SYS-PL-14	Compliant	N.A.	Recovered vehicle contains blackboxes
SYS-PL-15	Compliant	N.A.	Can be controlled through umbilical
SYS-PL-16	Intend to comply	T.B.D	Requires calibration and characterisation of sensor
SYS-PL-17	Intend to comply	T.B.D	Requires calibration and characterisation of sensor
SYS-PL-18	Intend to comply	T.B.D	Requires calibration and characterisation of sensor
SYS-PL-19	Intend to comply	T.B.D	Requires calibration and characterisation of sensor
SYS-PL-20	Intend to comply	T.B.D	Requires calibration and characterisation of sensor
SYS-PL-21	Intend to comply	T.B.D	Requires calibration and characterisation of sensor
SYS-PL-22	Compliant	N.A.	Payload contains sample collector
SYS-PL-23	Intend to comply	T.B.D	Requires structural analysis and testing of payload
SYS-PL-24	Intend to comply	T.B.D	Requires structural analysis and testing of payload
SYS-PL-25	Intend to comply	T.B.D	Requires structural analysis and testing of payload
SYS-PL-26	Intend to comply	T.B.D	Requires structural analysis and testing of payload
SYS-PL-27	Intend to comply	T.B.D	Requires structural analysis and testing of payload
SYS-PR-01	Intend to comply	N.A.	Viable syntheses are available for the propellant but approach needs proven
SYS-PR-02	Compliant	N.A.	Both hardware and software arming
SYS-PR-03	Compliant	N.A.	Indicated by audio and data interface
SYS-PR-04	Intend to comply	N.A.	Requires hydrostatic testing of motor
SYS-PR-05	Intend to comply	T.B.D	Requires qualification burn tests of motor
SYS-PR-06	Intend to comply	T.B.D	Requires hydrostatic testing of motor
SYS-PW-01	Compliant	No	Worst case battery life is sized for 2 hours, sufficient margin to prevent sensitivity

Table 9.1: Requirements Compliance Matrix

Code	Compliance	Sensitive?	Comment
SYS-PW-02	Compliant	No	Telemetry system has a 5 W output, sufficient margin to prevent sensitivity
SYS-PW-03	Compliant	N.A.	Separate power systems are used for the payload
SYS-PW-04	Intend to comply	N.A.	Depends on payload design
SYS-PW-05	Compliant	N.A.	Avionics have redundant power sources
SYS-PW-06	Compliant	N.A.	System contains a battery management system and external charging
SYS-RC-01	Intend to comply	T.B.D	Requires demonstration of reuse during test flight
SYS-RC-02	Intend to comply	T.B.D	Requires demonstration of reuse during test flight
SYS-RC-03	Intend to comply	T.B.D	Requires demonstration of reuse during test flight
SYS-RC-04	Intend to comply	T.B.D	Requires demonstration of reuse during test flight
SYS-RC-05	Intend to comply	T.B.D	Requires wind tunnel or drop testing of parachute
SYS-RC-06	Intend to comply	T.B.D	Requires wind tunnel or drop testing of parachute
SYS-RC-07	Intend to comply	T.B.D	Requires wind tunnel or drop testing of parachute
SYS-RC-08	Compliant	N.A.	Visible parachute colors used (orange)
SYS-RC-09	Intend to comply	T.B.D	Requires testing to measure deployment reaction time

9.2. Design Tool Verification & Validation

Transporting a scientific payload to the upper atmosphere is a difficult task. To have confidence in a design that is capable of achieving such a task, the design has to be simulated, verified and validated. A computational model was made to simulate the flight of the rocket, as previously mentioned in Section 8.1. The verification and validation of the simulation are explained below, in Section 9.2.1 and in Section 9.2.2, respectively.

9.2.1. Verification

Authors: S. Yorucu, M. Beenders
Editor: C. Kendall

To ensure the accurate representation of reality in the computational model, verification methods must be used to assess the computational model and its outputs. The methods used are, test, analysis, and inspection. For example, unit tests are performed to test the accuracy of the implementation of components of the model. Plots can also be generated and analysed to see if a system is performing as it should.

Unit Tests & Visual Inspection

Unit tests are a tool, critical for verifying and ensuring that the individual functions of a program, that form a part of the larger software model, are correctly functioning. These unit tests were executed for subsystem-level equations from Chapter 8, by comparing the outputs of the equations, to analytical solutions, or hand calculations. The program utilises a Python package, **pytest**[47] to perform these tests. The visual inspections and unit tests undertaken are summarised in Table 9.2, below.

Note that the **ID** of the tests are grouped according to subsystems, itemised below.

- **EN**: Engine
- **DR**: Drag
- **AV**: Avionics
- **SC**: Stability and control
- **RE**: Recovery

[47] `https://docs.pytest.org/en/7.3.x/` [21/06/2023]

Table 9.2: Visual inspection and unit tests of individual functions in the program.

ID	Test Goal & Relevance	**Test Description** (Check accuracy between...)	Status
DR1	Ensure correct skin friction drag.	...manually and computationally calculated skin friction drag for body and fins throughout the speed regime.	$\varepsilon < 10^{-6}$
DR2	Ensure correct fin pressure drag.	...manually and computationally calculated fin pressure drag throughout the speed regime.	$\varepsilon < 10^{-6}$
DR3	Ensure correct nose cone pressure drag.	...manually and computationally calculated nose cone pressure drag throughout the speed regime.	$\varepsilon = 0$
DR4	Ensure correct shoulder pressure drag.	...manually and computationally calculated shoulder pressure drag throughout the speed regime.	$\varepsilon = 0$
AV1	Ensure correct behaviour for infinite gain.	Check that the software does not throw an error when initial frequency or diameter is set to zero	$\varepsilon < 10^{-3}$
AV2	Ensure correct antenna gain.	...manually and computationally calculated antenna gain	$\varepsilon < 10^{-3}$
AV3	Ensure correct power received.	...manually and computationally calculated power received	$\varepsilon < 10^{-3}$
AV4	Ensure correct minimum bandwidth.	...manually and computationally calculated minimum bandwidth based on datarate and chosen modulation technique	$\varepsilon < 10^{-3}$
AV5	Ensure correct Doppler shift.	...manually and computationally calculated	$\varepsilon < 10^{-3}$
AV6	Ensure correct Shannon capacity.	...manually and computationally calculated shannon capacity	$\varepsilon < 10^{-3}$
AV7	Ensure correct total electronics power.	...manually and computationally calculated total electronics power based on depth of discharge and the margin	$\varepsilon < 10^{-3}$
AV8	Ensure correct electronics energy.	...manually and computationally calculated total required energy	$\varepsilon < 10^{-3}$
AV9	Ensure correct power-current unit conversion.	...manually and computationally calculated energy to amp-hour calculations	$\varepsilon < 10^{-3}$
SC1	Ensure correct centre of pressure location.	...manually and computationally calculated	$\varepsilon < 10^{-6}$
SC2	Ensure correct centre of mass location.	...manually and computationally calculated	$\varepsilon < 10^{-6}$
SC3	Ensure correct stability margin calculation.	...manually and computationally calculated	$\varepsilon < 10^{-6}$
RE1	Ensure correct parachute, mass and cost calculations.	...manually and computationally calculated value for fabric mass and cost of the main parachutes and drogue.	$\varepsilon < 10^{-6}$
RE2	Ensure correct suspension lines, mass and cost calculations.	...manually and computationally calculated value for suspension lines mass and cost of the main parachutes and drogue.	$\varepsilon < 10^{-6}$
RE3	Ensure correct cold gas system, mass and cost calculations.	...manually and computationally calculated value for cold gas system mass and cost.	$\varepsilon < 10^{-6}$
EN1	Ensure the initial acceleration calculation is accurate	Visually inspect the equation	pass
EN2	Ensure the thrust force calculation is accurate	Visually inspect the equation	pass
EN3	Ensure the effective exhaust velocity calculation is accurate	Visually inspect the equation and compare to literature	pass
EN4	Ensure the propellant mass calculation is accurate	Visually inspect the equation	pass

Table 9.2: Visual inspection and unit tests of individual functions in the program.

ID	Test Goal & Relevance	**Test Description** (Check accuracy between...)	Status
EN5	Ensure the mass flow calculation is accurate	Visually inspect the equation	pass
EN6	Ensure the casing thickness calculation is accurate	...manually and computationally calculated value	$\varepsilon < 10^{-6}$
EN7	Ensure the chamber volume calculation is accurate	Visually inspect the equation	pass
EN8	Ensure the propellant outer diameter calculation is accurate	Visually inspect the equation	pass
EN9	Ensure the chamber length calculation is accurate	Visually inspect the equation	pass
EN10	Ensure the nozzle throat area calculations are correct	...manually and computationally calculated value	$\varepsilon < 10^{-6}$
EN12	Ensure the nozzle exit area calculations are correct	...manually and computationally calculated value	$\varepsilon < 10^{-6}$
EN13	Ensure the nozzle length calculation is accurate	...manually and computationally calculated value	$\varepsilon < 10^{-6}$
EN14	Ensure the casing mass calculations are correct	...manually and computationally calculated value	$\varepsilon < 10^{-6}$
EN15	Ensure the nozzle mass calculations are correct	...manually and computationally calculated value	$\varepsilon < 10^{-6}$
EN15	Ensure the total length calculation is accurate	Visually inspect the equation	pass
EN16	Ensure the motor mass calculation is accurate	Visually inspect the equation	pass
EN17	Ensure the regression rate calculation is accurate	Visually inspect the equation	pass
EN18	Ensure the burn area calculation is accurate	Visually inspect the equation	pass

In Table 9.2, ε is the error, or deviation between the manually and computationally calculated values. All functions have passed the unit tests and/or visual inspections. Therefore, there is confidence in the correctness of the functions used to assess the compliance to requirements.

Sensitivity Testing

At startup, the program first fills the rocket data class with initial values. These initial values consist of constants and estimations about the rocket. During sensitivity testing, the estimated values are varied to check if the model would converge to the same value, independent of a change in initial values. The sizing model uses a total of 232 initial values, of which 65 are first estimations. During the sensitivity test, all 65 estimated values are multiplied by a uniformly randomised value, which ranges between 0.5 and 2. Then the full program is run until it converges, and the final values are saved. The runs that do not converge are saved but also flagged.

After the runs have been completed, the iterations are plotted and checked for their variance. There are a few possibilities for the final distribution of converged values. All values could converge to a single point, which would mean that none of the initial values have an influence on the final values of the rocket. The values could also converge to a few points, meaning that there would be multiple sets of final values for which the rocket would comply with the requirements. Lastly, the values could vary around a central value, which means that one or more values do have an influence on the final values of the rocket.

During sensitivity testing, a total of 35 sizing runs were completed, of which 12 runs failed to converge. The runs of the total mass and length are plotted in Figure 9.1, where the red crosses represent failed runs, the blue dots represent the converged cases and the line with the highlighted area represents the average value and the one sigma value of the vertical distribution of the blue dots.

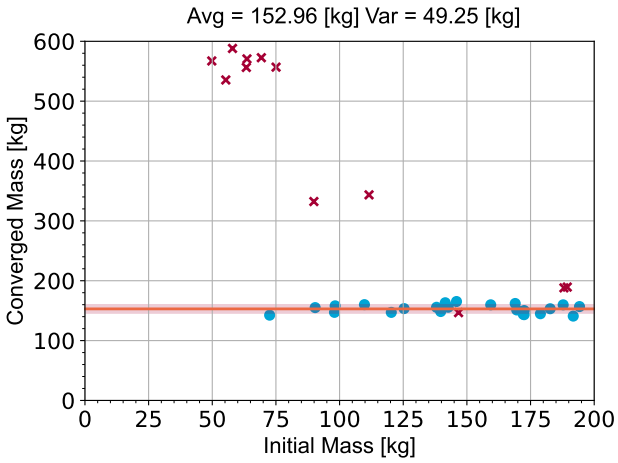

(a) Mass sensitivity analysis

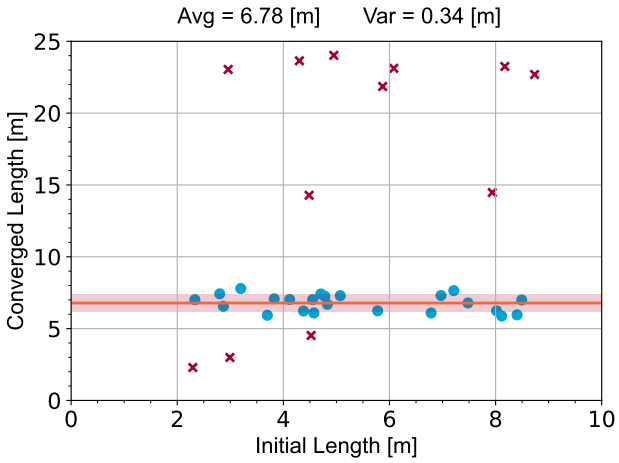

(b) Length sensitivity analysis

Figure 9.1: Sensitivity tests on the total mass and length of the rocket

The distribution of both the total mass and length do not converge to a single or a few values, instead, they collect around an average and vary slightly run by run, as discussed in the third hypothesis. This means that one or more of the estimated values does have an influence over the final convergence of the program. These variables can be found by varying every initial value one by one and inspecting when they do not converge to one of a few points anymore. However, because of time constraints, this is left for a later design phase.

The deviation between the different runs is relatively small for this stage of the design, with 15 of the 23 runs being within 4.59% of the average mass and within 8.60% of the average length. The biggest contribution to the overall mass and length variations comes from the engines, as they have to change their thrust, and therefore mass and size, to make sure the rocket attains the 110 km apogee target. The runs of the engine masses have been plotted in Figure 9.2, where the first stage is the booster stage and the second stage is the sustainer stage.

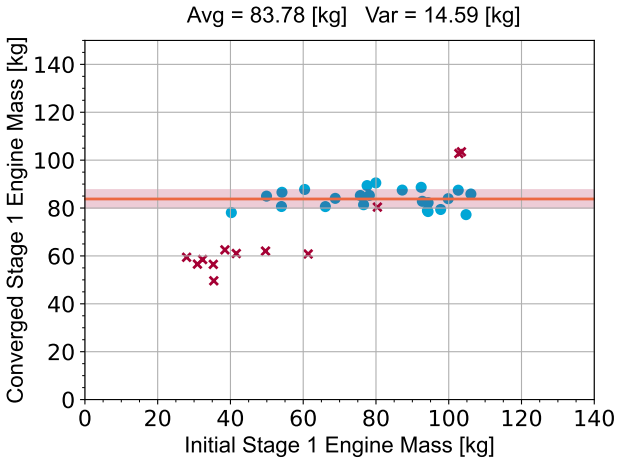

(a) First stage engine mass sensitivity analysis

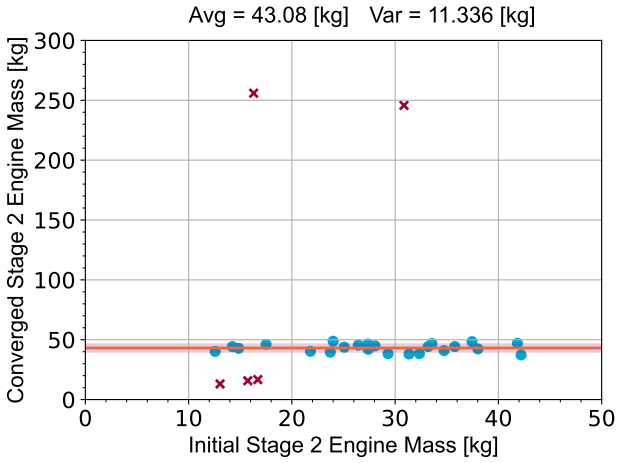

(b) Second stage engine sensitivity analysis

Figure 9.2: Sensitivity tests on first and second stage engine mass

The second stage engine has a lower variance. However, due to its lower mass, that deviation has a bigger impact

on the rocket. Moreover, the first stage engine size is based on the vehicle mass, which consequently also starts deviating due to the changes in the upper stage. The adjustment in the bottom stage will cause the rocket to reach a different altitude, which then changes the vehicle mass again, creating a loop. This interdependence makes sizing the engine relatively sensitive to adjustments, not only due to its own mass but also due to the masses and aerodynamic effects of the other systems.

Other subsystems have a relatively low influence on the rocket variances. For example, the fins only have a variance of 5.51×10^{-5} m and 5.07×10^{-6} m during runs of the first and second stage fins respectively. Another example, the first and second stage recovery masses have a variance of only 7.86×10^{-5} kg and 6.25×10^{-4} kg respectively. The engines are the main sensitive subsystem compared to other systems, as they rely on the cumulative masses and lengths of all other systems. Consequently, the variances of the other systems add up in the engine. The stability sizing also depends on the total rocket mass and length, however, a variation in these values can have a relatively small effect. For example, if the length of a section increases, this can both move the centre of pressure and centre of gravity forward, only marginally changing the stability margin.

In conclusion, for this stage of the design, the variation in the convergence is small enough to proceed with the design of the vehicle. However, more research should be done into the sensitivity of separate values to understand which are the cause of the variance in the converged values, such that the most influential parameters can get more attention during the detailed design.

9.2.2. Validation

Authors: S. Yorucu, E. Chen
Editor: C. Kendall

The degree of accuracy of the model to its real-life counterpart is determined through validation methods. Since a new simulation and sizing tool has been developed, this requires validation. Normally, the results gathered from the simulated model would be compared to experimental data, but due to the lack of publicly available flight data from missions with similar flight profiles, the program will initially be compared to a another validated program with the same simulation inputs, namely OpenRocket [48, 110].

The accuracy of OpenRocket for rocket simulations has been validated in amateur rocketry. Using low power B4-4 and C6-3 model rocket motors, the simulations have a 16% and 7% error respectively [110]. A report about an amateur high power rocket indicated errors up to 6.3% for launches up to 1800 m [111]. A separate mission reaching 1800 m experienced a 1.9% error between the simulated and achieved apogee [112]. In general, rockets with a maximum speed below Mach 1.5 have an expected simulation error within 15% when simulated using OpenRocket [110].

The extent of the available validation documentation is limited to low altitude and low speed flights, with a lack of validation data for highly supersonic rockets [48]. With the Altus mission exceeding Mach 4, there are uncertainties about the accuracy of the drag estimations. Similarly, the high velocity drag estimations based on the sizing calculations from Section 8.2 have similar uncertainties. Due to their purpose as preliminary sizing tools, uncertainties are tolerated with adequate design margins, and may later be reduced using computational fluid dynamics or wind tunnel testing in the detailed aerodynamic design phase.

To validate the Altus simulation tool and quantify the differences compared to OpenRocket, the vehicle resulting from the iterative design process was recreated in OpenRocket with identical mass and thrust curves. In Figure 9.3, the Altus simulation software and OpenRocket are compared for the nominal flight. The Altus software indicates an apogee of 110 km, while OpenRocket indicates 180 km. This represents a significant difference of around 60%, leading to an analysis of the sensitivity of the design.

It was found that the exact altitude reached is high dependent on the vehicle aerodynamics. For instance, increasing the second stage fin thickness from 6 mm to 10 mm decreased the OpenRocket simulated apogee to 154 km. Additional sources of uncertainty in the vehicle aerodynamics are in the surface roughness, differences in the treatment of supersonic correction, simulated wind effects, and fin geometry. Varying these parameters in OpenRocket result in apogees ranging from 100 km to 180 km. Taking these uncertainties into account, and given that the result from

the Altus simulation tool lie in the lower bound of the altitude estimation from OpenRocket, the uncertainty can be treated as a performance margin on top of the existing margin between 90 km to 110 km.

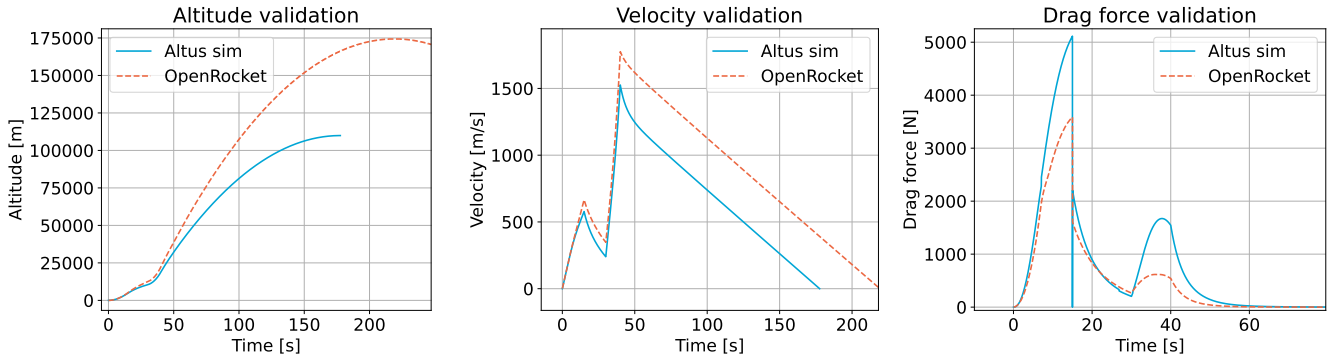

(a) Altitude comparison **(b)** Velocity comparison **(c)** Drag comparison

Figure 9.3: Comparison between Altus Simulation program and OpenRocket

For the purpose of validating the trajectory simulation code, the OpenRocket parameters were tweaked to match the altitude of the Altus simulation. This entailed modifying the fin geometry, while keeping the masses identical. The result of this is a more comparable set of plots, shown in Figure 9.4.

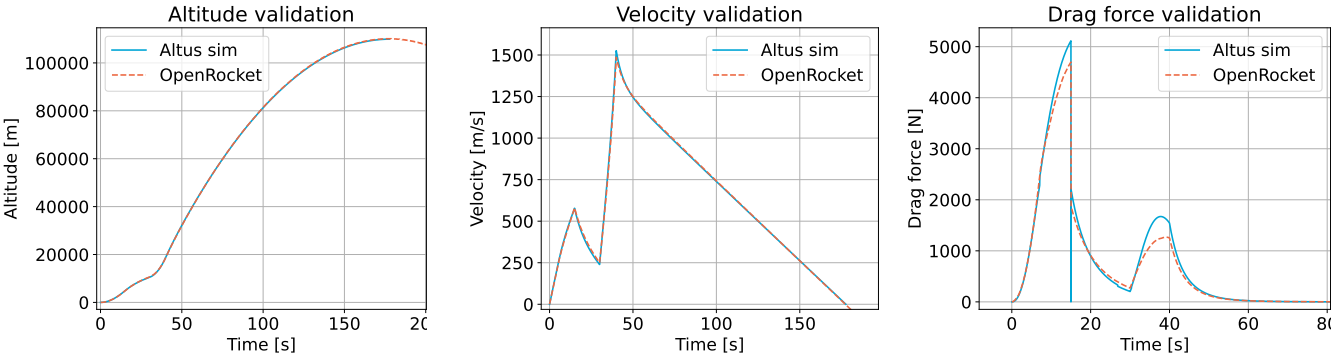

(a) Altitude comparison **(b)** Velocity comparison **(c)** Drag comparison

Figure 9.4: Comparison between Altus Simulation program and OpenRocket after adjustments

The comparison indicates that the approach to drag estimation used in the Altus simulation tool results in significantly higher drag forces compared to the drag model in OpenRocket. Although the individual contributions to the total drag contribution have been verified, it is recommended to reevaluate the implemented drag computation based on additional supersonic drag estimation methods, along with validation against wind tunnel testing, or computational fluid dynamics.

Note that some parts of the drag computation were derived from the methods used by the original OpenRocket implementation, but the software has since experienced improvements, which may explain the observed differences.

Simulation of T-Minus DART Rocket

Author: S. Aurori

Editor: L. Tabaksblat

The T-Minus DART Rocket is a two-stage rocket with similar performance parameters to the Altus vehicle [113]. With an apogee of 110 km, a maximum Mach number of 5.2, and a two-stage configuration, it is deemed a good case for the simulation tool to run, since it is assumed to perform similarly to the Altus vehicle. One main difference between the two vehicles is the fact that the Dart stage, meaning the upper stage of the DART rocket, is not propelled.

The measurements of the rocket are taken from [114, Appendix A]. The performance parameters, such as the reached apogee, thrust, and burn time are based on the T-minus fact sheet [113]. Those respective measurements are displayed in Table 9.3.

Table 9.3: T-Minus DART Rocket Parameters. Taken from [113]

Parameter Name	Value	SI Units
First Stage Booster Length	2.3	m
Second Stage Dart Length	1.12	m
First Stage Booster Diameter	118	mm
Second Stage Dart Diameter	35	mm
First Stage Total Booster Mass	25.7	kg
First Stage Propellant Mass	19.7	kg
Second Stage Dart Mass	3.5	kg
First Stage Booster Average Thrust	8000	N
First Stage Booster Burn Time	7	s

Several runs of the program based on the input variables of the T-Minus rocket have been performed. The reached apogee measures 40 km. However, a reduction in the coefficients for the drag of 50%, allowed for the apogee to change to the desired 113 403.33 km. This matches with the conclusion drawn from the OpenRocket based validation, which suggested that the drag calculation within the in-house simulation assumes the vehicles to produce higher drag than expected.

However, these results need to be interpreted also based on the assumptions that are made within the process. Values such as the booster fins thickness has been assumed based on an engineering drawing, as well as the nose-cone half angle. The fineness ratio is also assumed to be 15. The nose-cone type is also not revealed in the sources. Not having the exact values for several parameters introduces a level of uncertainty in the confidence of these results. However, as the development of the Altus vehicle is in its infancy, the results are encouraging, based on the small amount of iterations required to reach the achieved apogee of the DART vehicle.

10
Subsystem Analysis

During the development of an aerospace vehicle, functionality of both the vehicle and its subsystems need to be determined and defined. This chapter describes a number of tools are used to assess and give overviews of the system functionality. Section 4.2.1 presents a Functional Flow Diagram (FFD) is used to show the sequential steps during the entire life-cycle of the vehicle. Section 4.2.2 further expands the FFD into a Functional Breakdown Structure (FBS).Section 10.1, Section 10.2, and Section 10.3, show block diagrams that are created to further specify how the functionalities from the FBS are included in the Altus vehicle.

10.1. Hardware Block Diagram and Interfacing

Author: E. Chen

Editor: C. Kendall

The interfacing of the hardware can be shown in the form of a block diagram. The interfaces between the subsystems can represent either a structural interface, a power transfer interface, or a data transfer interface. Note that the information shown in the hardware block diagram can be treated as an supplement to the N2 chart shown in Section 10.6. The high level hardware block diagram is shown in Figure 10.1.

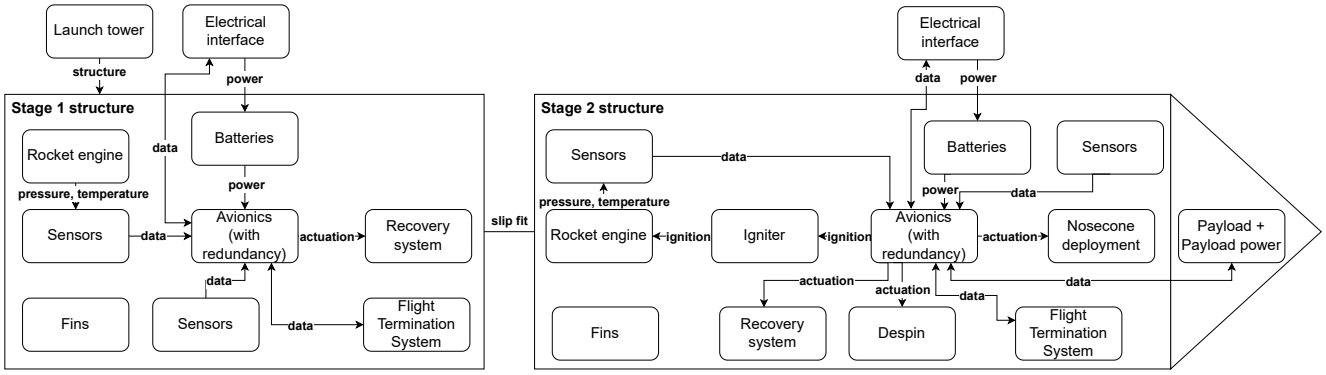

Figure 10.1: Hardware diagram for the vehicle

Since the structure of the vehicle interfaces with all individual components to facilitate load transfer, this is indicated as boxes encompassing the remaining vehicle components. The interfaces and connections between the components are important, since these represent links in which different hardware has to be compatible.

10.1.1. Power and Data Interfaces

The data interfaces between the subsystems depend on the required speed of data transfer and number of connections, along with the voltage and current requirements. The exact details of the data interfacing are beyond the scope of the preliminary design phase, but examples of possible options widely used for component interfacing are CAN and asynchronous serial such as RS232 and RS422, with RS422 being used in REXUS for payload interfacing [90].

In addition to the data interfacing, the interfaces facilitate power transfer need to be defined. This interface can be a

vehicle-wide power rail powered by the batteries. The exact requirements and design largely dependent on the exact sensors used.

10.1.2. Mechanical Interfaces

The mechanical interfaces between the subsystems and components should be defined to allow standardised mechanical connections. The internal connections within a subsystem are left for the detailed design, but the mechanical interconnections will be standardised based on metric fasteners whenever possible. Furthermore, as discussed in Section 8.6.4, the joints between the payload sections use Radax joints. To mount the motor to the rest of the rocket, a screw joint is used, since these allow for rapid assembly and integration.

As mentioned in the trade-off in Chapter 7, the staging separation mechanism will use aerodynamic staging. This requires no hardware retention, but uses a slip fit coupling which is indicated in Figure 10.1. The mechanical interfacing for the avionics, sensors, and batteries largely depend on exact placement, and so are not treated in detail in this design phase.

10.1.3. Payload Form Factor and Mounting

The interface between the payload and the rest of the rocket is important since this is different from mission to mission. The form factor of the payload is based on the CubeSat form factor, with up to 6U of space. This would allow two 3U CubeSats to be launched, or a scientific payload with cylindrical volume up to 14 cm radius by 60 cm length. The mechanical mounting of the payload depends on the exact configuration. The PMC payload requires fastening direct to the interface, while a standardised CubeSat can be contained within a cage similar to the Poly Picosatellite Orbital Deployer (P-POD) used in orbital missions [115]; this cage would subsequently be attached to the payload interface as well.

10.2. Electrical Block Diagram

Author: L. Tabaksblat
Editor: C. Kendall

The functionality of the electronics is determined by the other subsystems. For this reason a high-level diagram was created to show the functional blocks that the processor(s) will perform. These diagrams differ per stage, as the second stage needs to ignite the second stage motor (the first stage ignition is controlled from the ground), deploy the payload, and monitor the payload. These diagrams can be found at the end of the chapter, together with the low-level block diagrams. Where further information was known, some of the functional blocks have been worked out in further detail to show the steps required for, e.g. telemetry or cold gas deployment. Note that the green coloured "Processor" block represents the same component across the different diagrams.

The indicators in the system are intended to be used for indicating when the system enters a dangerous state. This means either when the system arms the ignition systems or when the system ignites the motors or deploys the parachute. Both visual and sound indications are used. The sound indicator is intended to alert anybody standing near the rocket, while the visual indicator can be used during testing of the electronics to confirm that the actuation signal has been sent.

As the system will use LiPo batteries, it is important to have a system that monitors for under-voltage, cell-imbalance, and other issues. This system is important, because if it fails, then the batteries could get damaged which can lead to a potential battery fire or to permanent damage to the batteries. The battery management system also allows for the system to switch over from external power (supplied to the rocket via the umbilical) to internal power. This is why this subsystem has been worked out in greater detail than some other subsystems.

Based on SYS-PW-03, the payload must have a separate power system to the rest of the rocket. The power block in the payload block diagram should thus be treated as its own power system independent from the main vehicle power system.

10.3. Software Block Diagram

Author: L. Tabaksblat
Editor: C. Kendall

The behaviour of the electronics and software is dependent on the current flight phase. For example, the payload data is only logged from nosecone deployment until touchdown. Similarly, the avionics data is only logged from start of flight until touchdown. For this reason, a state diagram has been made for both the first and second stage electronics. A state diagram describes the states of the system and the conditions required for the system to go from one state to another. Furthermore, in the future, the behaviour of each state can be described including more detailed transition requirements. The state diagrams can be found at the end of the chapter.

In the state diagram, each unringed black dot indicates a starting point. The arrows indicate the transition from either a starting point to a state, or from state to state. The text on the arrow indicates the requirements for the transition to occur. Each rounded block indicates the state and the state name. Finally, each ringed black dot indicates a final state. In this case, each diagram contains two final states as the system can end in error mode or in touchdown mode.

The most important states are the deployed state for both stages, the ignited state for the second stage, and the payload state for the second stage. The deployed mode is responsible for deploying the parachute at the right moment and, for this reason, is not only controlled by altitude measurements but also a backup timer based on simulations in case the sensors fail. Similarly, for the second stage motor ignition multiple conditions are implemented as the second stage can easily lose control if the motor still ignites in a non-nominal flight profile. These conditions consist of rotational acceleration being within an acceptable margin along with the correct orientation of the rocket to prevent the motor from igniting while pointing sideways or pointing downwards. Furthermore, the altitude and timing should be around the expected values to prevent an accidental hot staging from occurring. Finally, the payload similarly to the parachute checks both the timer and altitude before deploying the payload.

10.4. Data Handling

Author: E. Chen
Editor: C. Kendall

The combination of the vehicle hardware and software allows data to flow between the various systems. Measurement data flows from the sensors to the main processor, and out to the various receiving systems. A data-flow diagram is used to illustrate this. The scope of this diagram is not limited to a specific processor or computer, so each block can represent both hardware or software processing steps. The individual blocks represent either input/outputs, data stores, or functions processing the data [116]. The data-flow diagram applicable for both the first and second stage is shown in Figure 10.2. In the case of the first stage, no payload data is present.

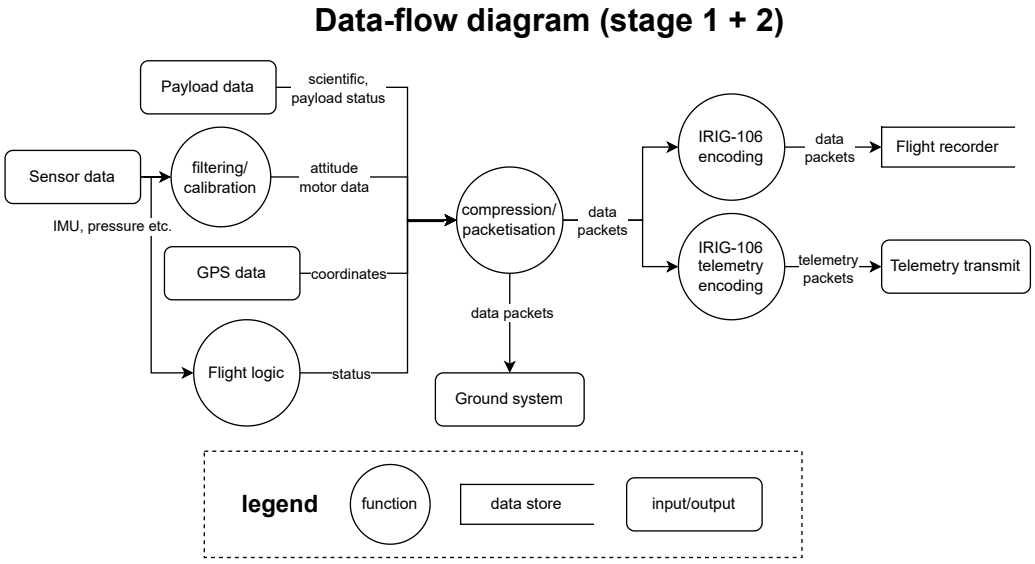

Figure 10.2: Data-flow diagram for the vehicle

10.5. Engineering Budgets

Authors: L. Tabaksblat, M.Beenders, L. Alonso
Editor: C. Kendall

The mass, datarate, power, and link budget are important to keep track of as they can influence each other. They are also dependent on the design choices of the vehicle as the need for things such as extra sensors or deployment devices will affect the datarate or power budget. For this reason, these budgets are only presented after the preliminary design. Section 10.5.1 presents the mass budget of the complete rocket. Section 10.5.2 presents the datarate budget for both the payload and avionics. Section 10.5.3 presents the power budget for both subsystems and finally Section 10.5.4 presents the link budget for the vehicle.

10.5.1. Mass Budget

Authors: M. Beenders, L. Alonso

An important metric for the rocket is the mass, as it influences the transportation, handling, flight profile and, generally, costs. Therefore, the total mass is kept track of by summing all the subsystem masses into a total dry and wet mass. These summations are shown in Table 10.1.

Table 10.1: Vehicle Mass Budget

Parameter	Value (kg)
Total mass	157.96
Total dry mass	62.46
Booster mass	90.95
Booster dry mass	26.95
Sustainer mass	67.01
Sustainer dry mass	35.51

Subsystem	Mass (kg)
Payload	12.00
Propulsion	125.01
Stability	7.07
Structure	7.22
Recovery	1.83
Avionics	4.83

10.5.2. Datarate Budget

Author: L. Tabaksblat

As the current required logging time is still very preliminary and as the data rate is important for the determination of the minimum bandwidth, it was decided to make a data rate budget instead of a data storage budget. Furthermore, the data rate budgets have been split up as the payload will have its own margins and flight recorder. Furthermore, the budget has also been split up into a table with the data rate of the first and second stages.

Avionics

The data rate of each system was estimated by finding sensors suitable for the rocket as can be seen in Table 10.2. However some data rates do not follow the maximum data rate of the data sheet. For the motor pressure sensor the update frequency is limited to 60 Hz, as this is only used for live monitoring during the flight and therefore does not need to be greater than the maximum refresh rate that can be perceived by humans. The 64 bits reserved for the general electronics are used for monitoring the status of the system during the flight and has therefore also been limited to 60 Hz. All data sizes were set to 32 bits unless specified otherwise.

The camera data rate was estimated by first assuming the quality of the footage. This was set to 480p, as anything better would required a data rate that would make sending all the footage via telemetry difficult. This means that each frame contains 640 times 480 pixels. Furthermore, a colour depth of 24 bits was set. By multiplying the amount of pixels with the colour depth the uncompressed frame size can be found. After this, a frame rate of 30 fps was chosen as this is generally sufficient for failure analysis. To decrease the data rate the MPEG video standard was chosen, giving a compression ratio of 52:1.

Table 10.2: Estimated data rate budget for the avionics

Instrument	Data	Amount	Size (bits)	Frequency (Hz)	Data rate (kbits/s)
Gyroscope [103]	$\mathrm{rad\,s^{-1}}$	2	48	2000	192
Accelerometer [103]	$\mathrm{m\,s^{-2}}$	2	48	2000	192
Magnetometer [103]	G	2	192	100	38.4
Barometer [103]	Pa	2	64	50	6.4
Temperature sensor [103]	°C	2	12	1	0.024
GNSS [104]	m	2	96	1	0.192
pressure sensor (engine) [105]	Pa	2	32	60	3.84
Thermocouple	°C	2	32	60	3.84
Camera [106]	-	2	141785	30	8507.077
General	-	2	64	60	7.68
				Total data rate (kbits $\mathrm{s^{-1}}$):	8951.45
			Total data rate with margin (kbits $\mathrm{s^{-1}}$):		11189.32

Payload

As there are no data sheets available for the payload, the size of the data points are assumed to be 32 bits, as this should provide a high enough resolution. Similarly to Section 10.5.2 a margin of 25 % has been applied as can be seen in Table 10.3. This is because, despite the payload instruments having already been chosen, the payload will have to be adapted due to the instruments currently not meeting all of the requirements. This can cause the data rate to change, depending on the adjustments required.

Table 10.3: Estimated data rate budget for the payload

Instrument	Data	Amount	Size (bits)	Frequency (Hz)	Data rate (kbits/s)
Sonic thermometer [117]	°C	1	32	700	22.4
Lymann-alpha [48]	ppmv	1	32	1	0.032
DAPMT [59]	Pa	1	32	1000	32
				Total data rate (kbits s^{-1}):	56.35
				Total data rate with margin (kbits s^{-1}):	70.44

Data Rate Estimate Per Stage

As can be seen in Table 10.4 the data rate between the two stages does not differ much. This is caused by the largest contribution to the data rate being the camera footage, as both stages currently contain two cameras. If these cameras are no longer required or if a camera with a lower data rate is chosen, the required bandwidth and SNR will change significantly.

Table 10.4: Estimated data rate budget per stage

Stage	Data rate (kBits/s)
1	11189.32
2	11259.76

10.5.3. Power Budget

Author: L. Tabaksblat

Similarly to the data rate budget, the power budget has been split into multiple tables. However, as the payload has a separate battery there will not be a table containing the power based on each stage. A margin of 25 % was chosen as to prevent the power draw being underestimated.

Avionics

Editor: C. Kendall

Almost all power estimates are derived from the data sheets for the relevant parts. The only exceptions are the general electronics and the pressure sensor data. The general electronics are a preliminary estimate. The pressure sensor power is based on the maximum resistance for 12 V. Using the equation $P = V^2/R$, the power draw can be calculated. In Table 10.5 the total power draw per stage can be found for the avionics.

Table 10.5: Power budget for the avionics

Instrument	Amount	Power (W)	Total power (W):
IMU [103]	2	0.52	1.04
GNSS [104]	2	0.2	0.4
pressure sensor (engine) [105]	2	1	2
Camera [106]	2	5	10
Telemetry [107]	1	5	5
General	2	5	10
		Total power (W):	27.44
		Total power with margin (W):	34.3

Payload

Editor: C. Kendall

Both the power of the Lymann-α hygrometer and the Dual Absolute Pressure Measuring Transducer can be found from their respective data sheets. The sonic thermometer power however needs to be adapted. This is due to the sensor being developed for ground use [118]. As sound intensity is approximately 25 dB stronger at ground level than at near vacuum [117], the power output will have to be increased to match this decrease in sound intensity. The power will therefore be increased by a factor of 100.

The sampling mechanism will also draw power by keeping the housing open during sampling. This is estimated by assuming that a servo motor is used for actuation. This servo motor is estimated to draw around 1.2 W of power when keeping the mechanism open.[49]

Instrument	Power (W)
Sonic thermometer	10
Lymann-α [61]	24
DAPMT [59]	0.959
Sampling mechanism	1.2
Total power	36.16
Total power with margin	45.2

Table 10.6: Power budget payload

10.5.4. Link Budget

Author: L. Tabaksblat

Editor: C. Kendall

The preliminary link budget was only calculated for the second stage. This is because the maximum required range compared to the first stage is much larger and any other differences are insignificant. This means that if the first stage has an adequate SNR, then the first stage SNR will be sufficient as well. Some losses are difficult to estimate, such as the atmospheric losses, and the losses due to the rocket body. Furthermore, losses due to polarisation mismatch and component losses are also difficult to estimate without a more detailed design. For this reason, a general loss of 10 dB has been added to decrease the risk of overestimating the SNR.

Table 10.7: Link Budget

Parameter name	Symbol	Initial Value Stage 1	Units
Carrier frequency	f_c	2.4	GHz
max range	d_{max}	200	km
data rate	R	9.01	Mbits/s
Modulation	-	QPSK	-
Bandwidth	B	6	MHz
Transmission Power	P_{Tx}	6.99	dB
Transmission gain	G_{Tx}	0	dBi
Free space loss	L_{FS}	-146.07	dB
Other losses	-	-10	dB
Receiver gain	G_{Rx}	38.98	dBi
Received power	P_{Rx}	-110.1	dB
Signal-to-noise ratio	SNR	24.01	dB

[49] https://nl.rs-online.com/web/p/servo-motors/7813046 [20/06/2023]

10.6. N2 Chart

Author: T. Odijk

Editor: C. Kendall

To properly visualise all the interactions between the different systems in the mission an N2 chart has been produced, displayed in Figure 10.3. This chart shows these interactions by linking the cells on the central diagonal. The chart should be read in a clockwise manner, from a yellow system cell on the diagonal to a linking cell, to the diagonal again. For instance, between the ground systems and communication there is a telemetry link to transfer data.

The N2 chart highlights the different functions that are required to make the systems cooperate. This makes it an important tool to generate requirements about system interaction. It can also be used to highlight where different departments needs to exchange information and thus provide a framework for clearer communication. The FBS and the various block diagrams supplement the N2 chart; together these resources give a complete overview of the functionality of the complete system and the interfaces of the various subsystems.

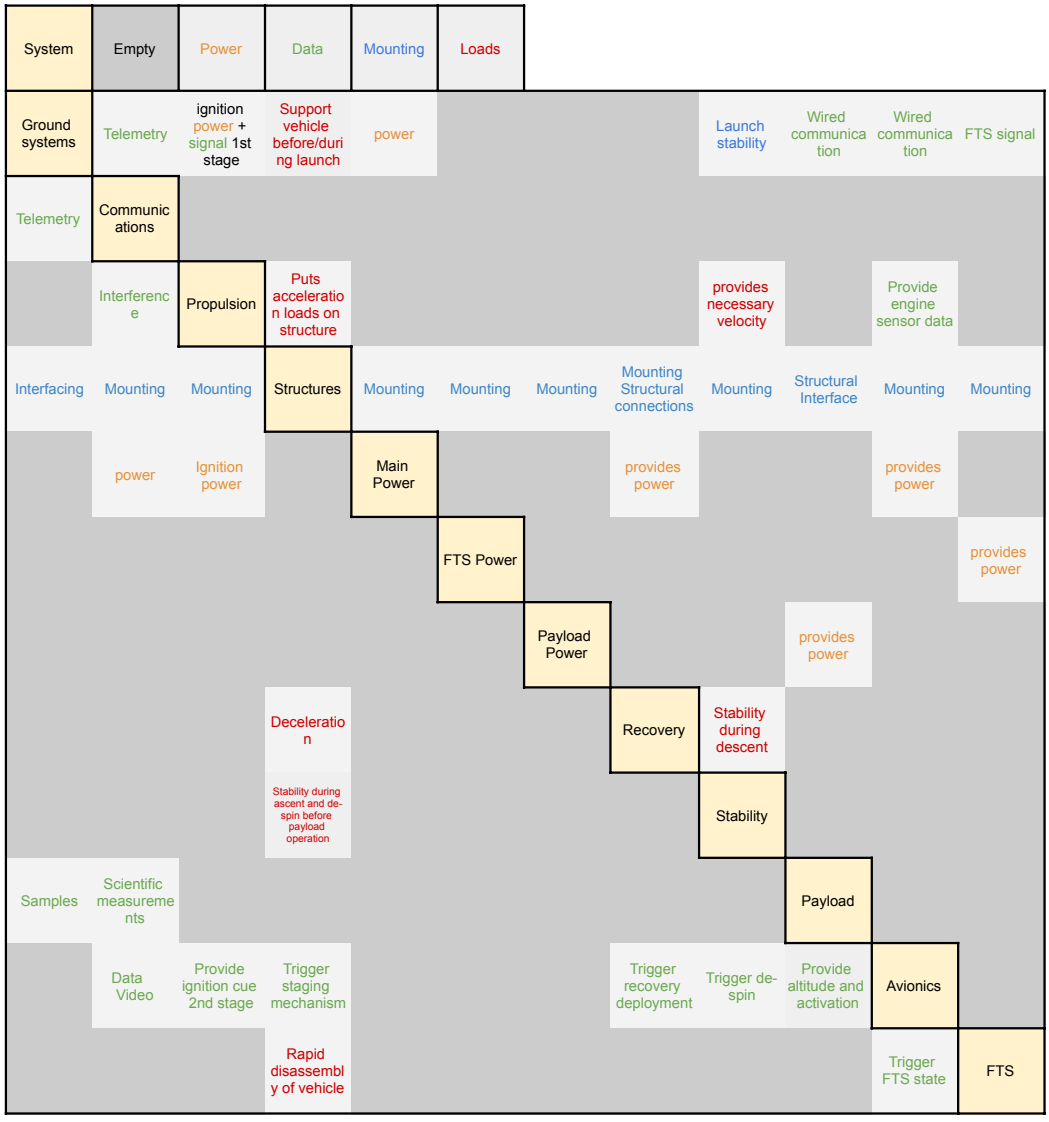

Figure 10.3: N2 Chart for the Altus Sounding Rocket

Stage 1 electrical block diagram

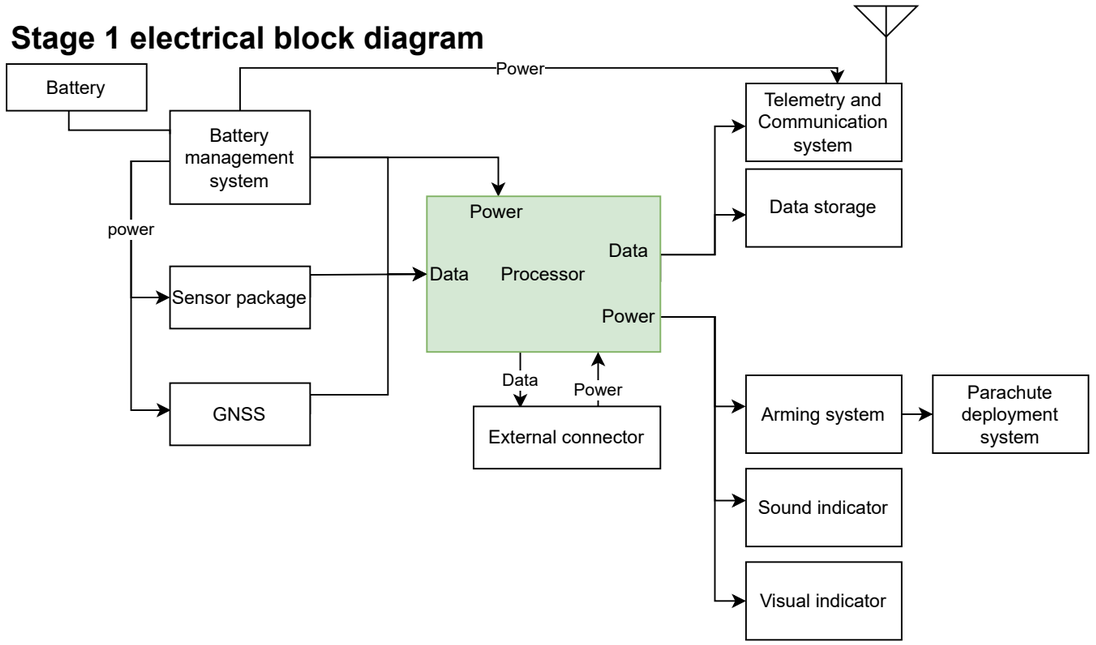

Stage 2 electrical block diagram

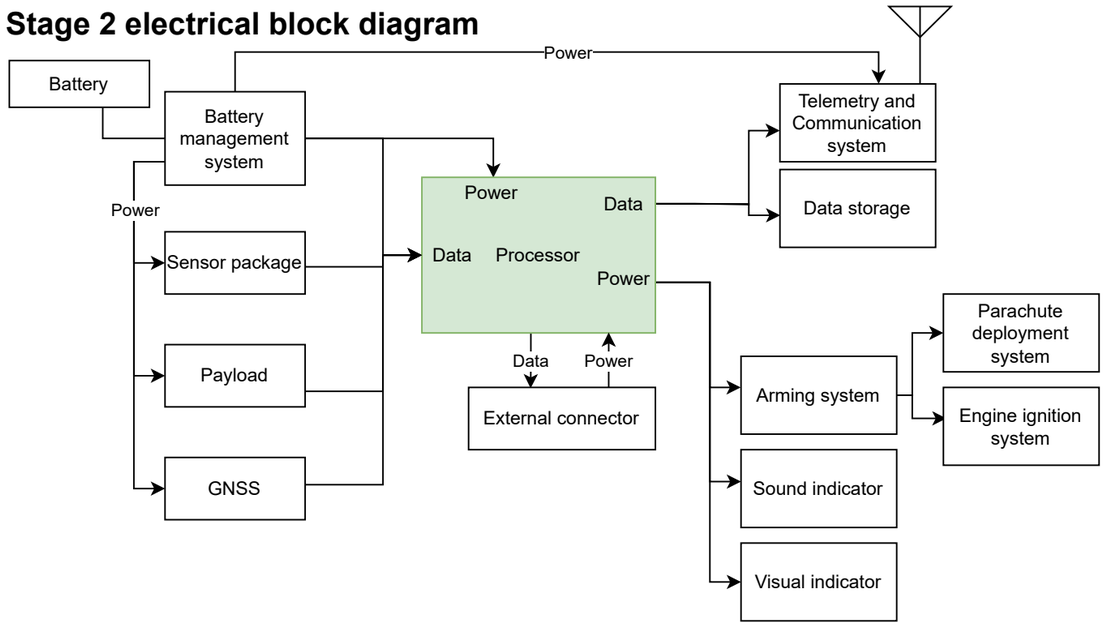

Engine ignition

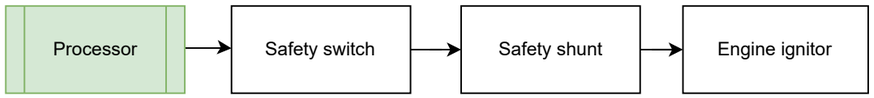

Cold gas deployment

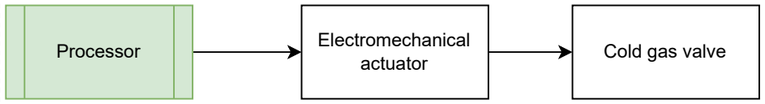

Telemetry transmitter

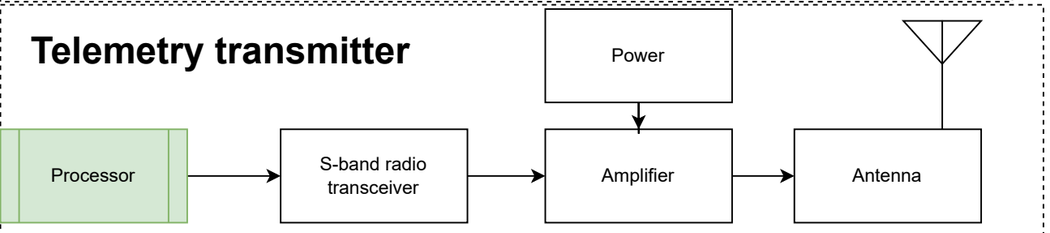

Power handling

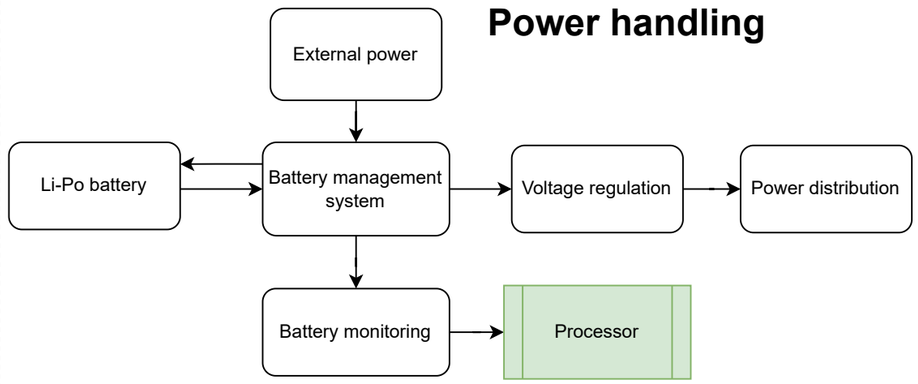

Data handling

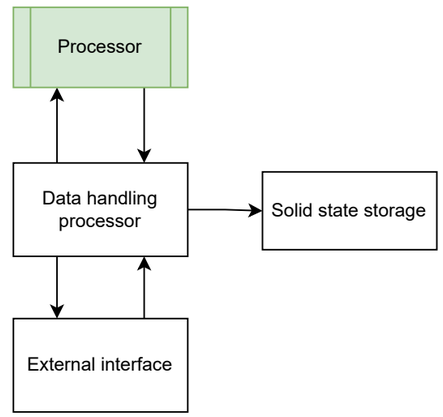

Sensor suite

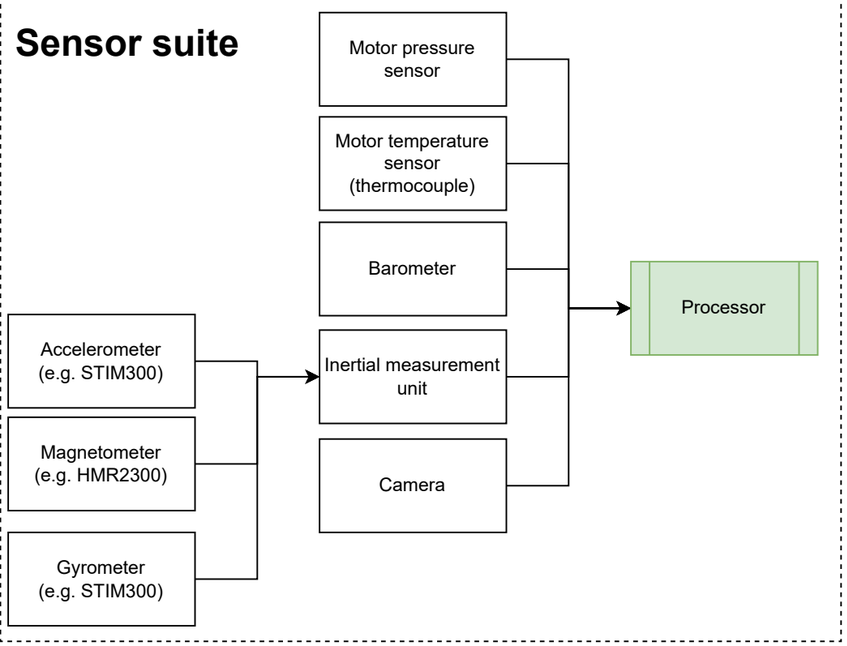

Payload

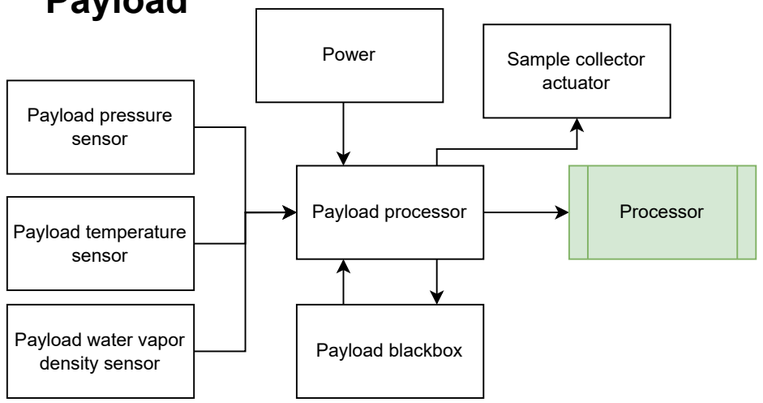

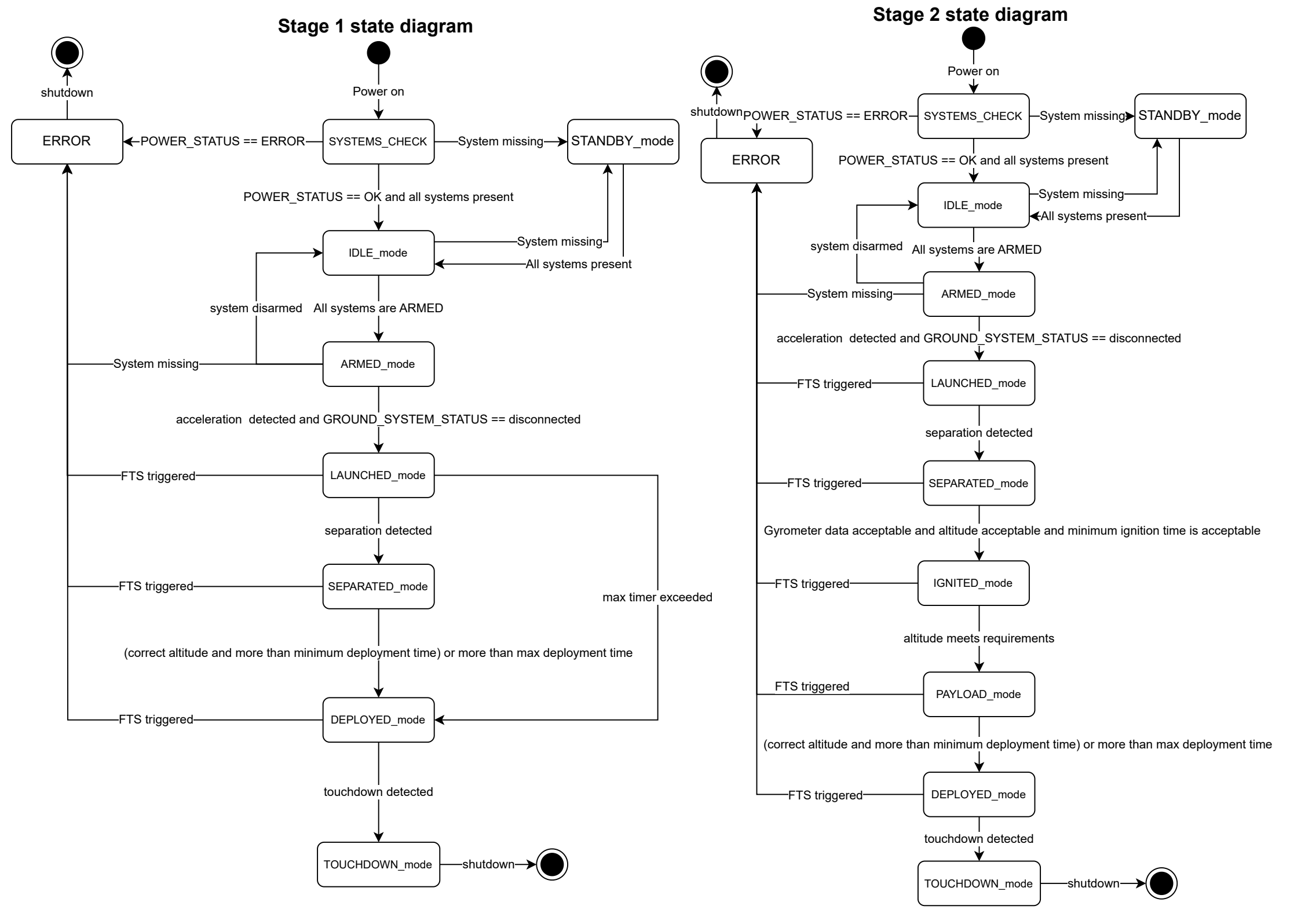
Stage 1 state diagram
shutdown
Power on
ERROR
POWER_STATUS == ERROR
SYSTEMS_CHECK
System missing
STANDBY_mode
POWER_STATUS == OK and all systems present
IDLE_mode
System missing
All systems present
system disarmed
All systems are ARMED
System missing
ARMED_mode
acceleration detected and GROUND_SYSTEM_STATUS == disconnected
FTS triggered
LAUNCHED_mode
separation detected
FTS triggered
SEPARATED_mode
max timer exceeded
(correct altitude and more than minimum deployment time) or more than max deployment time
FTS triggered
DEPLOYED_mode
touchdown detected
TOUCHDOWN_mode
shutdown
Stage 2 state diagram
Power on
shutdown
POWER_STATUS == ERROR
SYSTEMS_CHECK
System missing
STANDBY_mode
ERROR
POWER_STATUS == OK and all systems present
IDLE_mode
System missing
All systems present
system disarmed
All systems are ARMED
System missing
ARMED_mode
acceleration detected and GROUND_SYSTEM_STATUS == disconnected
FTS triggered
LAUNCHED_mode
separation detected
FTS triggered
SEPARATED_mode
Gyrometer data acceptable and altitude acceptable and minimum ignition time is acceptable
FTS triggered
IGNITED_mode
altitude meets requirements
FTS triggered
PAYLOAD_mode
(correct altitude and more than minimum deployment time) or more than max deployment time
FTS triggered
DEPLOYED_mode
touchdown detected
TOUCHDOWN_mode
shutdown

11 Vehicle overview

This chapter outlines the overall design and flight characteristics of the vehicle. This section starts with an overview of the vehicle layout and the materials used in Section 11.1. This is followed by the vehicle dynamics in Section 11.2. These characteristics are used for a simulation of which the results are highlighted in Section 11.3. Lastly, the green viability of the vehicle is discussed in Section 11.4.

11.1. Vehicle Layout and Material

11.1.1. Vehicle Layout

Author: T. Odijk

The vehicle is designed to be a two stage rocket. This choice was made as it allowed the rocket to be significantly lighter and thus more sustainable. The two stages will be referred to as the booster for the bottom stage, and the sustainer for the top stage. The sustainer is split between the motor module and the payload module. The motor module only houses the motor. The payload module houses the recovery, avionics, and payload. For the two stages an overview of the mayor dimensions and masses can be found in Table 11.1. An initial impression of the vehicle can be seen in Figure 11.1.

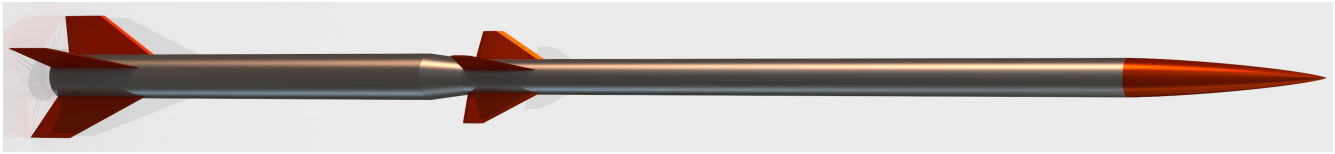

Figure 11.1: A render of the preliminary vehicle

11.1.2. Materials

Author: T. Odijk

The vehicle will use two main structural materials. For the motor aluminium 6082-T6 was chosen, it's properties can be found in [119]. This alloy was chosen as it has better thermal properties and corrosion resistance than the

Table 11.1: Vehicle Size Characteristics

Parameter	Value
Total length	6.23 m
Booster length	2.59 m
Sustainer length	3.64 m
Booster outer diameter	0.2 m
Sustainer outer diameter	0.15 m

Parameter	Value
Total mass	157.96 kg
Total dry mass	62.46 kg
Booster mass	90.95 kg
Booster dry mass	26.95 kg
Sustainer mass	67.01 kg
Sustainer dry mass	35.51 kg

Subsystem	Value
Payload	12 kg
Propulsion	125 kg
Stability	7.07 kg
Structure	7.22 kg
Recovery	1.83 kg
Avionics	4.83 kg

Table 11.2: Vehicle materials

Parameter	Value
Vehicle structure	Aluminium 7075-T6
7075-T6 Yield strength	503 MPa
7075-T6 Tensile strength	572 MPa
7075-T6 Density	2810 km^{-3}
7075-T6 Modulus of elasticity	71.7 GPa
7075-T6 Melting range	477 °C-635 °C

Parameter	Value
Engine casing	Aluminium 6082-T6
6082-T6 Yield strength	250 MPa
6082-T6 Tensile strength	290 MPa
6082-T6 Density	2700 km^{-3}
6082-T6 Modulus of elasticity	70 GPa
6082-T6 Melting range	585 °C-650 °C
6082-T6 Loss of temper	250 °C

Table 11.3: Main vehicle flight parameters influencing the aerodynamics

	Combined stage	Stage 2
Max velocity [m/s]	578.00	1525.90
Max acceleration [g]	4.94	19.27
Max dynamic pressure [pa]	125299.43	126926.31
Max Mach number [-]	1.80	5.17

aluminium 7075-T6 [50] used for the main structure. The 7075-T6 has better mechanical properties but is more sensitive to higher temperatures. An overview of the properties can be seen in Table 11.2.

11.2. Vehicle dynamics

11.2.1. Astrodynamics

Author: S. Aurori

The Altus payload requires reaching an altitude of 110 km, in order to properly perform measurements of the clouds, as well as collect particle samples. As it is not an orbital mission, orbit insertion is not required. The main target of the performance of the launcher is to reach the desired altitude. However, providing an overview of the Δv is useful when assessing the performance of the Altus vehicle when comparing it to other vehicles. For missions such as CubeSat microgravity assessment, it is relevant to see what the Δv values are for the launcher. Furthermore, due to the technology demonstrator aspect of the vehicle, with possible up-sizing of the system for future technology demonstrations, these values are useful when placing the Altus vehicle in context with the other commercial orbital launchers. The Δv of the booster motor is 2526.18 $m\,s^{-1}$ while the Δv of the sustainer motor measures 1842.61 $m\,s^{-1}$.

11.2.2. Aerodynamics

Author: E. Chen

Based on the Altus flight simulation, the velocities and accelerations and dynamic pressures are indicated in Table 11.3.

In order to find the aerodynamic coefficient at high mach numbers for the preliminary vehicle design, the RASAero II simulation software is used. RASAero uses advanced aerodynamic calculations for transonic and supersonic aerodynamic calculations [120], and thus gives more representative values than the ones used in the Altus simulation software. Shown in Figure 11.2 is the simulated drag coefficient as a function of the mach number. The circular cross-sectional area is used as the reference area for the drag coefficient based on the 200 mm and 150 mm for the combined and the second stage, respectively. RASAero has previously been validated on flights up to 90 km with an

[50] https://www.matweb.com/search/DataSheet.aspx?MatGUID=4f19a42be94546b686bbf43f79c51b7d&ckck=1 [20-06-2023]

altitude error of less than 2% [121].

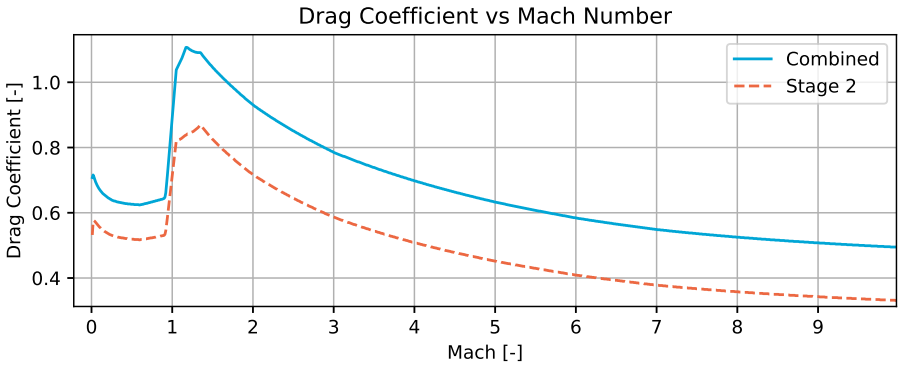

Figure 11.2: Drag coefficient simulations based on RASAero II

The geometric model used in RASAero for the drag coefficient estimation is based on the dimensions estimated during the preliminary design. This model is shown in Figure 11.3.

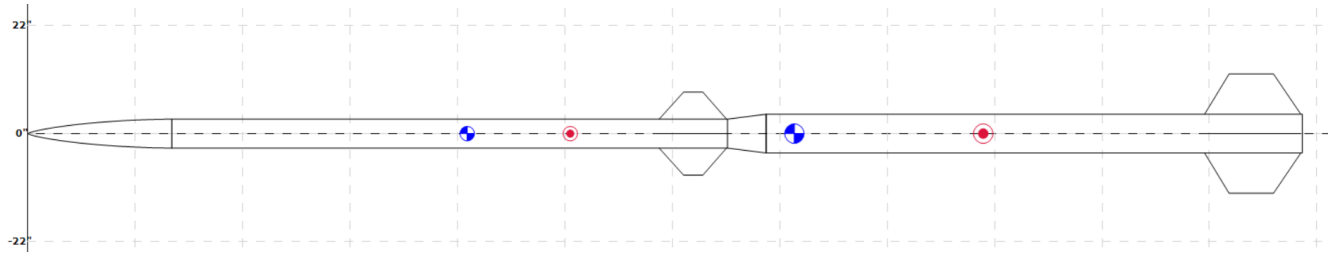

Figure 11.3: Geometric sounding rocket model used in RASAero II

11.2.3. Stability and Control

Author: T. Odijk

It is important for the vehicle to remain stable throughout the entire flight. Since the stability margin generally reduces with increasing Mach number it was decided to size the vehicle to have a stability margin of four body calibres. This ensures that the vehicle retains positive stability throughout the entire flight. To retain the stability the fins will be used. These fins have been sized to move the centre of pressure such that the four body calibres stability margin is reached. It is also important to make sure the fins do not flutter as this can lead to structural failure of said fins. The equations used for this sizing are explained in Section 8.5.2. This lead to having a thickness of at least 5 mm the booster fins and at least 7 mm for the sustainer fins. Lastly to make sure that the deviations do not cause a great dispersion of the vehicle landing location the rocket will be given a low spin rate. This makes sure that any deviations cancel out over the flight. A yo-yo de-spin mechanism will be used to cancel the spin in order to take better measurements.

11.3. Flight profile

11.3.1. Payload Altitude

Author: E. Chen

Although the vehicle is designed for a payload mass of 12 kg at a target altitude of 110 km, it is possible to reach higher altitudes by by lowering the payload mass. Figure 11.4 shows the simulated apogee with a payload mass varying from 0 kg to 15 kg. As indicated by the figure, an altitude of above 150 km may be possible with a lightweight payload of 2 kg. The effect of payload mass on the altitude can also be used for controlling the target altitude for a given mission through the addition of weights.

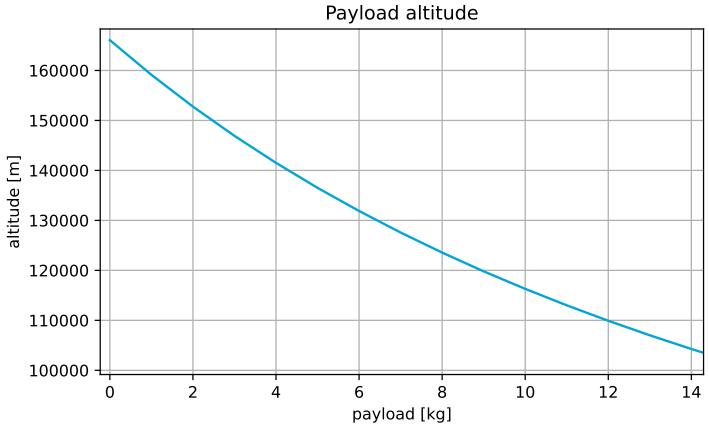

Figure 11.4: Altitude as a function of the vehicle payload mass

11.3.2. Flight Profile

Author: E. Chen

The Altus simulation tool lacks the simulation of the vehicle descent under parachute, therefore, OpenRocket is used for the visualisation of the complete trajectory. The exact flight profile of the mission depends on factors such as the launch tower angle and the wind. The tower angles were varied from 83° to 88° with winds that are randomized around 2 $\mathrm{m\,s^{-1}}$. With this variation of tower angles and wind velocities, the touchdown location is estimated to be between 60 km to 220 km. An example of one of these flight profiles is shown in Figure 11.5. Shown on Figure 11.6 is the simulated altitude as a function of time with the main mission events marked. Based on the trajectory and mission profile, representative flight events are Table 11.4.

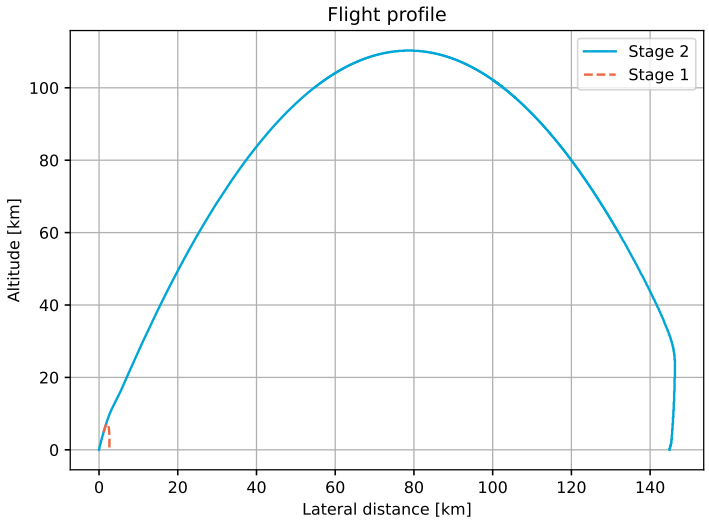

Figure 11.5: Launch trajectory simulated using OpenRocket

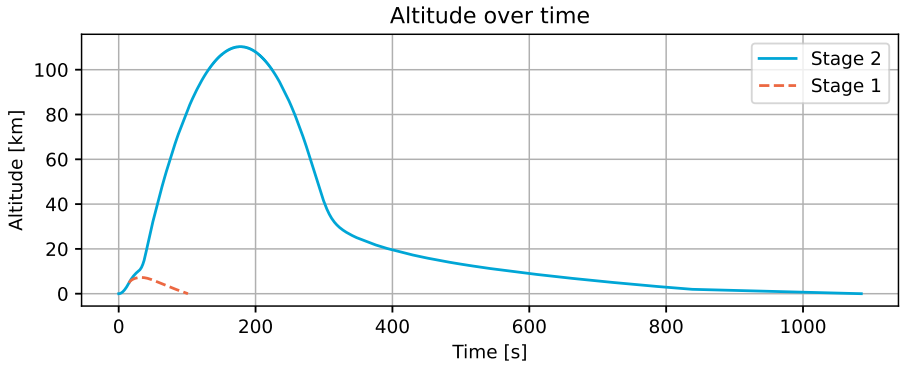

Figure 11.6: Altitude vs time of the vehicle using OpenRocket

Table 11.4: Mission events during flight

Event	Altitude [km]	Time [s]
Liftoff	0	0
first stage burnout/separation	5	15
Second stage ignition	10.5	30
Second stage burnout	19.5	40
First stage apogee, parachute deployment	7.3	34
First stage touchdown	0	100
Nosecone deployment	60	74
Second stage apogee	~110	180
Drogue deployment	60	287
Main parachute deployment	2	841
Second stage touchdown	0	1090

Note that these times may change with differing launch angles and payloads, and are thus only indicative of the sequence of events during a flight.

11.4. Quantification of Altus Vehicle Green Viability

Author: S. Aurori
Editor: E. Chen

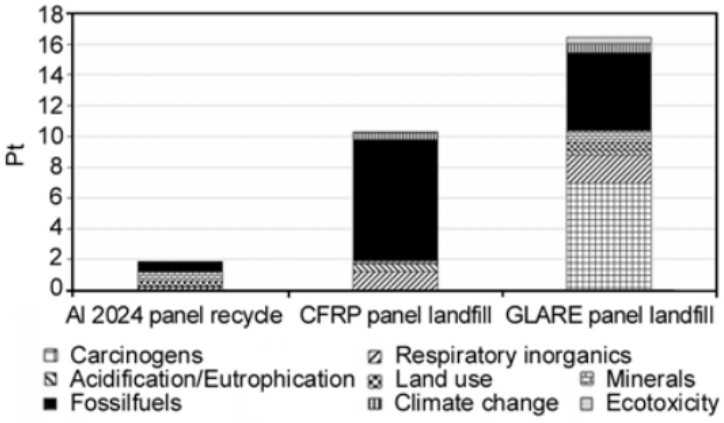

Figure 11.7: Single score impact results for manufacturing and disposal of Al 2024, CFRP and GLARE panels [122].

To fulfil its stakeholder requirements on sustainability, reuse, the Altus vehicle needs to prove reusability, which is a topic of high interest in the field of sounding rockets. History has shown that solid motors and various systems related to them can be properly reused, according to a Space Shuttle Refurbishability Document [123]. In the document, it is stated that the structural components of the motor have been designed to survive 40 launches, whereas the Thrust Vector Control and electronics viable for only 20 launches, and finally, the recovery parachutes for 10 launches. This puts confidence in the thoroughly designed Altus vehicle as well, due to the various similarities to the Shuttle Booster systems, such as the materials used and operations. Despite having been recovered from salt ocean water, the report confirms the refurbishment of various systems, namely, the solid motor booster, the onboard electronics, and parts of the Thrust Vector Control (TVC) system.

In terms of materials, an assessment of the chosen material, aluminium, and its strong competitor options is performed. Within the Aerospace industry, composites are gaining more and more attention, due to their high performance to mass ratio. However, within the Altus mission, the main focus is placed on the reusability, recyclability and sustainability of the system, as previously mentioned in Chapter 2 and Section 5.2. This entails that the performance metrics of materials, must fall under these factors, yet complete functionality of the material needs to be ensured.

Moreover, a comparison between an aluminium alloy and two composites is shown in Figure 11.7, showcasing the

environmental impact of these material choices, based on a Eco-indicator score index from literature [122]. As a result, the aluminium alloy is more sustainable, provided all the aluminium is recycled. Note that, the production of these composites is costly in terms of energy, as well as having no feasible recycling method yet. To conclude, due to its common use within the aerospace industry, proven technological readiness level, reliability, and recyclability, the aluminium alloys win on both performance, as well as sustainability.

The propulsion system of the Altus vehicle, is well constrained by the stakeholder requirements, namely, *STK-PR-01*, *STK-PR-02*, *STK-PR-03*. They outline the main factors that the propulsion system needs to be comprised of, such as, the absence of fossil fuel derivatives within the system, a clean exhaust according to World Health Organization (WHO) guidelines, and no toxicity produced by the motors. Based on conventional AP-based solid motor configurations, these are not achievable due to Hydrogen Chloride, present in the exhaust. This compound, combines with oxygen in the atmosphere and creates hydrochloric acid, a highly toxic compound responsible for the formation of acid rain, which damages the environment. Figure 11.8 shows the reduction of 100% of hydrogen chloride emissions in the exhaust, as well as an average reduction of 3% in carbon monoxide and water emissions. Furthermore, ADN is proven to have been extracted from ethanol [124], which allows for STK-PR-01 to be complied with quickly through the chosen oxidiser configuration.

Table 11.5: Exhaust compounds present for sample formulations of ADN- and AP-Based propellants calculated using ProPEP. 0.00 indicates trace amounts of compound present, – indicates compound not present. Taken from [17]

		% w/w Exhaust	
Compound	**Common Name**	**ADN-Based**	**AP-Based**
H_2	Hydrogen	38.62	35.27
CO	Carbon Monoxide	25.19	27.16
HCl	Hydrogen Chloride	–	13.60
N_2	Nitrogen	23.42	6.97
H_2O	Water	6.17	8.98
Al_2O_3	Alumina	3.82	4.23
CO_2	Carbon Dioxide	2.76	3.79
CH_4	Methane	0.01	0.00
NH_3	Ammonia	0.00	0.00
HCN	Prussic Acid	0.00	0.00
H	Monatomic Hydrogen	–	0.00
Cl	Monatomic Chlorine	–	0.00

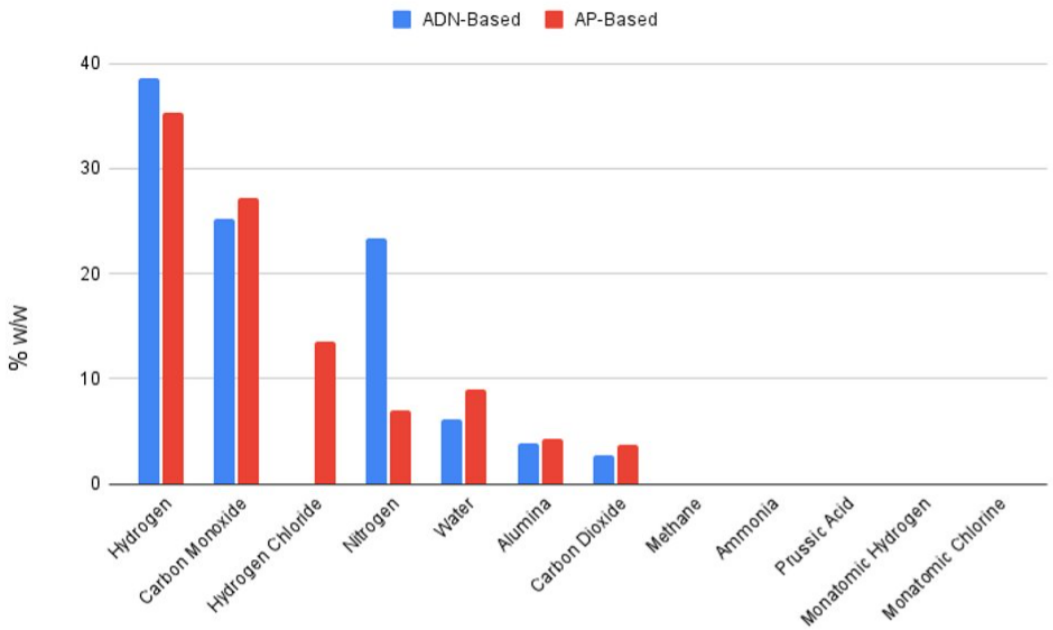

Figure 11.8: Overview of Comparison in Exhaust Products between AP and ADN based solid propellants

12
Operational Assessment

In this chapter, the realisation and operation of the Altus mission is discussed. This is first done by highlighting the MAI plan, described in Section 12.1. After which, the Operational and Logistical Concept is outlined in Section 12.2, where the post-MAI phase of the mission is discussed. Finally, the total project cost is broken down and depicted in Section 12.3.

12.1. Manufacturing, Assembly, Integration Plan

Authors: T. Odijk, L. Alonso, L. Tabaksblat
Editors: M. Rusch, S. Yorucu, C. Kendall

The MAI phase starts after the test flight is complete and the development stage is closed, as discussed in Section 4.1. To construct the 22 required operational vehicles, various components need to be manufactured, assembled, and integrated into a complete system. These activities will be covered during prototyping, the integrated system testing, and the operational phase. The manufacturing strategy of the subsystems, is described in the prototyping section. The integrated system test section, will elaborate on the integration and final assembly of the system. Next, the MAI and pre-flight testing of the payload is explored. Afterwards the full scale manufacturing of the operational vehicles is discussed. Finally, the operational and logistical concept is discussed in Section 12.2, where some of the MAI-related aspects of the operation, in particular the refurbishment process, is highlighted in more detail.

Prototyping

The goal of prototyping is to catch mistakes that are difficult to uncover, during either the performance analysis, or the verification and validation process. Part of this phase is included in the Project Design & Development Logic (PD&DL), as conveyed in Figure 4.1. Note that, it extends to the post-PD&DL manufacturing phase, since changes are likely based on the outcome of the test flights. This phase is important because it is difficult to predict issues in manufacturing during these phases. These issues can be unpredictable due to a lack of awareness that such a mistake can occur. During this phase, individual parts will be manufactured, starting from the lowest level and slowly moving up to larger scale subsystems to ensure that all parts can be manufactured and assembled to specifications within the budget, time, and cost constraints available. If the design specifications cannot be met within these constraints, iteration is necessary to make sure this becomes the case.

During the prototyping phase, the manufacturing of independent subsystems will be performed in parallel. This means, for example, that the engine and avionics subsystems, will be manufactured and verified simultaneously. Moreover, for the purpose of verification, the subsystems individual components will be verified first, after which, these respective components are assembled and they verified, as a whole. These steps are taken to ensure the efficiency of the manufacturing and integration of the system. Once all subsystems have been verified to a sufficient level the project will move on to the integrated system test phase.

Integrated System Test

By the time the initial prototyping tests are finished, the system is manufactured and subsystems are assembled. Subsequently, the system is integrated. During integration, the system should be checked with respect to ease of assembly, to ensure that at the launch site the vehicle is set up in a timely manner. The first step is integrating the system to its portable configuration. This is followed by assembling the entire vehicle according to launch procedures.

Afterwards, extended sub-system integration tests are executed. If the system falls short of the requirements, then parts need to be iterated in the design, or the procedures changed. Once the parts pass the test, the sub-systems can be moved on to the full assembly and integration test of the complete system. This will involve flying the vehicle multiple times to ensure that it is fully operational, which consists of another iteration, as shown in Figure 12.1.

Payload

To integrate and use the payload on the rocket, steps must be taken, both before and after the launch to ensure successful operation and sample collection. The approach taken before the flight, heavily depends on the number of previous launches with that payload, given that the payload is brand new. New payloads will be subject to extensive flight acceptance testing, however, this testing can be less rigorous if the payload is pre-flown. The testing will require vibration and acceleration testing, but also spin stabilising the payload, such that it does not negatively impact the stability characteristics of the vehicle.

After the payload has been assembled and tested, it undergoes isolated system checkouts before integration into the launch vehicle. The testing environment has to be carefully controlled in order to avoid contamination of sensitive instruments and sample collection systems. Depending on how sensitive the instrumentation is, some of these tasks may require a cleanroom environment. During the testing of the payload, instrumentation can be characterised and calibration in preparation for the flight.

During the transportation of the payload between different testing and integration facilities, the payload should also be protected against contamination and stresses [125]. The final step in the payload integration is to assess the flight readiness of the system. After this step, the payload is flight ready and may be integrated into the vehicle. From the logistics side, both the payload and launch vehicle are brought to the launch side, where the final integration occurs.

After the rocket has landed, the payload will be recovered and, depending on its integration procedure, it will be brought to a laboratory. Here, the samples will be examined and stored for later investigation. Both the sensor data and the sample data will be extracted and stored in a digital database to track the recordings. Afterwards, the payload undergoes health checks and is re-integrated into the next launcher if it passes these checks.

Full Scale Manufacturing

When the prototyping and integrated system testing is complete, the design is frozen and manufacturing can begin. In this section first the philosophy behind sourcing the materials is outlined. Afterwards the manufacturing phase is discussed. Finally, the method of casting the propellants is presented.

Sourcing of Materials

To minimise the impact of this mission, the aim is to source the raw materials and components from reliable sources that make significant efforts to reduce climate impact of their products: this could for instance mean sourcing recycled metals and components produced in the EU or United States as good working conditions and climate awareness are significantly more prevalent here than in many other countries.

To produce the solid rocket propellants, it is necessary to obtain the necessary chemical precursors. The most critical precursors are typically restricted under dual-use regulations such as EU Regulation 2021/821 [126]. Therefore, there is a significant regulatory overhead required to obtain these materials.

HTPB may be obtained from Evonik Industries (DE) or Cray Valley (FR). Of these, Evonik is preferred, as there is previous experience purchasing HTPB from this company for DARE. Evonik's brand of HTPB, 'Polyvest HT' [127], requires an End-User Certificate (EUC) for the government of Germany to ensure that the HTPB will be used as intended. It is expected that a similar requirement will exist in order to obtain Ammonium DiNitramide from EURENCO.

Manufacturing

Manufacturing, assembly, and integration will take place in the Netherlands. Easy access to highly skilled personnel and many different suppliers make this a very attractive location to base the production of the rockets. Most of the production will take place in-house to minimise cost and possible delays. However, the payload integration will be

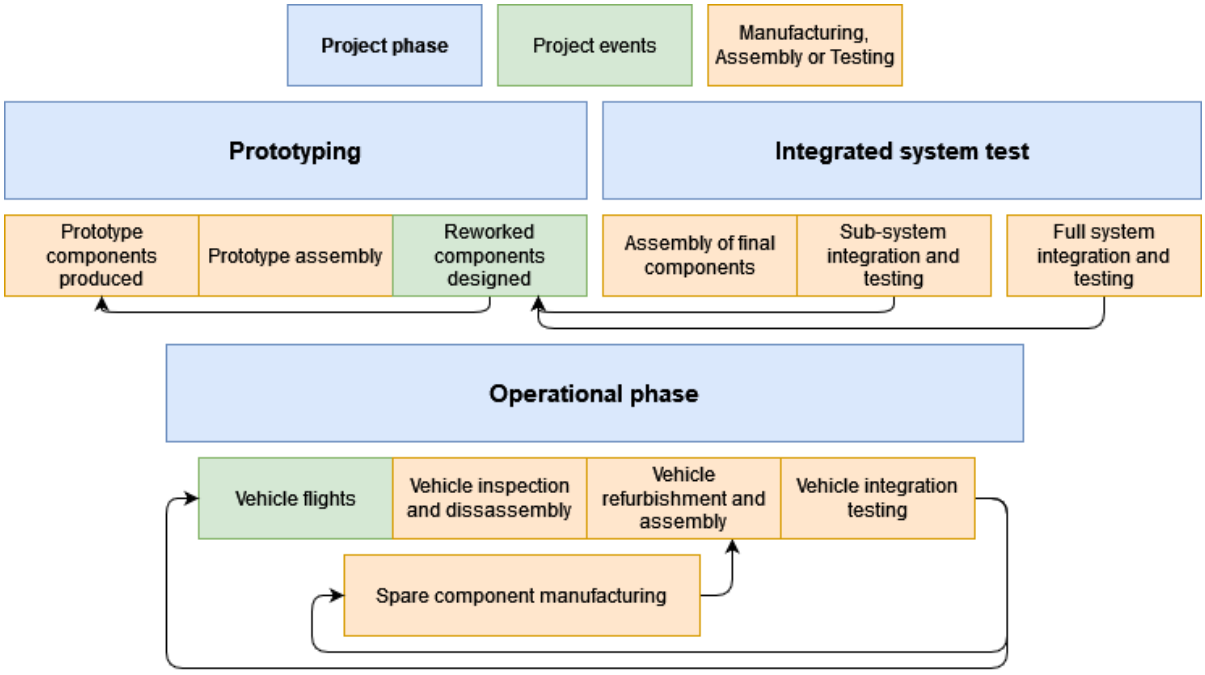

Figure 12.1: A flow diagram showing the different manufacturing, assembly and integration steps.

outsourced, since our company lacks the expertise to assemble the payload instruments. During the manufacturing phase, extensive quality control will be performed to ensure the components are made to the specification; the in-house manufacturing with skilled personnel ensures control over this quality.

Casting

During casting, safety is of paramount importance. Therefore, it is suggested that the casting shall be performed in a stand-alone building with a minimum distance of 30 m from other structures. Furthermore, the building shall have a blow-out wall or roof, to be able to vent any gasses in case of an explosion. The other walls of the building shall be made out of steel-reinforced concrete with a minimum thickness of 1 m, to contain an explosion in unwanted directions.

Operational Phase

During the operational phase MAI is also required since the launchers will be refurbished. Every launch season more rockets are taken to the launch site than required, ensuring that refurbishment can be carried out over the winter, in the Netherlands, such that scheduling risks are minimised. As outlined in the Section 4.2.2, the vehicle is disassembled and analysis performed on the parts to assess their reusability. This data will be used to create models for the wear of the components allowing for the optimisation of the refurbishment process. After refurbishment of components, re-assembly will occur. Post-assembly integration tests, will be conducted to ensure that the vehicle is flight-ready. Note that, excess materials are recycled. Additional information about refurbishment can be found in Section 12.2.

12.2. Operational and Logistical Concept

Author: M. Rusch

Editors: S. Yorucu, C. Kendall, E. Chen

The Altus mission is scheduled to start in the summer of 2026, and run for a period of 26 years. This section aims to give an overview of the operations and logistics required to successfully complete the mission. An overview of the logistical and operational concept is illustrated in Figure 12.2. First, the transportation of the equipment and vehicle to the launch site is briefly discussed, after which the mission operation during the summer period is elaborated on.

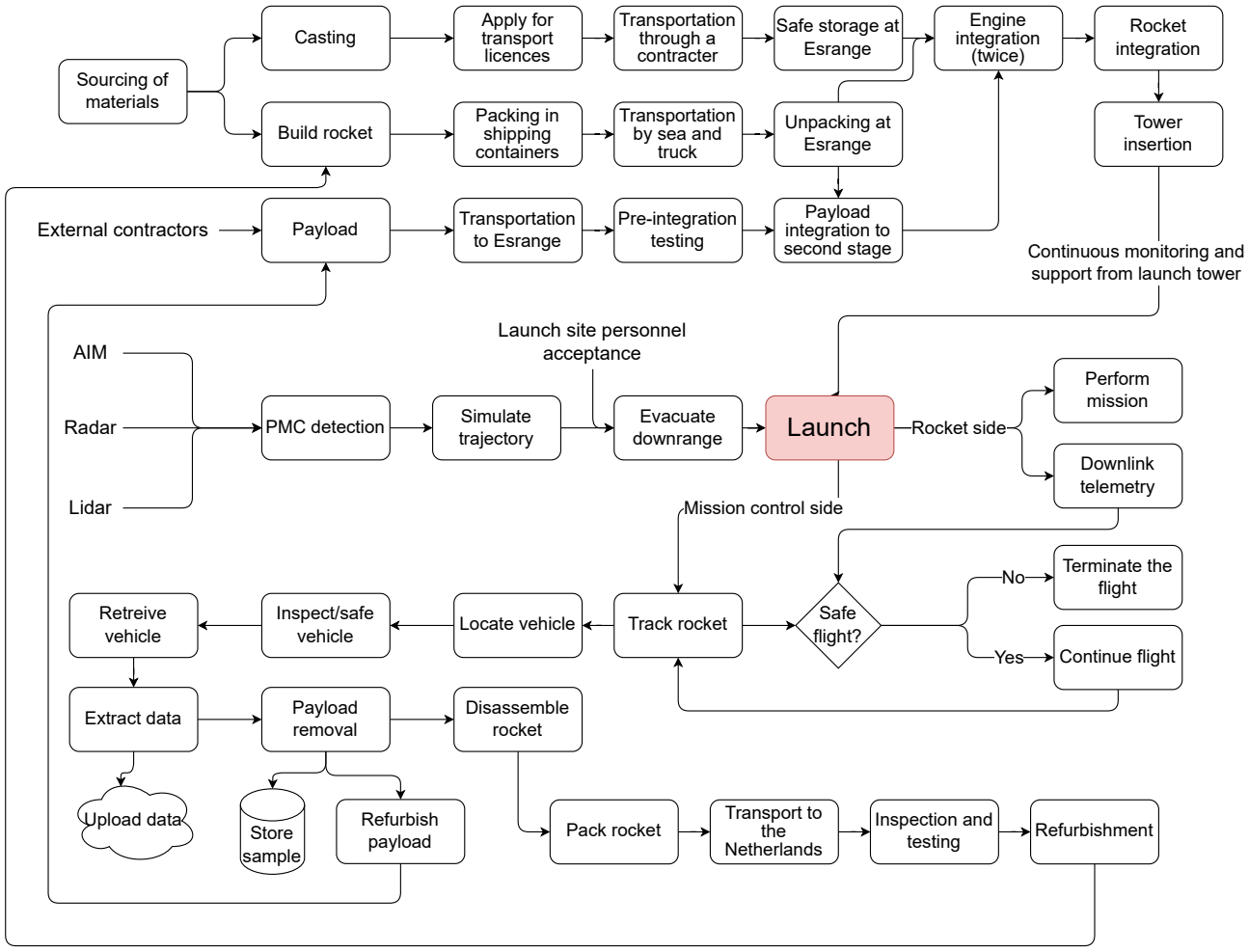

Figure 12.2: Logistics and timeline concept

Transportation to Launch Site

In this section, the logistics of reaching the launch site is discussed, initially for the equipment, and then for the rocket propellants, and personnel.

Transportation of Equipment

To simplify transportation, an effort will be made to pack all the equipment into one or two 40-foot shipping containers. Before the operational period in summer, these containers are packed with the vehicle, payload, and supporting equipment in the Netherlands, before being shipped to Esrange.

Transportation of Explosives and Propellants

The oxidiser Ammonium DiNitramide is classified as a class 1.1 explosive,[51] and the propellant itself is expected to be a class 1.3 explosive (fire hazard and either a minor blast hazard or a minor projection hazard or both) under United Nations (UN) transport regulations. Due to the nature of this transport, it will be outsourced to an external logistics company.

Transporting explosives and propellants is subjected to stringent regulations in the EU. This increases the logistical overhead of the program. Within the Netherlands, before getting a licence to transport explosives, everybody that uses them, the company and individuals, needs to have a "erkenning".[52] This certificate can is obtained from the Dutch police force, and has to be renewed every five years. This has to be done in the municipality where the company is located and in the municipality where the employee officially resides.[53] To be able to apply for such a licence, the recipient needs to have no criminal charges in weapon-related fields.[54] The chief of the local police force needs to give permission to acquire the certificate. They will use their judgement to determine if there is a risk of misuse of the explosives. If that is the case, or if there are other indications that the individual or company can not be trusted with these substances, then the certificate will not be granted.[55]

After the certificate has been granted, it is possible to apply for transportation of explosive materials. There are two different sets of rules looked at: transport within the Netherlands, and international transport between EU member states. Within the Netherlands, a so-called "overbrengingsvergunning" has to be applied for at the College van Burgemeester en Wethouders (College van B&W) in the municipality where the transport will end.[52] The College will then decide if the transportation is possible and if so, what safety measures are required. Additionally, the minister of Infrastructuur en Waterstaat (IenW) also has to agree on the transport.[55]

The normal road system has regulations in place for the movement of dangerous goods. The driver should be certified with the "ADR-Certificate",[56] for which a theoretical exam is required. This exam must be renewed every five years.[57] There are also requirements on parking locations, which roads you can use, certification of the transport vehicles, required personal protective equipment, etc.

When transporting across borders in the EU, both the minister of IenW and Inspectie Leefomgeving en Transport (ILT) have to agree to the transport.[53]Each country through which the propellants are transported or where the propellants are stored will too have to agree on the transport. The procedure to apply for hazardous materials transport varies by country but is unified under EU Directive 2008/68/EC [128].

Launch Operations

To minimise the amount of operations necessary on the launch site, all the vehicles necessary for the summer operational window and two spares are prepared over winter in the Netherlands and shipped to Sweden. This means

[51] https://echa.europa.eu/information-on-chemicals/cl-inventory-database/-/discli/details/101013 [22/05/2023]

[52] https://www.ilent.nl/onderwerpen/explosieven-voor-civiel-gebruik [17/05/2023]

[53] https://ondernemersplein.kvk.nl/werken-met-explosieven/ [17/05/2023]

[54] https://wetten.overheid.nl/BWBR0006962/2021-01-01 [17/05/2023]

[55] https://wetten.overheid.nl/BWBR0006803/2023-04-19 [17/05/2023]

[56] https://ondernemersplein.kvk.nl/gevaarlijke-stoffen-vervoeren-over-de-weg/ [17/05/2023]

[57] https://www.cbr.nl/nl/beroepsexamens/gevaarlijke-stoffen/adr-basiscertificaat.htm [17/05/2023]

no refurbishment is required during operations and this will significantly decrease personnel costs and schedule risks. Several payloads are taken, but due to the costs associated with this, the payloads will be reused; most likely two or three payloads will be on rotation, with a spare on hand.

Launch Preparations

At Esrange, the container is unpacked and pre-integration testing is performed on the payload. After these tests are completed the payload is integrated to the rocket structure. The final preparations for launch include integrating the rocket motors to the structure, connecting the two stages and rolling out to the pad. There the rocket will be inserted into a launchtower that will guide it during the first few meters of flight until it has sufficient speed to remain stable.

Launch Window

After the launch preparations are complete, the launch itself can be conducted. In the summer period, the launches will be spaced approximately eight days apart, but in order to determine the exact moment to launch the sounding rocket, the presence of PMCs has to be monitored, either using satellites or ground-based methods. An operational satellite suitable for this task is the AIM (Aeronomy of Ice in the Mesosphere) satellite, launched in 2007. One challenge in using satellites for determining launch opportunities is the lack of continuous detection above the launch site. The AIM satellite is in a 600 km Sun-synchronous orbit, which results in one continuous map of the polar region every day. Since only one measurement is conducted over the launch site each day [13] this data needs to be supplemented with ground-based data.

Ground-based lidar can be used as a supplement to the satellite observations in determining the timing of the launches [129]. The lidar measurements allow for frequent measurements, as opposed to the satellite measurements which only occur once per day. An added benefit is that the data is available sooner than the third-party satellite data. Satellites, on the other hand, do allow for a larger observational area, which may be used in order to predict the distribution of PMCs and indicate a chance of these clouds appearing above the launch site. Similar measurements can be conducted using Radar, but this does not directly measure the PMCs, but rather the Polar Mesospheric Summer Echoes (PMSEs), which are an indication of PMCs. Putting satellite-, radar-, and lidar-data together, the presence of PMCs can be confirmed and the launch can be scheduled.

Mission Control

From the point that the rocket is attached to the launch tower and its electronics are turned on, its health will be monitored digitally from the operations building. When a PMC is observed, the trajectory is simulated and passed by the launch site personnel. As soon as the trajectory is approved, all personnel in the downrange area are evacuated. When the downrange is cleared, the rocket is launched. From detecting PMCs, to actually launching, will take less than two hours; the launch warning sirens will be turned on starting from T-60 minutes [45]. The preparation for the launch will be minimal as the rocket will already be prepared in the tower.

As soon as the rocket leaves the launch tower, its trajectory is tracked. If the rocket starts to deviate too far from its intended path, the FTS is activated, to ensure that it will not land outside the allocated landing zone. The nosecone is ejected at 60 km altitude, such that the payload can perform its experiment. Afterwards, the rocket will start to descend and the recovery system will actuate to decelerate the vehicle to safe touchdown speeds. As soon as the vehicle lands, the location will be sent to the retrieval team, who will recover it, so that it can be refurbished again.

Telemetry

To obtain the highest gain, the ground station first points its antenna at the launch tower. Next, the rocket starts its electronic systems, and the ground station tries to make contact with the antenna of the rocket. As soon as the rocket launches, the ground antenna starts the track the rocket. The data sent over the telemetry link will consist of the payload data, any essential video footage (depending on the phase of the mission), the status and mission phase of the rocket, and the vehicle sensor data such as altitude, GNSS position, etc. This data will then be processed and presented live for the mission control while also being stored raw in a flight recorder as a backup in case of an anomaly and to provide more high frequency data post recovery. During the final descent phase the most important data transmitted will be the GNSS data. This data will be used to determine the touchdown location of the rocket.

Furthermore, radar tracking will be used for redundancy as this is an independent system, if the GNSS or telemetry fails the rocket can still be located. The exact data and resolution of the data send over the downlink is not yet known.

Retrieval

Upon the touchdown of the vehicle, it is important that it is retrieved. At Esrange, this is generally done though use of one or two helicopters. The vehicle has systems that enable the retrieval team to locate it. Firstly, radar and GNSS telemetry are transmitted to mission control throughout the descent phase. This gives a rough indication of where the rocket has touched down. For more accurate positioning a radio locator beacon and an Iridium GNSS beacon can be used. The first indicates the proximity of the receiver to the rocket; the second transmits the GNSS location via satellite to mission control. Once close, the brightly coloured parachute (SYS-RC-08) makes it easy to visually find the vehicle. When the helicopters arrive at the vehicle, an inspection is performed to ensure no hazards are present, and afterwards the rocket is attached to the helicopter and airlifted back to the launch site.

Post Flight Operations

After the retrieval, the data will need to be extracted from the rocket and the payload recycled for the next mission.

Data Handling

After each successful retrieval, the experimental data can be extracted from the rocket and is uploaded to the cloud of the customer so that scientists have instant access to the raw measured data. Additionally, the sample collection system collects particles, which are first stored in a cryocooler at Esrange. Every measurement is labelled with the time and place it is recorded and then saved into a digital database. At the end of the operational window, the eight samples are transported back to the Netherlands where they are transferred over to the customer, who will perform the laboratory analysis of the sample. They obtain the grain size, composition of the particles, and how many were found. These variables can both be compared over time and compared to other methods, like satellite measurements [130]. The changes over time result in a trend-line, which can be compared with other climate data (for example atmospheric temperatures and composition), to find if there is a correlation between climate change and the particle samples. The particles will be returned to long-term storage after analysis, so that if better instrumentation is created in the future or new theories are created the samples can be re-evaluated.

Similarly, the sensor data is compared to satellite, ground station and other rocket data and then compared to other climate data [13]. The data from satellites measuring similar properties to Altus will be stored in the database to allow for this data to be validated and correlated with the data gathered by the sounding rocket. Additionally any avionics data needed for calibration of the sensors will be provided.

After a season of data gathering a processed version of the data will be provided and graphed for the scientific community to use. Since this process depends on data over time, this will not be done after every launch. A first comparison between the data the rocket has collected and what other sources have documented will be done after the first launch, to confirm the accuracy of the instruments. This is also done for subsequent launches if the sensor suite is changed. After the sensor suite is calibrated and tested, the comparisons will happen further apart.

Refurbishment

The refurbishment process is two-fold. First of all, the payload will need to be refurbished on the launch site ahead of the next mission. This happens inside a clean-room: here, a new sample container is installed and the sensors are cleaned if necessary. Pre-integration testing and acceptance testing is once more performed.
The rockets will be packed in the shipping container after retrieval. At the end of the operational window the container is shipped back to the Netherlands where, over winter, the rockets are refurbished and updated and made ready for the next operational window. Refurbishment starts with system health checks. Depending on the outcome of these checks, the steps required for refurbishment are established and subsequently executed. Parts that are consumed often are kept in stock and tooling is put in place to aid in the execution of common procedures. This is to speed up the refurbishment as around eight rockets need to be refurbished in the span of nine months, in addition

to manufacturing new rockets if some are lost. Moreover, a speedy refurbishment lowers the costs associated to personnel.

12.3. Project Cost Budget

Author: L. Alonso
Editor: E. Chen

The project cost budget is a crucial tool in project management to plan and control the financial aspect of the project. It is necessary in order to achieve an estimate of the total project cost, allowing for its comparison with the project budget. In this manner the financial manager can check if the total cost is over or ideally under the budget resulting in contingencies. Additionally, the budget allows for the identification of cost components that are driving the majority of the total cost and further managerial action can be made. Note for this project cost budget, a margin of 30% was chosen, which is slightly larger to the 25% industry standard margin for flight systems according to the Johnson Space Center Cost Handbook.[58]

The project cost budget is shown in Table 12.1. The first price category is the labour cost which involves the salary of aerospace engineers and aerospace manufacturing technicians, estimated to be equal to €70,000 and €58,500 per year, respectively. [59] Note, these values are derived from engineering judgement and online sources. For the phases consisting of the detailed design, MAI, testing and design iterations, it was chosen to hire 4 aerospace engineers and 3 manufacturing technicians. Meanwhile, for the phases consisting of the launch, operations, refurbishing, and end of life, it was chosen to hire 1 aerospace engineer and 2 manufacturing technicians.

The next price category involves the costs for each vehicle sub-system part. Since it was chosen to manufacture 22 vehicles in Section 12.1, the cost is shown per 22 vehicles to cover the whole project cost. The cost is derived by multiplying 22 by the total sub-system cost found in Table 8.2, Table 8.12, Table 8.21, Table 8.29, Table 8.26 for the payload, propulsion, structures, avionics, and recovery sub-systems respectively. For the propulsion sub-system, a margin of 40% was chosen because of the uncertainty in the costs of the ADN propellant. This is due to the fact that this compound is manufactured in custom-made batches. In the future, the amounts that are demanded by Project Altus are expected to drive the shift from a batch-based production method to a continuous process, further decreasing the price. Even though the payload costs, mentioned in Section 2.4, are also uncertain, the chosen instruments, and hence, its costs are from before the year 2000. Therefore, it is expected that because of the drastic technological advancement in the previous decades that the cost nowadays would be lower. Hence, the margin of the payload is kept at 30%.

The physical parts price category consists of the manufacturing machines, ground systems, subsystems testing hardware and the flight testing hardware. The manufacturing machines component consists of the cost of a manufacturing and storage work space, a 5-axis CNC mill, and a large diameter lathe. The work space is based on a 350 m^2 area with a cost of €120 per m^2 per year. A budget of €100,000 and €25,000 is given to the 5-axis CNC mill and a large diameter lathe, respectively. These values are based on engineering experience. The ground systems component consists of the cost of a van used for transportation at Esrange and miscellaneous physical parts such as an antenna, cables, etc. A total of €100,000 was allocated towards the ground systems cost component. The subsystems testing hardware costs consists of the cost of tools for prototyping and tools and material needed for all the sub-system tests covered in Section 4.1. A budget of €50,000 was provided for it. Similarly, the cost for the flight testing hardware covers all tools and materials needed for three test flights. A budget of €50,000 was set for one test flight.

The last price category is cost related to operations, which includes the transportation, the launch site, as well as, the sub-system and flight tests. The transportation involves the use of a round trip shipping container every year for a total of 26 years to transport the vehicles from the Netherlands to Sweden. The cost is based on a one way

[58] URL https://www.nasa.gov/sites/default/files/atoms/files/14_historical_inst-spacecraft_growth_2016-08-04_tagged.pdf 27/06/2023

[59] URL https://www.payscale.com/research/NL/Job=Aerospace_Engineer/Salary 21/06/2023

shipping container estimated to be €4,500. Meanwhile, the launch site cost was approximated to be €100,000 a week. However, since the vehicle is only launched once a week, it was assumed that another team or project would be able to launch as well on a different day of the week. This will half the costs to €50,000 a week for a total of 8 weeks for 26 years. A budget of €300,000 was provided for the operational costs of all the sub-system tests. Meanwhile, a budget of €200,000 was set for one test flight. Since we estimate to have 3 full test flights, this results in an operational cost of €600,000 for the flight tests. Note, these values are based on past engineering experience. Since these values are uncertain at this stage of the project, an increased margin of 40% was applied to all operational cost components, as shown in Table 12.1.

By adding up all the development costs, the total development cost is equal to €4.35MM. While the total operational cost is equal to €15.98MM. Therefore, the total cost of the project is equal to €20.33MM. A 30% margin was added to this total cost, resulting in €26.42MM. Since the total budget for this project is equal to €35MM, €8.58MM is left for contingencies. Such margins are necessary to account for unforeseen circumstances, for example, the costs involved in the loss of a shipping container or higher costs than expected of certain components. Even though this cost is currently inestimable, the margin and contingencies allow for covering these potential circumstances.

Table 12.1: Project cost budget

Price category:	**Cost component:**	**Cost (million €):**	**Margin (+%):**	**Cost incl. Margin (million €):**
Labour:	Detailed Design MAI Testing Iterations	1.37	30	1.78
	Launch Operations Refurbish End of Life	4.86	30	6.32
Vehicle Parts per 22 Vehicles:	Payload	0.95	30	1.24
	Propulsion	0.14	40	0.20
	Structures & Stability	0.02	30	0.02
	Avionics	0.52	30	0.67
	Recovery	0.04	30	0.06
Physical Parts:	Manufacturing Workspace	1.32	30	1.71
	Ground Systems	0.10	30	0.13
	Subsystems Testing Hardware	0.05	30	0.07
	Flight Testing Hardware	0.15	30	0.20
Operations:	Transportation	0.23	40	0.33
	Launch Site	10.40	40	14.56
	Subsystem Tests	0.30	40	0.42
	Flight Tests	0.60	40	0.84
Total Development Cost:		4.35	-	5.67
Total Operational Cost:		16.70	-	22.86
Total Cost:		21.05	-	-
Total Cost including Margin:		-	-	28.53
Total Budget:		35.00	-	-
Contingency incl. Margin:	Budget Leftover	-	-	6.47

13
Sustainable Rocketry Industry Proposal

13.1. Assessment of Orbital Launcher Impact on the Environment

Author: S. Aurori
Editor: C. Kendall

The Altus mission is set to demonstrate sustainable technologies within the rocketry and launcher industry. In order to highlight the proposed advancements, an assessment of the effect of currently used technologies in the field is needed. Various studies have been carried out in order to assess the environmental impact of orbital launches, however most were related to the effects of the Space Shuttle Program [19]. The article sourced at [19], entitled "The environmental impact of emissions from space launches: A comprehensive review", is a meta-analysis of the environmental impact of orbital launchers over the past 40 years. It encompasses an assessment of 40 launcher reports and articles revealing the impact of these vehicles, out of which 32 sources reflect on Solid Rocket Motors (SRMs) only. This source is the backbone of the sustainability assessment within this chapter.

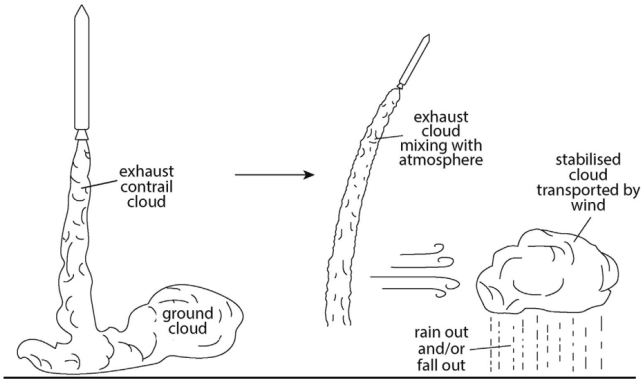

Figure 13.1: Cloud formation in the upper atmosphere due to orbital launcher exhaust products. Taken from [19].

Large scale SRMs are an industry standard as a first stage choice, due to their high propellant density, high thrust values, and simplicity [19]. This can be seen in [19, Table 1], due to the high number of orbital launchers that utilise APCP based motors. As previously outlined in Section 11.4, some of the main exhaust products of APCP are: hydrochloric acid, water vapour, carbon dioxide, oxides of nitrogen, aluminium oxide (alumina), and soot, also showcased in [19, Table 1]. The way these exhaust products are incorporated into the atmosphere is shown in Figure 13.1. Clouds are formed, and further transported by wind as a result, from the launcher exhausts. Furthermore, the exhausts themselves combine with the atmospheric products and can result in acid rain or fallout [131]. Such phenomena have been observed following Space Shuttle and Titan III launches, where acidic rain has occurred approximately 20 km away from the launch site [19]. Effects on the soil surrounding the launch sites have been quantified as well – the results and long term effect of these exhaust-induced alterations are dependent on the age and chemical composition of the soil itself [19, 131]. Fish killings, as well as damage to the vegetation surrounding the launchsite was measured following Space Shuttle operations [29, 131, 132]. This is where the atmospheric research of the PMCs is very valuable, by assessing the direct impact of orbital launcher vehicles onto the atmosphere [19], while developing a sustainable propulsion technology demonstrator.

A link between the ozone layer depletion and SRM firings has been established, by means of both simulations and in-situ measurements [19]. The amounts of chlorine present in the launcher exhaust plume has been assessed and linked to the ozone layer depletion, as it is responsible for two thirds of launcher-induced ozone reduction [19]. Although the effect is strongly dependent on the launch time, meaning that a lesser effect was spotted during night-time launches, more long term ozone layer depletion has been measured in small portions of the atmosphere

[19]. Additionally, AP is currently analysed to possibly negatively influence the endocrine system [60][19-06-2023]. Based on this, AP is currently under investigation in the EU under REACH, which brings further urgency in the need to replace this propellant component.

13.2. Green Propellant Development and Research

Author: S. Aurori
Editor: C. Kendall

The GRASP project is a consortium between 11 research parties across 7 countries, funded by the European Commission, with the purpose of researching and creating an overview of green alternatives to toxic industry standard propellants [133]. Due to their extremely high toxicity, negative impact on the environment and on system operators propellants such as hydrazine, monomethyl hydrazine (MMH), unsymmetrical dimethylhydrazine (UDMH), and dinitrogen tetroxide are planned to be replaced by cleaner and more sustainable alternatives [133]. To encourage the industry to switch to these alternatives, a database of performance values and experimental results is worked on within the GRASP initiative. The values attained experimentally are compared to the performance of the toxic counterparts. Such a comparison can be seen in Figure 13.2, where the performance of ADN-based monopropellants and that of HTPB in the context of a hybrid motor are compared to hydrazine. Not only are good performances indicated compared to hydrazine, but the inclusion of these propellants in the comparison is a confirmation of their sustainability.

The experiments consist of a performance assessment of various hot-fire tests, where a standard engine with different propellant configurations is tested. The scale of the thrust obtained through these hot-fires is around 200 N [134]. From a toxicity point of view, the chemicals are assessed based on a scale established within the GRASP program. Points are awarded based on the severity of consequences upon contact with the propellant, alongside a classification of contact method: oral, dermal or inhalation [133].

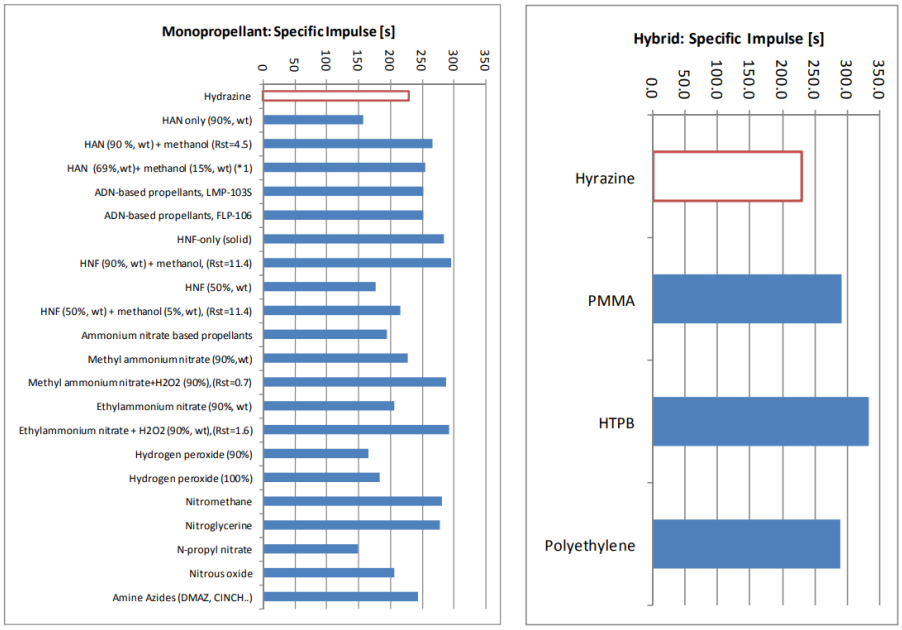

Figure 13.2: Overview of Green Monopropellant and Hybrid Propellant Alternatives to Hydrazine. Taken from [133].

The GRASP initiative is set to demonstrate the performance of these sustainable alternatives, as well as to create a database which gives confidence in these propellants to industry parties. However, within this consortium, only liquid propellants have been assessed [134].

As the Altus mission is developing a sustainable technology demonstrator for ADN-based solid rocket motors, it is proposed that a similar approach to that of GRASP is taken within the project. Moreover, the GRASP initiative showcases the need and urgency of researching sustainable propellants, and based on that, it is proposed that a similar initiative to take place in the assessment of SRM propellants and development.

[60] https://echa.europa.eu/substance-information/-/substanceinfo/100.029.305

14
Conclusion

Authors: L. Tabaksblat, S. Aurori, M. Beenders
Editor: M. Rusch

The behaviour of PMCs are changing with regards to, frequency of appearance, location, and brightness. Scientists suspect that this is due to climate change. However, it cannot yet be proven due to a lack of long-term data. For this reason, the goal is to launch for 26 years 8 times a year during the summer in Esrange. During these launches, a sensor suite records the pressure, temperature, and humidity, and collects samples. These variables are suspected the be the biggest contribution to the formation of the PMCs. Collecting these values over time will make it possible for researchers to search for correlations in the data, and find out if there are any links to climate change.

Parallel to this, the rocketry industry has a sizeable environmental impact. The use of hydrazine, nitric acid, AP, and many other hazardous chemicals, in addition to expendable vehicles, has been the industry standard for decades. This is because performance was always more important than sustainability. This needs to change, therefore the mission need statement of project Altus was defined as follows:

Catalyse a shift towards sustainable rocketry by means of a polar mesospheric cloud research mission, demonstrating technologies that can be applied to reduce the environmental impact of rockets.

This mission need statement is fulfilled in this report by placing this technology demonstrator into an industry-relevant context. To make this possible first an assessment of orbital launcher's environmental impact has been made. Based on continuous research carried out over the past 40 years, it is concluded that the need for new, sustainable alternatives exists. Similarly to the focus within the research community on coming up with clean alternatives for liquid propellants, the Altus project members have found a gap between the environmental impact of SRMs and the research conducted in attenuating this impact. Within the establishment of the readiness level phase, approximately 2 years into the mission, the Altus project is set to demonstrate the reliability and sustainability of the system, by means of numerous engine tests, as well as at least 10 qualification flight tests. By means of measurements, data analysis and performance assessment of the system, the new ADN-based propulsion system shall serve as a benchmark for new technologies meant to influence the industry to shift towards more environment-cautious systems.

15 Recommendations

This chapter gives recommendations for the further phases of this project. These are tasks that have been omitted due to time constraints, or suggestions on how to perform tasks better in the future. Section 15.1 explains these for the Systems Engineering tools, Section 15.2 for the Propulsion system, Section 15.3 for the avionics, Section 15.4 for the drag calculation and finally Section 15.5 for the structure sub-system.

15.1. Systems Engineering Tools

Authors: T. Odijk, M. Rusch

On of the areas where the understanding has evolved the most is the use of systems engineering tools. For the reports up until now the tools were globally understood as individual tools. The different tools, functional assessment, requirements, risks etc. were all used as individual blocks and in that sense completed to the best of our ability. However after doing more research into the topic and consulting a variety of different experts over the span of a number of days the understanding of the tools evolved. More of the links between them became apparent and a better way to utilise them to give our work a proper foundation was made clear.

As mentioned before, systems engineering was mostly regarded as some tools that had to be completed. But after more investigation the links and scope of systems engineering became a lot clearer. The tools are supposed to complement one another and give a solid foundation for the steps that are taken. It can even give rise to a plan that can be followed to achieve the goal.

Throughout the report it was attempted to also make more links back the the systems engineering tools. It is important at all steps to reflect on the requirements and risks such that your design is adequate for the task. It was also attempted to link things back to the timeline and project phases more often.

15.1.1. Product Functions

The product functions flow from the stakeholder requirements of the mission and will dictate the functional requirements. This was done implicitly but it would be nice if that can be made more clear for the future. This can help when the number of functions and requirements will expand and traceability is needed.

15.1.2. Requirements

For the requirements too much depth was explored in the previous reports. The importance of traceability was recognised, as all requirements had this indicated. However the method to find requirements did not always fully reflect this. It is therefore recommended that in the continuation of the project that the requirements are developed with the traceability more in mind and are clearly categorised to assist in this. This will also allow for the requirements to flow into the risks.

15.1.3. Risk Management

The risk management was initially done by trying to come up with the most important risks without consulting anything but our experience and what we thought the design would look like. What this meant is that the risks were developed in way too much depth in some areas and way too little in others. Since it was noticed for this report that it was the case some background research was done. This lead into a much deeper investigation of systems engineering as a whole. Here it was found that your risks come directly from your stakeholder requirements. Also

the difference between prevention and mitigation was made clear. Previously the difference between the probability and severity was not linked to the prevention and mitigation. For the next stages of the project it is also highly recommended that the investigation into root causes for risks is done. This should be combined with identification of departure likelihood, severity and the time at which it can occur. The risks can also lead to a plan for the verification and validation plan.

15.1.4. Market analysis

The main aspect that is currently lacking in the market analysis is evaluating the current competitors, and the competitiveness of the Altus design in the current market. Furthermore, while difficult, it is important to also take into account any future competition that will arise as technology advances. It is recommended to do more research into these two aspects. It is recommended to investigate how this evolving technology will affect Altus, and if a mid-life update is required in order to stay competitive.

15.1.5. Design and Development Logic

After reconsidering, and listening to expert feedback. It is clear that the level of detail and the substantiation behind the PD&DL is lacking. The recommendation for the next phase is that this is worked out into more detail and a comparison is drawn to similar programs to validate the estimates. More detail on how this should take shape will be given in Section 15.7 when the requirements compliance is discussed.

15.2. Propulsion System

Author: S. Aurori

Various recommendations are to be made regarding the propulsion system design. These are expected to be considered in later design phases, by means of extensive testing and iterations.

Firstly, starting with the sizing and simulations program of the propulsion system. Within the preliminary design phase of the Altus vehicle motors, the burn time has been assumed to be a constant input. It was planned that various iterations on the burn time shall be implemented, by means of OpenRocket simulations, where a indication of the necessary burn time would be provided. However, due to short amount of time and an oversimplification of the assumptions made throughout the process, this iterative burn time assessment has been skipped, meaning that only the thrust, and total impulse respectively, were iterated upon within the sizing tool with respect to the burn time. This introduced errors, due to the lack of flexibility between the input variables.

Moreover, in relation to the propellant composition, the current configuration has assumed characteristics, such as burn rate, pressure coefficient and exponent based on numerous OpenMotor simulations and indications based on literature. It is advised for the later stages of design, that numerous strand burner tests are performed, where a sample of propellant is ignited and its burn profile is measured. The process in which the propellant is cast and purchased from, which includes chemical purity, particle size, and compound ratios influence the burn behaviour heavily. Hence, determining these values for the Altus specific propulsion system is necessary.

Furthermore, the current propellant formulation includes aluminium powder, which has been incorporated for performance reasons. This further translates to having alumina particles in the exhaust, which although not toxic, are not desirable to be released in the environment. As previously outlined within the report, the ADN tends to burn aggressively, meaning that the addition of ammonium nitrate was necessary. Additionally, the presence of aluminium, following various standard motor configuration, allowed for the desired performance to be obtained within a short amount of iterations. Similarly to the previously outlined point, specific strand testing is advised, to determine the real performance of the propellant, including options that do not contain aluminium as well.

15.3. Avionics

Author: L. Tabaksblat

Editor: E. Chen

There are three big recommendations to be made for the avionics. The first is to improve the accuracy of the

power budget by analysing the required power over the entire flight as not all sensors and devices will be powered constantly. Furthermore, as this more detailed power budget will mostly lead to lower energy requirements, the feasibility of using LiFePO4 batteries, a form of lithium-ion batteries, instead of LiPo batteries should be reevaluated. Using LiFePO4 batteries would greatly reduce the risk of battery fires and increase the lifespan of the battery, thus increasing the sustainability of the avionics.

The second recommendation is to evaluate the possibility of using a lower amount of transmission power for the telemetry. The current telemetry system uses a large amount of power, to ensure that the required data rate is feasible and the data loss is minimal. However, the data rate will most likely decrease, since not all footage and data will be transmitted. Furthermore, the current SNR is greater than required and can therefore be decreased significantly. A decrease in transmission power would reduce the required battery mass, which would also make the heavier LiFePO4 batteries a feasible option. Therefore, a more detailed link budget should be set up to evaluate this possibility, and an estimation of the bit error rate should be created.

The last recommendation is to add a satellite communication module to the avionics. After touchdown, the connectivity between the ground stations and the rocket will worsen significantly due to ground obstacles hindering the signal propagation. As a satellite communication module works by line of sight to satellites, it increases the chance of receiving the location data of the landed vehicle.

15.4. Drag

Author: S. Yorucu

In the simulation, the drag components of the launch lugs, rail guides, and launch shoes were not included [48, p. 51-52]. During the detailed design phase, it is recommended that this drag component is implemented into the simulation tool to more accurately estimate trajectory and performance.

Moreover, an analysis of the accuracy of the Barrowman method for calculating drag components should have been done. Specifically by comparing the Barrowman equations outputs with existing experimental results, for example from Missile DATCOM.

15.5. Structure

Author: S. Yorucu

In Section 8.6.1, it was mentioned that the tip of the nose cone undergoes significant heating due to drag and atmospheric effects. It is recommended that, a thermal test is performed on the nose cone, and that an aerodynamic protective layer to cover the nose cone tip, such as a ceramic heat shield, is implemented into the design.

15.6. Model Verification and Validation

There is a lot of additional validation that needs to be performed in the future. Mainly, the simulation software needs to be validated more. The individual aspects such as the cost estimation, drag estimations and other subsections of the code have not been validated. This makes validating the model as a whole much more difficult. Furthermore, the software needs to be validated with more vehicles and more data. Furthermore, the precision of the model need to be estimated to define the reliability of the program and under what conditions.

Another point of interest to perform in the future is the validation of the trade-off. By putting our different trade-off options in the simulator we can verify that the right choices were made during the concept selection phase and that the estimated numbers were correct. This increases the confidence in the design significantly. The tool should also be evaluated against other more accurate simulation tools.

Finally, not only does the code needs to be validated but the subsystems need to be as well. For this reason a detailed plan should be created for the subsystem verification and validation. This should include details on what will be tested and which requirements the test will prove.

15.7. Requirements Compliance

The advice for the future is that a more detailed V&V or Test plan is created that will shape the PD&DL. For every requirement, a concrete test should be designed with fail-pass conditions and a list of necessary resources. This information will help fill in the timeline and make a more accurate budget.

15.8. Payload

One of the most difficult parts of the design was the design of the payload. This was due to how limited the options for sounding rocket instruments are. This meant that all options had to found from old papers where the instruments were custom made. It is therefore recommended to approach payload specialists for the preliminary design of the payload. This means that the payload will be custom made and perfectly adapted to the requirements of a sounding rocket.

15.9. Operational and Logistical Concept

The recommendation is to start soon with laying out a more detailed Operational and Logistical concept. This should include more information specific to the launchsite and high-level procedures for the launch and refurbishment process. This information will once more help in further detailing the timeline and cost budgets.

15.10. Project Cost Budget

For the next project phases, it is recommended to create a further detailed project cost budget, and hence, decrease the respective margins used. For example, the operational costs should also include the transportation and storage costs of the payload samples that will be collected after every successful launch. Another example is to include the costs for all the certifications needed. Once the budget is further detailed, the margins can decrease because of an increase in certainty in the cost of each component. Furthermore, the budget for testing and certification needs to be increased significantly to be able to account for possible test failures and for if multiple launches are required for the licensing. This does require the Operational and Logistical Concept, Design and Development Logic, and Manufacturing, Assembly, Integration, and Test plan to be worked out in more detail.

References

[1] J. D. Hunley. *The History of Solid-Propellant Rocketry: What We Do and Do Not Know*. Edwards, CA: National Aeronautics and Space Administration Dryden Flight Research Center, 1999. URL: https://www.nasa.gov/centers/dryden/pdf/88635main_H-2330.pdf.

[2] R.H. Varney and M.C. Kelley. 'MESOSPHERE | Polar Summer Mesopause'. In: *Encyclopedia of Atmospheric Sciences*. Elsevier, 2015, pp. 436–443. DOI: 10.1016/B978-0-12-382225-3.00221-8.

[3] Franz-Josef Lübken, Uwe Berger and Gerd Baumgarten. 'On the Anthropogenic Impact on Long-Term Evolution of Noctilucent Clouds'. In: *Geophysical Research Letters* 45 (13 July 2018), pp. 6681–6689. ISSN: 0094-8276. DOI: 10.1029/2018GL077719.

[4] Matthew T. DeLand and Gary E. Thomas. 'Updated PMC trends derived from SBUV data'. In: *Journal of Geophysical Research: Atmospheres* 120 (5 Mar. 2015), pp. 2140–2166. ISSN: 2169897X. DOI: 10.1002/2014JD022253.

[5] Jodie Barker-Tvedtnes. 'Polar Mesospheric Clouds: A Satellite and Ground-Based Comparison'. Logan, UT: Utah State University, 2009. URL: https://digitalcommons.usu.edu/cgi/viewcontent.cgi?article=1010%5C&context=honors.

[6] Peter Dalin et al. 'The strong activity of noctilucent clouds at middle latitudes in 2020'. In: *Polar Science* 35 (Mar. 2023), p. 100920. ISSN: 18739652. DOI: 10.1016/j.polar.2022.100920.

[7] Vincent B. Wickwar. 'Visual and lidar observations of noctilucent clouds above Logan, Utah, at 41.7°N'. In: *Journal of Geophysical Research* 107 (D7 Apr. 2002), p. 4054. ISSN: 0148-0227. DOI: 10.1029/2001JD001180.

[8] R.P. Turco et al. 'Noctilucent clouds: Simulation studies of their genesis, properties and global influences'. In: *Planetary and Space Science* 30 (11 Nov. 1982), pp. 1147–1181. ISSN: 00320633. DOI: 10.1016/0032-0633(82)90126-X.

[9] C. L. Hemenway, R. K. Soberman and G. Witt. 'Sampling of noctilucent cloud particles'. In: *Tellus* 16 (1 Feb. 1964), pp. 84–88. ISSN: 00402826. DOI: 10.1111/j.2153-3490.1964.tb00146.x.

[10] Gary E. Thomas et al. 'Relation between increasing methane and the presence of ice clouds at the mesopause'. In: *Nature* 338 (6215 Apr. 1989), pp. 490–492. ISSN: 0028-0836. DOI: 10.1038/338490a0.

[11] James M. Russell et al. 'The Aeronomy of Ice in the Mesosphere (AIM) mission: Overview and early science results'. In: *Journal of Atmospheric and Solar-Terrestrial Physics* 71 (3-4 Mar. 2009), pp. 289–299. ISSN: 13646826. DOI: 10.1016/j.jastp.2008.08.011.

[12] John M C Plane et al. 'Opinion: Recent Developments and Future Directions in Studying the Chemistry of the Mesosphere and Lower Thermosphere'. In: *EGUsphere [preprint]* (2023). DOI: https://doi.org/10.5194/egusphere-2023-680.

[13] Matthew T. DeLand et al. 'A quarter-century of satellite polar mesospheric cloud observations'. In: *Journal of Atmospheric and Solar-Terrestrial Physics* 68 (1 Jan. 2006), pp. 9–29. ISSN: 13646826. DOI: 10.1016/j.jastp.2005.08.003.

[14] Gary E. Thomas. 'Are noctilucent clouds harbingers of global change in the middle atmosphere?' In: *Advances in Space Research* 32 (9 Jan. 2003), pp. 1737–1746. ISSN: 02731177. DOI: 10.1016/S0273-1177(03)90470-4.

[15] Mark E. Hervig et al. 'The Missing Solar Cycle Response of the Polar Summer Mesosphere'. In: *Geophysical Research Letters* 46 (16 Aug. 2019), pp. 10132–10139. ISSN: 0094-8276. DOI: 10.1029/2019GL083485.

[16] C. E. Robert et al. 'First evidence of a 27 day solar signature in noctilucent cloud occurrence frequency'. In: *Journal of Geophysical Research* 115 (Mar. 2010), p. D00I12. ISSN: 0148-0227. DOI: 10.1029/2009JD012359.

[17] Luca Alonso et al. *Project Altus Midterm Report: Concept Selection and Conceptual Design for a Sustainable Upper Atmospheric Vehicle*. Delft: Delft University of Technology, May 2023.

[18] Luca Alonso et al. *Project Altus Baseline Report: Mission Establishment, Requirements Discovery, and Concept Generation for a Sustainable Upper Atmospheric Vehicle*. Delft: Delft University of Technology, May 2023.

[19] J.A. Dallas et al. 'The environmental impact of emissions from space launches: A comprehensive review'. In: *Journal of Cleaner Production* 255 (May 2020), p. 120209. ISSN: 09596526. DOI: 10.1016/j.jclepro.2020.120209.

[20] Benjamin J. Murray and Eric J. Jensen. 'Homogeneous nucleation of amorphous solid water particles in the upper mesosphere'. In: *Journal of Atmospheric and Solar-Terrestrial Physics* 72 (1 Jan. 2010), pp. 51–61. ISSN: 13646826. DOI: 10.1016/j.jastp.2009.10.007.

[21] Markus Rapp and Franz-Josef Lübken. 'Comment on "Ice iron/sodium film as cause for high noctilucent cloud radar reflectivity" by P. M. Bellan'. In: *Journal of Geophysical Research* 114 (D11 June 2009), p. D11204. ISSN: 0148-0227. DOI: 10.1029/2008JD011323.

[22] R. J. Francey et al. 'A history of $\delta^{13}C$ in atmospheric CH_4 from the Cape Grim Air Archive and Antarctic firn air'. In: *Journal of Geophysical Research: Atmospheres* 104 (D19 Oct. 1999), pp. 23631–23643. ISSN: 01480227. DOI: 10.1029/1999JD900357.

[23] Luke M. Western et al. 'Global increase of ozone-depleting chlorofluorocarbons from 2010 to 2020'. In: *Nature Geoscience* 16 (4 Apr. 2023), pp. 309–313. ISSN: 1752-0894. DOI: 10.1038/s41561-023-01147-w.

[24] Jennifer C. Mabry et al. 'No evidence for change of the atmospheric helium isotope composition since 1978 from re-analysis of the Cape Grim Air Archive'. In: *Earth and Planetary Science Letters* 428 (Oct. 2015), pp. 134–138. ISSN: 0012821X. DOI: 10.1016/j.epsl.2015.07.035.

[25] Jia Yue et al. 'Increasing Water Vapor in the Stratosphere and Mesosphere After 2002'. In: *Geophysical Research Letters* 46 (22 Nov. 2019), pp. 13452–13460. ISSN: 0094-8276. DOI: 10.1029/2019GL084973.

[26] Earle Williams et al. 'Calibrated Radiance Measurements with an Air-filled Glow Discharge Tube: Application to Sprites in the Mesosphere'. In: May 2006, pp. 237–251. ISBN: 1-4020-4627-8. DOI: 10.1007/1-4020-4629-4_11.

[27] Michael Alexander et al. *Systems Engineering Handbook, NASA SP-2016-6105 Rev2*. Washington, DC: National Aeronautics and Space Administration, 2016. URL: https://www.nasa.gov/sites/default/files/atoms/files/nasa_systems_engineering_handbook_0.pdf.

[28] Luca Pozzoni, Christian Paravan and Luciano Galfetti. 'ADN-based Formulations Analysis for Green Solid Propellants'. In: 9th European Conference for Aeronautics and Space Sciences (EUCASS). Milan, IT, 2022. DOI: 10.13009/EUCASS2022-4909.

[29] William E. Hawkins, Robin M. Overstreet and Mark J. Provancha. 'Effects of Space Shuttle Exhaust Plumes on Gills of Some Estuarine Fishes: A Light and Electron Microscopic Study'. In: *Gulf Research Reports* 7 (4 Jan. 1984), pp. 297–309. ISSN: 0072-9027. DOI: 10.18785/grr.0704.01.

[30] *2022-2026 Strategic Plan*. United States National Science Foundation, 2022. URL: https://www.nsf.gov/publications/pub_summ.jsp?ods_key=nsf22068.

[31] *Wetenschap Werkt! NWO-Strategie 2023-2026*. Den Haag: Nederlandse Organisatie voor Wetenschappelijk Onderzoek, July 2022. URL: https://www.nwo.nl/sites/nwo/files/media-files/NWO_strategie-Wetenschap-werkt_2023-2026.pdf.

[32] Daniel A. Sullivan et al. 'Development of an Ejectable Cubesat Onboard a Sounding Rocket'. In: 2nd Symposium on Space Educational Activities. Budapest, Hungary, Apr. 2018. URL: https://www.mse.tu-berlin.de/wp-content/uploads/2018/09/SSEA2018_proceedings_Alex.pdf.

[33] Leonardo Kessler Slongo et al. 'Pre-flight qualification test procedure for nanosatellites using sounding rockets'. In: *Acta Astronautica* 159 (June 2019), pp. 564–577. ISSN: 00945765. DOI: 10.1016/j.actaastro.2019.01.035.

[34] Daniel Levack, Bryan DeHoff and Russel Rhodes. 'Functional Breakdown Structure (FBS) and Its Relationship to Life Cycle Cost'. In: 45th AIAA/ASME/SAE/ASEE Joint Propulsion Conference. Reston, Virigina: American Institute of Aeronautics and Astronautics, Aug. 2009. ISBN: 978-1-60086-972-3. DOI: 10.2514/6.2009-5344.

[35] Bruno Gagnon, Roland Leduc and Luc Savard. 'Sustainable Development in Engineering: A Review of Principles and Definition of a Conceptual Framework'. In: *Environmental Engineering Science* 26 (10 Oct. 2009), pp. 1459–1472. ISSN: 1092-8758. DOI: 10.1089/ees.2008.0345.

[36] T. H. G. Megson. *Aircraft Structures for Engineering Students*. 6th ed. Oxford, UK: Butterworth-Heinemann, 2017. ISBN: 978-0-08-100914-7.

[37] Chetan, Sudarsan Ghosh and P. Venkateswara Rao. 'Application of sustainable techniques in metal cutting for enhanced machinability: a review'. In: *Journal of Cleaner Production* 100 (Aug. 2015), pp. 17–34. ISSN: 09596526. DOI: 10.1016/j.jclepro.2015.03.039.

[38] Fu-yao Chen et al. 'A review on the high energy oxidizer ammonium dinitramide: Its synthesis, thermal decomposition, hygroscopicity, and application in energetic materials'. In: *Defence Technology* 19 (2023), pp. 163–195. ISSN: 2214-9147. DOI: https://doi.org/10.1016/j.dt.2022.04.006. URL: https://www.sciencedirect.com/science/article/pii/S221491472200071X.

[39] John B. Rae. 'Synthetic Rubber: A Project that Had to Succeed. By Vernon Herbert and Attilio Bisio. Westport: Greenwood Press, 1985. Pp. xi, 243.' In: *The Journal of Economic History* 46.4 (1986), pp. 1096–1097. DOI: 10.1017/S0022050700051135.

[40] Jin Wei Fan and Fu Tao Tan. 'Analysis of Major Defects and Nondestructive Testing Methods for Solid Rocket Motor'. In: *Applied Mechanics and Materials* 365-366 (Aug. 2013), pp. 618–622. ISSN: 1662-7482. DOI: 10.4028/www.scientific.net/AMM.365-366.618.

[41] Christian Garb et al. 'Statistical analysis of micropore size distributions in Al–Si castings evaluated by X-ray computed tomography'. In: *International Journal of Materials Research* 109 (10 Oct. 2018), pp. 889–899. ISSN: 2195-8556. DOI: 10.3139/146.111685.

[42] Prabhu Paramasivam and S. Vijayakumar. 'Mechanical characterization of aluminium alloy 6063 using destructive and non-destructive testing'. In: *Materials Today: Proceedings* 81 (2023), pp. 965–968. ISSN: 22147853. DOI: 10.1016/j.matpr.2021.04.312.

[43] George Sutton and Oscar Biblarz. *Rocket Propulsion Elements*. 9th ed. Hoboken, NJ: John Wiley & Sons, 2017. ISBN: 9781118753651.

[44] F. Beach. *Electrical Systems and Equipment*. Ed. by D.J. Littler. 3rd ed. Oxford: Pergamon Press, 1992, pp. 748–798. ISBN: 9780080405148. DOI: 10.1016/C2009-0-16016-6.

[45] Peter Lindström et al. *Esrange Safety Manual, SCIENCE-60-4208*. Kiruna: Swedish Space Corporation, June 2020. URL: https://sscspace.com/wp-content/uploads/Esrange-Safety-Manual.pdf.

[46] Allen K Mears. *Report on the Effects of Parachutes on Risk Mitigation to Third-party Property and Individuals*. 1993. URL: https://rosap.ntl.bts.gov/view/dot/12796.

[47] Homayoon Dezfuli et al. *Risk Management Handbook, NASA/SP-2011-3422 Version 1.0*. Washington, D.C.: National Aeronautics and Space Administration, Nov. 2011. URL: https://ntrs.nasa.gov/api/citations/20120000033/downloads/20120000033.pdf.

[48] Sampo Niskanen. *OpenRocket Technical Documentation: Development of an Open Source Model Rocket Simulation Software*. 2013. URL: https://openrocket.sourceforge.net/techdoc.pdf.

[49] Gary A. Crowell. *The Descriptive Geometry of Nose Cones*. 1996. URL: http://servidor.demec.ufpr.br/CFD/bibliografia/aerodinamica/Crowell_1996.pdf.

[50] William E. Stoney. *Collection of Zero-lift Drag Data On Bodies of Revolution from Free-flight Investigations, NASA TR R-100*. Langley Field, Va: National Aeronautics and Space Administration Langley Research Center, 1961. URL: https://ntrs.nasa.gov/api/citations/19630004995/downloads/19630004995.pdf.

[51] James S Barrowman. 'The Practical Calculation of the Aerodynamic Characteristics of Slender Finned Vehicles'. Washington, D. C.: Catholic University of America, Mar. 1967. URL: https://ntrs.nasa.gov/api/citations/20010047838/downloads/20010047838.pdf.

[52] Sighard F. Hoerner. *Fluid-dynamic Drag Theoretical, Experimental and Statistical Information*. 2nd ed. Bakersfield, CA: Hoerner Fluid Dynamics, 1965. ISBN: 9781124136226.

[53] Eugene L. Fleeman. 'Tactical Missile Design'. In: *The Aeronautical Journal* 106 (1056 Feb. 2002), pp. 115–115. ISSN: 0001-9240. DOI: 10.1017/S0001924000096020.

[54] R. K. Soberman et al. 'Techniques for rocket sampling of noctilucent cloud particles'. In: *Tellus* 16 (1 Feb. 1964), pp. 89–95. ISSN: 00402826. DOI: 10.1111/j.2153-3490.1964.tb00147.x.

[55] Eric Jensen and Gary E. Thomas. 'A growth-sedimentation model of polar mesospheric clouds: Comparison with SME measurements'. In: *Journal of Geophysical Research* 93 (D3 1988), p. 2461. ISSN: 0148-0227. DOI: 10.1029/JD093iD03p02461.

[56] M. J. Burchell et al. 'Characteristics of cometary dust tracks in Stardust aerogel and laboratory calibrations'. In: *Meteoritics & Planetary Science* 43 (1-2 Feb. 2008), pp. 23–40. ISSN: 10869379. DOI: 10.1111/j.1945-5100.2008.tb00608.x.

[57] Jennifer A. Grier and Andrew S. Rivkin. 'Comparing Sample and Remote-Sensing Data – Understanding Surface Composition'. In: *Airless Bodies of the Inner Solar System*. Elsevier, 2019, pp. 95–119. DOI: 10.1016/B978-0-12-809279-8.00005-6.

[58] Tore R. Christiansen. *Development of an Airborne Sonic Thermometer*. Cambridge, MA: Aerophysics Laboratory Massachusetts Institute of Technology, Sept. 1982.

[59] O. V. Shtyrkov and V. A. Yushkov. 'A dual absolute pressure measuring transducer'. In: *Instruments and Experimental Techniques* 59 (1 Jan. 2016), pp. 139–141. ISSN: 0020-4412. DOI: 10.1134/S0020441216010140.

[60] André Zuber and Georg Witt. 'Optical hygrometer using differential absorption of hydrogen Lyman-α radiation'. In: *Applied Optics* 26 (15 Aug. 1987), p. 3083. ISSN: 0003-6935. DOI: 10.1364/AO.26.003083.

[61] Stuart P. Beaton and Mike Spowart. 'UV Absorption Hygrometer for Fast-Response Airborne Water Vapor Measurements'. In: *Journal of Atmospheric and Oceanic Technology* 29 (9 Sept. 2012), pp. 1295–1303. ISSN: 0739-0572. DOI: 10.1175/JTECH-D-11-00141.1.

[62] B. V. S Jyoti. *Exercise Thermal Rocket Propulsion AE4S01 (P). Lecture 1*. Delft, Feb. 2023.

[63] Edwin D Brown. 'An Introduction to PROPEP, A Propellant Evaluation Program for Personal Computers'. In: *Journal of Pyrotechnics* (1 1995), pp. 11–18. URL: http://www.jpyro.co.uk/wp-content/uploads/j01_11_htfsr.pdf.

[64] W. T. Brooks. *Solid Propellant Grain Design and Internal Ballistics, NASA SP-8076*. Cleveland, OH: National Aeronautics and Space Administration Lewis Research Center, Mar. 1972. URL: https://ntrs.nasa.gov/citations/19730007077.

[65] Weiqiang Pang et al. 'Burning Rate Prediction of Solid Rocket Propellant (SRP) with High-Energy Materials Genome (HEMG)'. In: *Crystals* 13 (2 Jan. 2023), p. 237. ISSN: 2073-4352. DOI: 10.3390/cryst13020237.

[66] Alain Davenas. *Solid Rocket Propulsion Technology*. Oxford, UK: Pergamon Press, 1993. ISBN: 0-08-040999-7. DOI: 10.1016/C2009-0-14818-3. Transl. *Technologie des Propergols Solides*, 1989.

[67] George P. Sutton and Oscar Biblarz. *Rocket Propulsion Elements*. 7th ed. Hoboken, NJ: John Wiley & Sons, 2001. ISBN: 978-0471326427.

[68] Luigi Tonino DeLuca. 'Innovative Solid Formulations for Rocket Propulsion'. In: *Eurasian Chemico-Technological Journal* 18 (3 Nov. 2016), p. 181. ISSN: 1562-3920. DOI: 10.18321/ectj424.

[69] Nasser Sheibani. 'Simulation and experimental study on the incompatibility issue between ADN and isocyanate'. In: *Journal of Molecular Modeling* 28 (12 Dec. 2022), p. 405. ISSN: 1610-2940. DOI: 10.1007/s00894-022-05399-y.

[70] Arnau Pons Lorente. *Study of Grain Burnback and Performance of Solid Rocket Motors*. Universitat Politècnica de Catalunya, Jan. 2013.

[71] F A Anderson and W R West. *Alternate Propellant Program Phase I Final Report, NASA-CR-158815*. Pasadena, CA: National Aeronautics and Space Administration Jet Propulsion Laboratory, July 1979. URL: https://ntrs.nasa.gov/api/citations/19790020174/downloads/19790020174.pdf.

[72] Liang Yin et al. 'High-temperature mechanical properties of constructional 6082-T6 aluminum alloy extrusion'. In: *Structures* 48 (Feb. 2023), pp. 1244–1258. ISSN: 23520124. DOI: 10.1016/j.istruc.2023.01.043.

[73] D.R. Bartz. *Turbulent Boundary-Layer Heat Transfer from Rapidly Accelerating Flow of Rocket Combustion Gases and of Heated Air*. Pasadena, CA: Jet Propulsion Laboratory, California Institute of Technology, 1965, pp. 1–108. DOI: 10.1016/S0065-2717(08)70261-2.

[74] David A. Reese, Darren M. Wright and Steven F. Son. 'CuO/Al Thermites for Solid Rocket Motor Ignition'. In: *Journal of Propulsion and Power* 29 (5 Sept. 2013), pp. 1194–1199. ISSN: 0748-4658. DOI: 10.2514/1.B34771.

[75] Homer E. Newell. *Sounding Rockets*. 1st ed. New York: McGraw-Hill, 1959.

[76] Charles J. Piper. *Manufacture of Boron / Potassium Nitrate (BKNO3) Ignition Granules, And Pellets*. 1st ed. Patterson, CA: Rocket Research Institute, 2013.

[77] *Pellets/Granules Boron/Potassium Nitrate, MIL-P-46994B*. 1982. URL: http://everyspec.com/MIL-SPECS/MIL-SPECS-MIL-P/MIL-P-46994B_8387/.

[78] *Mersen Benelux B.V. Graphite Nozzle Insert*. Invoice. Schiedam, NL. URL: www.mersen.com.

[79] *Evonik Industries AG Polyvest HT*. Invoice. Essen, DE. URL: www.evonik.com.

[80] *Design of Aerodynamically Stabilized Free Rockets, MIL-HDBK-762(MI)*. US Army Missile Command, 1990.

[81] Ryan Hannaford et al. *Project BOGO: Research and Design of a Two-Stage Supersonic Rocket*. Akron, OH: University of Akron, 2020.

[82] Kishorkumar Ukirde et al. 'Aerodynamic Study of Various Fins for Missile Body'. In: *International Journal for Research in Applied Science and Engineering Technology* 11 (2 Feb. 2023), pp. 1240–1252. ISSN: 23219653. DOI: 10.22214/ijraset.2023.49235.

[83] Zachary Howard. 'How To Calculate Fin Flutter Speed'. In: *Peak Of Flight 291* (291 July 2011). URL: https://www.apogeerockets.com/PeakOfFlight/Archive.

[84] T. V. Milligan. 'What is the best fin shape for a model rocket?' In: *Peak Of Flight 442* (442 May 2017). URL: https://www.apogeerockets.com/PeakOfFlight/Archive.

[85] J. V. Fedor. *Theory and Design Curves for a Yo-Yo De-Spin Mechanism for Satellites, NASA TN D-708*. Greenbelt, MD: National Aeronautics and Space Administration Goddard Space Flight Center, Aug. 1961.

[86] Gary Stroick. *Nose Cone & Fin Optimization*. Tripoli Minnesota, Jan. 2011.

[87] Mark W. Hilburger. *Buckling of thin-walled circular cylinders, NASA SP–8007-2020/REV 2*. Hampton, VA: National Aeronautics and Space Administration Langley Research Center, Nov. 2020. URL: https://shellbuckling.com/papers/classicNASAReports/NASA-SP-8007-2020Rev2FINAL.pdf.

[88] Florin Mingireanu, Nicolae Jula and Cristian Boboc. 'Boosted Dart Sounding Vehicle'. In: 2017 International Conference on Control, Artificial Intelligence, Robotics & Optimization (ICCAIRO). IEEE. 2017, pp. 319–324. DOI: 10.1109/ICCAIRO.2017.65.

[89] John C. Weydert. *A Discussion of Rocket Vehicle Joint Characteristics*. Albuquerque, NM: Sandia Laboratory, May 1968. URL: https://www.osti.gov/servlets/purl/5007820.

[90] Katharina Schüttauf et al. *REXUS User Manual*. EuroLaunch, Sept. 2017. URL: https://rexusbexus.net/rexus/rexus-user-manual/.

[91] Michael Ashby, Hugh Shercliff and David Cebon. *Materials*. 3rd ed. Oxford: Butterworth-Heinemann, 2014. ISBN: 978-0-08-097772-0.

[92] J. Guery et al. 'Thrust Oscillations in Solid Rocket Motors'. In: 44th AIAA/ASME/SAE/ASEE Joint Propulsion Conference & Exhibit. Reston, Virigina: American Institute of Aeronautics and Astronautics, July 2008. ISBN: 978-1-60086-992-1. DOI: 10.2514/6.2008-4979.

[93] E. L. Petersen and J. W. Murdock. 'Active control of vortex-driven oscillations in a solid rocket motor using a cold-flow simulation'. In: *37th Aerospace sciences meeting and exhibit* (Jan. 1999). DOI: 10.2514/6.1999-860.

[94] Roohollah Taherinezhad and Gholamreza Zarepour. 'Evaluation of pressure oscillations by a laboratory motor'. In: *Chinese Journal of Aeronautics* 33.3 (2020), pp. 805–825. ISSN: 1000-9361. DOI: 10.1016/j.cja.2019.11.010.

[95] Daniel J. Inman. *Engineering Vibration*. 4th ed. Upper Saddle River, NJ: Pearson, 2014. ISBN: 9780136809531.

[96] Y. Li et al. 'Fatigue properties and cracking mechanisms of a 7075 aluminum alloy under axial and torsional loadings'. In: *Procedia Structural Integrity* 19 (2019). Fatigue Design 2019, International Conference on Fatigue Design, 8th Edition, pp. 637–644. ISSN: 2452-3216. DOI: https://doi.org/10.1016/j.prostr.2019.12.069.

[97] Theo W. Knacke. *Parachute Recovery Systems Design Manual*. Santa Barbara: Para Publishing, Mar. 1991. ISBN: 0-915516-85-3. URL: https://apps.dtic.mil/sti/citations/ADA247666.

[98] Mattias Abrahamsson. *Esrange User's Handbook, Volume III, Launch Range Instrumentation*. Swedish Space Corporation, 2022. URL: http://www.sscspace.com..

[99] *IRIG standard 106-22*. Range Commanders Council, 2022. URL: https://irig106.org/wiki/irig_106-22.

[100] Leon W. Couch. *Digital and Analog Communication Systems*. Ed. by Andrew Gilfillan. 8th ed. London, UK: Pearson Education, Inc. ISBN: 978-0-13-291538-0. URL: https://www.pearson.com/en-us/subject-catalog/p/digital--analog-communication-systems/P200000003176/9780132915380.

[101] Nimal Navarathinam, Regina Lee and Hugh Chesser. 'Characterization of Lithium-Polymer batteries for CubeSat applications'. In: *Acta Astronautica* 68 (11-12 June 2011), pp. 1752–1760. ISSN: 00945765. DOI: 10.1016/j.actaastro.2011.02.004.

[102] Michele Pastorelli, Salvatore Musumeci and Fabio Mandrile. 'Battery Sources and Power Converters Interface in Waterborne Transport Applications'. In: 2021 AEIT International Conference on Electrical and Electronic Technologies for Automotive (AEIT AUTOMOTIVE). 2021, pp. 1–5. DOI: 10.23919/AEITAUTOMOTIVE52815.2021.9662776.

[103] *MTi User Manual, MT0605P*. Feb. 2020. URL: https://www.xsens.com/hubfs/Downloads/usermanual/MTi_usermanual.pdf.

[104] *Teseo-VIC3DA Automotive GNSS dead-reckoning module with 6-axis IMU*. Geneva, CH: STMicroelectronics, Oct. 2021. URL: https://www.st.com/en/positioning/teseo-vic3da.html.

[105] *PT-100-SEG14-A-ZVG/US Pressure Transmitter*. Essen, DE: ifm Electronic GmbH. URL: https://www.ifm.com/de/en/product/PT5402.

[106] *Hero 8 Black*. San Mateo, CA: GoPro, Inc. URL: https://gopro.com/content/dam/help/hero-2018/HERO_UM_ENG_REVA.pdf.

[107] *AFE7769 Quad-Channel RF Transceiver With Feedback Path*. Texas Instuments, 2019. URL: https://www.ti.com/lit/ds/symlink/afe7769.pdf?ts=1687015297783.

[108] *bq76pl536a-Q1 3-to-6 Series Cell Lithium-Ion Battery Monitor and Secondary Protection IC for EV and HEV Applications*. Texas Instruments, 2016. URL: https://www.ti.com/lit/ds/symlink/bq76pl536a-q1.pdf.

[109] *ASFC8G31M-51BIN*. Alliance Memory, 2021. URL: https://www.alliancememory.com/wp-content/uploads/pdf/eMMC/AllianceMemory_8GB_ASFC8G31M-51BIN_eMMCdatasheet_Jan2022_v1.1.pdf.

[110] Sampo Niskanen. *OpenRocket*. Computer Program. Feb. 2023. URL: https://github.com/openrocket/openrocket.

[111] Frank O. Chandler. 'Design and Testing of a Small Launch Vehicle with Lessons Learned'. In: AIAA Propulsion and Energy 2019 Forum. Reston, Virginia: American Institute of Aeronautics and Astronautics, Aug. 2019. ISBN: 978-1-62410-590-6. DOI: 10.2514/6.2019-4148.

[112] Ben C. Stringer et al. 'Student Design of Altitude Controlled High Powered Rocket and Deployable Autonomous Multirotor'. In: 53rd AIAA/SAE/ASEE Joint Propulsion Conference. Reston, Virginia: American Institute of Aeronautics and Astronautics, July 2017. ISBN: 978-1-62410-511-1. DOI: 10.2514/6.2017-4842.

[113] T-Minus Engineering. *DART System for fast and low-cost probing of the upper atmosphere*. 2017. URL: https://www.t-minus.nl/_files/ugd/b7ff60_f56fe10a98464ea08a7933b8dee02749.pdf.

[114] Wouter Dubois. 'Enhanced Radiation Cooling Design of an Active Thermal Protection System'. Delft, NL: Delft University of Technology, 2017.

[115] Jordi Puig-Suari, Clark Turner and William Ahlgren. 'Development of the standard CubeSat deployer and a CubeSat class PicoSatellite'. In: 2001 IEEE aerospace conference proceedings (Cat. No. 01TH8542). Vol. 1. IEEE. 2001, pp. 1–347. DOI: 10.1109/AERO.2001.931726.

[116] Qing Li and Yu-Liu Chen. 'Data Flow Diagram'. In: *Modeling and Analysis of Enterprise and Information Systems*. Berlin, Heidelberg: Springer, 2009, pp. 85–97. DOI: 10.1007/978-3-540-89556-5_4.

[117] M Posch et al. 'An Acoustic Balloon-Borne Instrument to Measure Temperature Fine Structure Near The Tropopause'. In: 14th ESA Symposium on European Rocket and Balloon Programmes and Related Research. Ed. by B. Kaldeich-Schúrmann. Potsdam, DE: European Space Agency, May 1999. URL: https://ui.adsabs.harvard.edu/abs/1999ESASP.437..359P.

[118] Ken Hamotani and Nobutaka Monji. 'A New, Low-Power Consumption, One-Dimensional Sonic Anemometer-thermometer.' In: *Journal of Agricultural Meteorology* 55 (2 1999), pp. 109–115. ISSN: 0021-8588. DOI: 10.2480/agrmet.55.109.

[119] Nedal Aluminium. *Alloy Data Sheet EN AW-6082 [AlSi1MgMn]*. June 2005. URL: https://www.nedal.com/wp-content/uploads/2016/11/Nedal-alloy-Datasheet-EN-AW-6082.pdf.

[120] Charles E. Rogers and David Cooper. *Rogers Aeroscience RASAero II Aerodynamic Analysis and Flight Simulation Program Users Manual*. URL: https://www.rasaero.com/dloads/RASAero%5C%20II%5C%20Users%5C%20Manual.pdf.

[121] Charles E. Rogers. *RASAero II Flight Simulation Comparison with Kip Daugirdas MESOS 293K ft Altitude Rocket Flight Data*. URL: https://www.rasaero.com/dloads/RASAero%5C%20II%5C%20Users%5C%20Manual.pdf.

[122] L. Scelsi et al. 'Potential emissions savings of lightweight composite aircraft components evaluated through life cycle assessment'. In: *Express Polymer Letters* 5 (3 2011), pp. 209–217. ISSN: 1788618X. DOI: 10.3144/expresspolymlett.2011.20.

[123] Donald Bush et al. *Recommended Techniques for Effective Maintainability, NASA-TM-4628*. National Aero., Space Admin. Reliability and Maintainability Steering Committee, Dec. 1994. URL: https://ntrs.nasa.gov/api/citations/19950025109/downloads/19950025109.pdf.

[124] Valery P. Sinditskii et al. 'Combustion of Ammonium Dinitramide, Part 1: Burning Behavior'. In: *Journal of Propulsion and Power* 22 (July 2006). DOI: 10.2514/1.17950.

[125] Priscia Lynch and Magdi Rizk. 'Thin-layer Navier-Stokes solutions for transonic multi-body interference'. In: 29th Aerospace Sciences Meeting. Reston, Virigina: American Institute of Aeronautics and Astronautics, Jan. 1991. DOI: 10.2514/6.1991-71.

[126] *Regulation (EU) 2021/821 of the European Parliament and of the Council of 20 May 2021 Setting Up a Union Regime for the Control of Exports, Brokering, Technical Assistance, Transit and Transfer of Dual-use Items*. May 2021. URL: https://eur-lex.europa.eu/legal-content/EN/TXT/?uri=CELEX:02021R0821-20230112.

[127] *Product information Polyvest ® HT Hydroxyl-Terminated Polybutadiene*. Marl, DE: Evonik Industries GmbH, 2018. URL: https://products.evonik.com/assets/88/68/Asset_1218868.pdf.

[128] *Directive 2008/68/EC of the European Parliament and of the Council of 24 September 2008 on the inland transport of dangerous goods (Text with EEA relevance)*. Sept. 2008. URL: https://eur-lex.europa.eu/legal-content/EN/TXT/?uri=CELEX:02008L0068-20221229.

[129] M.J. Taylor et al. 'Coordinated optical and radar image measurements of noctilucent clouds and polar mesospheric summer echoes'. In: *Journal of Atmospheric and Solar-Terrestrial Physics* 71 (6-7 May 2009), pp. 675–687. ISSN: 13646826. DOI: 10.1016/j.jastp.2008.12.005.

[130] M. N. Eremenko. 'Shape and composition of PMC particles derived from satellite remote sensing measurements'. In: *Geophysical Research Letters* 32 (16 Aug. 2005), L16S06. ISSN: 0094-8276. DOI: 10.1029/2005GL023013.

[131] Thomas W. Dreschel and Carlton R. Hall. 'Quantification of hydrochloric acid and particulate deposition resulting from space shuttle launches at John F. Kennedy space center, Florida, USA'. In: *Environmental Management* 14 (4 July 1990), pp. 501–507. ISSN: 0364-152X. DOI: 10.1007/BF02394138.

[132] Paul A C Schmalzer et al. *Effects Of Space Shuttle Launches STS4 Through STS9 On Terrestrial Vegetation Of John F. Kennedy Space Center, Florida, NASA-TM-83103*. Kennedy Space Center, FL: The Bionetics Corporation, Sept. 1985. URL: https://ntrs.nasa.gov/citations/19870011225.

[133] C Scharlemann. *Green Propellants: Global Assessment of Suitability and Applicability*. Siebersdorf, AT: Austrian Research Centers GmbH. URL: https://www.eucass.eu/component/docindexer/?task=download%5C&id=6118.

[134] C. Scharlemann. 'Green Advanced Space Propulsion - A project status'. In: 47th AIAA/ASME/SAE/ASEE Joint Propulsion Conference & Exhibit. Reston, Virigina: American Institute of Aeronautics and Astronautics, July 2011. ISBN: 978-1-60086-949-5. DOI: 10.2514/6.2011-5630.